

1995

Two-dimensional nuclear magnetic resonance studies of thymosin-alpha(1) (a myosin light chain kinase activating peptide), and ribonuclease a in the presence of uridine vanadate.

Timothy Daniel. Veenstra
University of Windsor

Follow this and additional works at: <http://scholar.uwindsor.ca/etd>

Recommended Citation

Veenstra, Timothy Daniel, "Two-dimensional nuclear magnetic resonance studies of thymosin-alpha(1) (a myosin light chain kinase activating peptide), and ribonuclease a in the presence of uridine vanadate." (1995). *Electronic Theses and Dissertations*. Paper 4441.

This online database contains the full-text of PhD dissertations and Masters' theses of University of Windsor students from 1954 forward. These documents are made available for personal study and research purposes only, in accordance with the Canadian Copyright Act and the Creative Commons license—CC BY-NC-ND (Attribution, Non-Commercial, No Derivative Works). Under this license, works must always be attributed to the copyright holder (original author), cannot be used for any commercial purposes, and may not be altered. Any other use would require the permission of the copyright holder. Students may inquire about withdrawing their dissertation and/or thesis from this database. For additional inquiries, please contact the repository administrator via email (scholarship@uwindsor.ca) or by telephone at 519-253-3000ext. 3208.



National Library
of Canada

Acquisitions and
Bibliographic Services Branch

395 Wellington Street
Ottawa, Ontario
K1A 0N4

Bibliothèque nationale
du Canada

Direction des acquisitions et
des services bibliographiques

395, rue Wellington
Ottawa (Ontario)
K1A 0N4

Your file *Votre référence*

Our file *Notre référence*

NOTICE

The quality of this microform is heavily dependent upon the quality of the original thesis submitted for microfilming. Every effort has been made to ensure the highest quality of reproduction possible.

If pages are missing, contact the university which granted the degree.

Some pages may have indistinct print especially if the original pages were typed with a poor typewriter ribbon or if the university sent us an inferior photocopy.

Reproduction in full or in part of this microform is governed by the Canadian Copyright Act, R.S.C. 1970, c. C-30, and subsequent amendments.

AVIS

La qualité de cette microforme dépend grandement de la qualité de la thèse soumise au microfilmage. Nous avons tout fait pour assurer une qualité supérieure de reproduction.

S'il manque des pages, veuillez communiquer avec l'université qui a conféré le grade.

La qualité d'impression de certaines pages peut laisser à désirer, surtout si les pages originales ont été dactylographiées à l'aide d'un ruban usé ou si l'université nous a fait parvenir une photocopie de qualité inférieure.

La reproduction, même partielle, de cette microforme est soumise à la Loi canadienne sur le droit d'auteur, SRC 1970, c. C-30, et ses amendements subséquents.

Canada

**TWO-DIMENSIONAL NUCLEAR MAGNETIC RESONANCE
STUDIES OF THYMOSIN α_1 A MYOSIN LIGHT CHAIN
KINASE ACTIVATING PEPTIDE, AND RIBONUCLEASE A
IN THE PRESENCE OF URIDINE VANADATE**

by

Timothy Daniel Veenstra

A Dissertation

**Submitted to the Faculty of Graduate Studies and Research
through the Department of Chemistry and Biochemistry
in Partial Fulfillment of the Requirements for the
Degree of Doctor of Philosophy at the
University of Windsor**

Windsor, Ontario, Canada

1994



National Library
of Canada

Acquisitions and
Bibliographic Services Branch

395 Wellington Street
Ottawa, Ontario
K1A 0N4

Bibliothèque nationale
du Canada

Direction des acquisitions et
des services bibliographiques

395, rue Wellington
Ottawa (Ontario)
K1A 0N4

Your file *Votre référence*

Our file *Notre référence*

THE AUTHOR HAS GRANTED AN IRREVOCABLE NON-EXCLUSIVE LICENCE ALLOWING THE NATIONAL LIBRARY OF CANADA TO REPRODUCE, LOAN, DISTRIBUTE OR SELL COPIES OF HIS/HER THESIS BY ANY MEANS AND IN ANY FORM OR FORMAT, MAKING THIS THESIS AVAILABLE TO INTERESTED PERSONS.

L'AUTEUR A ACCORDE UNE LICENCE IRREVOCABLE ET NON EXCLUSIVE PERMETTANT A LA BIBLIOTHEQUE NATIONALE DU CANADA DE REPRODUIRE, PRETER, DISTRIBUER OU VENDRE DES COPIES DE SA THESE DE QUELQUE MANIERE ET SOUS QUELQUE FORME QUE CE SOIT POUR METTRE DES EXEMPLAIRES DE CETTE THESE A LA DISPOSITION DES PERSONNE INTERESSEES.

THE AUTHOR RETAINS OWNERSHIP OF THE COPYRIGHT IN HIS/HER THESIS. NEITHER THE THESIS NOR SUBSTANTIAL EXTRACTS FROM IT MAY BE PRINTED OR OTHERWISE REPRODUCED WITHOUT HIS/HER PERMISSION.

L'AUTEUR CONSERVE LA PROPRIETE DU DROIT D'AUTEUR QUI PROTEGE SA THESE. NI LA THESE NI DES EXTRAITS SUBSTANTIELS DE CELLE-CI NE DOIVENT ETRE IMPRIMES OU AUTREMENT REPRODUITS SANS SON AUTORISATION.

ISBN 0-612-01496-7

Canada

© Timothy Daniel Veenstra 1994
All Rights Reserved

ABSTRACT

TWO-DIMENSIONAL NUCLEAR MAGNETIC RESONANCE STUDIES OF THYMOSIN α_1 A MYOSIN LIGHT CHAIN KINASE ACTIVATING PEPTIDE, AND RIBONUCLEASE A IN THE PRESENCE OF URIDINE VANADATE

by

Timothy Daniel Veenstra

1. The structure of the peptide thymosin α_1 has been investigated by circular dichroism and one- and two-dimensional nuclear magnetic resonance spectroscopy. Thymosin α_1 is a highly acidic peptide composed of 28 amino acid residues. Through the use of circular dichroism and two-dimensional nuclear magnetic resonance techniques, the structure of thymosin α_1 in 30% (v/v) deuterated 2,2,2-trifluoroethanol has been solved. Thymosin α_1 contains an α -helix extending from residue 16 to 26 and a turn between residues 5 and 8. Thymosin α_1 has been shown to be a potent activator of skeletal muscle myosin light chain kinase a well known calmodulin-dependent enzyme. Using the solution structures of thymosin α_1 and the calmodulin binding domain of skeletal muscle myosin light chain kinase, computer modelling suggests that electrostatic interactions comprise the major interacting force between these two peptides.

2. The binding of the proposed transition state analog, uridine vanadate to ribonuclease A has been investigated by one- and two-dimensional nuclear magnetic resonance spectroscopy. Analysis of the homonuclear nuclear Overhauser and exchange

spectroscopy spectrum of the uridine vanadate/ribonuclease A complex exhibits cross peaks between the H ϵ 1 proton of histidine 12 of RNase A and both the C₆H and C₅H protons of uridine vanadate. No cross peaks were observed between the H ϵ 1 proton of histidine 119 of ribonuclease A and the C₆H and C₅H protons of uridine vanadate. However, the distances calculated from the crystallographic structure show that the H ϵ 1 proton of histidine 119 is closer to the C₆H and C₅H protons of uridine vanadate, than is the H ϵ 1 proton of histidine 12. These results suggests that there is a significant difference in the position of the histidine 119 side chain in the crystallographic and solution structures of the uridine vanadate/ribonuclease A complex.

DEDICATION

I wish to dedicate this work to my beautiful wife, Christine and to our wonderful son, Jacob. Your love and encouragement has made this day possible. I promise you that I will spend the rest of my life trying to make our lives together the best they possibly can be. I love you both very much.

What we are is God's gift to us, what we become is our gift to God.

ACKNOWLEDGEMENTS

I would like to express my gratitude to my supervisor, Dr. Lana Lee and to my committee members Dr. Khosrow Adeli, Dr. Keith Taylor, and Dr. Alden Warner for their evaluation of this dissertation. I also wish to thank Dr. Joseph O'Neil for participating as my external examiner.

I wish to thank the University of Windsor for providing me with tuition scholarships and travel grants during the course of my study. Many thanks also go to the Dr. William A. Remond Memorial Bursary foundation for the financial support they have given me. I am also indebted to Dr. Su Sun Wang of ALPHA-1 Biomedicals Inc., Foster City, California for the gift of thymosin α_1 , Dr. G. S. Shaw of Western University, London, Ontario for the help in the acquisition of the thymosin α_1 nuclear magnetic resonance data, and Dr. S. N. Vinogradov of Wayne State University for allowing me the use of his circular dichroism spectropolarimeter.

I would also like to thank Jeffery Baldwin and Dr. T. K. Christopoulos for their critical evaluation of this dissertation. I would also like to acknowledge the University of Windsor Research Board for financial assistance.

I would like to express my eternal gratitude to my parents, Peter and Shirley Veenstra. You taught me the things that are truly important. Finally, I would like to thank God for always providing for me and guiding me on my path through life.

TABLE OF CONTENTS

	Page
ABSTRACT	iv
DEDICATION	vi
ACKNOWLEDGEMENTS	vii
LIST OF TABLES	xiv
LIST OF FIGURES	xvi
LIST OF ABBREVIATIONS	xx

PART A: Two-dimensional Nuclear Magnetic Resonance Studies of Thymosin α_1

1	INTRODUCTION	1
1.1	Two-dimensional Nuclear Magnetic Resonance	1
1.2	Circular Dichroism	14
1.3	Chou-Fasman Analysis	16
1.4	Primary Structure and Function of Thymosin α_1	17
1.5	Myosin Light Chain Kinase	28
1.5.a	Function	28
1.5.b	Binding Region and Interaction with Calmodulin	28
1.6	Stabilization of Peptide Structures by Fluorinated Alcohols	36
1.7	Objectives of this Research	39

2	MATERIALS AND METHODS	40
2.1	Materials	40
2.1.a	Proteins	40
2.1.b	Enzymes	40
2.1.c	Chemicals	40
2.2	Instrumentation	41
2.3	Methodology	44
2.3.a	Chou-Fasman Analysis of the Primary Structure of Thymosin α_1	44
2.3.b	Circular Dichroism	44
2.3.c	α -Chymotryptic Digestion of Thymosin α_1	45
2.3.d	Peptide Mapping	45
2.3.e	Amino Acid Analysis	46
2.3.f	NMR Spectroscopy	48
2.3.g	NOE Distance and Volume Restraints	50
2.3.h	Structure Calculations	50
2.3.i	Analysis of the Structure of Thymosin α_1	51
2.3.j	Modelling the Interaction with Myosin Light Chain Kinase	52
3	RESULTS	53
3.1	Chou-Fasman Analysis of Thymosin α_1	53
3.2	One-Dimensional NMR Measurements of Thymosin α_1	56
3.3	Circular Dichroism of Thymosin α_1	60
3.4	α -Chymotryptic Digestion of Thymosin α_1	69

3.5	Two-Dimensional NMR of Thymosin α_1	69
3.5.a	Amino Acid Spin System Identification	69
3.5.b	Non-Sequential NOE's	88
3.6	Chemical Shift Index for Thymosin α_1	93
3.7	Determination and Description of the Three-Dimensional Structure of Thymosin α_1	93
3.8	Modelling the Interaction of Thymosin α_1 with Myosin Light Chain Kinase	103
4	DISCUSSION	119
4.1	Solution Structure of Thymosin α_1	119
4.2	Stabilization of Thymosin α_1 by Trifluoroethanol	129
4.3	Modelling the Interaction of Thymosin α_1 with skMLCK	133
4.4	How Does Thymosin α_1 Cure Hepatitis B?	136
	REFERENCES	142

PART B: Two-Dimensional Nuclear Magnetic Resonance
 Studies of RNase A in the Presence of
 Uridine Vanadate

5	INTRODUCTION	162
---	--------------	-----

5.1	Ribonuclease A	162
5.1.a	Specificity and Enzymatic Mechanism	162
5.1.b	Structure	165
5.2	Position of Histidine 119 and Histidine 12	170
5.3	NMR Studies of RNase A	175
5.4	Interaction with Uridine Vanadate	175
5.5	Objectives of this Research	178
6	MATERIALS AND METHODS	180
6.1	Materials	180
6.1.a	Proteins	180
6.1.b	Chemicals	180
6.2	Instrumentation	180
6.3	Methodology	181
6.3.a	NMR Spectroscopy	181
6.3.b	pH* Titration of RNase A	182
6.3.c	3'-Cytidine Monophosphate Titration of RNase A	182
6.3.d	pH* Titration of the 3'-CMP/RNase A Complex	183
6.3.e	⁵¹ V-NMR of Uridine Vanadate	184
6.3.f	Uridine Vanadate Titration of RNase A	184
6.3.g	pH* Titration of the U-V/RNase A Complex	185
6.3.h	Preparation of Sample for Two-Dimensional ¹ H-NMR Studies	185

6.3.i	Modelling the Interaction of U-V with RNase A	186
7	RESULTS	188
7.1	pH* Titration of RNase A	188
7.2	3'-CMP Titration of RNase A	192
7.3	pH* Titration of the 3'-CMP/RNase A Complex	197
7.4	⁵¹ V-NMR of Uridine Vanadate	197
7.5	Uridine Vanadate Titration of RNase A	205
7.6	pH* Titration of the U-V/RNase A Complex	207
7.7	Two-Dimensional NMR of the U-V/RNase A Complex	211
7.8	Modelling the Interaction Between RNase A and Uridine Vanadate	217
7.9	Energy Changes in the U-V/RNase A Complex as a Consequence of Varying the Postions of the His119 Side Chain	220
8	DISCUSSION	225
8.1	pH* Titration of RNase A	225
8.2	Titration of RNase A with 3'-CMP	225
8.3	pH* Titration of the 3'-CMP/RNase A Complex	226
8.4	Titration of RNase A with U-V	227

8.5	pH* Titration of the U-V/RNase A Complex	229
8.6	Binding of U-V to RNase A	229
8.7	Position of His119 in the U-V/RNase A Complex	231
8.8	Modelling the Catalytic Mechanism of RNase A	234
	REFERENCES	239
	APPENDIX	249
	VITA AUCTORIS	263

LIST OF TABLES

TABLE	TITLE	Page
I	Observable ^1H - ^1H Distances for Identifying Secondary Structural Elements by Nuclear Overhauser Enhancement Spectroscopy	10
II	Conformational Parameters for the Residues of Thymosin α_1	54
III	Conformational Parameters for the Sequence Asp6, Thr7, Ser8 and Ser9 Within Thymosin α_1	57
IV	Helical Content of Thymosin α_1 at Various Amounts of Trifluoroethanol	66
V	Amino Acid Composition of Peptides Recovered in the α -Chymotryptic Digestion of Thymosin α_1	71
VI	Sequence-Specific Assignments of Thymosin α_1	90
VII	Observed versus Random Coil Chemical Shifts of the αH Resonances of Thymosin α_1	94
VIII	Average Distances Between the (i,i+3) Backbone Nitrogen Atoms of the Eleven Best Structures Generated for Thymosin α_1	101
IX	List of the Hydrogen Bonds Observed in the Modelling of the Interaction Between Thymosin α_1 and the CaM-binding Domain of skMLCK	109
X	Comparison of the Helical Content of Thymosin α_1 Determined by Chou-Fasman, CD and NMR Analysis	126
XI	Position of Histidine 119 in the Crystal Structures of RNase A with Various Active Site Ligands	173
XII	pH* Titration Chemical Shift Data of the Histidyl Residues of RNase A	191

XIII	RNase A pH Titration Parameters	193
XIV	Chemical Shift Data of the Histidyl Residues in the 3'-CMP Titration of RNase A	196
XV	pH* Titration Chemical Shift Data of the Histidyl Residues in the 3'-CMP/RNase A Complex	201
XVI	3'-CMP/RNase A Complex pH* Titration Parameters	202
XVII	Chemical Shift Data for Histidine Residues 12 and 119 in the U-V Titration of RNase A	208
XVIII	Chemical Shift Data for Histidyl Residues 12 and 119 in the pH* Titration of the U-V/RNase A Complex	215

LIST OF FIGURES

FIGURE	TITLE	Page
1	COSY Spin Systems of the Twenty Common Amino Acids	5
2	Common Nuclear Overhauser Enhancement (NOE) Connectivities Between Neighbouring Residues	8
3	Circular Dichroism Spectra of an α -helix, β -strand and Random Coil	15
4	The Primary Structure of Thymosin α_1	21
5	The Primary Structure of Prothymosin α	24
6	The Calmodulin Binding Domains of Skeletal Muscle and Smooth Muscle Myosin Light Chain Kinase	30
7	Secondary Structure Prediction for Thymosin α_1	58
8	pH* Titration of Thymosin α_1	59
9	$^1\text{H-NMR}$ Spectra of Thymosin α_1 in 100% (v/v) D_2O and 60% (v/v) TFE- d_3	61
10	CD Spectrum of Thymosin α_1 in Aqueous Solution	62
11	CD Spectra of Thymosin α_1 in 0% (v/v) and 10% (v/v) TFE	63
12	CD Spectra of Thymosin α_1 in Various Amounts of TFE Added	64
13	TFE Titration Curves of the MRE $_{203\text{nm}}$ and MRE $_{222\text{nm}}$ Values for Thymosin α_1	67
14	Isodichroic Region in the CD Spectra of Thymosin α_1 at Various Amounts of TFE Added	68
15	HPLC Peptide Mapping of the α -chymotryptic Digest of Thymosin α_1	70
16	Phase-Sensitive DQF-COSY Spectrum of Thymosin α_1	73
17	Homonuclear TOCSY Spectrum of Thymosin α_1	74

18	Phase-Sensitive NOESY Spectrum of Thymosin α_1	75
19	High-Field Region of the DQF-COSY Spectrum of Thymosin α_1	76
20	Assignment of the Low-Field Resonances of Isoleucine 11 and Leucine 16	77
21	Sequence-Specific Assignment of the Valanyl Residues of Thymosin α_1	79
22	Assignment of the Side Chain Resonances of the Valanyl Residues of Thymosin α_1	80
23	Amide Region of the NOESY Spectrum of Thymosin α_1	81
24	Sequence-Specific Assignment of the Alanyl Residues of Thymosin α_1	82
25	Assignment of the Side Chain Resonances of the Glutamyl and Seryl Residues of Thymosin α_1	84
26	Sequence-Specific Assignment of Residues 11 to 14 of Thymosin α_1	85
27	Sequence-Specific Assignment of Aspartic Acid of Thymosin α_1	86
28	Fingerprint Region of the DQF-COSY Spectrum of Thymosin α_1	89
29	Medium-Range NOE Connectivities in the Amide Region of the NOESY Spectrum of Thymosin α_1	91
30	Summary of the Observed NOE Connectivities	92
31	Plot of the Number of NOE Distance Restraints for Each Amino Acid in Thymosin α_1	95
32	Stereoview of the Final Structures I	97
33	Stereoview of the Final Structures II	98
34	Stereoview of the Turn Region of Thymosin α_1	100

35	Analysis of the Dihedral Angles of Thymosin α_1	102
36	Helical Wheel of Thymosin α_1	104
37	Electrostatic Model of the Interaction of skMLCK by Thymosin α_1	106
38	Stereoview of the Electrostatic Interaction Between skMLCK and Thymosin α_1	107
39	Hydrophobic Model of the Interaction of skMLCK by Thymosin α_1	110
40	Stereoview of the Hydrophobic Interaction Between skMLCK and Thymosin α_1	111
41	The Primary Structure of Thymosin β_4	112
42	Helical Wheel of Thymosin $\beta_4(1-39)$	114
43	Hydropathic Plots of the Residues of Calmodulin	116
44	Hydropathic Plot for the Residues of Thymosin α_1	117
45	Hydropathic Plot for the Residues of Thymosin $\beta_4(1-39)$	118
46	Amino Acid Homologies Within the Basic Domains of Basic-Helix-Loop-Helix Proteins	139
47	The Primary Structure of Bovine Pancreatic RNase A	163
48	Transphosphorylation Mechanism of RNase A	166
49	Hydrolytic Mechanism of RNase A	167
50	The Three-Dimensional Structure of RNase A	169
51	The Observed Positions of His119 of RNase A	172
52	The Structure of Uridine Vanadate	176
53	pH* Titration of RNase A	189
54	pH* Titration Curves of the Histidyl Resonances of RNase A	190

55	3'-CMP Titration of RNase A	194
56	Chemical Shift Dependence of the Histidine Resonances of RNase A in the Presence of 3'-CMP	195
57	pH* Titration of the 3'-CMP/RNase A Complex	198
58	pH* Titration of the Histidine Resonances in the 3'-CMP/RNase A Complex	200
59	⁵¹ V-NMR of Ammonium Metavanadate	203
60	⁵¹ V-NMR of Uridine Vanadate	204
61	Uridine Vanadate Titration of RNase A	206
62	pH* Titration of the U-V/RNase A Complex	209
63	pH Titration Curve of His12 in the U-V/RNase A Complex	212
64	pH Titration Curve of His119 in the U-V/RNase A Complex	213
65	pH Titration Curve of His105 in the U-V/RNase A Complex	214
66	NOESY Spectrum of the Aromatic Region of the U-V/RNase A Complex	216
67	NOE Cross Peak Between His119P and Val118 in the U-V/RNase A Complex	218
68	Distances Within the Active Site of the X-ray Crystallographic Structure of the U-V/RNase A Complex	219
69	Distances Within the Active Site of the U-V/RNase A Complex with His119 in the B Position	221
70	Contour Plot of the Energy of RNase A Versus the χ_1 and χ_2 Angles of His119	222
71	Contour Plot of the Energy of the U-V/RNase A Complex Versus the χ_1 and χ_2 Angles of His119	224

LIST OF ABBREVIATIONS

Ala	alanine
Arg	arginine
Asp	aspartic acid
Asn	asparagine
Ca ²⁺	calcium ion
CaM	calmodulin
CD	circular dichroism
3'-CMP	3'-cytidine monophosphate
COSY	J-correlated spectroscopy
Cys	cysteine
Da	daltons
D ₂ O	deuterium oxide
DCl	deuterium chloride
DNA	deoxyribonucleic acid
DQF-COSY	double-quantum-filtered correlated spectroscopy
DSS	sodium 2,2-dimethyl-2-silapentane-5-sulfonate
ft	frequency of occurrence
¹ H-NMR	proton nuclear magnetic resonance
Gln	glutamine
Glu	glutamic acid

Gly	glycine
H-bond	hydrogen bond
HBV	hepatitis B virus
His	histidine
His 12P	histidine 12 of RNase A in the protonated state
His 12U	histidine 12 of RNase A in the unprotonated state
His 119P	histidine 119 of RNase A in the protonated state
His 119U	histidine 119 of RNase A in the unprotonated state
His 119A	histidine 119 of RNase A in the major position
His 119B	histidine 119 of RNase A in the minor position
HPLC	high performance liquid chromatography
ID	inner diameter
IFN	interferon
Ile	isoleucine
kDa	kilodalton
Leu	leucine
Lys	lysine
M	molar

Met	methionine
MLCK	myosin light chain kinase
mM	millimolar
MQF-COSY	multiple-quantum-filtered correlated spectroscopy
ms	millisecond
n	Hill coefficient
N	normal
NaOD	deuterated sodium hydroxide
NH ₄ VO ₃	ammonium metavanadate
nm	nanometer
NMR	nuclear magnetic resonance
NOESY	nuclear Overhauser enhancement spectroscopy
P _α	helical potential
P _β	β-strand potential
P _c	random coil potential
pH*	pH uncorrected for deuterium isotope effect
Phe	phenylalanine
PITC	phenylisothiocyanate
ppm	parts per million
Pro	proline
pt	product of the frequency of occurrence values
PTC	phenylthiocarbonyl

RELAY	relayed coherence transfer spectroscopy
RNA	ribonucleic acid
RNase A	ribonuclease A
SECSY	spin-echo-correlated spectroscopy
Ser	serine
sk	skeletal muscle
sm	smooth muscle
TFE	2,2,2-trifluoroethanol
TFE-d ₃	deuterated 2,2,2-trifluoroethanol
Thr	threonine
TOCSY	total correlated spectroscopy
Trp	tryptophan
Tyr	tyrosine
UV	ultraviolet
U-V	uridine vanadate
Val	valine
⁵¹ V-NMR	vanadium-51 nuclear magnetic resonance
Å	angstrom
δ _A	chemical shift of protonated species
δ _B	chemical shift of deprotonated species
μM	micromolar

PART A

**Two-dimensional Nuclear Magnetic Resonance
Studies of Thymosin α_1**

CHAPTER ONE

INTRODUCTION

1.1) Two-Dimensional Nuclear Magnetic Resonance

Recent advances in nuclear magnetic resonance (NMR) methodology and instrumentation have made it possible to determine the three-dimensional structures of small proteins in solution. The most important technique developed for the structural study of proteins was the introduction of two-dimensional NMR (Jeener, 1971). Two-dimensional NMR is now in widespread use, since the instrumental and computational requirements have been developed to utilize this type of experiment. In a two-dimensional NMR spectrum, the severely overlapped one-dimensional NMR spectrum of a protein becomes spread into two orthogonal frequency dimensions (Wüthrich, 1986). The result is a spectrum with much greater resolution, which is a necessity when attempting to assign overlapping resonances in a protein spectrum. The major instrumental improvement has been the development of spectrometers utilizing high-field strength (i.e. 500-600 MHz), which also leads to an improvement in resolution. The increase in field strength along with improvements in radio frequency technology have led to a large increase in NMR sensitivity (Williamson and Waltho, 1992). An increase in sensitivity allows for the study of proteins in solutions at millimolar concentrations which can be extremely important when dealing with proteins that are difficult to obtain in large quantities or may have low solubility in aqueous solutions.

Although technical advances have been the primary reason for the success of

protein studies by NMR, there are other special features of proteins which make them especially suitable for structure determination by NMR (Williamson and Waltho, 1992):

1) Since the interiors of proteins are densely packed, the relative positions of atoms in the centre of proteins are largely fixed due to steric constraints.

2) The globular nature of proteins allows for many observable short internuclear distances using nuclear Overhauser effects (NOE) measurements inside proteins.

3) Contacts between residues far apart in the primary sequence act as powerful distance constraints in determining the overall three-dimensional shape of a protein.

The information that may be gained from NMR measurements is largely determined by the extent to which the resonance lines within the spectrum can be assigned (Wüthrich, 1986). Prior to 1978, the assignments of the individual resonances in proteins were extremely difficult to obtain. Most of the assignment work was based on homologies with other proteins, selective chemical modification, isotopic labeling and the use of shift or broadening reagents together with references to crystal structures (Wagner, 1990). In recent years, useful experiments have been designed that allow the complete sequence-specific resonance assignment of all the residues of a polypeptide. Sequential assignments make use of the fact that in small proteins sequences larger than four or five amino acid residues are rarely repeated, therefore unique oligopeptide segments are usually observed in the primary structures of proteins. In a sequential assignment procedure, connectivities between the ^1H spin systems of sequentially

neighbouring monomeric units are established either by ^1H - ^1H NOE measurements or by heteronuclear scalar couplings (Wagner, 1990). The resulting short segments of neighbouring ^1H spin systems are then matched against corresponding sequences in the protein to obtain the sequence-specific assignments.

As alluded to above, the first step in the determination of the three-dimensional structure of a protein by NMR is to assign all of the resonances to particular amino acids within the protein. The resonances of each amino acid residue can be identified through experiments correlating the proton resonances via spin-spin coupling (Basus, 1989). Amino acid residues can be identified as individual spin-coupling networks (or commonly referred to as spin systems), since no coupling is observed between protons across peptide bonds. The two-dimensional NMR experiments that are most often performed for this purpose include spin-echo-correlated spectroscopy (SECSY) (Nagayama and Wüthrich, 1981), correlated spectroscopy (COSY) (Nagayama *et al.*, 1980; Bax and Freeman, 1981), double-quantum-filtered (DQF) -COSY (Piantini *et al.*, 1982), multiple-quantum-filtered (MQF) -COSY (Müller *et al.*, 1986; Rance and Wright, 1986), double relayed coherence transfer (RELAY) spectra (King and Wright, 1983) and total correlated spectroscopy (TOCSY) (Braunschweiler and Ernst, 1983). Often only COSY and TOCSY experiments are required to identify the individual spin systems within a peptide (Wagner, 1990).

The spin systems of some residue types are unique (glycine (Gly), alanine (Ala), threonine (Thr), isoleucine (Ile), valine (Val), leucine (Leu)); others must be assigned to groups of residues (tyrosine (Tyr), phenylalanine (Phe), histidine (His), tryptophan (Trp), cysteine (Cys), aspartic acid (Asp), asparagine (Asn), serine

(Ser)), 5-spin systems (glutamic acid (Glu), glutamine (Gln), methionine (Met)) and long spin systems (arginine (Arg), lysine (Lys), proline (Pro)) (Wagner, 1990). The connectivity diagrams for the spin systems of the protons in the common amino acids in a two-dimensional COSY experiment are shown in Figure 1.

The initial spin system assignment of the amino acids in a protein are usually done in D₂O solution (Nagayama *et al.*, 1980). Dissolving the protein in D₂O results in the exchange of all labile protons with deuterons and a simplification of the spectrum. Acquiring spectra in D₂O also does not require as severe a saturation of the solvent resonance which can result in the loss of some protein resonances due to overlap with the solvent resonance or saturation transfer (Basus, 1989). In order to exchange all of the labile protons, heating the sample in D₂O or a variation of the pH of the sample may be required. Once the assignments are completed in D₂O, the assignments are then done in H₂O so that the frequencies of the labile amide protons can be determined. The most important labile protons are the backbone amide protons whose assignment are necessary in making sequence-specific assignments of the residues within the protein in a homonuclear NMR study (Wüthrich, 1986).

As previously mentioned, COSY and TOCSY experiments allow the identification of the number and different type of spin systems within a protein, but do not allow the determination of the exact residue that gives rise to a particular spin system (Wüthrich, 1986). For example, it is possible to determine that there are four leucine (Leu) residues within a protein from observed spin system patterns, but it is not possible to assign any of the spin systems to a specific Leu residue based on the results of the COSY and TOCSY experiments. Sequence-specific connectivities between the spin

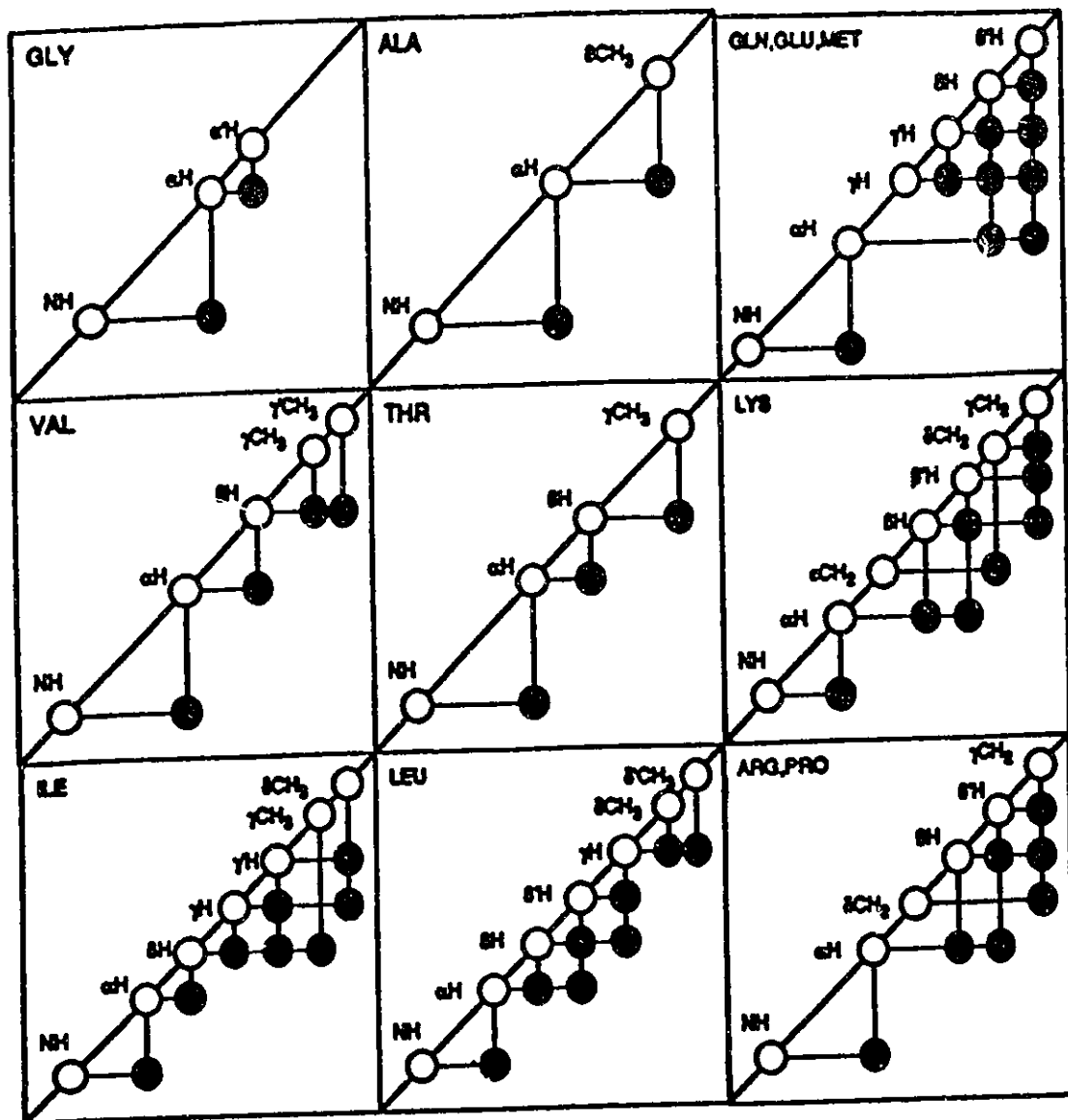


Figure 1. COSY Spin Systems of the Twenty Common Amino Acids. Spin systems are used to identify resonances belonging to a particular amino acid residue type in a two-dimensional COSY spectrum of a protein. All of the connectivities are between protons that are separated by three or fewer bonds, therefore no connectivities are seen between neighbouring residues. (Adapted from Wüthrich, 1986).

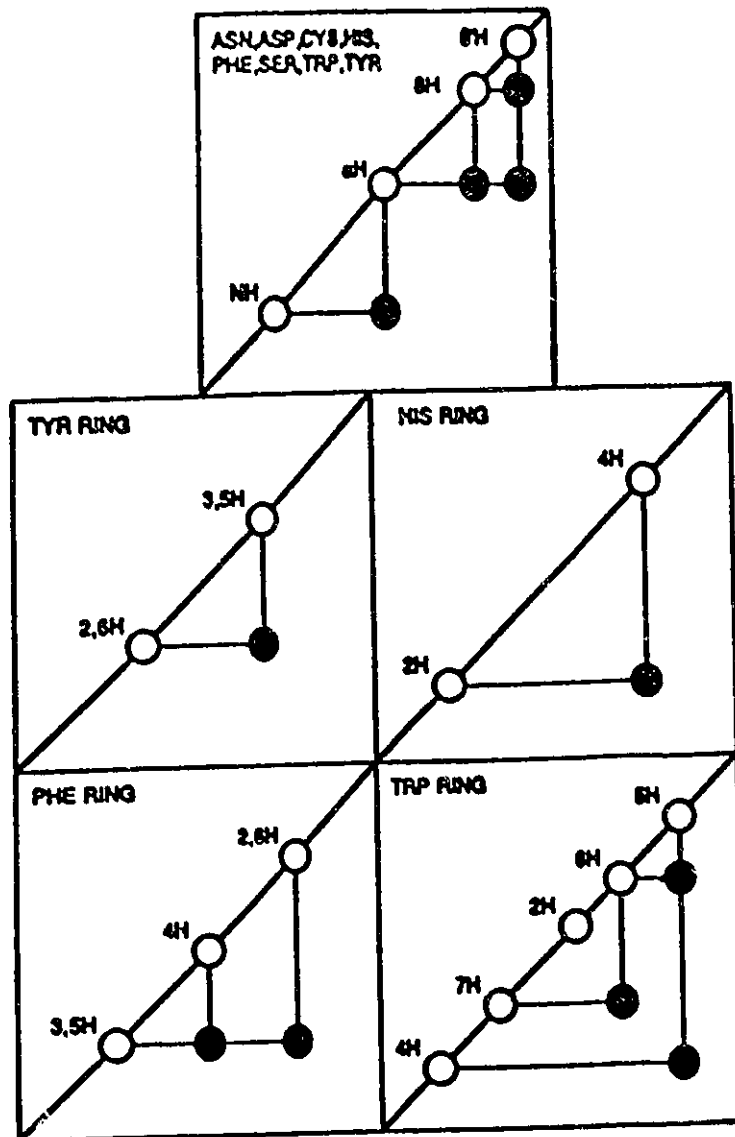


Figure 1 (continued). COSY Spin Systems of the Twenty Common Amino Acids.

systems of the amino acid residues are identified in a nuclear Overhauser enhancement spectroscopy (NOESY) spectrum (Wüthrich, 1986). The NOE is by far the most useful parameter for determining the structure of proteins. The NOE is a phenomenon arising from the cross-relaxation between two nuclei due to their spatial proximity. It is observed in a one-dimensional spectrum as a change in intensity of one resonance signal as a result of the saturation of another (Wagner, 1990). In the two-dimensional NOESY experiment the NOE is seen as a cross peak. The short sequential distances that are important for sequence-specific assignments are the distance between the C α proton of one residue and the amide proton of the next residue ($d_{\alpha N}(i,i+1)$), the distance between the β proton of one residue and the amide proton of the next residue ($d_{\beta N}(i,i+1)$) and the distance between sequential amide protons ($d_{NN}(i,i+1)$) (Wüthrich, 1986). Once a sequential connectivity between two amino acids is established, it may then be possible to correlate this result with a sequence in the polypeptide primary structure and make a sequence-specific assignment. Some of the sequential ^1H - ^1H distances observed in a NOESY experiment that are useful in the sequence-specific assignment of residues in a protein are shown in Figure 2.

The observation of NOE connectivities between residues separated by one or more residues within the primary structure of a polypeptide also makes it possible to determine regions of secondary structure, since it is well documented that regular secondary structures have typical NOE patterns (Wagner *et al.*, 1981). The most important protons for determining the secondary structural characteristics of proteins are the backbone α carbon and backbone amide protons. Since the amide protons are labile, it is necessary to acquire NOESY experiments in H₂O in order to gain the necessary structural data. Both α - and 3_{10} -helices are characterized by strong

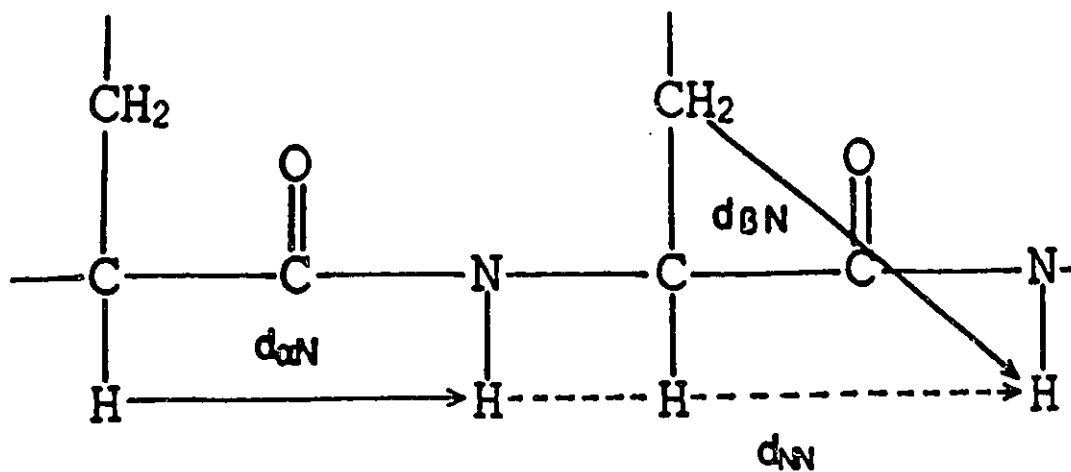


Figure 2. Common Nuclear Overhauser Enhancement (NOE) Connectivities Between Neighbouring Residues. The above connectivities are all (i,i+1) connectivities between neighbouring residues. These connectivities allow for the sequence-specific assignments of residues within the protein. (Adapted from Wüthrich, 1986).

$d_{NN(i,i+1)}$ NOE cross peaks which are not usually observed in β -sheets. The $d_{\alpha N(i,i+2)}$, $d_{\alpha N(i,i+3)}$ and $d_{NN(i,i+2)}$ NOE cross peaks are also often observed in helical regions. β -strands are identified through intense $d_{\alpha N(i,i+1)}$ cross peaks observed in the NOE spectrum (Wagner, 1990). Some of the more useful sequential and medium range ^1H - ^1H distances observed in helices and strands, based on x-ray diffraction structures of proteins, are listed in Table 1.

Tight turns are more difficult to identify than helices and β -sheets, except when they are hairpin turns at the bend of an antiparallel β -sheet (Wagner, 1990). The parameter most distinctive of tight turns, the H-bond between the carbonyl oxygen of residue 1 and the amide proton of residue 4, cannot be observed in a ^1H - ^1H NOESY spectrum. An isolated $d_{\alpha N(i,i+2)}$ or $d_{NN(i,i+2)}$ connectivity may be indicative of a tight turn with i being residue number 2 of the turn (Wagner, 1990).

One problem with the measurement of NOE cross peaks in protein spectra is that the buildup rate of the NOE can become non-linear when there are other protons nearby. This is a result of spin diffusion (Wüthrich, 1986). Spin diffusion is a phenomenon by which the intensity of the NOE cross peak is affected by two or several cross relaxation steps between nuclei of like spins (Wüthrich, 1986). For example in a three spin system of protons A, B, and C, spin A and spin C may cross relax via a pathway in which spin A first cross relaxes with spin B followed by spin B to spin C. In this case the NOE observed between A and C is no longer an accurate reflection of the distance between A and C (Wüthrich, 1986). In order to remain in the linear region, it is necessary to use very short mixing times (Wüthrich, 1986). Unfortunately short mixing times can lead to problems with poor signal-to-noise and artifacts. A second serious problem with NOE

Table 1

Observable ^1H - ^1H Distances for Identifying
Secondary Structural Elements by Nuclear
Overhauser Enhancement Spectroscopy

Distance*	<u>Secondary Structural Element</u>			
	α -helix	3_{10} -helix	β -antiparallel	β -parallel
$d_{\text{ON}}(i, i+1)$	3.5	3.4	2.2	2.2
$d_{\text{ON}}(i, i+2)$	4.4	3.8		
$d_{\text{ON}}(i, i+3)$	3.4	3.3		
$d_{\text{ON}}(i, i+4)$	4.2	>4.5		
$d_{\text{OS}}(i, i+3)$	2.5-4.4	3.1-5.1		
$d_{\text{NN}}(i, i+1)$	2.8	2.6	4.3	4.2
$d_{\text{NN}}(i, i+2)$	4.2	4.1		
$d_{\text{NN}}(i, i+3)$	4.8	5.2		

*all distances are reported in Å

(Table adapted from Wagner, 1990)

measurements is motion (Williamson and Waltho, 1992). Motion is much more of a problem when working with peptides than with large globular proteins. If intramolecular rearrangements are occurring at a fast rate compared to the overall tumbling rate, the NOE is averaged as r^{-6} , where r is the distance between the two observed nuclei (Williamson and Waltho, 1992). This leads to a strong biasing of the observed NOE, such that minor conformations can give rise to an intense NOE cross peak if the internuclear distances in the minor conformations are very short (Williamson and Waltho, 1992). Therefore the time-averaged conformation as determined by the measurement of the NOE cross peak intensity sometimes will poorly reflect the conformational ensemble populated by the peptide (Williamson and Waltho, 1992). Since the intensity of the NOE cross peak observed between two nuclei is a weighted average of the distance between the two nuclei, the NOE intensity is can be severely biased if the two nuclei are separated by a short distance for any significant time period (Williamson and Waltho, 1992). In reality the two nuclei may spend most of there time separated by a large distance in which would give rise to a weak NOE cross peak.

The structures of peptides are generally not as easily obtained by NMR as they are for proteins. Before 1980 it was thought that small peptides did not fold into stable conformations (Williamson and Waltho, 1992). There are far fewer packing restraints, there is a lower density of NOE cross peaks, there are often no contacts between residues far apart in sequence, and the ratio of surface area to interior is much greater (Williamson and Waltho, 1992). It is common to find that a peptide will have a certain region which is less flexible while the remainder of the peptide is unstructured or in a random coil configuration. An unstructured peptide has a range of conformational states available to it that are of similar free energy, and have little or no barrier to

interconversion between them (Williamson and Waltho, 1992). NOE measurements of random coil peptides are typified by large sequential $d_{\alpha N}(i,i+1)$ connectivities and small or non-existent $d_{NN}(i,i+1)$ connectivities, as seen in an α -helix (Wüthrich, 1986).

Once the complete assignment of the residues and the determination of the secondary structures within the peptide have been accomplished, the accumulated data sets are used as input in order to determine the three-dimensional structure of the peptide (Wagner, 1990). The data set is comprised of a list of observed NOE connectivities between atoms within the polypeptide along with a value of the approximate distance between them. The distance is based on the measured volume of the cross peak between the two atoms, with the volume of the cross peak proportional to the r^{-6} , where r is the distance between the two observed nuclei. Two atoms within close proximity of one another will give rise to a NOE cross peak with a large volume and vice versa. Since the data defines distances between two atoms based on an observed NOE cross peak, the parameters in the data set are commonly referred to as NOE distance restraints. Along with NOE distance restraints, generic distance restraints defining expected hydrogen bonds are often included in the data set for regions where NOE connectivity patterns suggest the presence of common secondary structures (Wagner, 1990). The locations of hydrogen bonds within the structure are most often based on the measurement of the rate of exchange of the amide proton with a deuterium atom by dissolving the protein in D_2O (Wüthrich, 1986). Hydrogen bond location can also be based on the observation of NOE connectivities that suggest a region of known stable secondary structure in which the expected hydrogen bonds are used as distance restraints (Wagner, 1990). In the past the locations of hydrogen bonds have been successfully determined by the measurement of

the amide proton exchange rate and the observation of distance NOE patterns of known secondary structures (Wüthrich, 1986).

The two main methods for determining the final peptide structure are distance geometry and molecular dynamics (Williamson and Waltho, 1992). Distance geometry calculations determine a consistent matrix of distance boundaries between all atoms, starting from a set of observed NOE and covalent distances that are put into the program. The distance constraints are then converted into a set of cartesian coordinates. This type of algorithm does not start with any initial structure and is thus considered to be the least biased computational method. A second type of distance geometry calculation method starts from an initial structure, which may be as simple as an extended chain. This algorithm, which also utilizes an input of observed NOE and covalent distance restraints, applies intra-residue constraints to the chain one residue at a time. The algorithm then recalculates the structure after adding (i,i+1) constraints along the peptide working on each dipeptide in sequence. The program then adds (i,i+2) constraints and continues adding constraints until all of the observed distances are utilized (Williamson and Waltho, 1992). The major problem with distance geometry calculations is that any of the calculated structures may represent a local minimum structure. Therefore more than one structure is calculated that represents the observed NOE constraints, and often several of the calculated structures are rejected because there is a poor fit with the experimental data. The final structure calculated using NMR data is not one unique structure but an ensemble of structures which all satisfy the NMR data and are closely related.

1.2) Circular Dichroism

Considerable information about the structure of proteins in solution can be obtained from the measurement of their optical activity. One of the more useful techniques in the determination of the secondary structure of a protein is circular dichroism (CD). CD is the measurement of a molecule's unequal absorption of right- and left-handed circularly polarized light as a function of the wavelength (Adler *et al.*, 1973). Even though all of the amino acids, except for glycine, contain a least one asymmetric carbon atom (the L or D configuration), most amino acids display only small CD bands (Toniolo, 1970). It is the conformation of the protein, with its asymmetric and periodic arrangement of peptide units that gives rise to their characteristic CD spectra (Adler *et al.*, 1973). The CD spectra observed for the α -helix, β -sheet and random coil forms of the model peptide poly-L-lysine are displayed in Figure 3 (Greenfield and Fasman, 1969).

Techniques such as X-ray diffraction, neutron diffraction and high resolution NMR spectroscopy have proven very successful in the determination of the three-dimensional structure of proteins. Neutron diffraction and NMR are able to provide information about hydrogen atoms within the protein (Adler *et al.*, 1973). Such specific structural determinations are beyond the capacity of CD. However CD has the advantage that the approximate percentages of the conformations present in a protein can be determined much faster than with the other techniques. A second advantage of CD over the other techniques is that a low concentration of protein is required to acquire a CD spectrum so that most often a sample of less than 0.1 mg is sufficient (Adler *et al.*, 1973). With the speed and low material requirement involved in acquiring a CD spectrum of a protein, it is often a useful first step in the determination of the three-dimensional structure of a

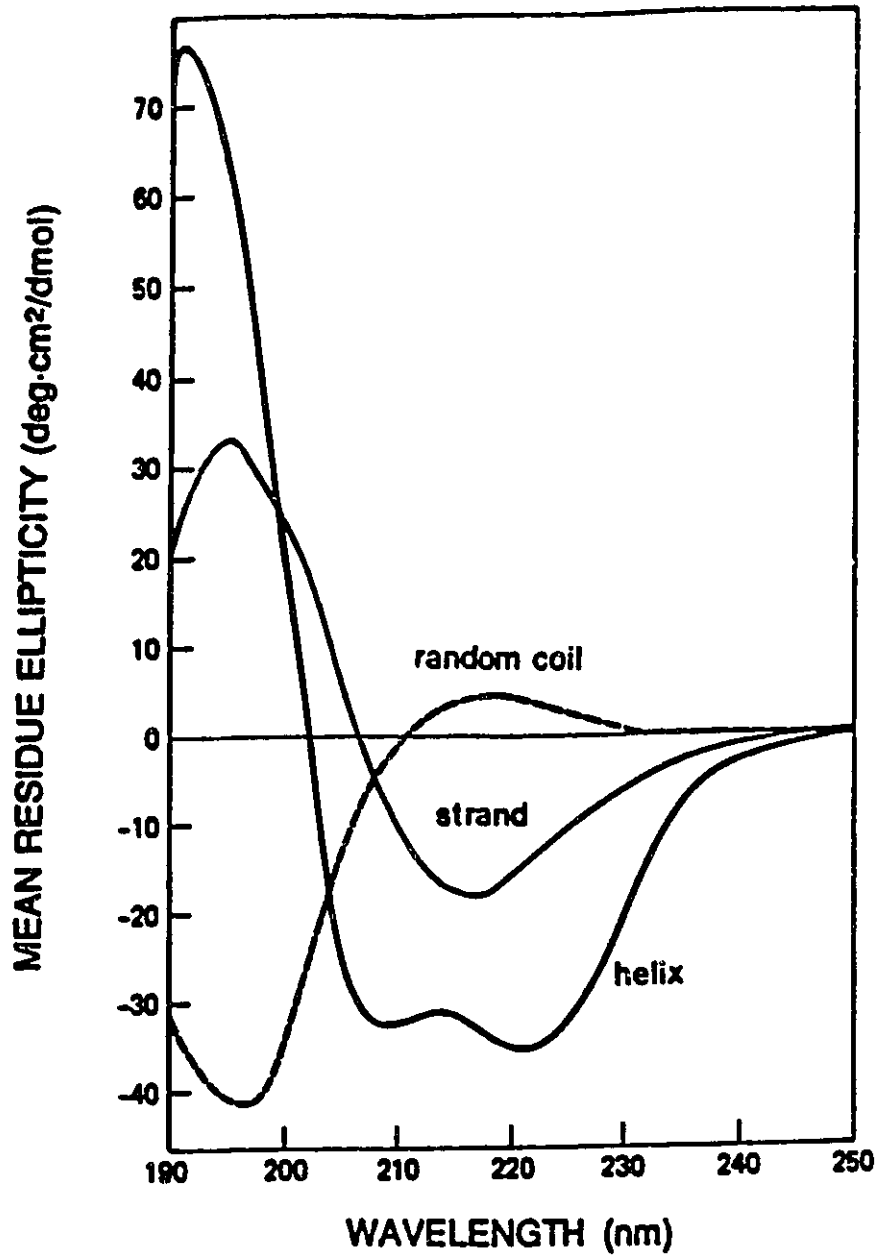


Figure 3. Circular Dichroism Spectra of an α -helix, β -strand, and Random Coil. The circular dichroism spectra show poly-L-lysine in the α -helical (helix), β -strand (strand), and random coil (random coil) conformations. (Reproduced with permission from N. J. Greenfield *et al.*, (1969) *Biochemistry* 6:1630-1637).

protein. Its use is even more essential when working with peptides in which the presence of stable secondary structure may not be certain, and steps must be taken in order to stabilize the secondary structure. Attempting to establish conditions in which the peptide's secondary structure is most stable by NMR may require days of acquisition time and months of analysis, whereas CD can make the same type of determination in hours.

CD is a very useful tool in studying any type of reaction that results in a change of optical activity. Such a reaction may involve the binding of substrates, inhibitors or coenzymes to an enzyme. CD is also excellent for measuring protein denaturation and helix-coil transitions in polypeptides (Adler *et al.*, 1973).

CD data is generally recorded as observed ellipticity (units of millidegrees) and is reported as the mean residue ellipticity (MRE). The MRE for proteins and peptides is defined as:

$$[\text{MRE}]_{\lambda} = \frac{\theta_{\text{obs}} \times \text{MRW}}{10(d)(c)}$$

where λ = wavelength; θ_{obs} = observed ellipticity in degrees; MRW = mean residue weight; d = pathlength in centimeters; c = concentration in grams per milliliter. The units of MRE are $\text{deg}\cdot\text{cm}^2/\text{dmol}$ (Adler *et al.*, 1973).

In order to determine the relative percentages of the conformations present in a protein molecule, a calculated CD curve is matched to the experimentally obtained spectrum. The procedure of matching the observed CD spectra to a calculated spectra is

known as multicomponent analysis (Freifelder, 1982). The CD curve is simulated from equations of the form

$$S = a[\alpha] + b[\beta] + c[R]$$

In the above equation, α , β and R represent the secondary structural types helix, β -strand and random coil respectively. The values of a, b and c are then varied until the simulated CD spectrum most closely matches the experimental CD spectrum.

In the study of peptides, a useful measurement is the MRE at 222 nm (MRE_{222nm}). The CD band at 222nm is assigned to the $n \rightarrow \pi^*$ amide transition for a helical polymer (Adler *et al.*, 1973). By measuring the MRE_{222nm} and comparing it to the MRE_{222nm} for a complete random coil and the MRE_{222nm} for a complete α -helix, an estimation of the helical content of a peptide can be made (Khan *et al.*, 1990).

1.3) Chou-Fasman Analysis

The primary structure of a peptide can sometimes be used to accurately predict its secondary structure by using a set of rules developed by Chou and Fasman (Chou and Fasman, 1974a,b). The basis of this analytical method is that the conformation of a protein is predominantly determined by its amino acid sequence (Anfinsen, 1973). Chou and Fasman analyzed the 20 amino acids in 15 proteins (containing a total of 2473 residues) whose X-ray crystallographic structures had been determined, and compared the frequency of the amino acids in various conformational states (Chou and Fasman, 1974a). The amino acid residues in helix, β -sheet and coil regions were tabulated. All

regions designated as helical, whether they were in a different helical type (i.e. α_1 , α_{II} , 3_{10} , distorted helix), were grouped as helical residues. The conformational parameters for the amino acids were determined by tabulating the frequency of all amino acids in the helical, β -sheet and coil regions of the 15 proteins and dividing each by their total occurrence (Chou and Fasman, 1974a).

Analysis of the helix-coil boundary residues and central helix residues of proteins (Chou and Fasman, 1974a) showed that residues with the highest helical potential, P_α , reside mostly at the helix center, while strong helix breakers (low P_α values) were found just beyond the helix ends. They proposed that helix nucleation could start at the center of a helix region and propagate in both directions, until a cluster of strong helix breakers terminated helix growth. In addition, the frequency of negatively charged residues at the amino terminus of the helix and positively charged residues at the carboxyl terminus of the helix (Cook, 1967; Ptitsyn, 1969; Chou and Fasman, 1974b) were used in locating helix region boundaries. These facts serve as useful starting points in predicting helical regions within proteins.

Before attempting to calculate the average helical potential P_α ($\langle P_\alpha \rangle$) and average β -strand potential ($\langle P_\beta \rangle$) values for regions within a protein, it is best to assign all of the residues as formers, breakers or indifferent to helix and β regions. By doing this it is easier to visually pick out regions having a high affinity for a certain type of conformation. The helix and β -sheet potentials are subdivided into the following classifications: H_α (strong helix former), h_α (helix former), l_α (weak helix former), i_α (helix indifferent), b_α (helix breaker), B_α (strong helix breaker); H_β (strong β former), h_β (β former), l_β (weak β former), i_β (β indifferent), b_β (β breaker), and

B_{β} (strong β breaker). The symbols H and h can be thought of as strong and moderate hydrogen bonding (Chou and Fasman, 1974b), respectively, with subscripts α and β denoting helical and β -strand conformation, respectively. In predicting the secondary structural elements present in a protein, the key is finding groups of residues that all have a high propensity for existing in a certain type of conformation (Chou and Fasman, 1974b). One disadvantage of the Chou-Fasman predictive algorithm is that the influence of the environment around is not considered in predicting the secondary structure possessed by a sequence of amino acids. Therefore, an isolated peptide and the identical sequence incorporated into a large protein would be predicted to have the same secondary structure, but this may be incorrect owing to influence of other nearby secondary structural elements felt by the peptide sequence in the protein that are not felt by the isolated peptide.

1.4) Primary Structure and Function of Thymosin α_1

Over the past 150 years researchers have been attempting to determine the role of thymic functions, yet the importance of the thymus gland and the function it plays in the immune system was not recognized until the early 1960's (Goldstein and White, 1970). The thymus gland has been shown to be essential in the development of the lymphoid system by the lack of postnatal lymphoid tissue growth and development in mice and rabbits that had undergone neonatal thymectomies (Miller, 1961). A principle role for the thymus gland in the maturation, proliferation and immunological competence of the lymphocyte (T-cell) has also been shown (Aisenberg and Wilkes, 1965).

The mechanism by which the thymus gland exerts control over T-cell development is

not definitively known. The process is believed to be controlled by hormonal stimulation (Goldstein and White, 1970). Much of the early research was directed towards isolating and identifying biologically active hormones that are able to restore immunological capabilities in thymectomized animals or enhance immunological ability within normal animals (Goldstein *et al.*, 1972; Goldstein, 1974; Hooper *et al.*, 1975).

A partially purified thymic fragment, thymosin Fraction 5, has been shown to correct some of the deficiencies resulting from a lack of thymic function in a number of animal studies (Zisblatt *et al.*, 1970; Bach *et al.*, 1971; Dauphinee *et al.*, 1974; Scheinberg *et al.*, 1976), as well as in humans with immunodeficiency diseases (Wara *et al.*, 1975; Goldstein *et al.*, 1976; Wara and Ammann, 1976) and in cancer patients suffering from immunosuppression (Goldstein *et al.*, 1976; Schafer *et al.*, 1976). Thymosin Fraction 5 is composed of a group of polypeptides with molecular weights ranging from 1000 to 15 000 Da (Low *et al.*, 1979). One of these polypeptides called thymosin α_1 has been purified and sequenced (Low and Goldstein, 1979; Low *et al.*, 1979). Thymosin α_1 is a potent immunopotentiating agent, being from 10 to 1000 times as active as the parent thymosin Fraction 5 preparation in a number of bioassays designed to measure the maturation and function of T-cells (Low and Goldstein, 1979). A chemically synthesized molecule of thymosin α_1 has been shown to be as active as the native molecule in several bioassay systems (Low and Goldstein, 1979).

Thymosin α_1 is composed of twenty eight amino acid residues giving it a molecular weight of 3108 Da (Low and Goldstein, 1979). The peptide is highly acidic, with an isoelectric point of 4.2 (Low and Goldstein, 1979). The primary structure of the peptide is known (Figure 4). Thymosin α_1 is composed of nine acidic residues (six Glu

and three Asp) and four basic residues (four Lys). Of the remaining residues, eight are hydrophobic (three Ala, three Val, one Leu and one Ile) and the remaining six are hydrophilic (three Ser and three Thr). Of the nine acidic residues in thymosin α_1 , six are located in the carboxyl terminal half of the peptide as are the five basic amino acids. The peptide contains no aromatic residues (His, Phe, Trp and Tyr) and is also devoid of Arg, Cys, Gln, Gly, Met and Pro.

Thymosin α_1 has been found in every known vertebrate tissue (Franco *et al.*, 1992). It is still debated as to whether thymosin α_1 is a native peptide (Franco *et al.*, 1992) or is only an artifact produced by proteolysis of its proposed precursor, prothymosin α (Haritos *et al.*, 1984), which contains the 28 residues of thymosin α_1 at its amino terminus. Purification studies under conditions preventing proteolytic activity have shown that the quantity of thymosin α_1 detected in specific tissues is greater than the quantity of prothymosin α detected, precluding the suggestion that thymosin α_1 is a proteolytic artifact of prothymosin α (Franco *et al.*, 1992). Since an obvious connection between thymosin α_1 and prothymosin α exists, it necessitates briefly introducing prothymosin α in order to get a better understanding of the specific function of thymosin α_1 .

Until recently thymosin α_1 (Low *et al.*, 1979) and prothymosin α (Haritos *et al.*, 1985) had been attributed immunological functions involved in extracellular mechanisms. This hypothesis is unlikely since neither thymosin α_1 nor prothymosin α contain a signal peptide (Eschenfeldt and Berger, 1986; Goodall *et al.*, 1986). The widespread distribution of both of these peptides seems to point to a general cellular function rather than a specific role in the immune system (Franco *et al.*, 1992).

Prothymosin α contains the karyophilic signal Lys-Lys-Glu-Lys (residues 101-104) within its sequence, which suggests that it may have a nuclear function. Prothymosin α has most recently been attributed a role in cellular division (Sburlati *et al.*, 1993) as nonsense oligomers of prothymosin α have been shown to arrest cell division. Elevated levels of prothymosin α have been detected in tumour samples taken from breast tissue (Dominiguez *et al.*, 1993) and in human colorectal cancers (Mori *et al.*, 1993). Radioimmunoassays specific for the amino and carboxyl termini of prothymosin α in human thymus, spleen and liver show that the levels of this protein are much greater in the spleen during the first decade of life, and in particular during the first year (Tsitsiloni *et al.*, 1993).

The levels of prothymosin α mRNA and protein levels have been measured in HL-60 myeloid leukemia cells (Smith *et al.*, 1993). The results showed an increase in the levels of prothymosin α mRNA and protein during cell proliferation, but not during cell differentiation. The levels of prothymosin α were found to decline during cell differentiation. The increase and decrease in prothymosin α levels during proliferation and differentiation respectively, paralleled those of c-Myc mRNA under the same conditions (Smith *et al.*, 1993). The c-Myc gene has been established as a well documented proto-oncogene (Ramsay *et al.*, 1984). The results of the study suggested that there might be some type of connection between prothymosin α and c-Myc expression in cell differentiation and proliferation (Smith *et al.*, 1993).

The primary sequence of prothymosin α is quite striking and is worth examining (Figure 5), if there is some type of connection between its function and the function of thymosin α_1 (Sburlati *et al.*, 1993). Prothymosin α contains 109 amino acids of

1 Ac-Ser-Asp-Ala-Ala-Val-Asp-Thr-Ser-Ser
10 Glu-Ile-Thr-Thr-Lys-Asp-Leu-Lys-Glu-Lys
20 Lys-Glu-Val-Val-Glu-Glu-Ala-Glu-Asn-Gly
30 Arg-Asp-Ala-Pro-Ala-Asn-Gly-Asn-Ala-Asn
40 Glu-Glu-Asn-Gly-Glu-Gln-Glu-Ala-Asp-Asn
50 Glu-Val-Asp-Glu-Glu-Glu-Glu-Glu-Gly-Gly
60 Glu-Glu-Glu-Glu-Glu-Glu-Glu-Glu-Gly-Asp
70 Gly-Glu-Glu-Glu-Asp-Gly-Asp-Glu-Asp-Glu
80 Glu-Ala-Glu-Ser-Ala-Thr-Gly-Lys-Arg-Ala
90 Ala-Glu-Asp-Asp-Glu-Asp-Asp-Asp-Val-Asp
100 Thr-Lys-Lys-Gln-Lys-Thr-Asp-Glu-Asp-Asp

Figure 5. The Primary Structure of Prothymosin α . The protein contains 109 residues of which 53 are acidic (Glu or Asp). The first 28 residues correspond to the primary structure of thymosin α_1 . The sequence was taken from Sburlati *et al.*, 1993.

which 53 are acidic (Glu or Asp). As previously mentioned, the first 28 residues correspond to the residues present in thymosin α_1 . The large number of acidic residues within prothymosin α suggests some type of interaction with histones, which contain a high percentage of basic residues. The amount of prothymosin α in the nucleus is similar to that of histones (Sburlati *et al.*, 1993). Barcia *et al.* (1992) showed that prothymosin α as well as thymosin α_1 were phosphorylated by casein kinase-2 at a Ser and a Thr residue located within the amino terminus of the peptides. The pattern of phosphorylation of prothymosin α and thymosin α_1 were identical. Shortly after these results were published another group (Sburlati *et al.*, 1993) reported *in vivo* phosphorylation of prothymosin α at a single site, identified as Ser1 by electrospray ionization mass spectrometry. Since this residue is also acetylated, prothymosin α has an acetylserine phosphate as the amino terminal residue. This group found no evidence of a phosphothreonine residue in the protein and attributed the different findings to an artifactual phosphorylation occurring during the isolation of prothymosin α . Unfortunately little is known about the significance of the phosphorylation of either of these polypeptides (Sburlati *et al.*, 1993).

A preliminary clinical trial studying the safety and efficacy of thymosin Fraction 5 and thymosin α_1 against chronic hepatitis B infection is presently underway (Mutchnick *et al.*, 1991). Chronic hepatitis B is a common form of liver disease associated with an increased risk of cirrhosis and liver failure. Epidemiological studies have shown a clear connection between hepatitis B virus (HBV) and hepatocellular carcinoma (HCC) (Tiollais *et al.*, 1985). The inability of host cellular immune mechanisms to remove HBV infected hepatocytes is believed to be responsible for the development of chronic hepatitis B (Mutchnick *et al.*, 1991). Of all the anti-viral agents previously used to

treat chronic hepatitis B, interferon (IFN)- α has been shown to be the most effective (Perrillo *et al.*, 1990). Unfortunately IFN- α treatment leads to remission in less than 50% of patients and the associated side effects are often severe enough to cause stoppage of the treatment (Perrillo *et al.*, 1990).

The clinical trial utilizing thymosin Fraction 5 and thymosin α_1 as a therapy against chronic hepatitis B was performed using twelve patients who had exhibited evidence of active liver disease and were positive for serum HBV DNA (Mutchnick *et al.*, 1991). Four of the patients were given thymosin Fraction 5, three received thymosin α_1 and the remaining five patients received a placebo. All of the patients were given their assigned medication by subcutaneous injection twice weekly for six months. Two of the patients who received thymosin Fraction 5 experienced discomfort at the site of injection two weeks into the trial and were switched over to injections of thymosin α_1 . Since the known biological effects of thymosin Fraction 5 and thymosin α_1 are similar (Mutchnick *et al.*, 1991), the results of the patients who received either were combined.

By the conclusion of the study, a significant improvement in thymosin treated patients was observed. No change was observed in patients who had received the placebo. Six of the seven thymosin treated patients and one patient receiving placebo cleared HBV DNA from serum. After treatment, six of the seven thymosin treated patients showed no signs of any replicative forms of HBV DNA, while replicative forms of HBV DNA were found in four of the five placebo receiving group. No significant side effects were observed in patients receiving thymosin or placebo treatment. The improvements in patients who responded to thymosin treatment were sustained during the 26 month

follow-up period. The results of the pilot study suggest that thymosin Fraction 5 and thymosin α_1 are non-toxic in the doses given and they promote disease remission and cessation of HBV replication in patients with chronic viral infection (Mutchnick *et al.*, 1991).

Investigations have shown that a class of compounds referred to as C-modulins (Galoyan *et al.*, 1992) isolated from bovine hypothalamus, are high-affinity stimulators of the basal activity of calcium/calmodulin ($\text{Ca}^{2+}/\text{CaM}$)-dependent cyclic nucleotide phosphodiesterase (Galoyan *et al.*, 1992). It was also shown that other $\text{Ca}^{2+}/\text{CaM}$ -dependent enzymes including myosin light chain kinase (MLCK), phosphorylase kinase, and CaM-dependent protein kinase were also stimulated by C-modulins. One of the C-modulins that was found to be a high-affinity stimulator of MLCK was identified as the first 39 residues of thymosin β_4 . Thymosin β_4 is a 43 residue peptide that has been shown to be a major actin sequestering protein in platelets. Subsequent experiments showed that another fragment of thymosin β_4 (residues 16-38) and thymosin α_1 were also high-affinity stimulators of rabbit skeletal muscle (sk) MLCK (Galoyan *et al.*, 1992). All three of the thymosin peptides stimulated skMLCK in a Ca^{2+} -independent manner. These findings suggested that C-modulins comprise a system of universal Ca^{2+} -independent enzyme regulators (Galoyan *et al.*, 1992). The activation of skMLCK by thymosin α_1 was the first specific function attributed to the peptide.

1.5) Myosin Light Chain Kinase

1.5.a) Function

Myosin light chain kinase (MLCK) is a key enzyme in the regulation of smooth and skeletal muscle contraction (Hartshorne, 1987). Phosphorylation of Ser19 on each of the two 20 kDa light chains of myosin by MLCK is thought to be essential for the initiation of muscle contraction (Hartshorne, 1987). Since MLCK is a $\text{Ca}^{2+}/\text{CaM}$ -dependent enzyme, the process of muscle contraction is ultimately linked to intracellular Ca^{2+} levels.

1.5.b) Binding Region and Interaction with Calmodulin

In order to attempt to model how thymosin peptides stimulate skMLCK, it is important to examine the background information that is known about the binding of $\text{Ca}^{2+}/\text{CaM}$ to $\text{Ca}^{2+}/\text{CaM}$ -dependent enzymes. The binding regions between $\text{Ca}^{2+}/\text{CaM}$ and smooth muscle (sm) MLCK (Lukas *et al.*, 1986), skMLCK (Blumenthal *et al.*, 1985) and several other $\text{Ca}^{2+}/\text{CaM}$ -dependent enzymes are known (O'Neil and DeGrado, 1990).

Calmodulin is a 148 amino acid residue protein present in all eukaryotic cells, that serves as the primary receptor for intracellular Ca^{2+} (O'Neil and DeGrado, 1990). The $\text{Ca}^{2+}/\text{CaM}$ -binding domains within $\text{Ca}^{2+}/\text{CaM}$ -dependent enzymes show considerable sequence diversity, yet most are predicted to form positively charged amphipathic helices (O'Neil and DeGrado, 1990). The affinity of peptides for CaM

appears to correlate with their ability to form positively charged amphipathic helices (Giedroc *et al.*, 1983). A synthetically prepared peptide composed of only Leu, Lys and Trp residues (Trp-Lys-Lys-Leu-Leu-Lys-Leu-Leu-Lys-Lys-Leu-Leu-Lys-Leu) in an amphipathic helical conformation, was found to bind CaM with a dissociation constant (K_d) of about 0.4 nM. Another synthetic peptide in which all of the Lys residues had been changed to neutral Gln residues was shown to bind to CaM with a K_d of 10 nM. It was concluded that about 15% of the total binding energy was contributed by electrostatic interactions (O'Neil and DeGrado, 1990).

Lukas *et al.* (1986) showed that the CaM-binding region of chicken gizzard smMLCK was made up of an 18-20 residue segment comprising amino acid residues 494 to 513. This region contained a cluster of basic amino acids and formed an amphipathic α -helical structure (Lukas *et al.*, 1986). The Ca^{2+} /CaM-binding region of smMLCK is shown in Figure 6. A synthetic peptide representing the binding domain within smMLCK, called RS20, inhibited the Ca^{2+} /CaM-dependent phosphorylation of myosin light chain with a K_d value of 1.6 nM. This peptide adopted an amphipathic α -helical conformation in the presence of Ca^{2+} /CaM with four Arg residues and one Lys residue on its polar face. An analogous peptide from the Ca^{2+} /CaM-binding protein, skeletal muscle phosphorylase kinase, that did not contain the first two Arg residues, inhibited Ca^{2+} /CaM only at concentrations 1000-fold greater than RS20 (Lukas *et al.*, 1986).

Fitzsimons *et al.* (1992) examined the role of some of the basic residues within the Ca^{2+} /CaM-binding region of smMLCK by site-directed mutagenesis. A mutant smMLCK molecule in which the sequence Arg1-Arg2-Lys3 within the Ca^{2+} /CaM-binding domain was changed to Glu-Glu-Asp did not bind biotinylated Ca^{2+} /CaM. This mutant also had a

	1	5	10
skMLCK	Lys-Arg-Arg-Trp-Lys-Lys-Asn-Phe-Ile-Ala		
smMLCK	Arg-Arg-Lys-Trp-Gln-Lys-Thr-Gly-His-Ala		
		15	20
skMLCK	Val-Ser-Ala-Ala-Asn-Arg-Phe-Lys-Lys-Ile		
smMLCK	Val-Arg-Ala-Ile-Gly-Arg-Leu-Ser-Ser		
		25	
skMLCK	Ser-Ser-Ser-Gly-Ala-Leu		

Figure 6. The Calmodulin Binding Domains of Skeletal Muscle and Smooth Muscle Myosin Light Chain Kinases. Residues 342-367 of skMLCK and residues 494-513 of smMLCK comprise the CaM-binding domain within each kinase. The cluster of positively charged residues at the amino terminus of each peptide is highlighted. Both sequences are taken from Ikura *et al.*, 1992.

K_{CaM} value 41 times greater than native MLCK. K_{CaM} is the concentration of CaM required for the half-maximal activation of MLCK. A second mutant in which Lys6 was changed to a Glu residue, had a K_{CaM} value 15 times greater than the native MLCK along with a decrease in Ca^{2+}/CaM affinity. This showed that Arg1, Arg2, Lys3 and Lys6 were important residues for high affinity CaM binding to smMLCK. The results were consistent with other studies using rabbit skMLCK and chicken non-muscle MLCK in which analogous residues in both were postulated to play an important role in Ca^{2+}/CaM binding (Bagchi *et al.*, 1992).

The role of basic residues in the binding of Ca^{2+}/CaM to MLCK is consistent with the experiments of Blumenthal and Stull (1982), in which the effects of ionic strength on the activation of skMLCK by Ca^{2+}/CaM were measured. The results showed a marked inhibition of Ca^{2+}/CaM activation of skMLCK with increasing ionic strength. This result led to the conclusion that ionic interactions play an important role in the stability of the $Ca^{2+}/CaM/skMLCK$ complex (Blumenthal and Stull, 1982).

Herring (1991) prepared a series of mutants of rabbit skMLCK in which basic residues homologous to those in the Ca^{2+}/CaM binding region of smMLCK were altered. The sequence near the binding region they examined was Lys-Lys-Tyr-Leu-Met-Lys-Arg-Arg-Trp-Lys-Lys, which comprised residues 337 to 347 of skMLCK. A series of mutants were prepared altering the basic residues. It was found that changing the first two Lys residues to Glu residues had little effect on the V_{max} and Ca^{2+} concentration required for half-maximal activation of the enzyme ($[Ca^{2+}]_{0.5max}$) in the presence of CaM. A second mutant in which the sequence of residues Lys6-Arg7-Arg8 were changed to the sequence Glu6-Thr7-Leu8 had a much higher $[Ca^{2+}]_{0.5max}$ than the native

enzyme. A third mutant in which the same residues (Lys6-Arg7-Arg8) were changed to three Glu residues had an even greater $[Ca^{2+}]_{0.5max}$. It was concluded that these three basic residues were probably interacting with Glu on the CaM molecule. The mutant which contained the three Glu residues also failed to exhibit high affinity Ca^{2+}/CaM binding. A final mutant in which Lys10 and Lys11 were changed to two Glu also had a low affinity for Ca^{2+}/CaM and an increased $[Ca^{2+}]_{0.5max}$ compared to the native enzyme. It was concluded that the important basic residues for high affinity Ca^{2+}/CaM binding in skMLCK were those within the sequence Lys-Arg-Arg-Trp-Lys-Lys (Herring, 1991).

An interesting question regarding the activation of MLCK in the presence of Ca^{2+}/CaM is how MLCK is inhibited in the absence of Ca^{2+}/CaM . It was proposed that the inhibition is due to the interaction of the MLCK active site with another segment of its polypeptide which can function as a pseudosubstrate, and that this interaction is dissociated by the binding of Ca^{2+}/CaM (Kemp *et al.*, 1987). This hypothesis of autoinhibition was first postulated by a comparison of the myosin light chain phosphorylation site with an homologous site on MLCK. The Ca^{2+}/CaM binding domains of both smMLCK and skMLCK contain a number of basic residues similar to the sequence found in the region around the phosphorylation site in smooth muscle myosin light chain. Another group (Walsh *et al.*, 1982) was able to prepare a Ca^{2+}/CaM -independent smMLCK by limited α -chymotryptic digestion. The 80 kDa fragment had a high specific activity compared to native Ca^{2+}/CaM -dependent smMLCK. They concluded that the Ca^{2+}/CaM -independence was a result of the removal of the Ca^{2+}/CaM binding site as the smMLCK fragment would no longer bind to a CaM affinity column. Subsequent digestion experiments showed that it was also the loss of the autoinhibitory region which

conferred Ca^{2+} -independent activity on MLCK.

Using a series of mutations in which acidic residues within the active site of MLCK were mutated to basic residues, Gallagher *et al.* (1993) were able to locate acidic residues that were responsible for binding to the autoinhibitory domain of MLCK. They were able to show that by changing the sequence Asp784-Glu785-Asp786 in rabbit smMLCK to Lys-Lys-Lys there was a large decrease in both $[\text{Ca}^{2+}]_{0.5\text{max}}$ and KCaM values with no other changes in the kinetic parameters. A similar mutation in skMLCK (Asp384-Glu385-Asp386 \rightarrow Lys-Lys-Lys) also resulted in a similar KCaM decrease and no change in the other kinetic parameters (Gallagher *et al.*, 1993). From these experiments they concluded that residues 384-386 in skMLCK and the analogous residues 784-786 in smMLCK were involved in binding to the autoinhibitory domains of these two kinases. These were the first experimental results that suggested the importance of ionic interactions in the inhibition of MLCK.

In order to specify the exact location of the autoinhibitory domain of smMLCK, the group of Ito *et al.* (1991) prepared a series of turkey gizzard smMLCK mutants which started at Leu447 of the protein and contained varying amounts of the remainder of the carboxyl terminus of the enzyme. The molecule containing the entire carboxyl terminus, from Leu447 to Glu972, possessed kinase activity that was $\text{Ca}^{2+}/\text{CaM}$ -dependent. A mutant that ended at Thr778 resulted in an active mutant that was $\text{Ca}^{2+}/\text{CaM}$ -independent. Thus it was concluded that the autoinhibitory domain lies on the carboxyl side of this residue. Truncation to Lys773 and Trp800 also resulted in constitutively active mutants, although the specific activity of the truncated Trp800 mutant was less than the other shorter mutants. These results led to the conclusion that

the critical region of the inhibitory domain is contained in the sequence of residues Tyr774-Trp800 (Tyr-Met-Ala-Arg-Arg-Lys-Trp), which are homologous to residues 491 to 497 of chicken gizzard smMLCK. None of the active mutants bound $\text{Ca}^{2+}/\text{CaM}$, but the postulated autoinhibitory region did overlap the postulated $\text{Ca}^{2+}/\text{CaM}$ binding region for five residues (Ala-Arg-Arg-Lys-Trp).

Since the putative $\text{Ca}^{2+}/\text{CaM}$ binding and autoinhibitory regions within MLCK were determined the attention now turned to how $\text{Ca}^{2+}/\text{CaM}$ interacted with the smMLCK and skMLCK on an atomic level. Laporte *et al.* (1980) were able to show that the binding of Ca^{2+} to CaM causes conformational changes in the protein which results in the formation of a surface with considerable hydrophobic character. This hydrophobic region was able to bind between four and six molecules of 9-anthroylcholine (Laporte *et al.*, 1980). Although this work showed the probable importance of hydrophobic interactions in the formation of a $\text{Ca}^{2+}/\text{CaM}$ -protein complex, it was also noted that the specificity of $\text{Ca}^{2+}/\text{CaM}$ associations with other proteins was most likely determined by the complementarity of surfaces and specific ionic or polar interactions between CaM and other proteins (Laporte *et al.*, 1980).

An early model (Blumenthal and Stull, 1982) proposed that the first step in the activation of MLCK by $\text{Ca}^{2+}/\text{CaM}$ involves the hydrophobic-driven binding of $\text{Ca}^{2+}/\text{CaM}$ to the enzyme. These hydrophobic interactions are Ca^{2+} -dependent, since the hydrophobic domain at the site of interaction on CaM is only exposed when Ca^{2+} is bound to the protein. As a consequence of the first interaction, short-range interactions such as electrostatic interactions, hydrogen bonds, and van der Waals interactions would become possible due to the proper alignment of amino acid residues. It is evident that the

short-range interactions cannot maintain the stability of the enzyme-protein complex in the absence of the hydrophobic interactions, since CaM activity is Ca²⁺-dependent. Any short range interactions are probably important in strengthening the stability of the complex, conferring CaM specificity to the interaction, and inducing structural changes in the complex which results in enzyme activation (Blumenthal and Stull, 1982).

The solution structure of the complex between Ca²⁺/CaM and a synthetic peptide comprising the binding region of skMLCK has been solved (Ikura *et al.*, 1992). The crystal structure of a complex between Ca²⁺/CaM and a synthetic peptide comprising the binding region of smMLCK has also been solved (Meador *et al.*, 1992). Both structures were similar overall and a tremendous conformational change was observed within the Ca²⁺/CaM molecule. The central helix of CaM (residues 65-93) was disrupted, bringing the two domains of the protein closer together. This conformational change results in the formation of a tunnel by the Ca²⁺/CaM molecule with the hydrophobic regions of the protein melded together along one side of the tunnel. Several hydrophobic interactions between the Ca²⁺/CaM protein and the binding regions of skMLCK and smMLCK were observed. In the crystal structure all seven basic residues of the binding region peptide (smMLCK) were observed to make salt bridges with Ca²⁺/CaM (Meador *et al.*, 1992). Also in the solution structure, calculated simulated annealing structures showed putative interactions between all of the basic residues of the binding peptide and Glu residues of Ca²⁺/CaM (Ikura *et al.*, 1992).

1.6) Stabilization of Peptide Structures by Fluorinated Alcohols

Until recently, experimental evidence for secondary structure in short linear peptides in water solution has been difficult to obtain (Dyson *et al.*, 1988a). Stable structures are not often observed in short peptides since they do not contain the medium and long range stabilizing interactions that are observed in proteins. With the advent of more sensitive techniques, such as high-resolution NMR spectroscopy, stable structures are being observed in localized regions of peptides. Fluorinated alcohols such as 2,2,2-trifluoroethanol (TFE) and hexafluoro-2-propanol (HFP) have been used in solution studies of a number of peptides (Tappin *et al.*, 1988; Gooley and MacKenzie, 1988; Khan *et al.*, 1990; Zagorski *et al.*, 1991). Studies have shown that the introduction of these alcohols to aqueous solutions of these peptides stabilizes the secondary structural elements of the peptides. The induction of secondary structure in these peptides by fluorinated alcohols, may be related to the fact that the peptides in question act in membranes. The co-solvent simulates the lipid environment reducing the water activity, thus stimulating the peptide to take up its *in vivo* conformation.

One suggestion is that the addition of these fluorinated alcohols to the peptide solution does not create new secondary structure but actually stabilizes α -helices which exist transiently in aqueous solutions (Dyson *et al.*, 1988b). An exception to this rule is in cases where sequences have nearly equal tendencies to exist as an α -helix or β -sheet, in which case the equilibrium will be shifted in favour of the helix. The reason these structures are not detected in aqueous solutions is that they exist in a rapid equilibrium with random coil structures and any qualitative detection is observed as a weighted average of the structural equilibrium state (Williamson and Waltho, 1992).

A study was done on a 19 residue synthetic peptide corresponding to the C-helix, containing residues 69 to 87, of myohemerythrin (Dyson *et al.*, 1988a). The two-dimensional NMR spectra of the C-helix peptide in aqueous solution and 20% (v/v) TFE were compared. The purpose of the comparison was to observe the structural differences of the peptide in the different solvents. In aqueous solution strong $d_{\alpha N(i,i+1)}$ NOE connectivities were observed over the whole of the C-helix showing that the conformational ensemble of the peptide included a substantial population of extended chain forms. Such structures appear to predominate in the unfolded form of a peptide in water solution (Dyson *et al.*, 1988b). In addition, $d_{NN(i,i+1)}$ and $d_{\alpha N(i,i+2)}$ NOE connectivities were observed, indicating a small but measurable population of folded conformations.

The $d_{NN(i,i+1)}$ connectivities were observed between residues 11 to 19 of the helix, which is suggestive of α or 3_10 helix (Wüthrich, 1986). For short linear peptides in solution the $d_{NN(i,i+1)}$ distance only becomes short enough to give observable NOEs between residues with ϕ and ψ angles in the helix region of (ϕ, ψ) space (Wüthrich, 1986). Therefore only regions which have a helical tendency would be expected to give rise to $d_{NN(i,i+1)}$ connectivities, the distances in all other structural types being too great. None of the characteristic long range $d_{\alpha N(i,i+3)}$ or $d_{\alpha \beta(i,i+3)}$ NOE connectivities which would confirm a helical structure in the C-helix peptide were detected. Instead what was observed were $d_{\alpha N(i,i+2)}$ NOE connectivities between Lys10 and Phe12 and Phe12 and Glu14 which indicated the presence of local structures and short range order (Dyson *et al.*, 1988a). These connectivities are characteristic of reverse turns in the peptide chain (Wüthrich *et al.*, 1984; Dyson *et al.*, 1988a) and taken with the observed d_{NN} NOE connectivities, implied a significant population of turn

conformations involving His9 to Phe12 and Asp11 to Glu14. Also observed were $d_{\beta N}(i,i+1)$ connectivities, which are commonly observed in helical structures (Wüthrich, 1986) in the carboxyl terminus half of the peptide. Thus the NOE data indicated that in the conformational ensemble of the C-helix, there is a significant population of turn-like structures (Dyson *et al.*, 1988a).

In contrast to the short range order that was seen in the aqueous sample of C-helix, the peptide formed a helix with long range order in a 20% (v/v) TFE solution (Dyson *et al.*, 1988b). Long range $d_{\alpha N}(i,i+3)$ and $d_{\beta N}(i,i+3)$ connectivities confirmed the presence of a helix between residues 11 and 15. From the d_{NN} and $d_{\beta N}$ connectivities observed, the group inferred that the helix extended from residue 9 or 10 to residue 18 or 19.

The important result that came from this research on the structure of the peptide in TFE was that the long-range connectivities were only seen in areas where short-range connectivities typical of helix formation were previously observed in aqueous solutions of the peptide. Therefore, the addition of TFE did not induce helix formation in new regions of the peptide, but merely stabilized regions that already possessed helical characteristics (Dyson *et al.*, 1988b). Therefore it can be concluded that the addition of fluorinated alcohols to aqueous solutions of peptides, does not result in the creation of secondary structure, but merely results in the stabilization of the structure the peptide already possesses (Dyson *et al.*, 1988b). The determination of the solution structure of the C-helix showed it had a helical content of approximately 50% which agreed very favourably with the CD analysis in 20% TFE and Chou-Fasman calculations on the primary structure of the peptide (Dyson *et al.*, 1988b).

1.6) Objectives of this Research

It is well documented that a structure-function relationship exists within proteins. That is, the functionality of a protein is directly related to its three-dimensional structure. Two-dimensional NMR has proven to be very successful in the determination of the three-dimensional structure of small proteins and peptides in solution. Thymosin α_1 is a small peptide that has been implicated in a wide-range of different functions. The three-dimensional structure of the peptide is not yet known nor is the mechanism behind any of its reputed functions. One of the first specific functions attributed to this peptide is the activation of skMLCK in a Ca^{2+} -independent manner. The objectives of this research is to determine the three-dimensional structure of thymosin α_1 by two-dimensional NMR and CD. The three-dimensional structure of the peptide will be presented, along with a model which shows the most probable mode of interaction of thymosin α_1 with skMLCK.

CHAPTER TWO

MATERIALS AND METHODS

2.1) Materials

2.1.a) Proteins

Synthetically prepared thymosin α_1 was the generous gift of Dr. Su Sun Wang of ALPHA-1 Biomedicals Inc. (Foster City, CA).

2.1.b) Enzymes

α -Chymotrypsin (EC 3.4.21.1) was purchased from Worthington Biochemical Corporation (Freehold, NJ 07728).

2.1.c) Chemicals

Sodium chloride (ACS 783), sodium phosphate (B10249), acetonitrile Omnisolv (B90014) and methanol Omnisolv (B90234) were purchased from BD Σ Inc. (Toronto, Ontario M8Z 1K5). Deuterium oxide (D₂O) (99.8 mol%) (MD-175), sodium 2,2-dimethyl-2-silapentane-5-sulfonate (DSS) (MX-1061) and deuterated sodium hydroxide (NaOD) (40% in D₂O) were purchased from MSD Isotopes (Pointe Claire-Dorval, Quebec H9R 4P7). Deuterated hydrogen chloride (DCI) (35% in D₂O), disodium hydrogen phosphate (S-0876), ammonium bicarbonate (A-6141),

trifluoroacetic acid (T-6508), sodium acetate (S-8625) and phenylisothiocyanate (protein sequencing grade) (P-8625) were purchased from Sigma Chemical Company (St. Louis, MO 63178). High performance liquid chromatography (HPLC) grade glacial acetic acid (9515-03) was purchased from J. T. Baker Chemical Co. (Phillipsbury, NJ 08865). Triethylamine (23962-3) and 2,2,2-trifluoroethanol (75-89-8) were purchased from Aldrich Chemical Company (Milwaukee, WI 53201). Deuterated 2,2,2-trifluoroethanol (99%) (75-89-8) was purchased from Cambridge Isotope Laboratories (Woburn, MA 01801). Phosphoric acid (8425-1) was obtained from Caledon Laboratories Ltd. (Georgetown, Ontario L7G 4R9). Amino acid standard H (20088) and 6 N HCl, Sequenal grade (24309) were obtained from Pierce Chemical Co. (Rockford, IL 61105).

2.2) Instrumentation

The masses of materials were determined using a Mettler AE50 electronic balance purchased from Fisher Scientific (Canada) Inc. (Ottawa, Ontario).

Small volume aliquots were dispensed using Gilson PipetmanTM P20, P200 and P1000 from Mandel Scientific Co. Ltd. (Guelph, Ontario N1H 6J3). The pipettes were equipped with tips purchased from Canlab distributed by American Hospital Supply Canada Ltd. (Mississauga, Ontario).

pH measurements were performed on a Fisher AccumetTM Model 810 pH meter manufactured by Allied Fisher Scientific (Pittsburgh, PA. 15219) and a Corning Model 240 pH meter from Corning Science Products (Corning , NY 14831), equipped with an

Ingold U457 combination electrode from Ingold Electronics Inc. (Wilmington, MA 01887). All pH measurements were calibrated with pH 4 (R01204-74), pH 7 (R01278-74) and pH 10 (R01206-74) buffer solutions from BDH Chemicals (Toronto, Ontario M8Z 1K5).

Ultraviolet and visible spectrophotometric measurements were performed on a Shimadzu UV-160 spectrophotometer from Shimadzu Corporation (Kyoto, Japan).

One-dimensional ^1H -NMR spectra were acquired at 300 MHz using an AC-300 NMR spectrometer manufactured by Bruker Spectrospin Ltd. (Milton, Ontario L9T 1Y6). The spectrometer was equipped with a 5 mm ^1H specific probe.

Two-dimensional homonuclear NMR spectra were acquired at the University of Western Ontario, London, Ontario at 500 MHz using a Unity-500 spectrometer manufactured by Varian Associates Inc. (Palo Alto, CA 94304-1030). The instrument was equipped with a 5 mm triple resonance probe.

Circular dichroism spectra were recorded on an On-Line Instrument Systems (OLIS) UV/VIS/CD spectrophotometric operating system manufactured by OLIS Inc. (Bogart, GA 30622). The CD was the property of Dr. S. Vinogradov of Wayne State University, Detroit, Michigan.

High performance liquid chromatography was performed using a Waters 600 multisolvent delivery system, a Waters 411 UV detector and a Waters 745 data module. Amino acid analysis was done using a Waters Pico-TagTM (15 cm x 3.9 mm I.D.)

column. Pre-column derivatization of the amino acids was carried out on a Waters Pico-TagTM Work Station. Peptide mapping was performed using a Waters Delta-PakTM C18-100 Å (30 cm x 3.9 mm I.D., 15 µm spherical resin) column from Nihon Waters Ltd., Tokyo, Japan. All Waters products were obtained from Waters Chromatography Division, Millipore Corporation (Milford, MA 01757). HAWP04700 (0.45 µm) and HVHP04700 (0.45 µm) membranes used to filter HPLC solvents were purchased from Millipore Corporation (Toronto, Ontario).

Deionized distilled water was obtained from a Milli-Q water system from Millipore Corporation (Milford, MA 01757).

Two-dimensional NMR data analysis was performed on a Silicon Graphics Indigo R4000 computer using Varian VNMRSGI software purchased from Varian Associates Inc. (Palo Alto, California, 94304-1030).

The three-dimensional structure of thymosin α_1 was determined using distance geometry, restrained simulated annealing and energy minimization. Structural calculations and analysis were performed using the NMR_Refine and INSIGHTII modules which are part of the BioSym software package purchased from Biosym Technologies Inc. (San Diego, California, 92121-2777).

Modelling studies were performed on a Silicon Graphics Indigo R4000 computer using the DOCKING and INSIGHTII modules which are part of the BioSym software package purchased from Biosym Technologies Inc.

2.3) Methodology

2.3.a) Chou-Fasman Analysis of the Primary Structure of Thymosin α_1

Calculations to predict if thymosin α_1 possessed any secondary structure were performed using the primary sequence of thymosin α_1 (Low and Goldstein, 1979) and the criteria for the prediction of protein conformation as outlined by Chou and Fasman (Chou and Fasman, 1974a,b).

2.3.b) Circular Dichroism

Sample Preparation. A thymosin α_1 stock solution was prepared in 0.15 M NaCl and 20 mM phosphoric acid, pH 3.50. In order to obtain the greatest accuracy, the concentration of the stock solution was determined using amino acid analysis. A CD spectrum of a 0.070 ml aliquot of the stock solution dissolved in 0.180 ml of buffer was acquired as were spectra of 0.070 ml of the stock solution dissolved in various concentrations of 2,2,2-trifluoroethanol (TFE). All samples were made up to 0.250 ml by adding appropriate amounts of buffer.

Spectra Acquisition. Circular dichroism measurements of thymosin α_1 were performed using an OLIS UV/VIS/CD spectrophotometer with a 1 mm path length quartz cell. Spectra were acquired from 250 to 198 nm and contained 52 points, with a time delay of 3 s at each point. The CD spectra were recorded in millidegrees (mdeg) and converted into mean residue ellipticity (MRE) using the concentration of the thymosin

α_1 stock solution determined by amino acid analysis. All CD spectra were acquired using the same cell and care was taken to place the cell in the same position for each spectrum. All spectra were baseline corrected. The CD spectropolarimeter was calibrated with a 0.1 mg/ml aqueous sample of (+)-10-camphorsulfonic acid.

The α -helix content of thymosin α_1 was determined by measuring the MRE at 222 nm (MRE_{222nm}) and comparing it to the value of MRE_{222nm} for a complete random coil (Greenfield and Fasman, 1969) and for a complete α -helix (Toniolo *et al.*, 1979).

2.3.c) α -Chymotryptic Digestion of Thymosin α_1

Enzymatic digestion of thymosin α_1 by α -chymotrypsin was performed in a 1% ammonium bicarbonate solution at pH 8.3 for 3 h at 37°C (Low and Goldstein, 1979). α -chymotrypsin was added to the peptide solution to give a final ratio of enzyme to substrate of 1:50 (w/w). The enzymatic digest was lyophilized to terminate the reaction. The peptide fragments were isolated by peptide mapping.

2.3.d) Peptide Mapping

Peptide mapping was performed using a Waters 600 HPLC system with a Model 440 UV detector and a Delta-Pak C-18 column. The initial column buffer was 0.05% trifluoroacetic acid (TFA) and the temperature was 28°C. The conditions for the isolation of peptides from the α -chymotrypsin digestion were as follows: 0-20% ACN in 20 minutes, 20-40% ACN (20-60 minutes), 40-70% (60-90 minutes), 70% ACN (90-100 minutes), 70-0% ACN (100-110 minutes) with a constant 0.05% TFA

concentration and a flow rate of 1 ml/min. The UV detector monitored peptide elution at a wavelength of 214 nm. Separated peaks were collected and lyophilized. The amino acid composition of the separated peaks was determined by amino acid analysis.

2.3.e) Amino Acid Analysis (Bidingmeyer et al., 1984)

Reagent Preparation. Eluent A was composed of 0.14 molal sodium acetate trihydrate and 0.05% (v/v) triethylamine, adjusted to pH 6.4 with HPLC grade glacial acetic acid. Eluent B was distilled deionized water collected through a Milli-Q water system. Both of the previous reagents were passed through a 0.45 μm HAWP filter before use on the HPLC. Eluent C was HPLC grade acetonitrile which was subsequently passed through a 0.45 μm HVHP filter before use. The sample diluent contained 5% (v/v) acetonitrile, 4.75 mM sodium hydrogen phosphate, pH 7.4. The redrying reagent was composed of a 2:2:1 mixture of methanol:water: triethylamine. The derivatizing reagent was composed of a 7:1:1:1 mixture of methanol:water:triethylamine:phenylisothiocyanate.

Procedure. Thymosin α_1 samples were hydrolyzed in acid washed, pyrolyzed culture tubes with vapor phase 6N HCl containing 1% phenol for 24 hours at 110^oC in a Waters reaction vial on the Picotag workstation. After hydrolysis the culture tubes were transferred to a fresh reaction vial and placed on the workstation to dry (until a vacuum of 65 millitorr was reached). Twenty microliters (μL) of the redrying reagent was then added to the thymosin α_1 culture tubes, which were replaced into the reaction vial and installed onto the workstation to re-dry. The hydrolyzed amino acids were then derivatized by adding 20 μL of derivatizing reagent to each culture tube, replacing the culture tubes into the reaction vial, and allowing the vial to sit at room temperature for

20 minutes. Excess reagent was then removed by re-installing the reaction vial onto the workstation and waiting for a vacuum of 65 millitorr to be achieved. The reaction vial was left on the workstation for 30 minutes after the suitable vacuum was reached to ensure all excess reagent was removed. An external standard composed of 5 μ L of Pierce amino acid standard was dried, redried and derivatized along with the samples of thymosin α_1 . The derivatized PTC amino acids were dissolved in the sample diluent and injected onto a Waters Picotag column installed in the Waters 600 multisolvent HPLC system with a model 441 detector set at 254 nm. The temperature of the column was maintained at 38^oC. The separation of amino acids occurred in under 13 minutes using the following gradient conditions:

Time (min)	Flow Rate (ml/min)	Eluent A (%)	Eluent B (%)	Eluent C (%)
0.0	1.0	94	0	6
10.0	1.0	56	16	28
10.3	1.0	0	40	60
12.0	1.0	0	40	60
12.5	1.5	0	40	60
13.3	1.5	0	40	60
14.0	1.5	94	0	6
30.0	1.5	94	0	6
30.5	1.0	94	0	6

Amino acids were quantified using response factors from an external amino acid standard.

2.3.f) NMR Spectroscopy

Sample Preparation. For the acquisition of one-dimensional ^1H -NMR spectra of thymosin α_1 , the peptide was dissolved in a buffer of 0.15 M NaCl, 20 mM phosphate, and 0.5 mM DSS in D_2O to give a final peptide concentration of 1.08 mM in a total volume of 0.45 mL. The thymosin α_1 sample was then transferred to a clean 5 mm NMR tube (535-PP), and the pH value measured with the Ingold NMR tube pH electrode. The pH^* of the peptide sample was adjusted by appropriate additions of 1 N DCl or 1 N NaOD in D_2O . pH^* refers to the direct pH meter reading uncorrected for the deuterium isotope effect (Glasoe and Long, 1960).

For acquisition of two-dimensional homonuclear spectra of thymosin α_1 , the peptide was dissolved in a buffer containing 0.15 M NaCl, 20 mM phosphate and 0.5 mM DSS in 70% H_2O and 30% TFE-d_3 in a final volume of 0.5 mL. The final peptide concentration was determined to be 1.93 mM by weight. The pH^* of the sample was adjusted to 6.0 with an appropriate addition of 1 N HCl or NaOH.

Data Acquisition and Processing. One-dimensional ^1H -NMR spectra of thymosin α_1 were recorded at 300 MHz on a Bruker AC-300 FT-NMR spectrometer with a 5 mm ^1H selective probe in quadrature detection mode. Typical NMR acquisition parameters were: 16K data points FID; sweep width, 3600 Hz; flip angle, 60° ; relaxation delay, 2 seconds; temperature, 298 K; number of transients, 500; line broadening, 0.462 Hz;

excitation and decoupling on the H₂O resonance. All reported chemical shifts are relative to the principal resonance of the internal standard DSS.

The phase-sensitive double-quantum filtered COSY and phase-sensitive NOESY spectra were collected according to standard procedures. Phase-sensitive spectra were recorded with the hypercomplex method (States *et al.*, 1982). The TOCSY experiment was recorded using an MLEV-17 spin lock of 50 ms. In all two-dimensional COSY, TOCSY and NOESY experiments 2048 data points were collected in the t_2 domain and zero-filled to 4096 points prior to Fourier transform. In all 2D COSY and NOESY experiments, 256 time increments were collected in the t_1 domain and zero-filled to 4096 points. In the TOCSY experiment 128 time increments were collected in the t_1 domain and zero-filled to 4096 points. In general, 8 transients were averaged for each t_1 time increment. Spectral widths of 6000 Hz were collected in both dimensions. Mixing times of 75, 150 and 300 ms were used in the NOESY experiments. All two-dimensional NMR spectra were recorded at 298 K. Prior to Fourier transformation, the DQF-COSY data were multiplied by a sinebell function in both dimensions with a small amount of sensitivity enhancement applied with a positive exponential. The TOCSY and NOESY spectra were multiplied by a Gaussian apodization function and a negative exponential for resolution enhancement. The intense solvent peak was removed in the DQF-COSY and TOCSY experiments by saturation of the solvent resonance frequency during the relaxation delay. In the NOESY experiments the solvent peak was saturated during the evolution period and mixing time.

2.3.g) NOE Distance and Volume Restraints

NOE distance and volume restraints were determined using two-dimensional NOESY experiments in 30% (v/v) TFE- d_3 and 70% (v/v) H_2O . Three NOESY experiments were performed with mixing times of 75, 150 and 300 ms. Cross peaks were integrated using VNMRSGI software by drawing a box around the desired cross peak and integrating the peak volume. The integrated intensities were classified as strong, medium or weak with associated upper distance limits of 3.0 Å, 4.0 Å and 5.0 Å, respectively. A lower distance limit of 1.8 Å was used for all observed crosspeaks. A total of 134 NOE distance restraints and 128 NOE volume restraints were measured. The NOE restraints were supplemented with seven generic distance restraints corresponding to hydrogen bonds for regions of regular secondary structure, based on characteristic NOE patterns and preliminary structure calculations. For each hydrogen bond, one restraint holds the distance between the amide proton and the carbonyl oxygen to less than 2.3 Å, while a second restraint keeps the distance from the amide nitrogen to the carbonyl oxygen between 2.5 Å and 3.3 Å to maintain the linearity of this bond.

2.3.h) Structure Calculations

The structure of thymosin α_1 was determined using the distance geometry algorithm contained in the program DGII (Havel, 1991), that is part of the NMR_Refine software package (Biosym Technologies, San Diego, California). The algorithm is based on the following three steps: bound smoothing, embedding, and annealing.

The experimentally determined NOE distance and volume restraints were loaded onto

the starting structure of thymosin α_1 . The starting structure used to generate the final conformation of the peptide was an extended chain. Tetragonal smoothing using a sequential strategy was performed. The bounds were smoothed using a tolerance level of 0.01 and convergence criteria of 0.005.

After the bound smoothing was performed, the embedding was done using 200 eigen iterations and an eigen criteria of 0.0001. Prospective metrization was chosen and inverse squared range plus squared average weighted majorization was selected. The embed dimension was set to four.

The deviations in the embedded coordinates were minimized by optimization. In optimization the initial energy of the system was set at 900 kcal/mol with a time step of 0.35 psec. The calculations gave a convergence for 11 out of 30 structures. Superposition and analysis of the structures were performed using INSIGHT II software.

2.3.1) Analysis of the Structure of Thymosin α_1

The analyses of the structures of thymosin α_1 were performed by visual inspection and by superimposing various regions of the structures on to one another. The backbone atoms (N, C α , C, O) of all of the residues, for the eleven converged structures, were superimposed on one another. The root mean square deviation (RMSD) of all of the structures compared to one another was recorded and an average RMSD was determined. The backbone atoms of the subset of residues from 16 to 26 were also superimposed and the average RMSD of all of the structures compared to one another was also recorded and averaged. The backbone atoms of residues 5-8 were also measured in the same manner.

The dihedral angles ϕ and ψ of all of the residues of the eleven structures of thymosin α_1 with the lowest convergence level were measured and averaged in order to determine the presence of known stable secondary structure within the peptide.

The distance between the backbone nitrogen atoms of residues separated by three amino acids residues (i.e. i,i+3) were measured and averaged for all of the residues of the eleven converged structures of thymosin α_1 .

2.3.j) Modelling the Interaction with Myosin Light Chain Kinase

The interaction between thymosin α_1 and skMLCK was performed using the structure of thymosin α_1 in 30% (v/v) TFE-d₃ and the structure of the CaM-binding domain of MLCK as determined in 30% (v/v) TFE-d₃ (Zhang *et al.*, 1993) and complexed to CaM (Ikura *et al.*, 1992). The total van der Waals and electrostatic energy between the two peptides was monitored using the DOCKING module which is part of the BioSym software package. The total nonbonded energy was calculated, while the position of one of the peptides was altered relative to the other. Some of the torsion angles within the side chains of residues that came into close intermolecular contact were also altered in order to find the system with the lowest total energy. The interactive forces between the peptides were measured *in vacuo* using all of the atoms within each peptide.

CHAPTER THREE

RESULTS

3.1) Chou-Fasman Analysis of Thymosin α_1

The first step in the Chou-Fasman analysis of the primary structure of thymosin α_1 is to locate a cluster of four residues out of six with a high propensity for forming an α -helix. Near the carboxyl terminus of the peptide, residues 24 to 27 (Glu-Glu-Ala-Glu) are all strong helix formers (Table II). Analyzing the sequence in both directions and calculating the helical affinity of every tetrapeptide encountered predicts how long the helix in the peptide is. The next residue after Glu27 is a helix breaker ($b\alpha$), Asn28, which is also the final residue of the peptide. Thus Glu27 is predicted to be the residue at the carboxyl terminus of the helix. The first tetrapeptide towards the amino terminus capable of stopping helix propagation is residues 12 to 15 (Thr-Thr-Lys-Asp). All four of these residues are either weak or indifferent helix formers. Examining the residues between Leu16 and Glu27 inclusive, each segment of six residues has an average $P\alpha$ ($\langle P\alpha \rangle$) value greater than 1.03 (Table II) and also the $\langle P\alpha \rangle$ value is greater than the $\langle P\beta \rangle$ or $\langle P_c \rangle$ value. Therefore the Chou-Fasman calculations predict that the helix begins at Leu16 and extends to Glu27. The predicted helical portion of thymosin α_1 is twelve residues in length.

The Chou-Fasman rules for predicting structural conformation within proteins also addresses the probability of finding particular residues at particular locations within a helical conformation. The helix in thymosin α_1 would have an amino terminus composed

Table II

Conformational Parameters for the Residues
of Thymosin α_1

<u>Amino Acid</u>	<u>Pα^a</u>	<u>Pβ^b</u>	<u>Pγ^c</u>
Ser1	0.79	0.72	1.27
Asp2	0.98	0.80	1.09
Ala3	1.45	0.97	0.66
Ala4	1.45	0.97	0.66
Val5	1.14	1.65	0.66
Asp6	0.98	0.80	1.09
Thr7	0.82	1.20	1.05
Ser8	0.79	0.72	1.27
Ser9	0.79	0.72	1.27
Glu10	1.53	0.26	0.87
Ile11	1.00	1.60	0.78
Thr12	0.82	1.20	1.05
Thr13	0.82	1.20	1.05
Lys14	1.07	0.74	1.05
Asp15	0.98	0.80	1.09
Leu16	1.34	1.22	0.66
Lys17	1.07	0.74	1.05
Glu18	1.53	0.26	0.87
Lys19	1.07	0.74	1.05
Lys20	1.07	0.74	1.05
Glu21	1.53	0.26	0.87
Val22	1.14	1.65	0.66
Val23	1.14	1.65	0.66
Glu24	1.53	0.26	0.87
Glu25	1.53	0.26	0.87
Ala26	1.45	0.97	0.66
Glu27	1.53	0.26	0.87
Asn28	0.73	0.65	1.33

^ahelical potential

^b β -strand potential

^crandom coil potential

(Table adapted from Chou and Fasman, 1974a)

of the residues Leu16-Lys17-Glu18 and a carboxyl terminus made up of the residues Glu25-Ala26-Glu27 based on the above prediction. The average value for any given residue occurring at the amino terminus or the carboxyl terminus of a helix is 0.097 (Chou and Fasman, 1974a). The values for Leu, Lys and Glu are 0.056, 0.057 and 0.195 respectively (Chou and Fasman, 1974a). Therefore Glu is the only residue to have a high affinity for the amino terminus of an α -helix. The frequency values for Glu or Ala to occur in the carboxyl region of an α -helix are 0.124 and 0.118, respectively (Chou and Fasman, 1974a) are well above the average for being found in this location. The frequency value of having an Asp residue at the amino terminus non-helical region is 0.081, which is comparable to the average for all residues of 0.082 (Chou and Fasman, 1974a). The frequency value for having an Asn residue at the carboxyl terminus non-helical region is 0.120, which is well above the average for all residues of 0.080 (Chou and Fasman, 1974a). This statistical examination of the composition of the carboxyl terminus of the predicted peptide corresponds reasonably well with the Chou-Fasman rules.

The residues making up the center of the helix region all have a higher than average frequency for being found in this region. The average value for all residues being found within the center of a helix is 0.112 (Chou and Fasman, 1974a). The residues comprising the centre region of the thymosin α_1 helix have frequency values as follows: Glu(0.177), Val(0.166) and Lys(0.126). There are no Pro residues within the helix which would disrupt the helical conformation.

The presence of β turns within a protein can also be predicted using the set of rules devised by Chou and Fasman (Chou and Fasman, 1974b). The frequency of occurrence

(ft) for a residue at each of the four positions within a β turn is listed in the Chou-Fasman rules for predicting secondary structure. To predict a β turn, the product of the ft values for each position (pt) must be greater than 0.5×10^{-4} , $\langle P\alpha \rangle$ for the sequence must be less than 0.90, and $\langle P\beta \rangle$ must be greater than $\langle P\alpha \rangle$. All of the above criteria are met by the sequence of residues 6 to 9 (Asp-Thr-Ser-Ser) of thymosin α_1 . For this sequence pt equals 1.26×10^{-4} , while $\langle P\beta \rangle$, $\langle P\alpha \rangle$ and $\langle P\beta \rangle$ equal 1.345, 0.845 and 0.860 respectively (Table III). Thus a β turn is predicted between residues 6 to 9 of thymosin α_1 . The complete prediction of the secondary structure of thymosin α_1 based on the Chou-Fasman rules is shown in Figure 7.

3.2) One-Dimensional NMR Measurements of Thymosin α_1

Initial one-dimensional $^1\text{H-NMR}$ spectra of thymosin α_1 in 20 mM sodium phosphate, 150 mM NaCl in D_2O , were acquired at 300 MHz at various pH values. Spectra were recorded at five different pH values in the order 9.0, 8.0, 7.0, 6.0 and 5.0 (Figure 8). The spectra did not change appreciably between pH values 9.0 and 6.0, but at pH 5.0 the spectrum changed dramatically, especially in the αCH region of the spectrum (4.0-4.5 ppm). All of the thymosin α_1 spectra in this pH range were characterized by very sharp resonances.

A one-dimensional $^1\text{H-NMR}$ spectrum of thymosin α_1 in 20 mM sodium phosphate, 150 mM NaCl in 60% (v/v) 2,2,2-trifluoroethanol- d_3 (TFE- d_3) and 40% (v/v) D_2O at pH 6.0, was acquired. When compared to a spectrum of thymosin α_1 in the same buffer conditions and 100% D_2O , the spectrum in 60% (v/v) TFE- d_3 was characterized by broader resonances and a change in position of some of the resonances

Table III

Conformational Parameters for the Sequence
Asp6, Thr7, Ser8 and Ser9 Within
Thymosin α_1

<u>Residue</u>	<u>Pα^a</u>	<u>Pβ^b</u>	<u>Pc^c</u>	<u>Pt^d</u>
Asp6	0.98	0.80	1.09	0.137
Thr7	0.82	1.20	1.05	0.093
Ser8	0.79	0.72	1.27	0.095
Ser9	0.79	0.72	1.27	0.104

^ahelical potential
^b β -strand potential
^crandom coil potential
^dturn potential

1		5						10		
Ac	Ser	Asp	Ala	Ala	Val	Asp	Thr	Ser	Ser	Glu
c	c	c	c	c	c	t	t	t	t	c
					15				20	
	Ile	Thr	Thr	Lys	Asp	Leu	Lys	Glu	Lys	Lys
	c	c	c	c	c	α	α	α	α	α
					25					
	Glu	Val	Val	Glu	Glu	Ala	Glu	Asn		
	α	α	α	α	α	α	α	c		

Figure 7. Secondary Structure Prediction for Thymosin α_1 . The predicted secondary structures are annotated α (helix), t (turn) and c (coil). Predictions were based on the procedure described by Chou and Fasman (1974a,b).

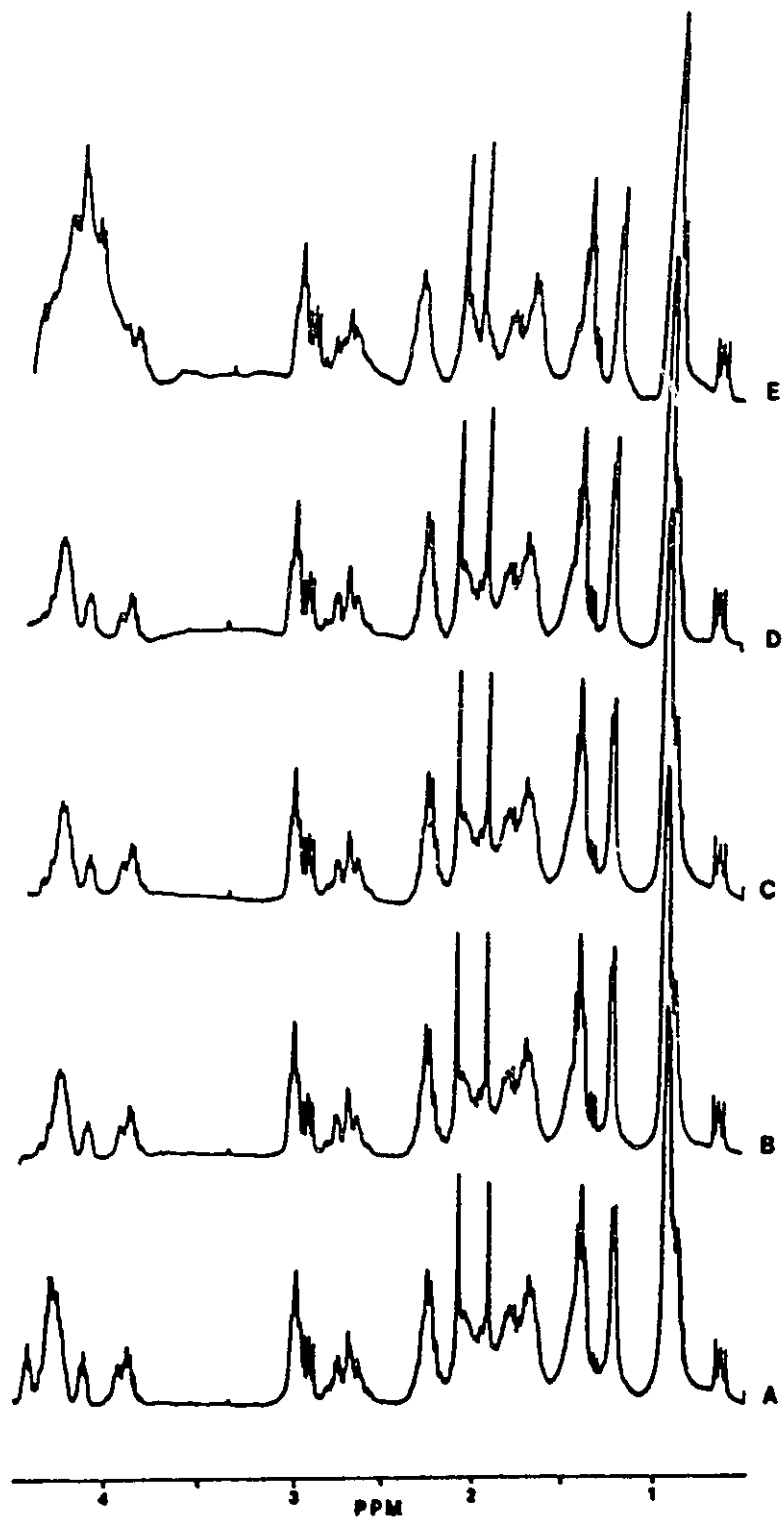


Figure 8. pH^{*} Titration of Thymosin α_1 . 300 MHz ¹H-NMR spectra of thymosin α_1 in 20 mM phosphate, 0.15 M NaCl, 0.5 mM DSS in D₂O at 300 K at pH^{*} 9.0 (A), 8.0 (B), 7.0 (C), 6.0 (D) and 5.0 (E).

in the α CH region of the spectrum (Figure 9).

3.3) Circular Dichroism of Thymosin α_1

A series of CD spectra of thymosin α_1 were recorded in the presence of various concentrations of TFE. The MRE_{222nm} was used to calculate the percentage of α -helical structures. The CD spectrum of thymosin α_1 in 0% (v/v) TFE showed the presence of a limited amount of stable secondary structure (Figure 10). The MRE_{222nm} was -3158.7 deg·cm²/dmol. Using a MRE_{222nm} of -38 000 deg·cm²/dmol for a complete α -helix (Toniolo et al., 1979) and 3900 deg·cm²/dmol for a complete random coil (Greenfield and Fasman, 1969), the calculated α -helical content of the peptide is 16.8% in aqueous solution, which corresponds to four residues being in an α -helical conformation. The calculation is based on the observation that a linear relationship exists between the MRE_{222nm} value and the helical content. There was a large minimum absorption band at 203 nm ($MRE_{203nm} = -12 499.3$ deg·cm²/dmol) which confirmed that most of the peptide was in a random coil form.

The subsequent spectrum of thymosin α_1 in 10% (v/v) TFE showed no change in the size of the band at 222 nm (Figure 11). There was an increase in the band at 203 nm ($MRE_{203nm} = -7788.7$ deg·cm²/dmol), which was still the position of minimum absorption (Figure 11). In subsequent CD spectra of the peptide in 20% (v/v) and 30% (v/v) TFE, the MRE_{222nm} decreased in value and the large negative band at 203 nm shifted to 208 nm (Figure 12). The minimum value of MRE_{222nm} was recorded with thymosin α_1 in a 30% (v/v) TFE solution (-13 141.3 deg·cm²/dmol). No further decrease in MRE_{222nm} was observed for the peptide in 40% (v/v) and 50%

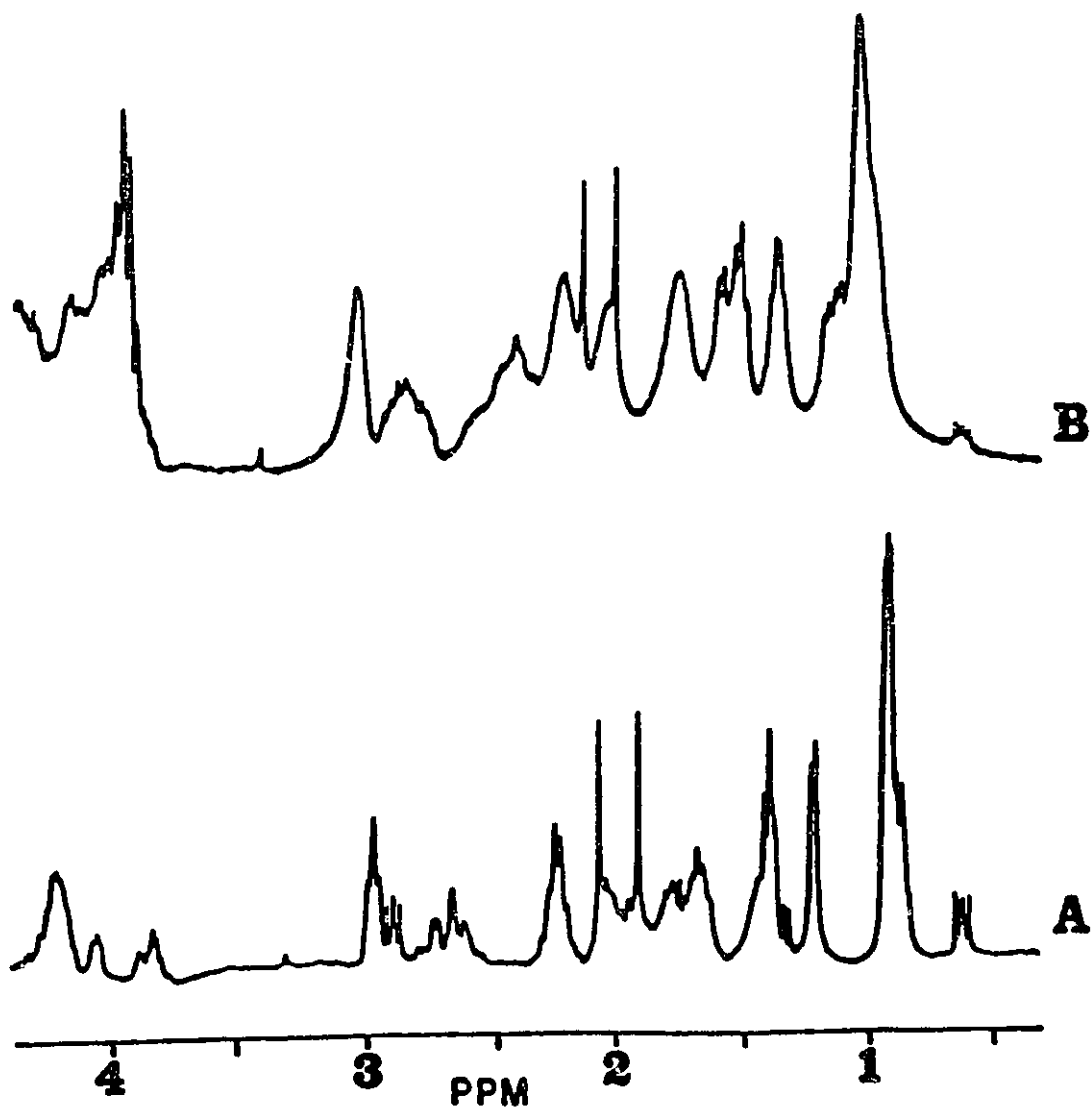


Figure 9. $^1\text{H-NMR}$ of Thymosin α_1 in 100% (v/v) D_2O and 60% (v/v) TFE-d_3 . The 300 MHz spectra of the peptide in 100% (v/v) D_2O (A) and 60% (v/v) TFE-d_3 (B) are shown. Both spectra contained 20 mM phosphate, 0.15 M NaCl, 0.5 mM DSS at pH 6.0. The spectra were recorded at 300 K.

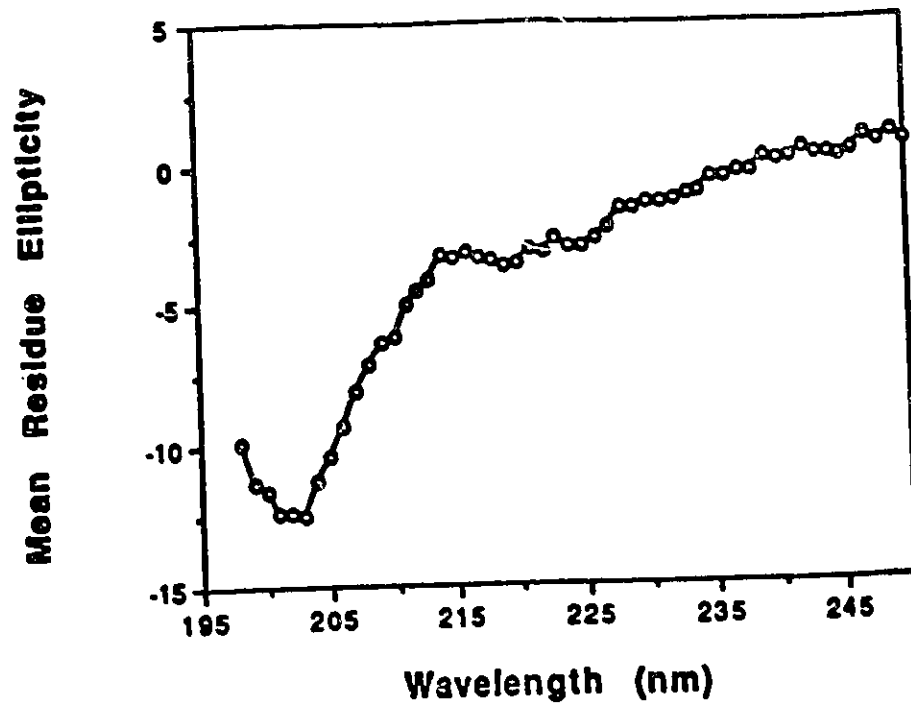


Figure 10. CD Spectrum of Thymosin α_1 in Aqueous Solution. The peptide concentration was 36 μM in 20 mM H_3PO_4 , pH 3.50. The spectrum was recorded using a 1 mm path length cell and was baseline corrected. The spectrum was recorded at ambient temperature. The mean residue ellipticity is reported as $\text{deg}\cdot\text{cm}^2/\text{dmol} \times 10^{-3}$.

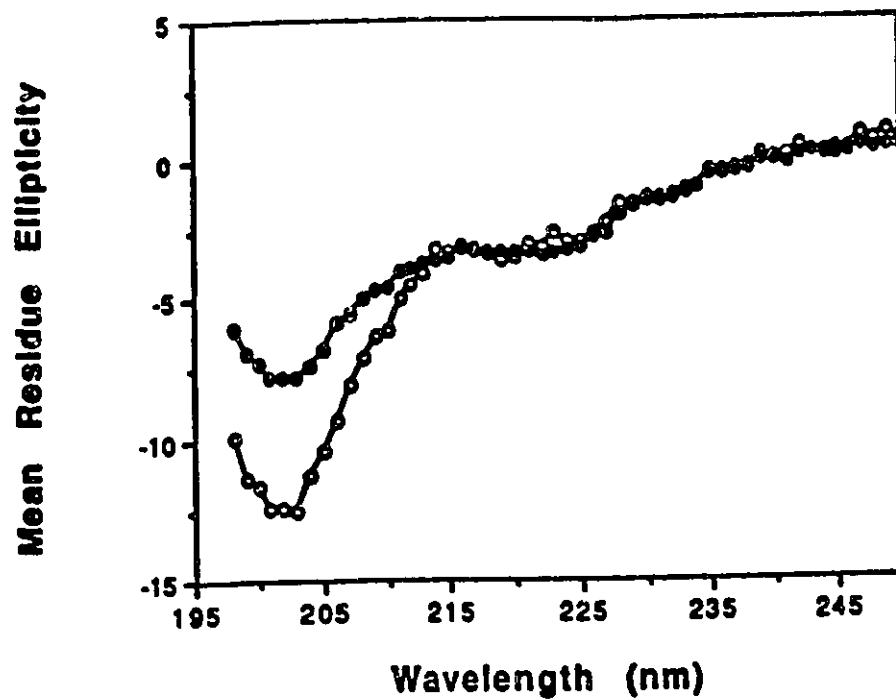


Figure 11. CD Spectrum of Thymosin α_1 in 0% (v/v) and 10% (v/v) TFE. The spectrum of the peptide in 10% (v/v) TFE is indicated by closed circles (●) and the spectrum of the peptide in 0% (v/v) TFE by open circles (○). The concentration of the peptide was 36 μ M in both spectra.

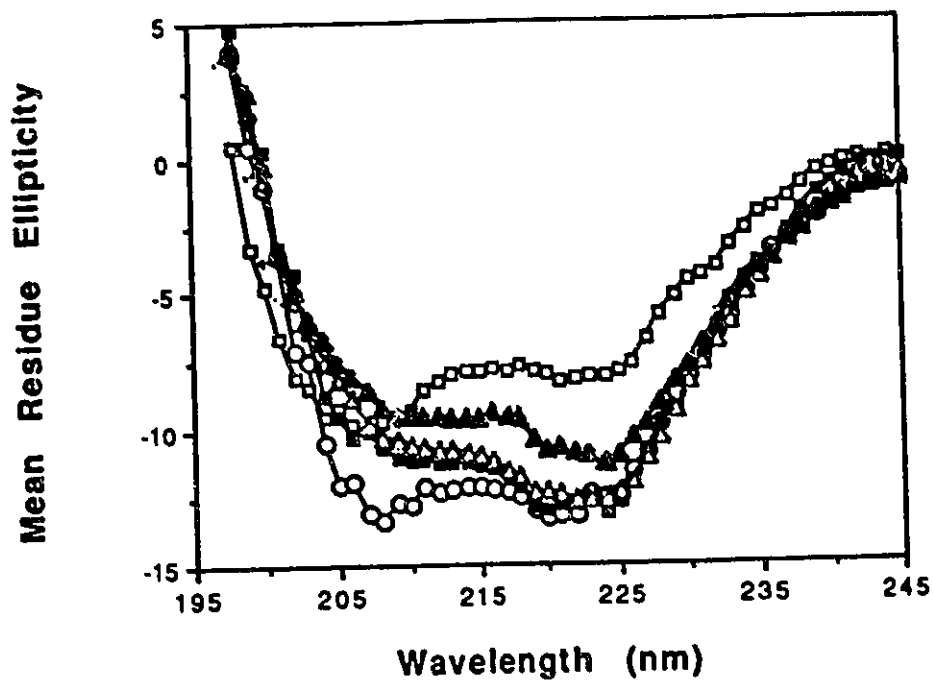


Figure 12. CD Spectra of Thymosin α_1 in Various Amounts of TFE Added. The spectra of thymosin α_1 in the following concentrations of TFE are shown: 20% (\square), 30% (\circ), 40% (\blacksquare), 50% (\triangle), and 60% (\blacktriangle). The CD instrument was calibrated with a 0.1 mg/ml aqueous solution of (+)-10-camphorsulfonic acid.

(v/v) TFE solutions but an increase was observed at 60% (v/v) TFE (Table IV).

Figure 13 shows a graphical representation of the change in the MRE values at 222 and 203 nm as a function of the amount of TFE added. The MRE_{222nm} value does not change significantly between 0% (v/v) and 10% (v/v) TFE added but a significant decrease is observed at 20% (v/v) TFE added and continues to decrease at 30% (v/v) TFE added. A significant increase in the MRE_{222nm} value is observed when 60% (v/v) TFE added. The MRE_{203nm} value increases dramatically between 0% (v/v) and 10% (v/v) TFE added, but shows little change in subsequent spectra of the peptide with increasing amounts of TFE added.

The CD titration data clearly shows a narrow isodichroic region from 202 to 207 nm (Figure 14). Since an isodichroic region, rather than an isodichroic point, exists the formation of secondary structure within thymosin α_1 may involve more than just two states (i.e. random coil and α -helix). In the TFE titration of the aqueous solution of thymosin α_1 there is very little change in the MRE_{222nm} value between 0% (v/v) and 10% (v/v) TFE added to the solution, yet there is a substantial increase in the MRE_{203 nm}. The calculated amount of helicity of thymosin α_1 in 0% (v/v) TFE is 16.8% while the amount of helicity in 10% (v/v) TFE is 17.5%. There is some change in the secondary structure of the peptide occurring which does not include any substantial increase in the helicity of the peptide. It is possible that the structural change is the β -turn predicted by the Chou-Fasman analysis of the primary structure of thymosin α_1 .

TABLE IV

Helical Content of Thymosin α_1 at Various
Amounts of Trifluoroethanol

<u>[TFE] % (v/v)</u>	<u>MRE_{222nm}</u>	<u>% α-helix</u>
0	-3158.68	16.8
10	-3430.55	17.5
20	-8119.45	28.7
30	-13141.28	40.7
40	-12739.06	39.7
50	-12629.45	39.4
60	-10861.03	35.2

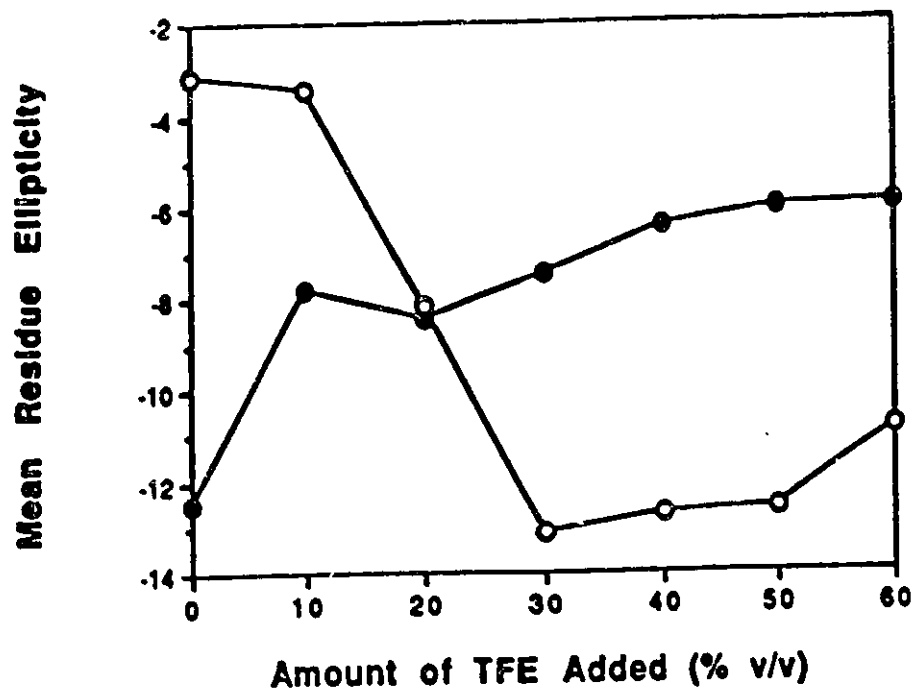


Figure 13. TFE Titration Curves of the MRE_{203nm} and MRE_{222nm} Values for Thymosin α_1 . The observed MRE_{203nm} and MRE_{222nm} values for the peptides as a function of the amount of TFE added are plotted. The MRE_{203nm} values are indicated by closed circles (●) and the MRE_{222nm} values by open circles (○).

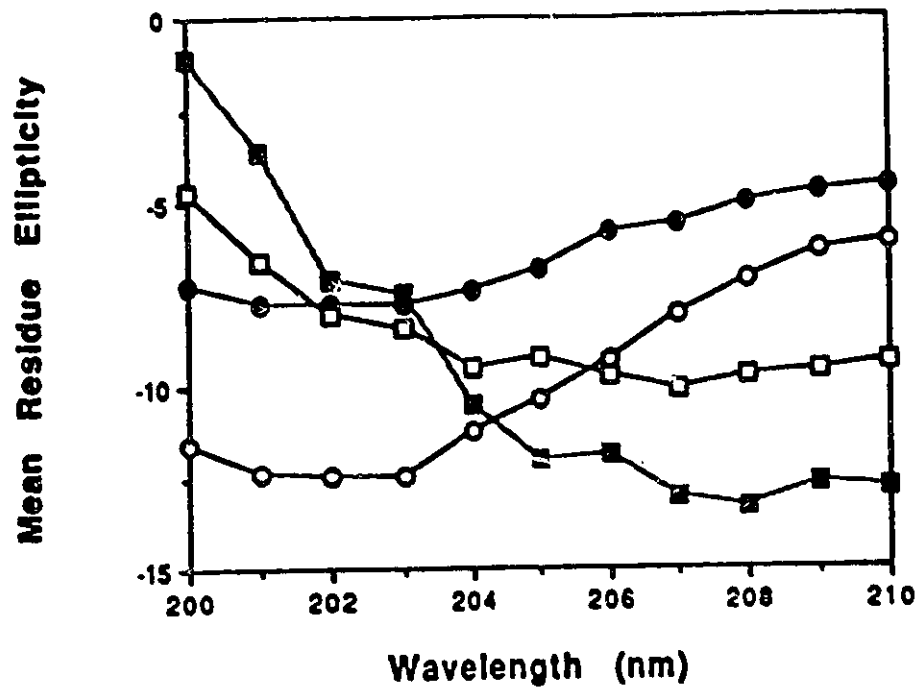


Figure 14. Isodichroic Region in the CD Spectra of Thymosin α_1 at Various Amounts of TFE. The spectra of the peptide in the following amounts of TFE added are shown: 0% (v/v) (○), 10% (v/v) (◻), 20% (v/v) (○) and 30% (v/v) (◼).

3.4) α -chymotryptic Digestion of Thymosin α_1

In the initial primary sequence determination of thymosin α_1 it was observed that α -chymotrypsin cleaved the peptide quite unexpectedly after Lys14 (Low and Goldstein, 1979). In order to confirm this result an α -chymotryptic digest of the peptide was performed under the same conditions. The α -chymotryptic digestion of thymosin α_1 produced five peaks when the peptides were separated by reverse phase HPLC (Figure 15). The peaks are well separated and were identified by amino acid analysis. The largest peak, representing 37.6% of the total peak areas, eluted at 24.1% ACN (28.6 min) and was identified as undigested thymosin α_1 . The next two largest peaks (19.6% and 18.2% of the area) eluted at 20.8% ACN (21.8 min) and 21.7% ACN (23.6 min) and were identified as thymosin α_1 (15-28) and thymosin α_1 (1-14). The two remaining peaks, representing 7.0% and 6.3% of the total area, eluted at 17.9% ACN (17.8 min) and 24.7% ACN (29.3 min) respectively, and were identified as thymosin α_1 (17-28) and thymosin α_1 (1-16). Examining the sequence of the peptide shows that α -chymotrypsin predominantly cleaved thymosin α_1 after Lys14, while a smaller amount of the peptide was cleaved after Leu16. The complete amino acid analysis of the peaks of digested thymosin α_1 collected in the α -chymotryptic digest of peptide is shown in Table V.

3.5) Two-dimensional NMR of Thymosin α_1

3.5.a) Amino Acid Spin System Identification

In order to identify and sequentially assign the amino acid spin systems within

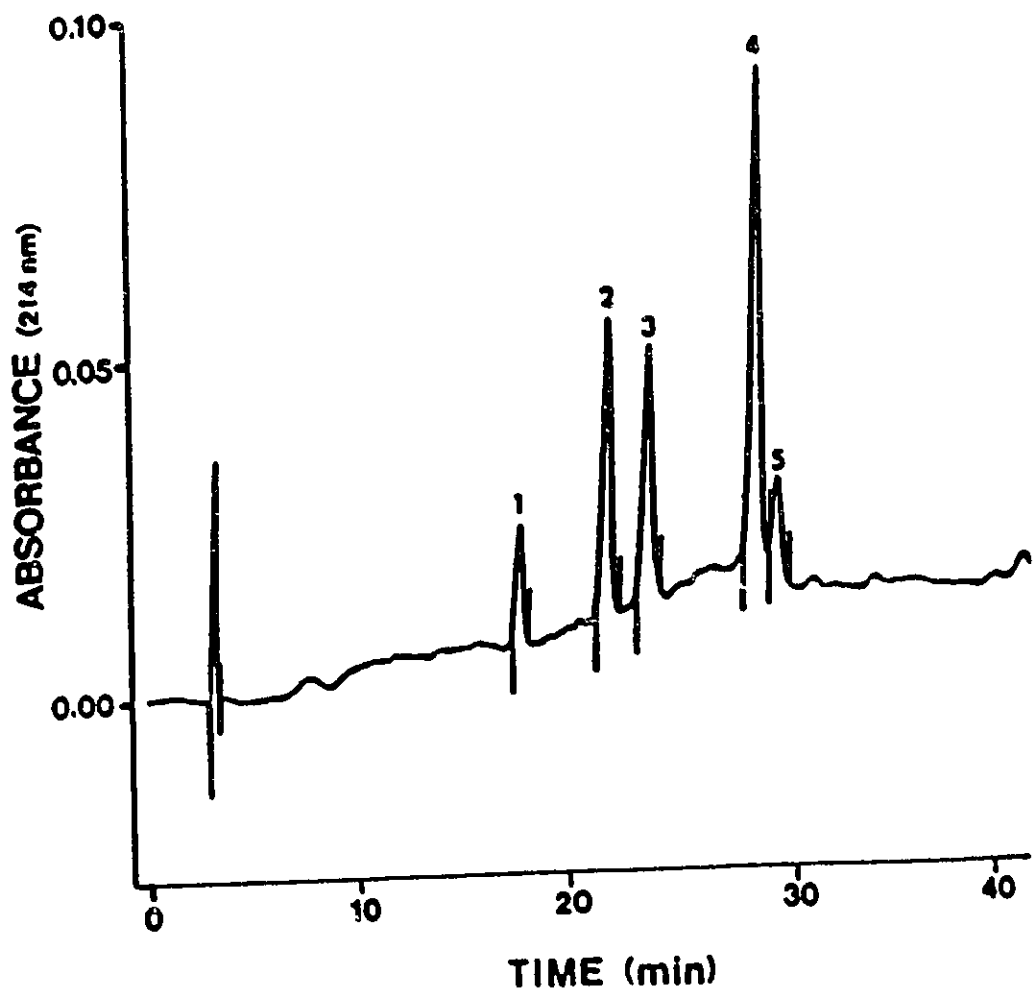


Figure 15. HPLC Map of the α -chymotryptic Digest of Thymosin α_1 . Thymosin α_1 that had been subjected to 3 hours of α -chymotryptic digestion was fractionated on a Waters Delta-Pak C18 column. The peaks correspond to the following peptides: (1) thymosin $\alpha_1(17-28)$; (2) thymosin $\alpha_1(15-28)$; (3) thymosin $\alpha_1(1-14)$; (4) thymosin α_1 ; (5) thymosin $\alpha_1(1-16)$.

TABLE V

Amino Acid Composition of Peptides Recovered
in the α -Chymotryptic Digestion of Thymosin α_1

<u>Peptide 1</u> (17-28) [@]			<u>Peptide 2</u> (15-28)			<u>Peptide 3</u> (1-14)		
<u>Residue</u>	<u>No.</u>	<u>Observed</u>	<u>Residue</u>	<u>No.</u>	<u>Observed</u>	<u>Residue</u>	<u>No.</u>	<u>Observed</u>
Asp	1.35	(1)*	Asp	1.87	(2)	Asp	2.17	(2)
Glu	5.56	(5)	Glu	6.23	(5)	Glu	1.52	(1)
Ser	0.69	(0)	Ala	0.98	(1)	Ser	2.79	(3)
Thr	0.25	(0)	Val	1.35	(2)	Thr	2.70	(3)
Ala	1.31	(1)	Leu	1.02	(1)	Ala	1.98	(2)
Val	1.52	(2)	Lys	2.55	(3)	Val	0.87	(1)
Lys	2.26	(3)				Ile	0.93	(1)
						Lys	1.03	(1)

<u>Peptide 4</u> (1-28)			<u>Peptide 5</u> (1-16)		
<u>Residue</u>	<u>No.</u>	<u>Observed</u>	<u>Residue</u>	<u>No.</u>	<u>Observed</u>
Asp	4.68	(4)	Asp	2.69	(3)
Glu	7.53	(6)	Glu	2.05	(1)
Ser	3.28	(3)	Ser	2.70	(3)
Thr	2.93	(3)	Thr	2.41	(3)
Ala	2.99	(3)	Ala	1.93	(2)
Val	2.01	(3)	Val	1.34	(1)
Ile	0.83	(1)	Ile	0.93	(1)
Leu	0.97	(1)	Leu	1.00	(1)
Lys	2.77	(4)	Lys	0.96	(1)

[@]Numbers in parentheses represent the sequence of residues represented by the fragment isolated from thymosin α_1 .

*Numbers in parentheses represent the number of expected amino acid residues for the corresponding peptide.

thymosin α_1 , three two-dimensional NMR experiments were utilized. The DQF-COSY (Figure 16) and TOCSY spectra (Figures 17) were initially used to identify the amino acid spin systems present. A NOESY spectrum with a mixing time of 300 ms (Figure 18) was used in order to sequentially assign the amino acid spin systems within thymosin α_1 . All of the homonuclear two-dimensional NMR experiments of thymosin α_1 were acquired with the peptide dissolved in 30% (v/v) TFE- d_3 and 70% (v/v) H_2O . It was shown by CD that the peptide possesses the highest amount of helical structure under these solvent conditions.

Assignment of the NMR resonances of Ile11 and Leu16 were easily accomplished since there is only one copy of each residue in thymosin α_1 . Only one copy of Asn exists within thymosin α_1 , but the assignment of this residue was not as straightforward since the spin system of this residue is similar to that of Asp, of which there are three copies in the peptide.

The assignment of Ile11 and Leu16 was initiated by observing the pattern of methyl resonances in the high field region of the DQF-COSY spectrum (Figure 19). For Ile11 the δCH_3 - γCH_2 connectivities at 0.98, 1.29 ppm and 0.98, 1.61 ppm are characteristic of the spin system of this residue (Wüthrich, 1986). These resonances are an excellent starting point for assigning the remaining resonances of Ile11. All of the remaining resonances of Ile11 were then assigned using the DQF-COSY spectrum and confirmed using the TOCSY spectrum (Figure 20).

The two remaining high field cross peaks at 0.90, 1.72 ppm and 0.96, 1.72 ppm, in the high field region of the DQF-COSY spectrum, could then be assigned to the γCH_2 -

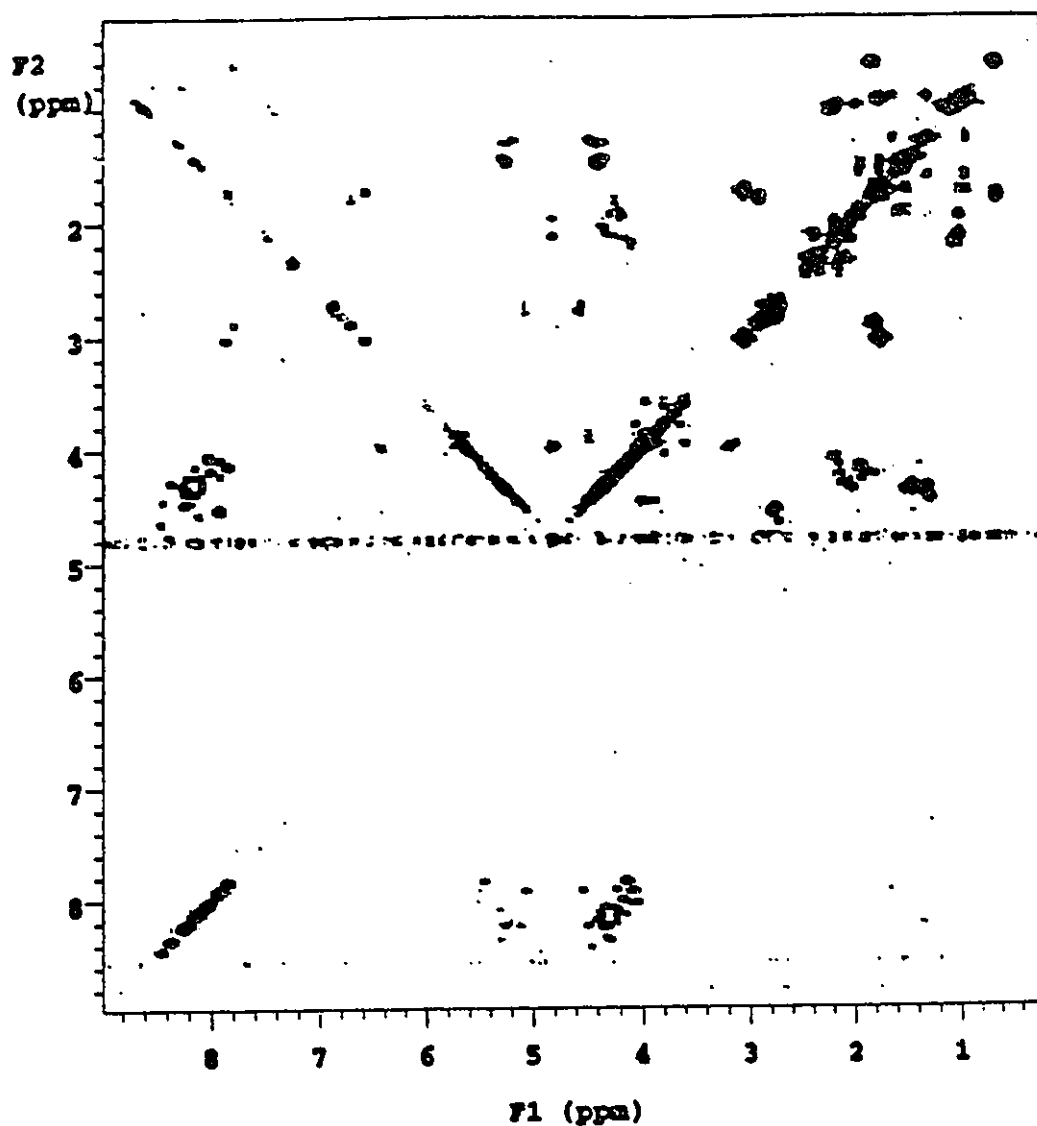


Figure 16. Phase-Sensitive DQF-COSY Spectrum of Thymosin α_1 . The sample for two-dimensional ^1H -NMR acquisition contained 1.93 mM of the peptide dissolved in 30% (v/v) TFE- d_3 and 70% (v/v) H_2O in 20 mM phosphate, 0.15 M NaCl, 0.5 mM DSS, pH 6.0. The spectrum was recorded at 500 MHz using spectral widths of 6000 Hz in both dimensions. A total of 2048 data points were collected in the t_2 domain and 128 t_1 increments were used. The spectrum was recorded at 298 K.

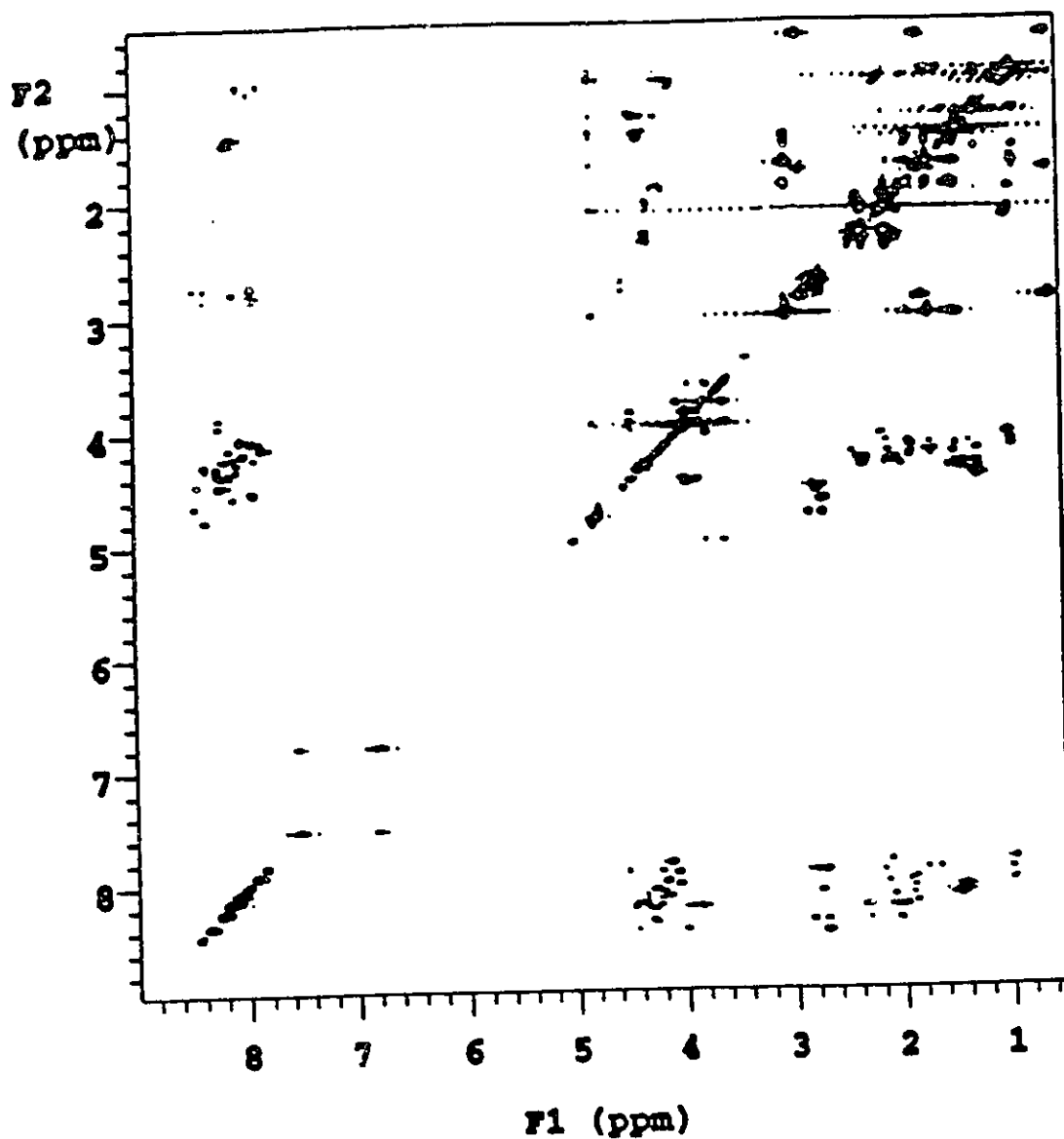


Figure 17. Homonuclear TOCSY Spectrum of Thymosin α_1 . The spectrum was recorded at 500 MHz using spectral widths of 6000 Hz in both dimensions. A total of 2048 data points were collected in the t_2 domain and 128 t_1 increments were used. The sample contained 1.93 mM of the peptide dissolved in 30% (v/v) TFE- d_3 and 70% (v/v) H_2O in 20 mM phosphate, 0.15 M NaCl, 0.5 mM DSS, pH 6.0.

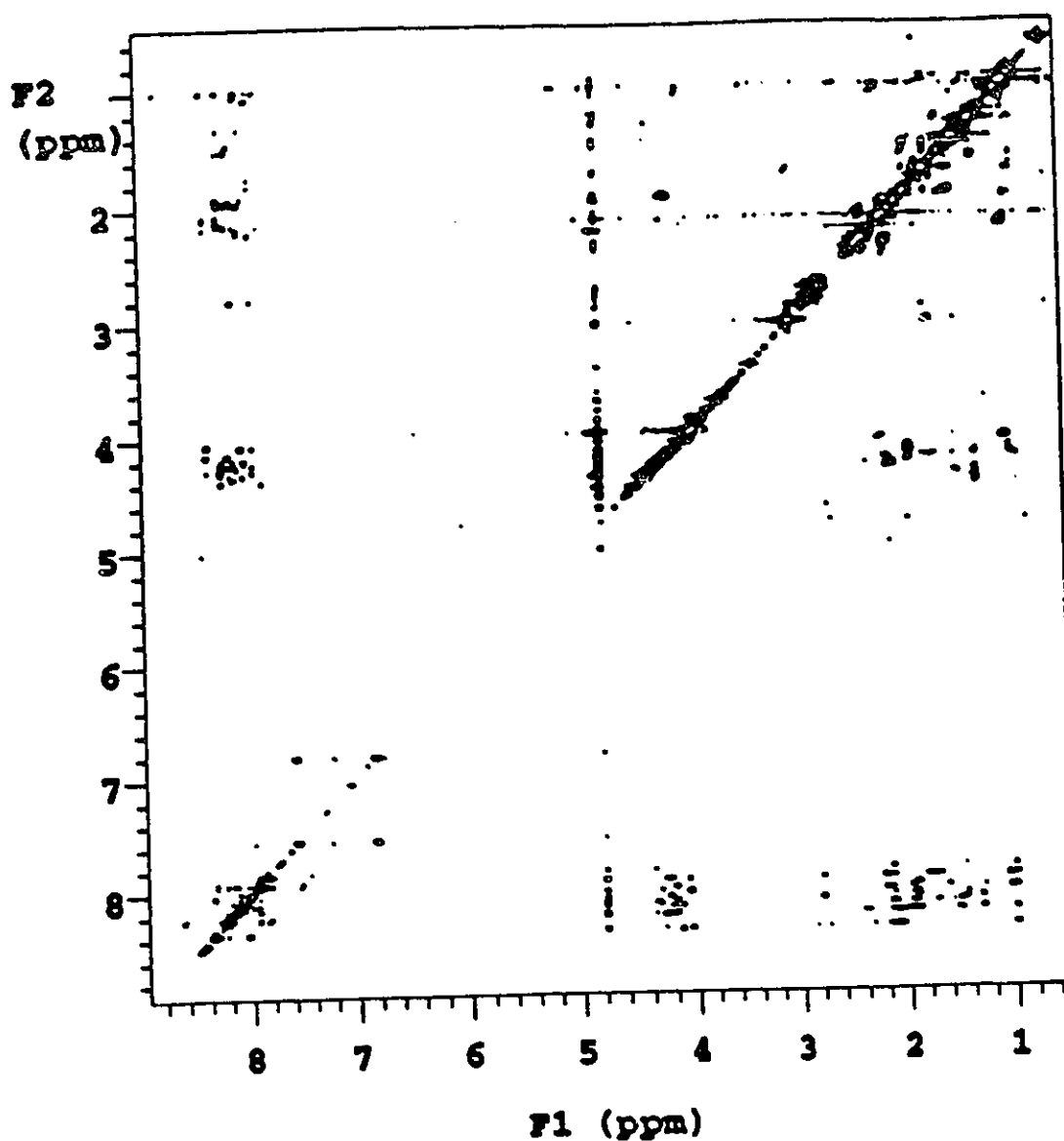


Figure 18. Phase-Sensitive NOESY Spectrum of Thymosin α_1 . The spectrum was recorded at 500 MHz with a mixing time of 300 ms. Two other NOESY spectra with mixing times of 75 and 150 ms were also acquired. The sample contained 1.93 mM of the peptide dissolved in 30% (v/v) TFE- d_3 and 70% (v/v) H_2O in 20 mM phosphate, 0.15 M NaCl, 0.5 mM DSS, pH 6.0.

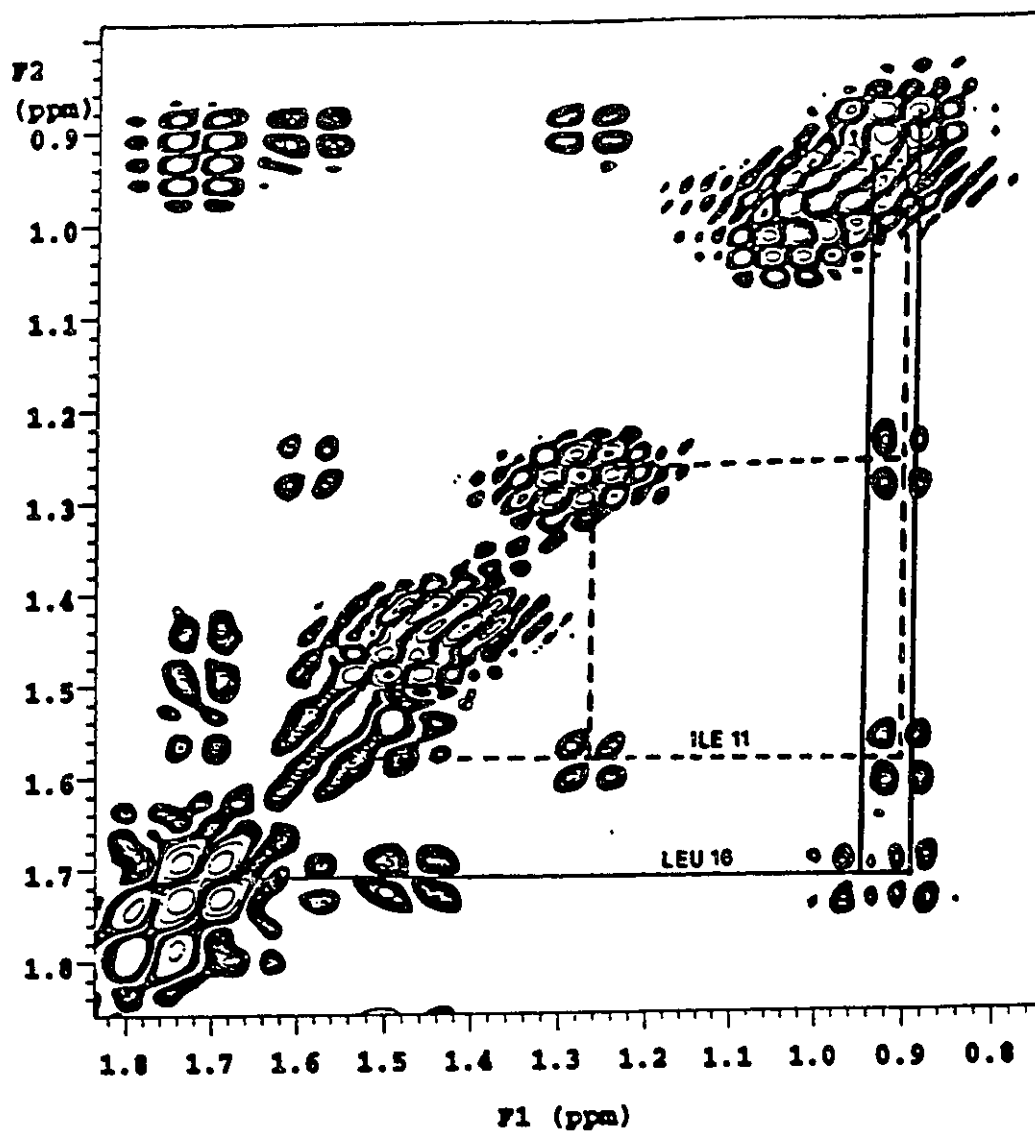


Figure 19. High-Field Region of the DQF-COSY Spectrum of Thymosin α_1 . The J-connectivities for Ile11 (---) and Leu16 (—) are shown. Sample conditions are as listed in Figure 16 for all spectra unless stated otherwise.

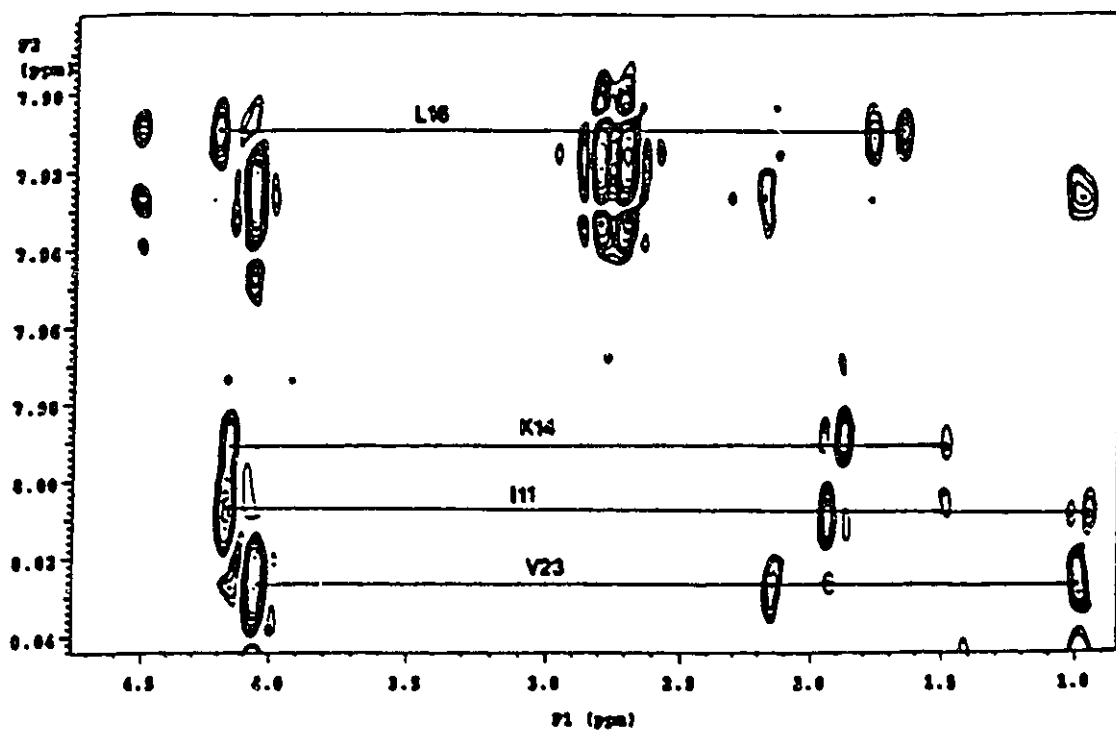


Figure 20. Assignment of the Low-Field Resonances of Isoleucine 11 and Leucine 16. The assignment of the NH- α CH (I,I) cross peaks for Ile11 (I11) and Leu16 (L16) are shown in the TOCSY spectrum of the peptide. Also shown are the resonances belonging to Lys14 (K14) and Val23 (V23).

δ CH₃ cross peaks of Leu16 (Figure 19). The remaining resonances of Leu16 could be assigned using the DQF-COSY and TOCSY spectra (Figure 20).

The remaining high field cross peaks in the DQF-COSY spectrum of the peptide belong to the γ CH₃- β CH cross peaks of the three Val residues. The α CH and NH resonances of the three Val residues were assigned at (7.84, 4.13 ppm), (7.93, 4.07 ppm) and (8.04, 4.06 ppm). Valine 22 and Val23 were sequence-specifically assigned using the α CH-NH(i,i+1) connectivity between these two residues at 4.07, 8.04 ppm (Figure 21) and the NH-NH(i,i+1) cross peak at 7.93, 8.04 ppm. This remaining α CH-NH cross peak at 7.84, 4.13 ppm is assignable to Val5. The complete assignment of the resonances of the Val residues is shown in the TOCSY spectrum in Figure 22.

Aspartic acid 6 (8.37, 4.46 ppm) was assigned via the α CH-NH, γ CH₃-NH and NH-NH (Figure 23) NOESY cross peaks with Val5. The NH proton of Asp6 could be seen in the NOESY spectrum, but the α CH resonance was assigned from the TOCSY spectrum where its position was more easily observed.

Alanine 4 (8.14, 4.37 ppm) was sequentially assigned through a NH-NH(i,i+1) NOESY cross peak with Val5 at 8.13, 7.84 ppm (Figure 23). The remaining resonances belonging to Ala4 were assigned from this initial assignment. The α CH-NH(i,i+1) and β CH-NH(i,i+1) cross peaks between Ala4 and Val5 at 4.36, 7.84 ppm and 1.45, 7.84 ppm, respectively, were also observed.

Alanine 3 (8.11, 4.34 ppm) could be assigned by using the α CH-NH(i,i+1) connectivity with Ala4 at 4.34, 8.14 ppm (Figure 24). The remaining Ala resonances

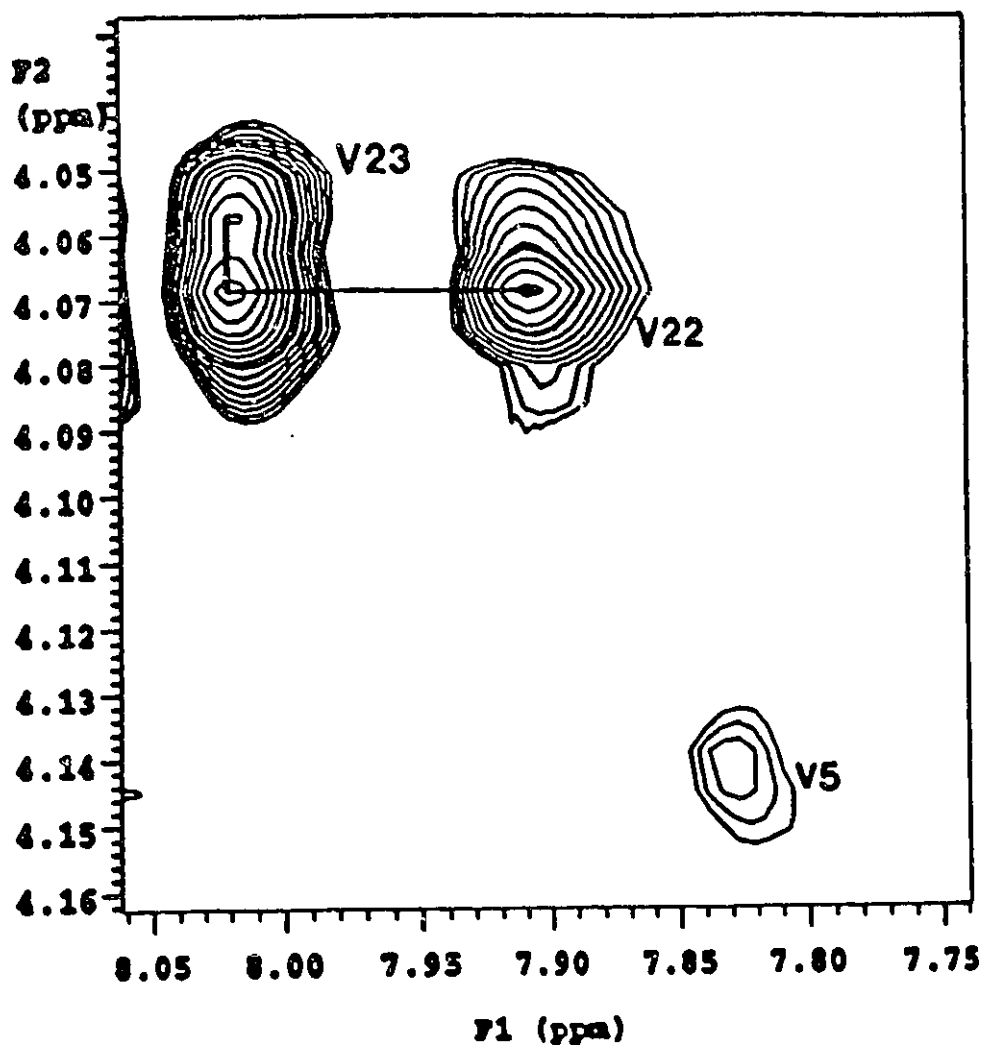


Figure 21. Sequence-Specific Assignment of the Valanyl Residues of Thymosin α_1 . The contour plot shows the α CH-NH (i,i+1) connectivity observed between Val22 and Val23 in the fingerprint region of the NOESY spectrum of the peptide. No connectivities between Val5 and the other Val residues were observed.

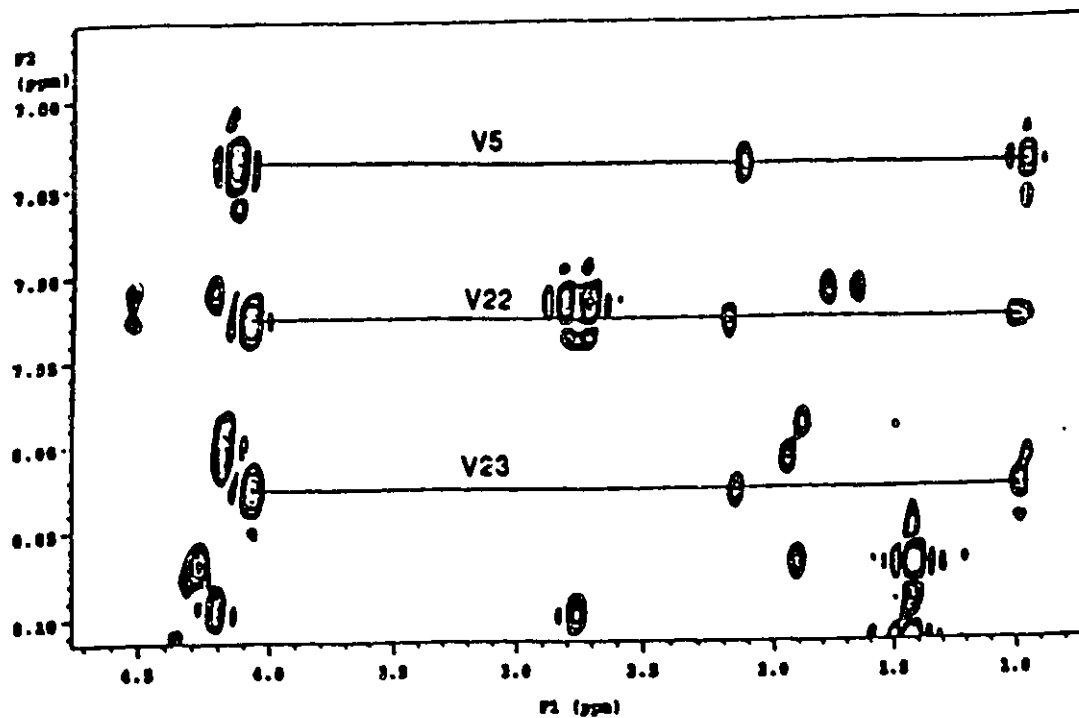


Figure 22. Assignment of the Side Chain Resonances of the Valanyl Residues of Thymosin α_1 . The α H, β CH₂ and γ CH₃ resonances belonging to the three valanyl residues in the peptide are shown in the TOCSY spectrum of thymosin α_1 .

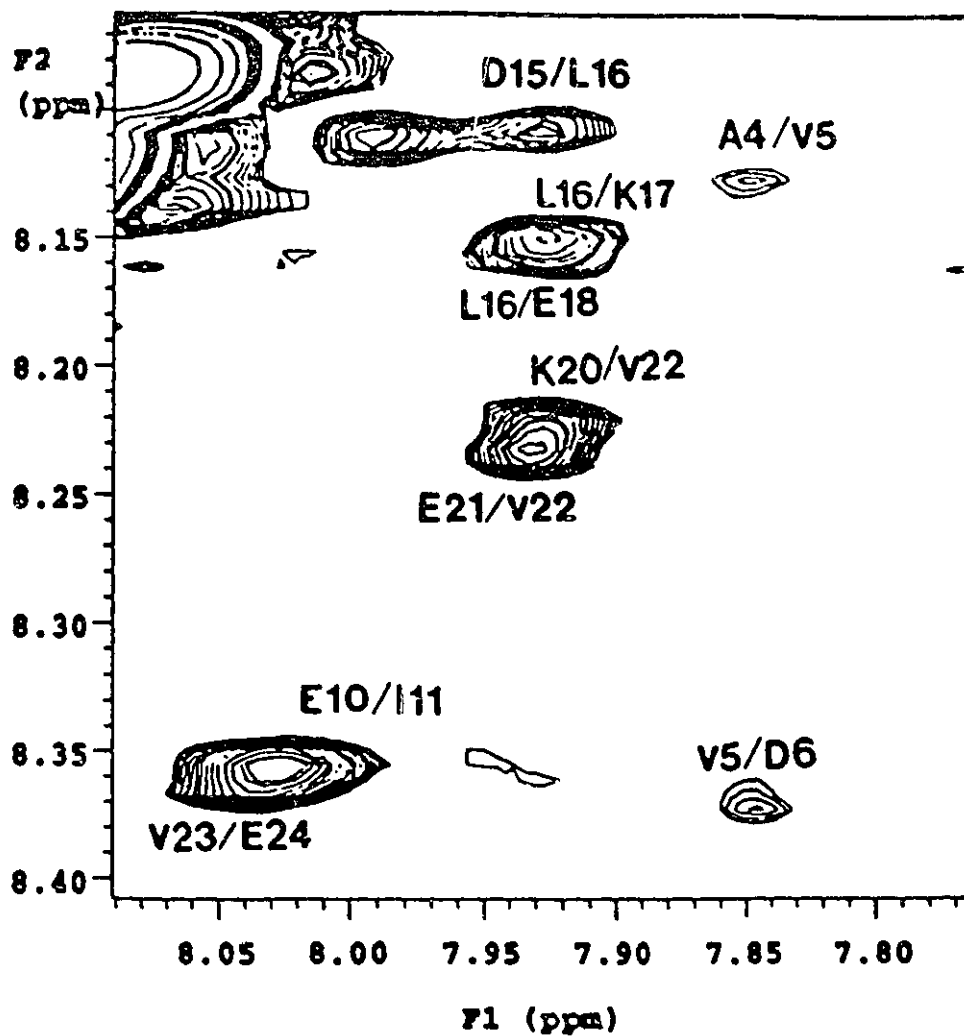


Figure 23. Amide Region of the NOESY Spectrum of Thymosin α_1 . The above region of the NOESY spectrum shows the NH-NH (i,i+1) connectivities between A4/V5, V5/D6, E10/E11, D15/L16, L16/K17, E21/V22 and V23/E24. Two NH-NH (i,i+2) connectivities between L16/E18 and K20/V22 are also shown.

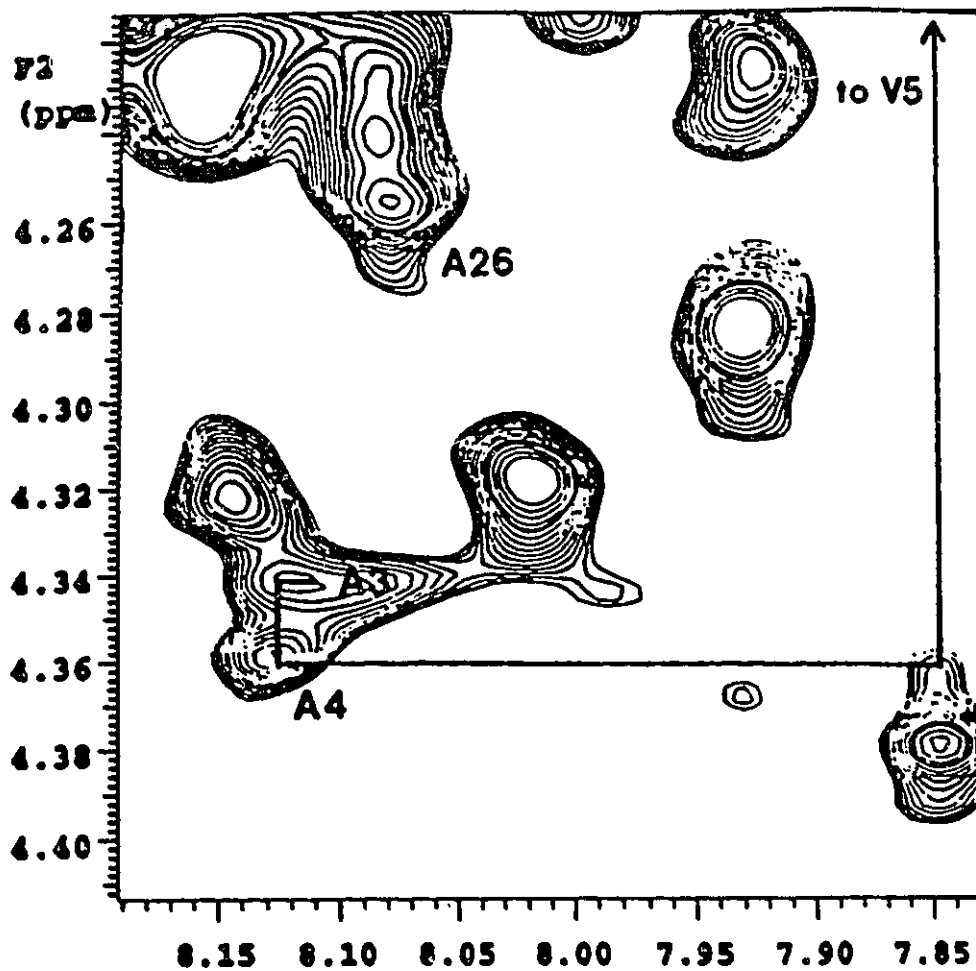


Figure 24. Sequence-Specific Assignment of the Alanyl Residues of Thymosin α_1 . The contour plot of the NOESY spectrum shows the $\alpha\text{CH-NH}$ ($i,i+1$) connectivity observed between Ala3 and Ala4. The $\alpha\text{CH-NH}$ ($i,i+1$) connectivity between Ala4 and Val5 is also displayed.

were assignable to Ala26 (8.06, 4.28 ppm). Alanine 26 showed no observable connectivities to the other two Ala residues (Figure 24).

Glutamic acid 24 (8.35, 4.27 ppm) was assigned from the NOESY cross peak with Val23 in the fingerprint region of the spectrum (4.27, 8.04 ppm). The NH-NH (Figure 23) and $\gamma\text{CH}_3\text{-NH}$ cross peaks between these residues were also observed at 8.35, 8.04 ppm and 2.35, 8.04 ppm, respectively. Glutamic acid 25 (8.24, 4.30 ppm) was assigned through its strong NH-NH cross peak (8.35, 8.24 ppm) with Glu24. The $\alpha\text{CH-NH}$ (4.27, 8.35 ppm), $\beta\text{CH-NH}$ (2.09, 8.24 ppm) and $\gamma\text{CH}_3\text{-NH}$ (2.33, 8.24 ppm) cross peaks between these two residues were also observed. A cross peak could be seen between Glu24 $\gamma\text{CH}_2\text{-Glu25 } \beta\text{CH}$ (2.33, 2.14 ppm) in the high field region of the spectrum. The assignment of the resonances belonging to Glu10, Glu18, Glu24, Glu25 and Glu27 is shown in the TOCSY spectrum in Figure 25.

Threonine 12 was sequentially assigned through its NOESY connectivity with Ile11 (Figure 26). The $\alpha\text{CH-NH}$ cross peak at 4.19, 8.22 ppm between these two residues was observable in the fingerprint region, as was an NH-NH cross peak at 8.02, 8.22 ppm. A strong $\gamma\text{CH}_3\text{-NH}$ cross peak between these two residues was seen at 1.29, 8.22 ppm (Figure 26). Threonine 13 was assigned through its NH-NH, $\alpha\text{CH-NH}$, and $\delta\text{CH}_3\text{-NH}$ (Figure 25) NOESY connectivities with Thr12. Lysine 14 was sequentially assigned through its $\delta\text{CH}_3\text{-NH}(i,i+1)$ cross peak with Thr13 at 1.31, 7.99 ppm (figure 26). Aspartic acid 15 was sequentially assigned through its $\alpha\text{CH-NH}(i,i+1)$ connectivity with Lys14 at 4.18, 8.11 ppm. The NH-NH($i,i+1$) (Figure 23) and $\beta\text{CH-NH}(i,i+1)$ (Figure 27) cross peaks between these two residues were also observed as was a weak $\gamma\text{CH}_2\text{-NH}$ cross peak. An $\alpha\text{CH-NH}$ cross peak between Asp15 and Leu16 was observed at

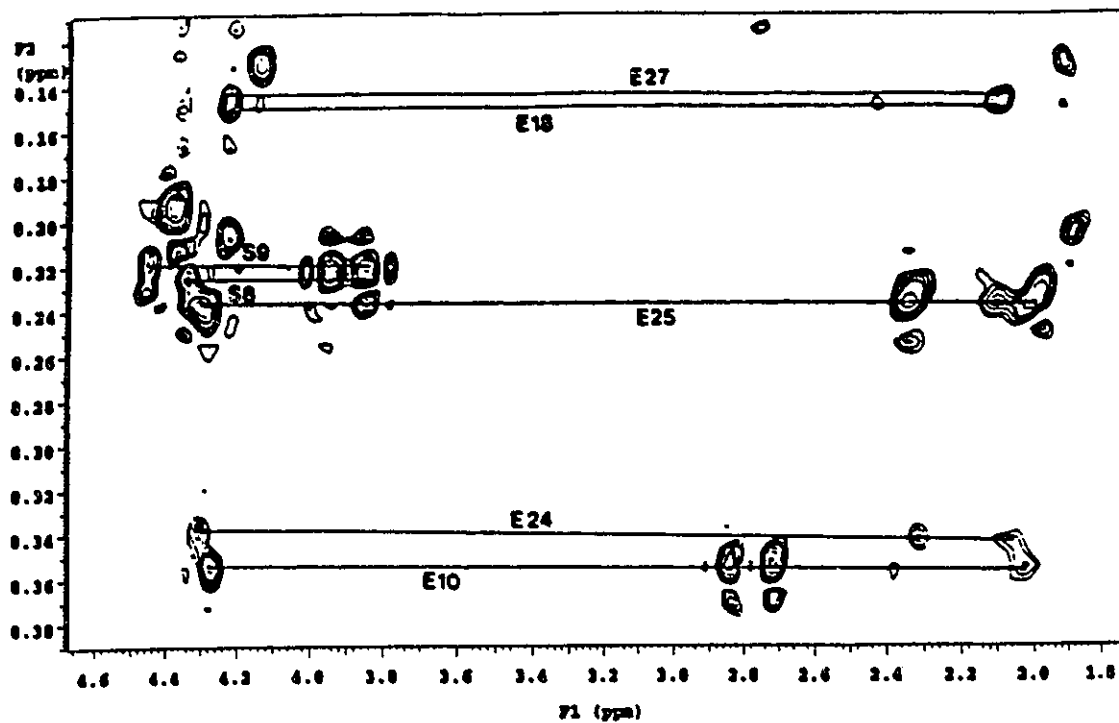


Figure 25. Assignment of the Side Chain Resonances of the Glutamyl and Seryl Residues of Thymosin α_1 . The assignment of the resonances belonging to Glutamyl (E) residues 10, 18, 24, 25 and 27 are shown along with Seryl (S) residues 8 and 9 in the TOCSY spectrum of the peptide. The residues were sequentially assigned using the NOESY spectrum.

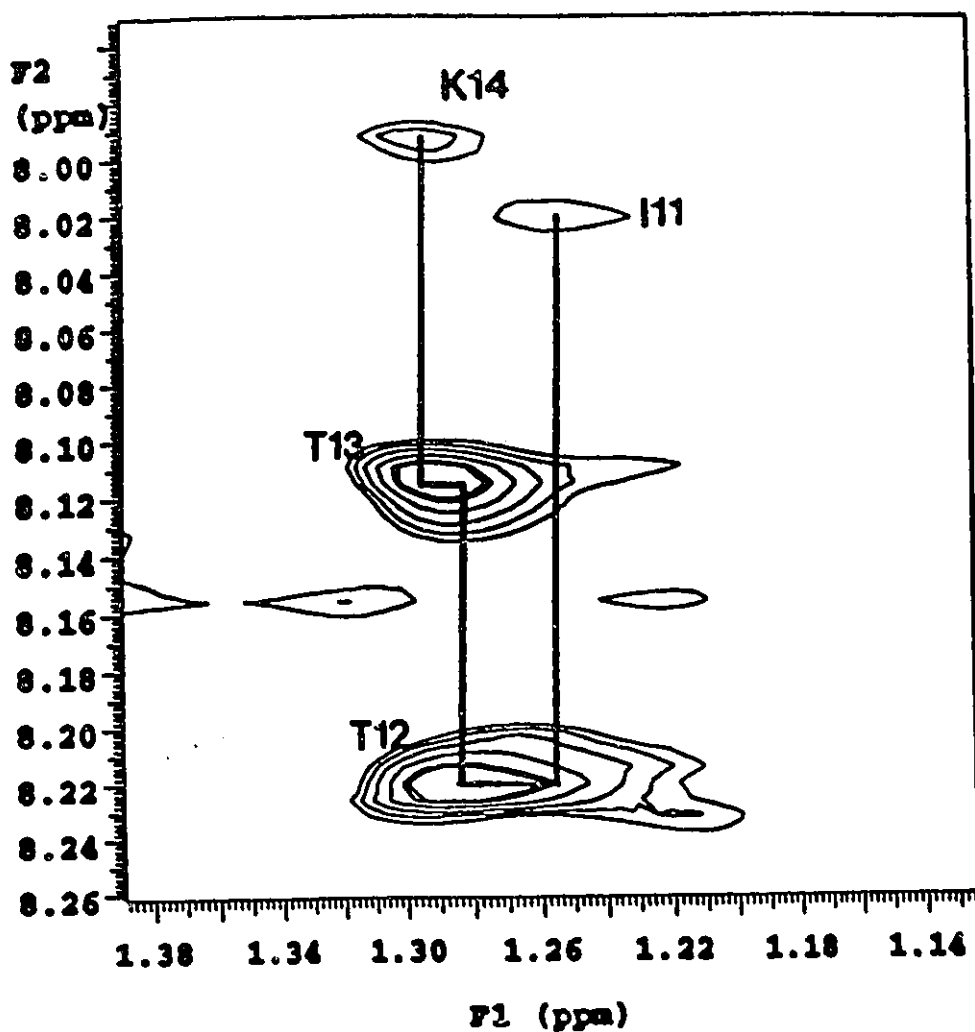


Figure 26. Sequence-Specific Assignment of Residues 11 to 14 of Thymosin α_1 . The contour plot shows the sequence-specific assignment of residues Thr12 (T12), Thr13 (T13) and Lys14 (K14) using Ile11 (I11) as a starting point. All connectivities are side chain to NH ($i, i+1$) connectivities between the residues.

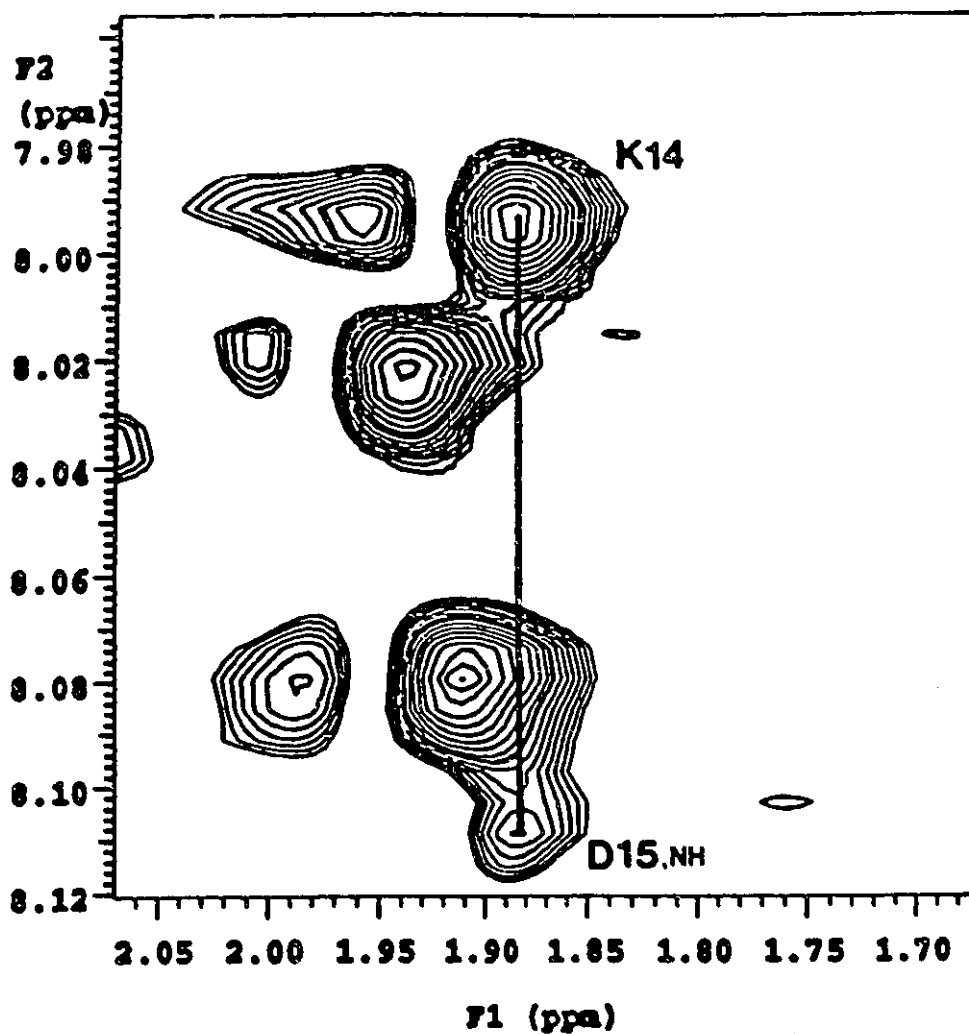


Figure 27. Sequence-Specific Assignment of Aspartic Acid 15 of Thymosin α_1 . The contour plot of the NOESY spectrum shows the BCH-NH (i,i+1) connectivity between Lys14 (K14) and Asp15 (D15) at 1.87, 8.11 ppm.

4.56, 7.92 ppm. A strong NH-NH cross peak was observed between these two residues at 8.11, 7.92 ppm (Figure 23).

Lysine 17 (8.15, 4.14 ppm) was initially assigned through a strong β CH-NH cross peak with Leu16. The NH-NH (Figure 23) and α CH-NH cross peaks between these two residues were also observed. Glutamic acid 18 (8.16, 4.23 ppm) was assigned through its α CH-NH connectivity with Lys17. Due to the similarity of their positions, no NH-NH cross peak could be observed for this pair of residues. Lysine 19 (8.07, 4.27 ppm) was assigned through its strong β CH-NH connectivity with Glu18 at 2.11, 8.07 ppm. The intensity of this cross peak strongly suggested an $i,i+1$ position between these two resonances. This is also the only position in the sequence of thymosin α_1 that a Glu residue is directly to the amino terminus of a Lys residue. After the initial β CH-NH cross peak between Glu18 and Lys19 was determined, the α CH-NH and NH-NH cross peaks were easily detected. Lysine 20 (8.22, 4.23 ppm) was the last Lys residue assigned. The α CH-NH and NH-NH cross peaks between Lys19 and Lys20 were observed. Glutamic acid 21 (8.23, 4.28 ppm) was assigned through the α CH-NH cross peak with Lys20. Glutamic acid 21 exhibited strong NH-NH (Figure 23) and α CH-NH cross peaks with Val22.

The assignment of the three Ser residues was not so straightforward as many expected cross peaks associated with these residues were either absent or very weak. Serine 8 (8.23, 4.39 ppm) and Ser9 (8.21, 4.47 ppm) were assigned through the α CH-NH cross peak between these two residues. The resonances assigned to Ser8 and Ser9 are shown in the TOCSY spectrum in Figure 25. No NH-NH cross peak was observed between these two residues in the NOESY spectra. The remaining Ser resonances are assignable to

Ser1 (8.44, 4.44 ppm). The assignment of the α CH-NH cross peaks for 24 of the 28 residues in thymosin α_1 is shown in the DQF-COSY spectrum in Figure 28. The complete sequence-specific assignments for the residues of thymosin α_1 are listed in Table VI.

3.5.b) Non-sequential NOE's

Numerous connectivities were identified between distant residues along the peptide chain, in addition to the sequential NOE cross peaks observed. In the fingerprint region medium-range α CH-NH($i,i+3$) cross peaks were observed between Leu16 α CH-Lys19 NH, Lys17 α CH-Lys20 NH, Lys19 α CH-Val22 NH, Glu21 α CH-Glu24 NH and Val22 α CH-Glu25 NH. Four medium range NH-NH($i,i+2$) NOESY cross peaks, Leu16 NH-Glu18 NH, Glu18 NH-Glu20 NH, Glu20 NH-Val22 NH and Val22 NH-Glu24 NH, were observed in the amide region of the NOESY spectrum (Figure 29). A $d_{NN}(i,i+3)$ cross peaks between Val23-Ala26 was also present in this region of the spectrum (Figure 29).

Other non-sequential $i,i+3$ cross peaks that were observed included; Lys19 β CH-Val22 NH, Lys19 γ CH₂-Val22 NH, Glu21 β CH-Glu24 NH and Val23 β CH-Ala26 NH cross peak. Two $i,i+4$ cross peaks were observed between Leu16 β CH-Lys20 NH and Glu18 β CH-Val22 NH. An $i,i+2$ cross peak was observed between the Lys20 α CH-Val22 NH cross peak at 4.23, 7.93 ppm. Figure 30 gives a summary of the sequential and medium-range NOEs observed between residues within thymosin α_1 .

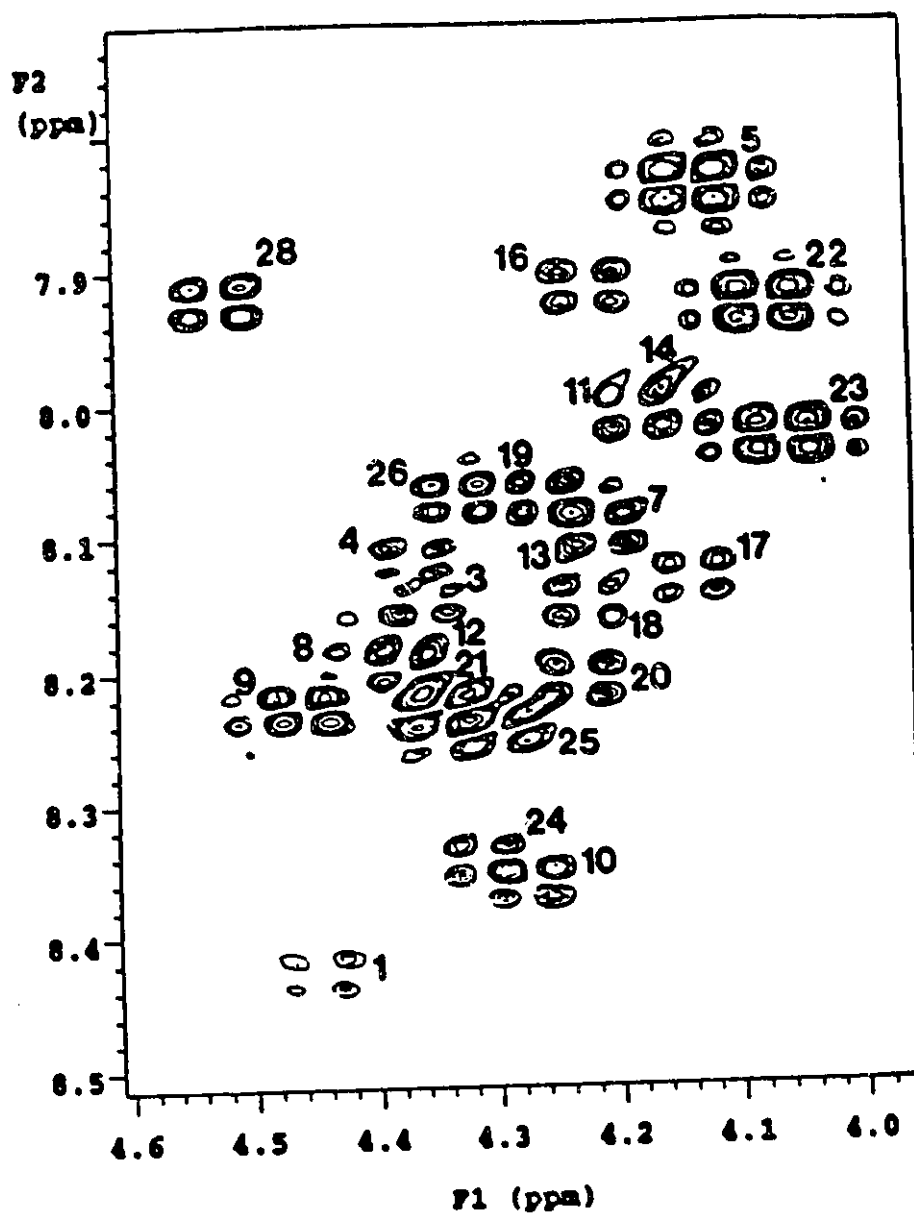


Figure 28. Fingerprint Region of the DQF-COSY Spectrum of Thymosin α_1 . The sequence-specific assignments of the α CH-NH (i,i) cross peaks of 24 of the 28 residues within the peptide are shown.

TABLE VI

Sequence-Specific Assignments of Thymosin α_1

residue	NH	α CH	β CH	others
Ser1	8.44	4.44	4.00	
Asp2	8.45	4.64	2.73, 2.69	
Ala3	8.11	4.34	1.48	
Ala4	8.14	4.36	1.45	
Val5	7.84	4.13	2.12	γ CH ₃ 0.98
Asp6	8.37	4.76	2.84, 2.72	
Thr7	8.10	4.18	4.33	δ CH ₃ 1.32
Ser8	8.23	4.39	3.94, 3.86	
Ser9	8.21	4.47	3.96, 3.87	
Glu10	8.37	4.32	2.12, 2.03	γ CH ₂ 2.42
Ile11	8.02	4.19	1.96	γ CH ₂ 1.61, 1.29, γ CH ₃ 0.98, δ CH ₃ 0.93
Thr12	8.22	4.32		δ CH ₃ 1.30
Thr13	8.12	4.21	4.33	δ CH ₃ 1.31
Lys14	7.99	4.18	1.91	γ CH ₂ 1.50, 1.52, δ CH ₂ 1.70, ϵ CH ₂ 2.99
Asp15	8.11	4.56	2.79	
Leu16	7.92	4.23	1.76	γ CH 1.72, δ CH ₃ 0.96, 0.90
Lys17	8.15	4.14	1.94	γ CH ₂ 1.49, δ CH ₂ 1.71, ϵ CH ₂ 3.02
Glu18	8.16	4.23	2.11	γ CH ₂ 2.44
Lys19	8.07	4.27	1.93	γ CH ₂ 1.51, δ CH ₂ 1.71, ϵ CH ₂ 3.02
Lys20	8.22	4.23	1.91	γ CH ₂ 1.50, δ CH ₂ 1.69, ϵ CH ₂ 2.99
Glu21	8.23	4.28	2.10, 1.96	γ CH ₂ 2.35
Val22	7.93	4.07	2.21	γ CH ₃ 1.06
Val23	8.04	4.06	2.18	γ CH ₃ 1.02
Glu24	8.35	4.27	2.09	γ CH ₂ 2.33
Glu25	8.24	4.30	2.14	γ CH ₂ 2.38
Ala26	8.08	4.28	1.42	
Glu27	8.14	4.23	2.09	γ CH ₂ 2.45
Asn28	7.92	4.52	2.81, 2.71	

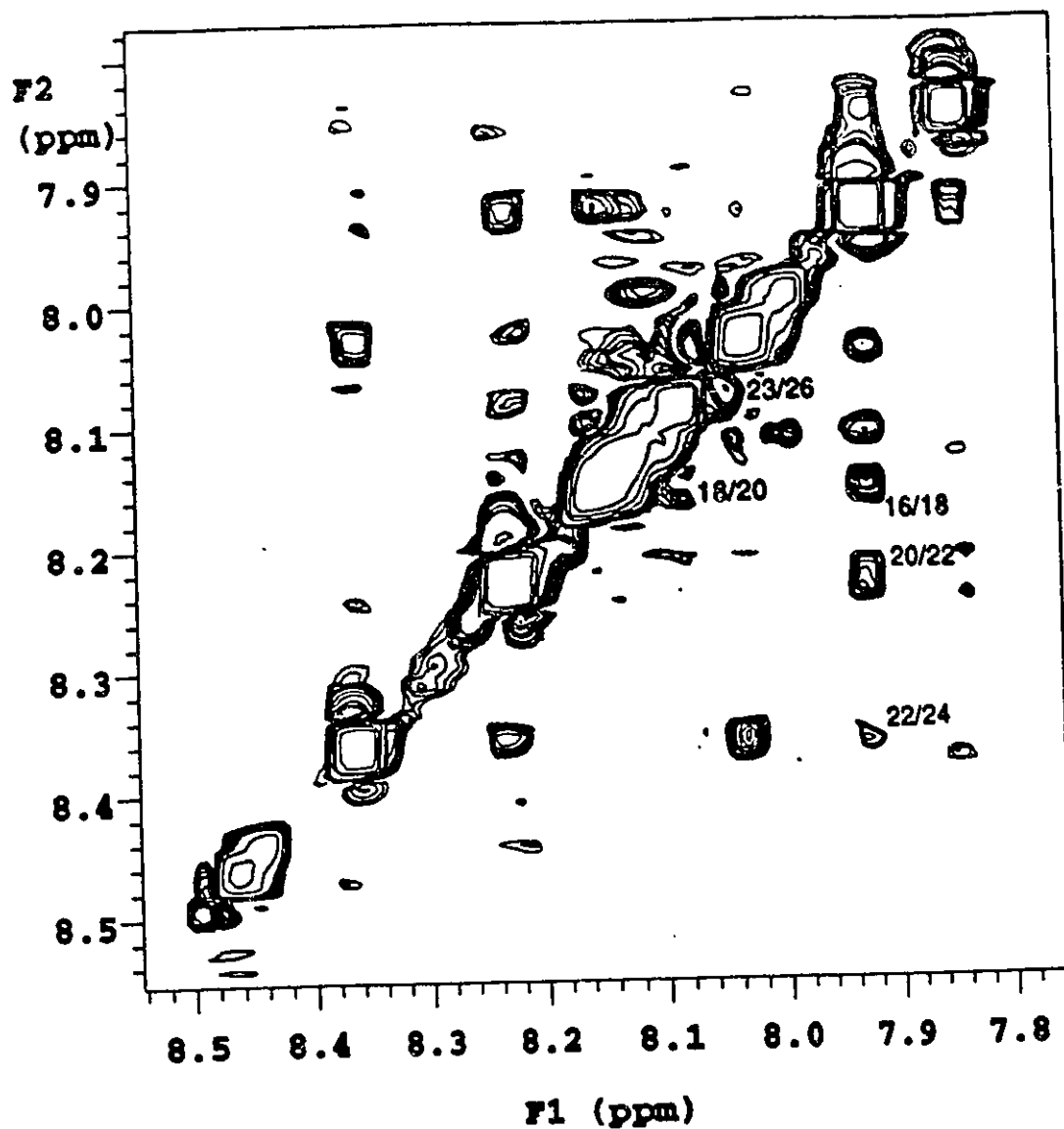


Figure 29. Medium-Range NOE Connectivities in the Amide Region of the NOESY Spectrum of Thymosin α_1 . The contour plot of the amide region of the NOESY spectrum shows medium-range NH-NH NOE connectivities observed between the amide protons of Leu16/Glu18, Glu18/Lys20, Lys20/Val22, Val22/Glu24, and Val23/Ala26.

Thymosin α_1 S D A A V D T S S E I T T K D L K K E K K E V V E E A E N
 1 5 10 15 20 25

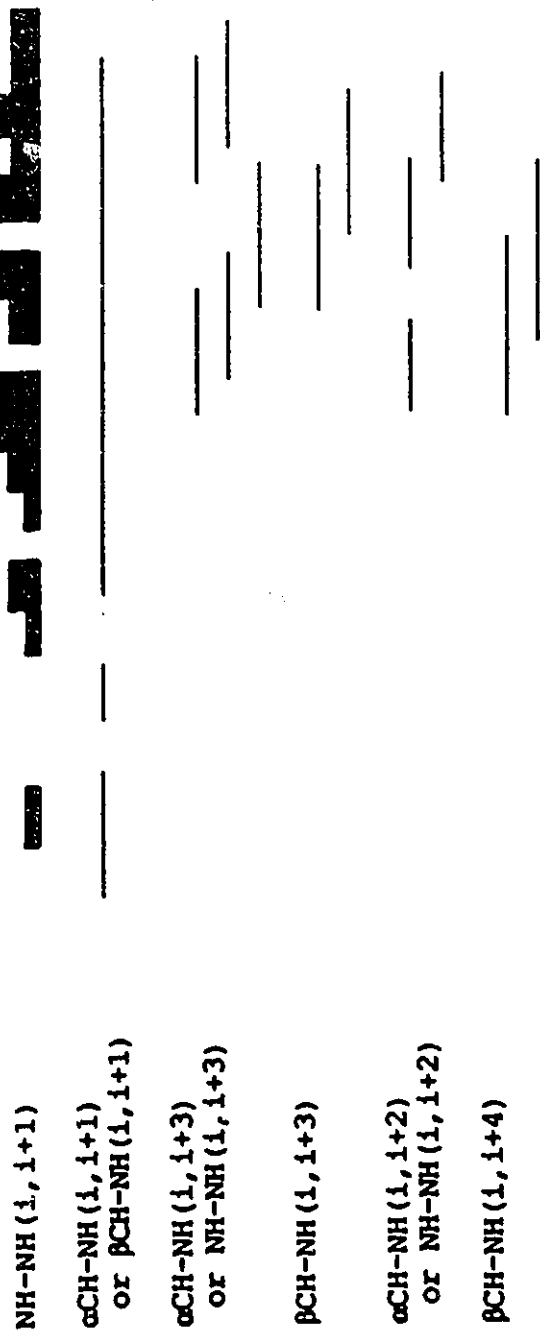


Figure 30. Summary of the Observed NOE Connectivities. A graphical summary of the sequential and non-sequential NOE connectivities observed in the NOESY spectrum of thymosin α_1 .

3.6) Chemical Shift Index for Thymosin α_1

The chemical shift values for all of the α H resonances of thymosin α_1 and the chemical shift values expected for these resonances in a random coil configuration are listed in Table VII. The chemical shift index is defined as the difference between the measured and random coil chemical shifts for a particular resonance (Wishart et al., 1991). Many of the α H protons are shifted upfield from their random coil positions, especially those within the carboxyl terminal half of the peptide. This upfield shift of the resonance position is indicative of these residues being within an α -helical conformation (Wishart et al., 1992).

3.7) Determination and Description of the Three-Dimensional Structure of Thymosin α_1

The calculation of the three-dimensional structure of thymosin α_1 was initiated using the primary structure of the peptide in an extended chain conformation. The pH of the system was set to 6.0 to correspond to the conditions of the two-dimensional 1 H-NMR acquisition. The starting structure was energy minimized until the root mean square deviation (RMSD) was 0.0001 Å. The final three-dimensional structure of thymosin α_1 was determined with a total of 134 NOE distance restraints and 128 NOE volume restraints. Figure 31 shows a distribution of the sequential and medium-range NOEs observed between residues within thymosin α_1 .

Thirty structures were generated using distance geometry, of which only eleven had acceptable convergence within the proposed helical region (residues 16-26).

TABLE VII

Observed versus Random Coil Chemical Shifts of the αH
Resonances of Thymosin α_1

<u>Residue</u>	<u>$\delta_{\text{obs}} \alpha\text{H}$</u>	<u>$\delta_{\text{coil}} \alpha\text{H}^*$</u>	<u>delta αH^{**}</u>
Ser1	4.44	4.50	-0.06
Asp2	4.64	4.76	-0.12
Ala3	4.35	4.35	0.00
Ala4	4.37	4.35	0.02
Val5	4.13	4.18	-0.05
Asp6	4.76	4.76	0.00
Thr7	4.18	4.35	-0.17
Ser8	4.39	4.50	-0.11
Ser9	4.47	4.50	-0.03
Glu10	4.28	4.29	-0.01
Ile11	4.19	4.23	-0.04
Thr12	4.32	4.35	-0.03
Thr13	4.21	4.35	-0.14
Lys14	4.18	4.36	-0.18
Asp15	4.56	4.76	-0.20
Leu16	4.23	4.38	-0.15
Lys17	4.14	4.36	-0.22
Glu18	4.23	4.29	-0.06
Lys19	4.27	4.36	-0.09
Lys20	4.23	4.36	-0.13
Glu21	4.28	4.29	-0.01
Val22	4.07	4.18	-0.11
Val23	4.06	4.18	-0.12
Glu24	4.27	4.29	-0.02
Glu25	4.30	4.29	0.01
Ala26	4.28	4.35	-0.07
Glu27	4.23	4.29	-0.06
Asn28	4.52	4.75	-0.23

*random coil chemical shift values taken from
 Wüthrich, 1986.

**delta αH = ($\delta_{\text{obs}} \alpha\text{H}$ - $\delta_{\text{coil}} \alpha\text{H}$)

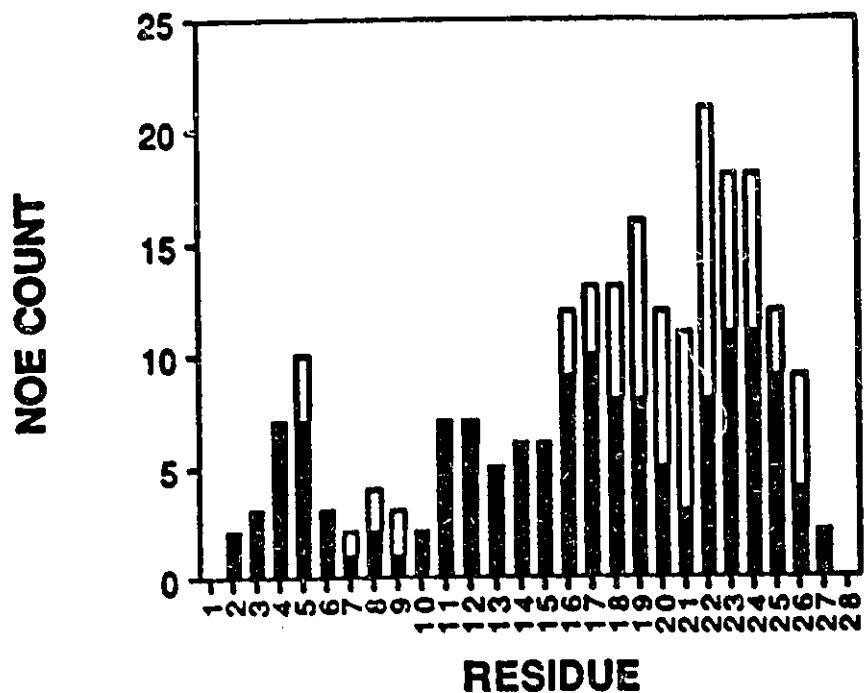


Figure 31. Plot of the Number of NOE Distance Restraints for Each Amino Acid in Thymosin α_1 . The number of sequential connectivities per residue is represented by closed columns and non-sequential connectivities by open columns. All constraints appear twice, once for each interacting residue. No Intra-residue connectivities were included in the graph.

Acceptable convergence in the helical region was set at a maximum RMSD of 2.0 Å between any two compared structures. Therefore the eleven structures that were selected had RMSD values less than 2.0 Å when the backbone atoms of residues 16 to 26 of the structures were superimposed on each other in a pairwise manner. Therefore each of the structures were compared to the remaining structures. All of the eleven structures had high RMSD values when the backbone atoms (N, C α , C and O) of all residues were superimposed. The average backbone RMSD between all pairs of structures for all residues is 5.78 ± 1.15 Å. This is a result of the lack of medium-range NOEs observed between residues within the sequences 1-4, 9-15 and 27-28. A stereoview of the superposition of the backbone atoms of all the residues is shown in Figure 32. It is obvious that no regular structure is obvious from superimposing the structures in this manner, although the density of atoms appears to be greater in the carboxyl terminal region than in the rest of the peptide.

When the backbone atoms of residues 16 to 26 are superimposed the \langle RMSD \rangle value is substantially lower. The average backbone RMSD between all pairs of structures for residues 16 to 26 is 0.86 ± 0.26 Å. A stereoview of the superposition of the backbone atoms of these residues is shown in Figure 33. Figure 33 shows residues 13 to 28 of thymosin α_1 with residues 16 to 26 superimposed. Visual inspection of the superimposed structures shows that residues 16 to 26 exhibit a helical-like structure.

Superimposing the backbone atoms of residues 5 to 8 gives an \langle RMSD \rangle value of 1.40 ± 0.37 Å. These residues comprise the putative turn region as determined by the presence of a small number of medium-range NOE measurements between residues within this sequence. A stereoview of residues 3 to 10 of thymosin α_1 with residues 5

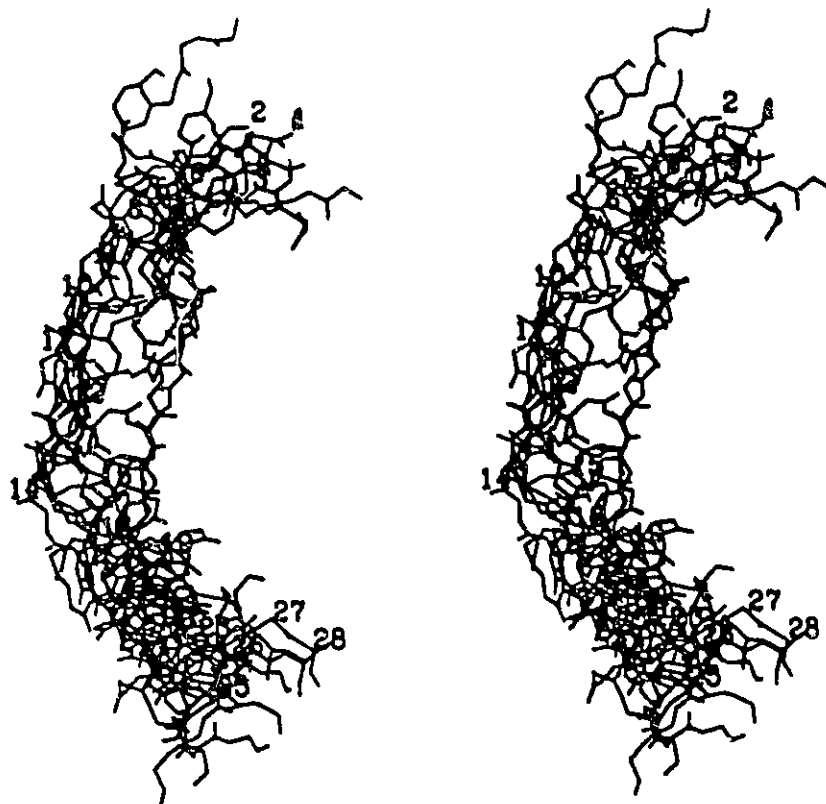


Figure 32. Stereoview of the Final Structures I. The eleven best structures calculated for the peptide are displayed with the backbone atoms (N, C α , C and O) of all residues superimposed.



Figure 33. Stereoview of the Final Structures II. The eleven best structures calculated for the peptide are displayed with the backbone atoms of residues 16 to 26 superimposed.

to 8 superimposed is shown in Figure 34. Visual inspection shows that there is some degree of order within residues 5 to 8 which comprise a turn-like structure.

The distances between the (i,i+3) backbone nitrogen atoms of the eleven best converged structures were measured. Table VIII gives a list of the average distance and the value of one standard deviation for each pair of atoms. A noticeable decrease in the distance is observed for the pairs of atoms within the proposed helical region (residues 16 to 26) as compared to those outside of this region. Most of the distances are within the range expected for an ideal α -helix (4.86 Å), and are much too low for those distances associated with an ideal β -strand (9.94 Å) or extended chain (10.88 Å). All of the average distances within the helical regions have low standard deviations associated with their averages. Within the proposed turn region the N,N(i,i+3) distances beginning from the first two atoms in the turn, Val5N and Asp6N, are 6.01 and 6.17 Å respectively. Again these distances are much lower than the same distances associated with a β -strand or random coil. In particular the distance between Asp6N and Ser9N (6.17 Å) is clearly within the range expected for a turn conformation of approximately 6.0 Å, and has a low standard deviation associated with the average of this distance.

The dihedral angles of the eleven best converged structures were measured and averaged. The presence of a helix between residues 16-26 is clear in the analysis of the backbone dihedral angles shown in Figure 35. The plot of ϕ and ψ versus the sequence of the peptide shows that residues 16-26 possess angles in the region characteristic of an α -helix. In an ideal α -helix the ϕ and ψ angles are equal to -57° and -47° ,

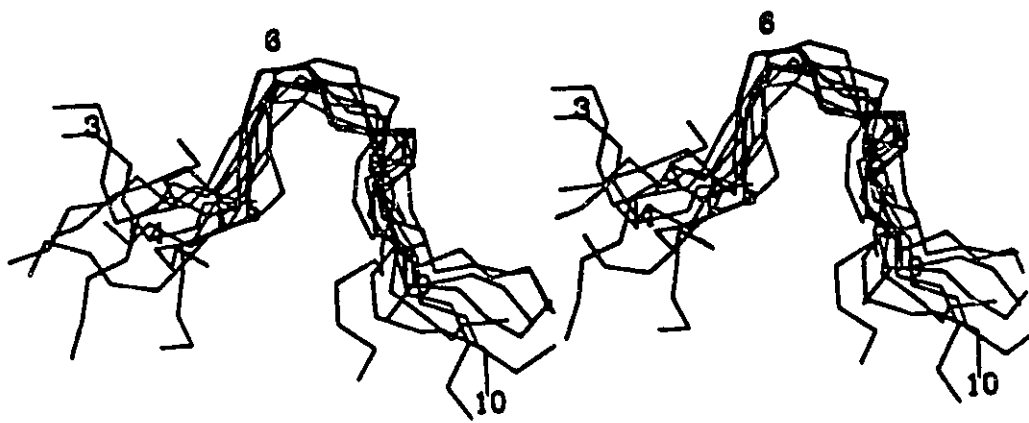


Figure 34. Stereoview of the Turn Region of Thymosin α_1 . The residues 3 to 10 of the eleven best structures are displayed with the backbone atoms of residues 5 to 8 superimposed.

TABLE VIII

Average Distances Between the (i,i+3) Backbone Nitrogen Atoms
of the Eleven Best Structures Generated for Thymosin α_1

<u>Residues</u>	<u>Distance (Å)</u>
Ser1/Ala4	8.17 (1.40)*
Asp2/Val5	9.01 (0.81)
Ala3/Asp6	8.34 (1.17)
Ala4/Thr7	8.03 (0.72)
Val5/Ser8	6.01 (1.00)
Asp6/Ser9	6.17 (0.34)
Thr7/Glu10	7.70 (0.98)
Ser8/Ile11	8.25 (0.94)
Ser9/Thr12	8.87 (1.21)
Glu10/Thr13	9.36 (0.80)
Ile11/Lys14	9.01 (1.21)
Thr12/Asp15	7.69 (1.07)
Thr13/Leu16	7.04 (1.18)
Lys14/Lys17	7.46 (0.73)
Asp15/Glu18	7.67 (0.33)
Leu16/Lys19	5.04 (0.56)
Lys17/Lys20	4.28 (0.36)
Glu18/Glu21	4.00 (0.43)
Lys19/Val22	3.69 (0.14)
Lys20/Val23	4.23 (0.24)
Glu21/Glu24	4.09 (0.17)
Val22/Glu25	4.87 (0.13)
Val23/Ala26	4.03 (0.17)
Glu24/Glu27	7.31 (0.70)
Glu25/Asn28	8.50 (0.99)

*standard deviation in parentheses.

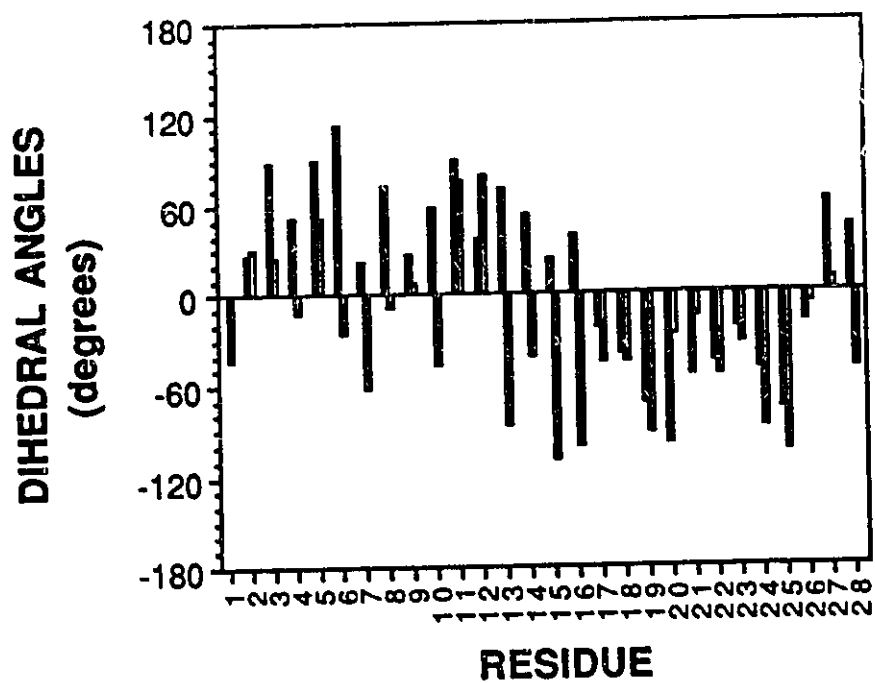


Figure 35. Analysis of the Dihedral Angles of Thymosin α_1 . The graph shows the average dihedral angles for all of the residues of the eleven best structures calculated for the peptide. The ϕ and ψ angles are shown by closed and open columns, respectively.

respectively (Creighton, 1993). The ϕ angle of Leu16 and the ψ angle of Ala26 are not characteristic for that expected for an α -helix, but this is not surprising as these two residues comprise the amino and carboxyl termini of the helical region. The presence of a turn starting at Val5 is not readily obvious from an examination of Figure 35.

A helical wheel depiction of the helical region of thymosin α_1 is shown in Figure 36. Examining the relative location of the side chains of the residues making up the helix, shows that this region is amphipathic. The four hydrophobic residues, Leu16, Val22, Val23 and Ala26, occupy one side of the helix, while the polar residues, Lys17, Glu18, Lys20, Glu21, Glu24 and Glu25, occupy the opposite side of the helix. One exception is the presence of Lys19 along the hydrophobic face of the helix. A closer examination of the division of the residues shows that the four Glu residues occupy an arc of approximately 133° along one face of the wheel, while the four hydrophobic residues occupy an arc of approximately 140° along the other face of the helix. Therefore the acidic and hydrophobic residues are tightly clustered along their respective sides of the helix.

3.8) Modelling the Interaction of Thymosin α_1 with Myosin Light Chain Kinase

The interaction between thymosin α_1 and skMLCK was modelled using the DOCKING module of the INSIGHTII software package manufactured by Biosym Technologies. The Ca^{2+} /CaM-binding domain of skMLCK was built into an α -helix using the BIOPOLYMER module of INSIGHTII. The peptide has been shown to exist in a helical conformation when complexed to Ca^{2+} /CaM (Ikura et al., 1992) and in a solution of 40% (v/v) TFE-d₃ (Zhang et al., 1993). The coordinates for the published structures of the Ca^{2+} /CaM-

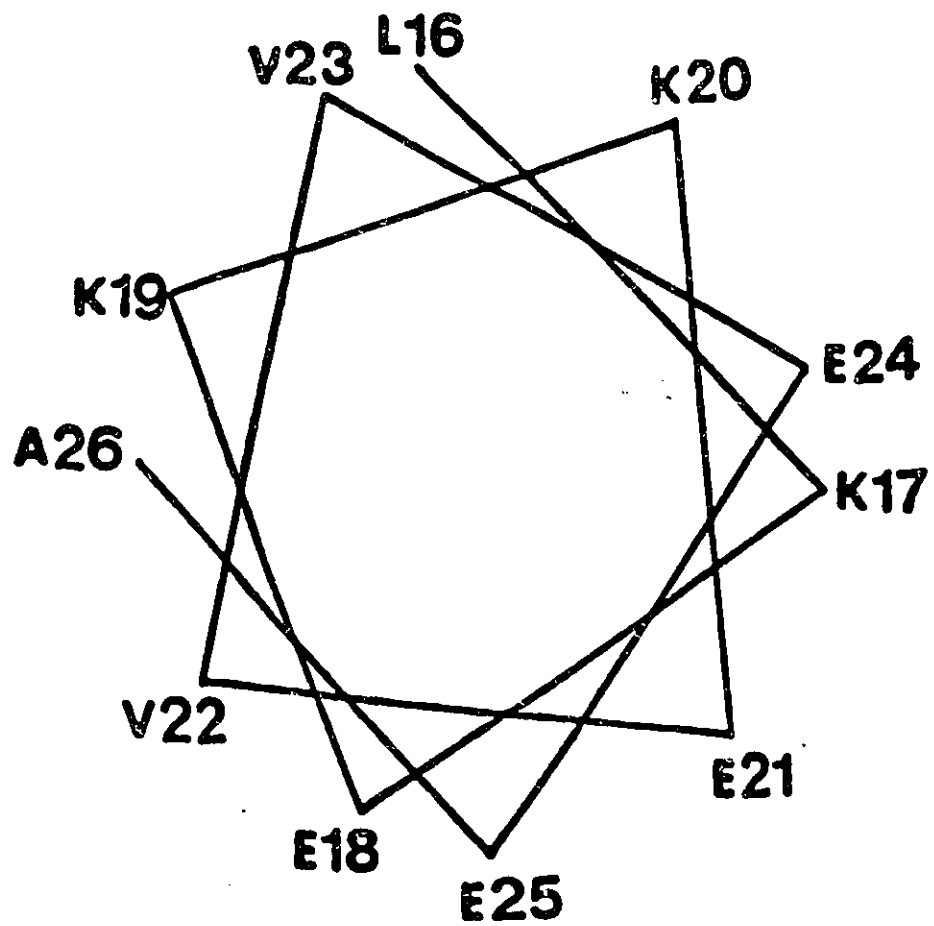


Figure 36. Helical Wheel of Thymosin α_1 . The helical wheel representation of residues 16 to 26 of the peptide is shown. Visual inspection shows that the helix is amphipathic.

binding domain of skMLCK were not available. The solution structure of thymosin α_1 showing the lowest consistent RMSD when compared to all of the other calculated structures above was used in the complex. The total intermolecular energy between the two peptides as they were brought close together was continuously calculated. The total energy measured was the sum of the van der Waals and coulombic energy between the two peptides.

To examine the possibility of an electrostatic interaction between the two peptides, residues Glu18, Glu21, Glu24 and Glu25, which lie along one side of the helical region of thymosin α_1 were aligned with the positively charged residues, Lys1, Arg2, Arg3, Lys5 and Lys6 at the amino terminal of the skMLCK peptide. The position of thymosin α_1 was altered relative to the skMLCK peptide while the total energy was monitored. When the lowest possible energy was obtained, the angles of the side chains of the residues that made intermolecular contacts of less than 6 Å were varied in order to attempt to find a lower energy system. No alteration in the backbone conformation of either peptide was made during the modelling study. The total energy of the system of intermolecular interactions possessing the lowest energy had a value of -1050.7 kcal/mol. Of this total energy -1059.7 kcal/mol was coulombic and 9.0 kcal/mol was van der Waals energy. Several short intermolecular interactions (<3.0 Å) were observed between the Glu residues of thymosin α_1 and the Lys and Arg residues of the skMLCK peptide (Figure 37). Residues Glu18, Glu21 and Glu24 of thymosin α_1 and Arg2, Lys5 and Lys6 of the skMLCK made particularly close contact. The stereoview diagram (Figure 38) of the electrostatic interaction model shows that the negatively and positively charged residues on the different peptides interlock in a zipper-like manner. A summary of the observed hydrogen bonds between the side chains of these residues is

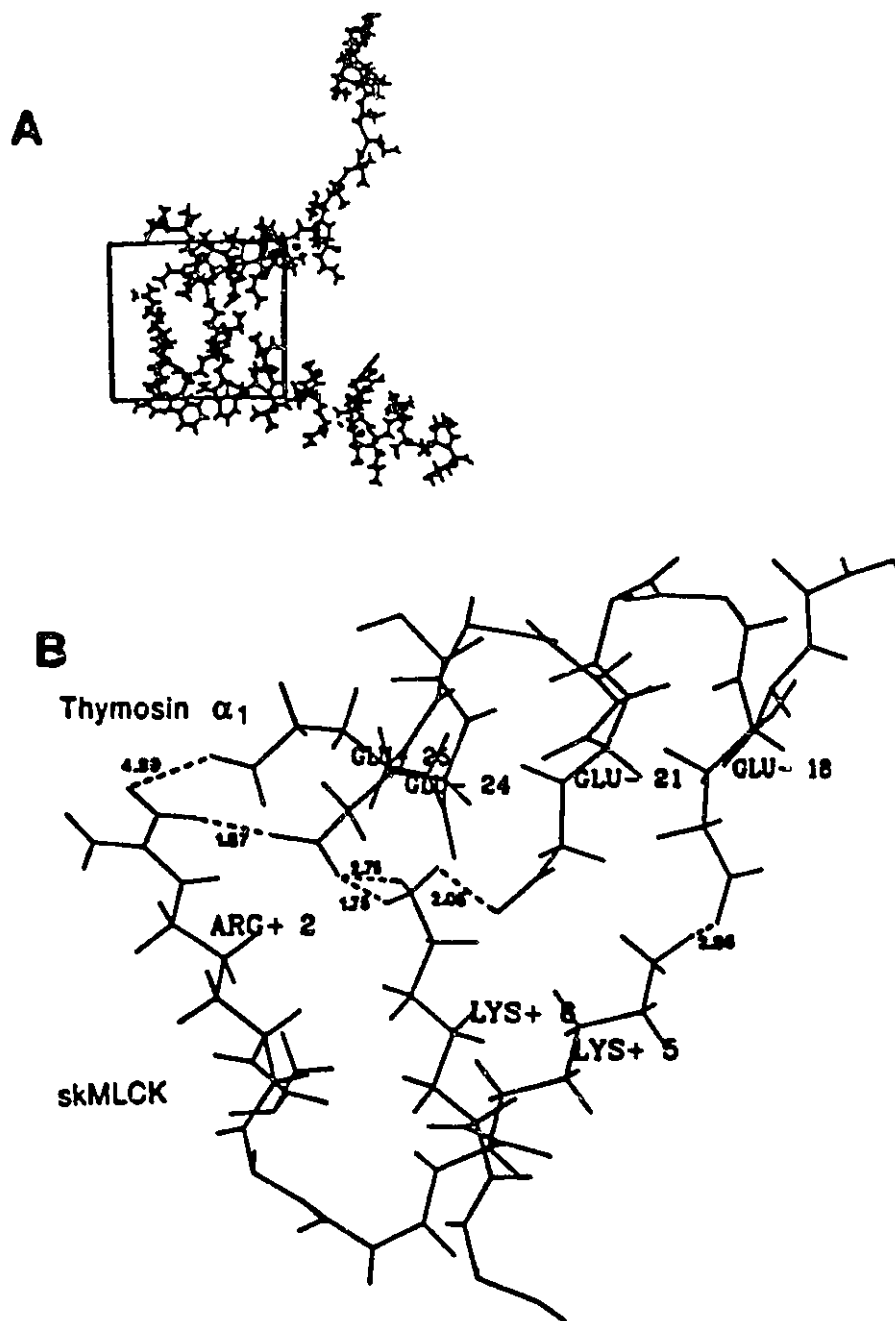


Figure 37. Electrostatic Model of the Interaction of skMLCK with Thymosin α_1 . The entire interaction between the two peptides is shown in (A), and an enlargement of the primary interacting regions is shown in (B).

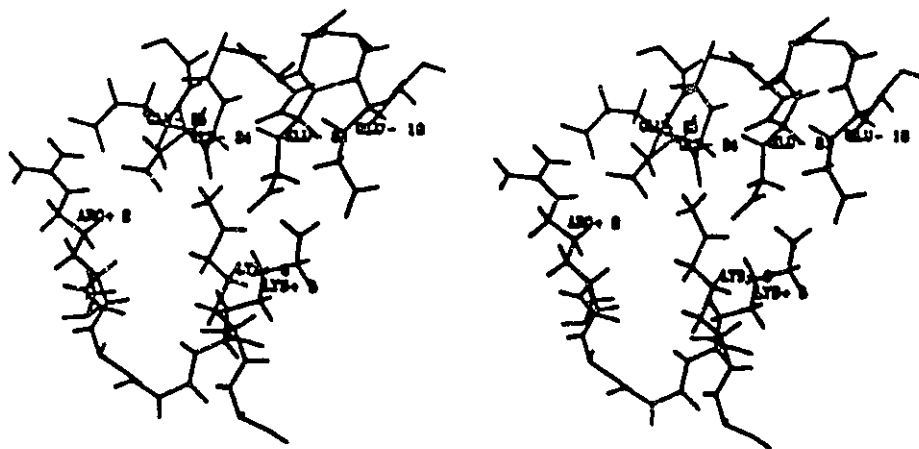


Figure 38. Stereoview of the Electrostatic Interactions Between skMLCK and Thymosin α_1 . The primary site of interaction between the Glu residues of thymosin α_1 and the basic residues of skMLCK is shown.

listed in Table IX.

To examine the possibility of the interaction between skMLCK and thymosin α_1 being hydrophobic in nature, the hydrophobic side of the helical region of thymosin α_1 was orientated so that it faced the large hydrophobic residues Trp4 and Phe8 of skMLCK. These two hydrophobic residues in skMLCK have been shown to be particularly important for the binding of CaM. Again several short intermolecular distances were observed between these two peptides as shown in Figure 39. The total energy of this system was -750.0 kcal/mol which is only 71% as low as the energy observed in the electrostatic model. A stereoview of the interaction between the two peptides (Figure 40) shows that Val23 does not participate in the hydrophobic interaction with Trp4 and Phe8 of skMLCK as it is oriented away from the region of interaction.

It has been shown that two thymosin α_1 related peptides, thymosin $\beta_4(1-39)$ and thymosin $\beta_4(16-38)$, are also high affinity stimulators of skMLCK (Galoyan *et al.*, 1992). The primary structure of thymosin β_4 is shown in Figure 41 (Low *et al.*, 1981). The solution structure of thymosin β_4 , a 43 amino acid residue peptide, in 50% hexafluoroisopropyl- d_2 alcohol is known (Zarbock *et al.*, 1990). Thymosin β_4 is made up of two helices comprising residues 4-16 and 30-40. In the first helical region of thymosin β_4 (residues 4-16) charged residues again predominate. There are four acidic residues (Asp5, Glu8, Glu10 and Asp13) as well as three basic residues (Lys11, Lys14 and Lys16). The second helical region of thymosin β_4 (residues 30-40) is dominated by charged and polar residues (Lys31, Glu32, Glu35, Gln36, Glu37, Lys38 and Gln39).

TABLE IX

List of the Hydrogen Bonds Observed in the Modelling
of the Interaction Between Thymosin α_1 and the
CaM-binding Domain of skMLCK

Atoms	Distance (Å)	Angle (N-H...O)
R2 HH11/E24 OE2	1.87	155.8°
R2 HH12/E25 OE1	4.89	63.9°
R2 HH12/E25 OE2	5.04	39.7°
K5 HZ1/E18 OE1	2.86	123.5°
K6 HZ1/E24 OE1	2.75	74.2°
K6 HZ2/E21 OE2	2.05	109.4°
K6 HZ3/E24 OE1	1.78	141.9°

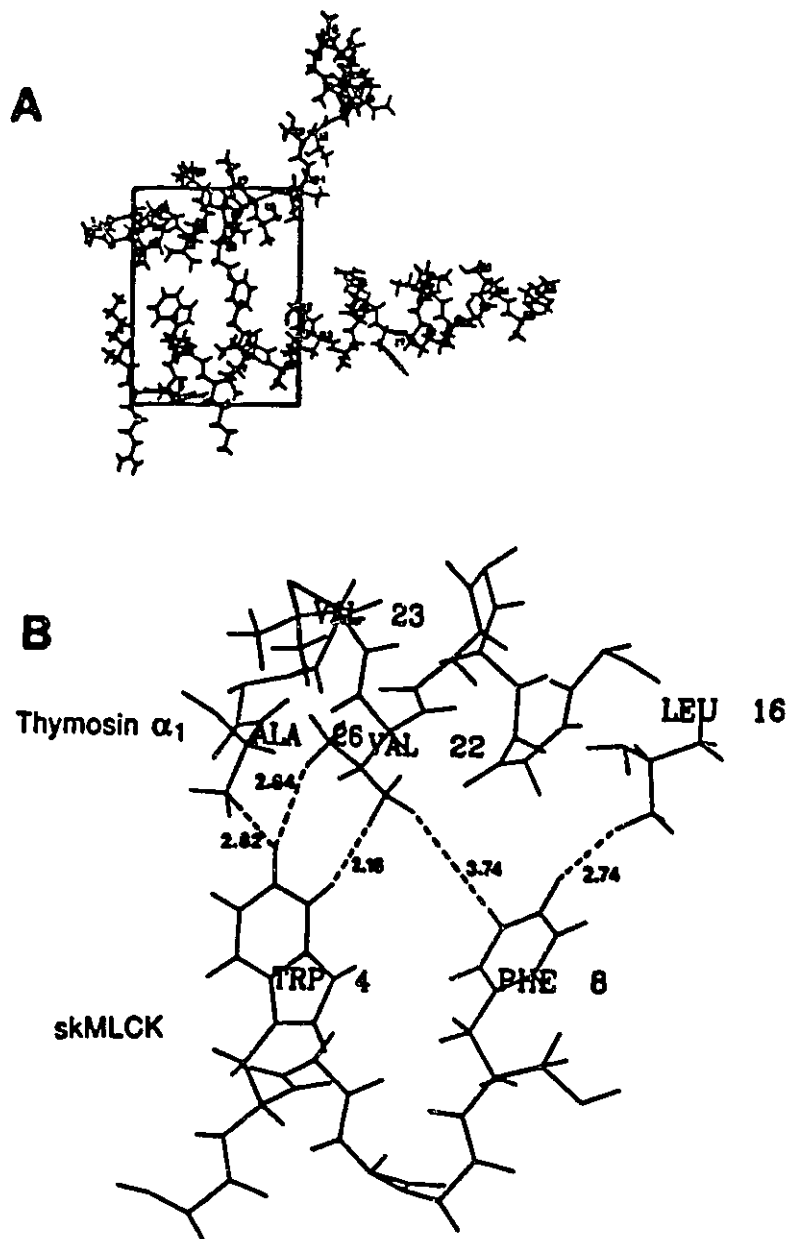


Figure 39. Hydrophobic Model of the Interaction of skMLCK with Thymosin α_1 .
 The entire interaction between the two peptides is shown in (A), and an enlargement of the primary interacting regions is shown in (B).

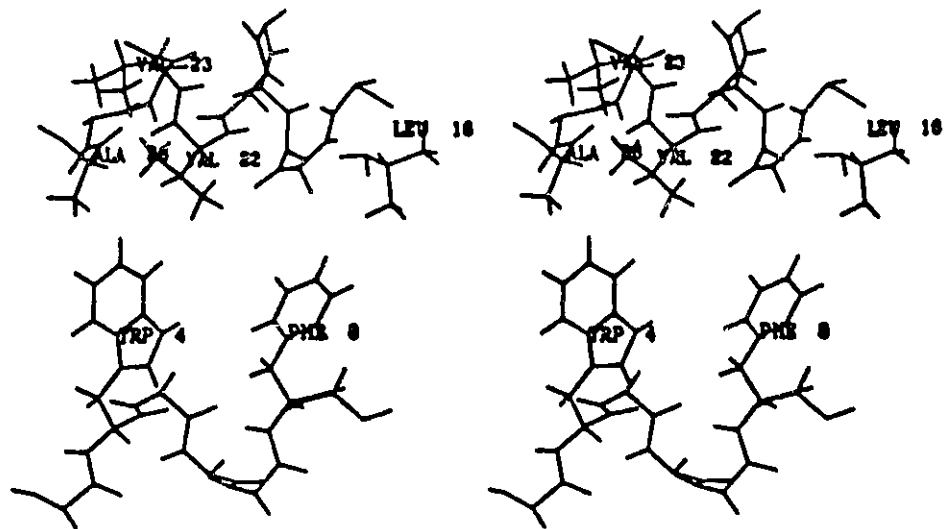


Figure 40. Stereoview of the Hydrophobic Interaction Between skMLCK and Thymosin α_1 . The primary site of interaction between the hydrophobic residues of thymosin α_1 (Leu16, Val22, Val23 and Ala26) and skMLCK (Trp4 and Phe8) is shown.

1	5	10
<u>Ser-Asp-Lys-Pro-Asp-Met-Ala-Glu-Ile-Glu</u>		
11	15	20
<u>Lys-Phe-Asp-Lys-Ser-Lys-Leu-Lys-Lys-Thr</u>		
21	25	30
<u>Glu-Thr-Gln-Glu-Lys-Asn-Pro-Leu-Pro-Ser</u>		
31	35	40
<u>Lys-Glu-Thr-Ile-Glu-Gln-Glu-Lys-Gln-Ala</u>		
41		
Gly-Glu-Ser		

Figure 41. The Primary Structure of Thymosin B4. The helical regions of the peptide, as observed in the solution structure (Zarbock *et al.*, 1990), are underlined. The sequence is taken from Low *et al.*, 1979.

The relative stimulating ability of skMLCK by the three thymosin peptides are in the order: thymosin $\beta_4(1-39)$ > thymosin $\beta_4(16-38)$ > CaM > thymosin α_1 . In the case of thymosin $\beta_4(1-39)$ and thymosin $\beta_4(16-38)$ the important region in the interaction of skMLCK would be expected to be within a sequence common to both peptides. This would involve the helical region comprised of residues 30-38. If this region is responsible for the activation of skMLCK it would then be appropriate to look for structural similarities between this region and the helical region within thymosin α_1 . In the helical wheel representation of thymosin $\beta_4(30-38)$ shown in Figure 42, polar residues Glu32, Glu35 and Gln36 lie along one face of the helix. Residues Glu32 and Glu35 are in analogous positions along the helix as residues Glu18 and Glu21 of thymosin α_1 . The helical region is definitely amphipathic, except for the case of Glu 37 which lies along the non-polar face of the helix.

The helical region of thymosin β_4 comprising residues 4-16 is less amphipathic than the previous helices examined (Figure 42). The boundaries between non-polar, basic, acidic and polar residues around the helix are not well-defined. No large areas of charge separation would be expected to predominate along any side of this helical region.

Hydrophobic interactions have been implicated in the binding of CaM to the binding peptide of smMLCK and skMLCK. In the structures of both complexes many possible sites of hydrophobic interactions were observed. Also seen though, were many possible ionic interactions between oppositely charged residues. Analyses of the hydrophobicities of the residues within the common helical segment of thymosin $\beta_4(1-39)$ and thymosin $\beta_4(16-38)$, shows that it is unlikely that hydrophobic interactions play a major role in its binding to MLCK since there is only one true hydrophobic residue in the sequence

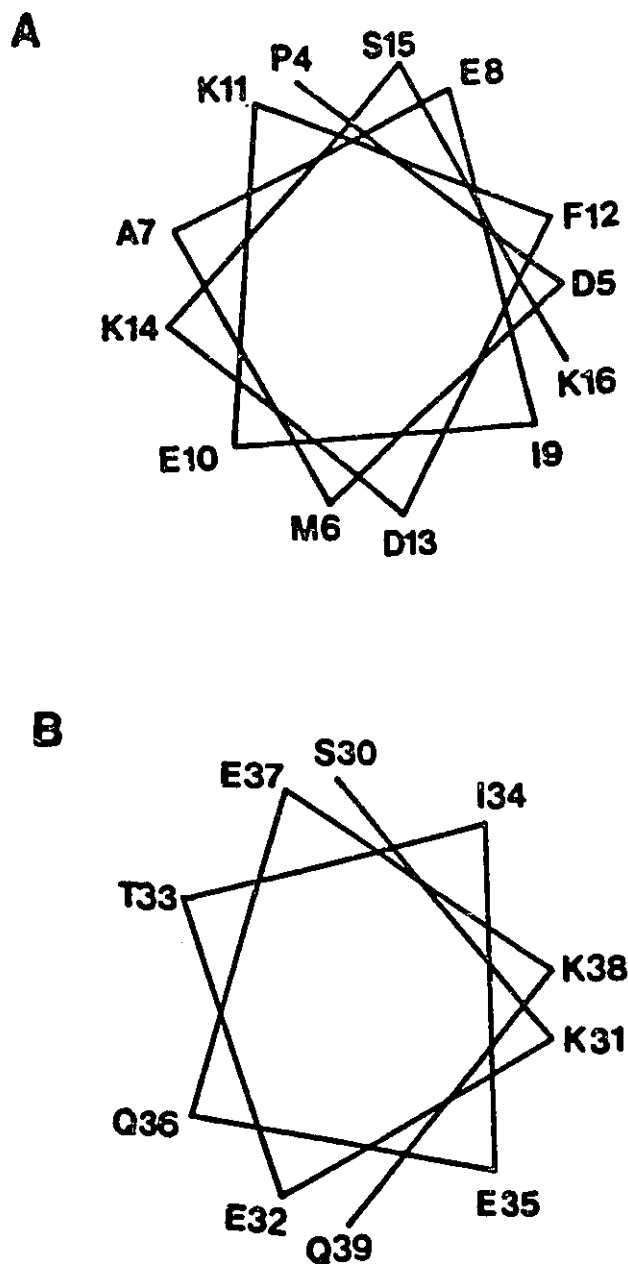


Figure 42. Helical Wheel of Thymosin $\beta_4(1-39)$. The two helical regions of thymosin $\beta_4(1-39)$ are shown. Wheel (A) depicts residue 4 to 16 while wheel (B) depicts residues 30-39. The helical wheel for thymosin $\beta_4(16-38)$ would contain residues 30 to 38 as depicted in wheel (B).

(Ile34). Although there is a conserved residue in the sequence of thymosin α_1 (Val23), it is unlikely that these residues are the dominant sites of interaction with MLCK, since they are on the opposite side of the helix and the electrostatic interactions would be expected to dominate.

Analyses of the hydrophobicity of the side chains of the residues making up the four MLCK-stimulating polypeptides (CaM, thymosin $\beta_4(1-39)$, thymosin $\beta_4(16-38)$ and thymosin α_1), show that CaM contains a much greater percentage of hydrophobic side chains than the other peptides. Figure 43 shows a plot of the hydrophathy of the side chains within CaM versus the residue number. Forty nine of the 148 side chains within the protein are hydrophobic (33.1%). Figure 44 shows a similar plot for thymosin α_1 , where only 8 out of 28 (28.6%) of the side chains of the residues are hydrophobic. The hydrophathy plot for thymosin $\beta_4(1-39)$ is shown in Figure 45. In this peptide only 7 of the 39 (17.9%) side chains are hydrophobic. Within helical regions common to both thymosin $\beta_4(16-38)$ and (1-39) (i.e. residues 30-38), there is a single residue with a hydrophobic side chain (Ile34). The analysis of the hydrophathies of the side chains of the thymosin peptides compared to the residues of CaM, show that the relative number of hydrophobic residues in the thymosin peptides is low compared to CaM. This result suggests that hydrophobic interactions would not be an important mode of interactions between the thymosin peptides and other molecules. In contrast hydrophobic interactions play a large role in the association of $\text{Ca}^{2+}/\text{CaM}$ with its target proteins.

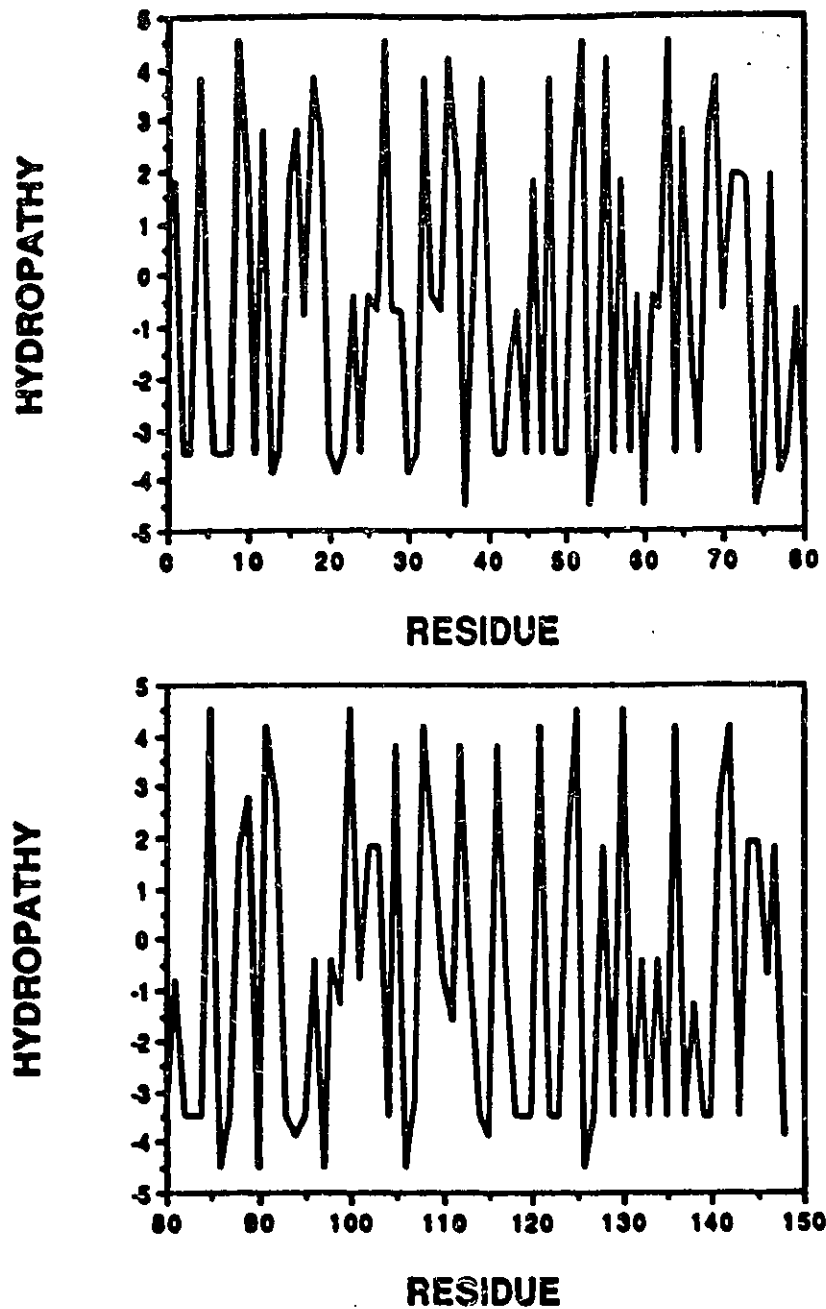


Figure 43. Hydrophobic Plots of the Residues of Calmodulin. The hydrophobicities of the side chains of residues 1 to 80 of CaM are displayed in (A) and those of residues 81 to 148 are shown in (B). The sequence is for *E. coli* expressed chicken calmodulin (Putkey *et al.*, 1985). The hydrophobicities for the side chains of the residues are taken from Kyte and Doolittle, 1982.

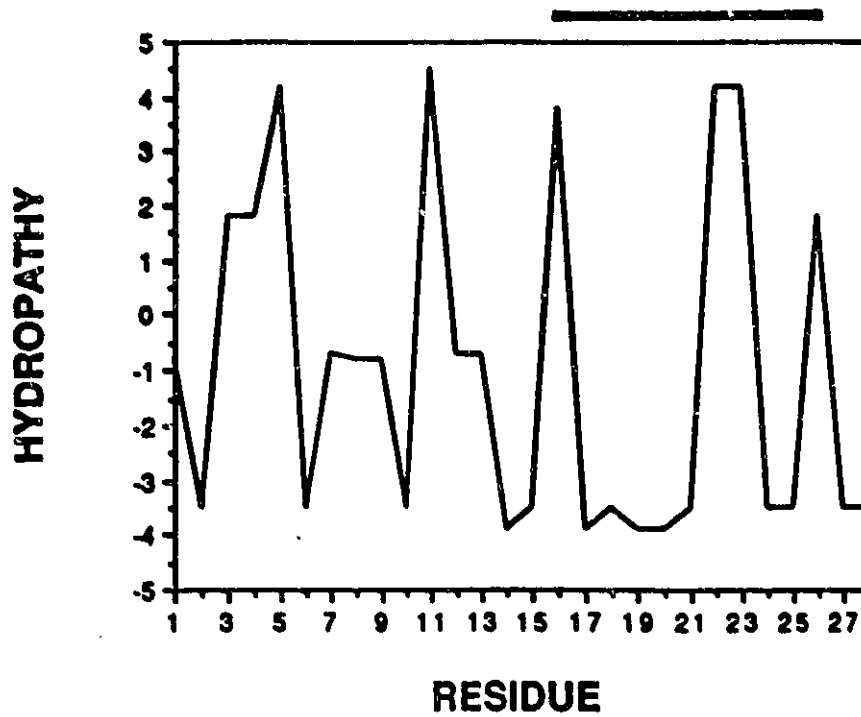


Figure 44. Hydropathic Plot of the Residues of Thymosin α_1 . The hydropathies of the side chains of the residues of thymosin α_1 are displayed. The bar above the plot shows the helical region within the peptide. The hydropathies for the side chains of the residues are taken from Kyte and Doolittle, 1982.

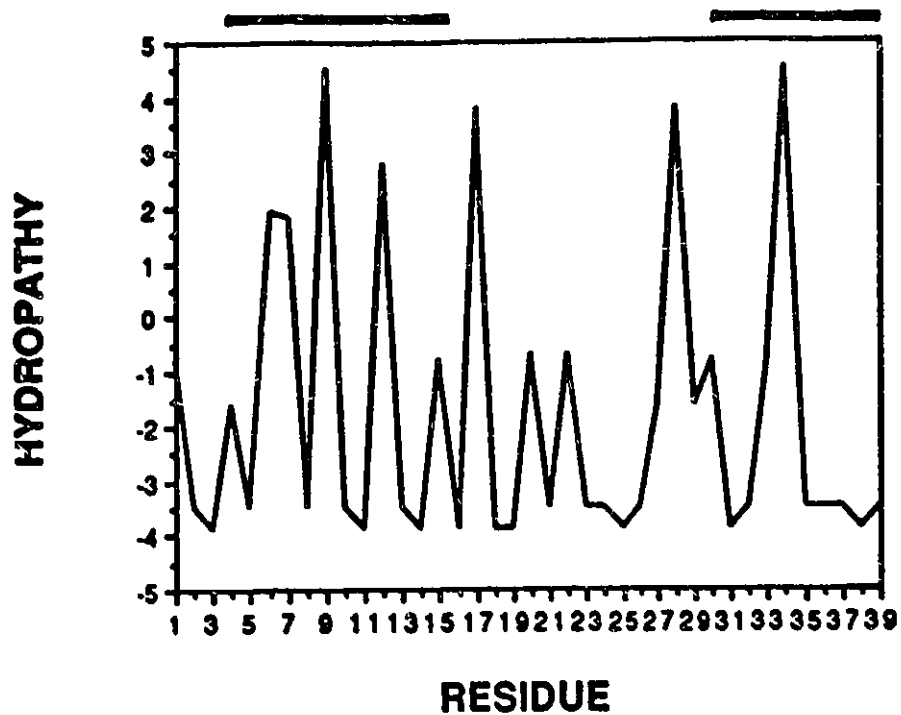


Figure 45. Hydropathic Plot of the Residues of Thymosin $\beta_4(1-39)$. The hydropathies of the side chains of the residues of thymosin $\beta_4(1-39)$ are displayed. The hydropathic plot of thymosin $\beta_4(16-38)$ is also contained within this plot. The bars above the plot show the helical regions within thymosin $\beta_4(1-39)$ based on the solution structure of thymosin β_4 (Zarbock et al., 1990). The hydropathies for the side chains of the residues are taken from Kyte and Doolittle, 1982.

CHAPTER FOUR

DISCUSSION

4.1) Solution Structure of Thymosin α_1

Thymosin α_1 is a highly active polypeptide isolated from thymus Fraction 5 (Low and Goldstein, 1979). The primary structure of the peptide is known (Figure 4) (Low and Goldstein, 1979) but the three-dimensional structure is not. Thymosin α_1 and Fraction 5 have shown promise as an effective therapy for chronic hepatitis B in ongoing clinical trials, yet the exact mode of action of either against hepatitis B is unknown (Mutchnick *et al.*, 1991). It is hoped that the determination of the three-dimensional structure of thymosin α_1 can help in determining the exact mechanism by which the peptide modulates immune responses against hepatitis B.

The Chou-Fasman analysis of the primary structure of the peptide predicts an α -helix region comprising residues 16 to 27 and a β -turn made up of residues 6 to 9 (Figure 7). It has also been shown that α -chymotrypsin cleaves thymosin α_1 at Lys14 instead of the nearby residue, Leu16, which suggests a conformational susceptibility at Lys14 (Low and Goldstein, 1979). The results show that the peptide is cleaved by α -chymotrypsin at Lys14 and Leu16 (Figure 15 and Table V) in a 3:1 ratio.

α -Chymotrypsin is known to clip proteins and peptides on the carboxyl terminal side of large hydrophobic aromatic residues (Phe, Tyr and Trp) (Creighton, 1993). Within the amino acid sequence of thymosin α_1 there are no aromatic residues. The cleavage

after Leu16 is explainable, since Leu is a hydrophobic residue and has a van der Waals volume of 124 \AA^3 , which is comparable to the volumes of Phe, Tyr and Trp (135 , 141 and 163 \AA^3 respectively) (Creighton, 1993). The cleavage after Lys14 is not so straightforward. Although Lys is a large residue, having a van der Waals volume of 135 \AA^3 , it is extremely hydrophilic. The closest large hydrophobic residue near Lys14, aside from Leu16, is Ile11 which is slightly more hydrophobic than Leu. The next two residues after Ile11 are Thr12 and Thr13. The catalytic centre of α -chymotrypsin is made up of a deep hydrophobic pocket containing several Thr and Ser residues (Creighton, 1993). It may be possible that Thr12 and Thr13 of thymosin α_1 interact favourably with the pocket of α -chymotrypsin leaving the peptide bond between Lys14 and Asp15 in a susceptible position.

The finding that thymosin α_1 is cleaved after Lys14 and Leu16 in a 3:1 ratio suggests that in aqueous solution, thymosin α_1 is rapidly converting between more than one conformational state. As seen by the CD analysis these states are predominantly a random coil and α -helix (Figure 12). Since the amount of α -helix within the peptide is small in aqueous solution (Figure 10), the α -chymotryptic digestion may suggest that thymosin α_1 is cleaved after Leu16 when the peptide is in a helical state and Lys14 when in a random coil configuration. These results also suggest that the helix in thymosin α_1 begins in the vicinity of Leu16.

The preliminary one-dimensional $^1\text{H-NMR}$ spectrum of thymosin α_1 acquired at 300 MHz in 20 mM phosphate, 150 mM NaCl, pH* 5.98 dissolved in 100% D_2O was characterized by very sharp resonances (Figure 9). Sharp resonances are characteristic of random coil structures (Wüthrich, 1986), since these structures

experience much less transverse (spin-spin) relaxation and therefore have much longer T_2 times which gives rise to sharper lines. The initial $^1\text{H-NMR}$ spectrum of the peptide in 60% (v/v) TFE- d_3 resulted in a spectrum with much broader resonances suggesting that the introduction of the fluorinated alcohol resulted in the stabilization of some type of secondary structure within the peptide. Although this experiment provided initial evidence that the peptide did possess some type of stable structure in TFE- d_3 , the amount of TFE required to provide the maximum amount of stable structure could not be precisely determined using this technique. Although the broadening of the resonances could also have been attributed to aggregation, subsequent CD experiments confirmed the addition of TFE resulted in an increase in the amount of stable helical structure. No evidence of aggregation was observed in the NOESY spectrum of the peptide in TFE- d_3 .

The above results made it necessary to acquire a CD spectrum of the peptide to confirm that thymosin α_1 in aqueous solution exists as a random coil or contains a very small amount of stable secondary structure. Secondly, it was important to determine the conditions under which the secondary structure of the peptide was most stable. The amount of TFE required to cause thymosin α_1 to adopt the maximum amount of secondary structure would then be added to the NMR samples in order to determine the three-dimensional structure of the peptide.

The CD spectrum of thymosin α_1 in aqueous solution confirms that the peptide is predominantly a random coil under these conditions with only 17% of the peptide in an α -helical conformation. As TFE is added to an aqueous solution of the peptide the CD spectrum begins to resemble that expected for an α -helical structure (Figure 12).

The shoulder at 222 nm clearly indicates the presence of α -helix. The MRE_{222nm} decreases significantly with increasing concentrations of TFE, up to 30% (v/v), which stabilizes the α -helix within the peptide. The MRE_{222nm} value reached a minimum value of $-13141.3 \text{ deg}\cdot\text{cm}^2/\text{dmol}$ in a sample of thymosin α_1 containing 30% (v/v) TFE. The α -helical content of thymosin α_1 , as measured by CD, is 40.7% in 30% (v/v) TFE.

The DQF-COSY, TOCSY and NOESY spectra of thymosin α_1 were initially used to make resonance assignments and determine the secondary structure of the peptide. In total, 24 out of 28 residues were assigned unambiguously. The residues whose assignments were ambiguous included Ser1, Asp2, Glu27 and Asn28. All three of these residues are located at the ends of the peptide and probably have little influence on the overall solution structure of the peptide. Since they are located at the ends of the peptide they would be expected to have greater mobility and thus give rise to less intense cross peaks with neighbouring residues. Ser1 and Glu27 were assigned by default since the other Ser and Glu residues were unambiguously assigned. Since Asp and Asn residues both belong to the AMX spin system (Wüthrich, 1986) they were more difficult to assign. Of the remaining possible cross peaks that were assignable to these residues, the α CH resonance positions were almost identical (c.f. 4.52 and 4.64 ppm) but they differed significantly in the position of their amide resonance (c.f. 7.92 and 8.45 ppm). It was concluded that Asn28 is at 7.92 and 4.52 ppm since it is at the carboxyl terminus and this would be expected to cause an upfield shift in the position of the resonances of this residue (Wüthrich *et al.*, 1984). The remaining AMX spin system is assignable to Asp2 at 8.45 and 4.64 ppm.

The pattern of observed medium-range NOE cross peaks clearly indicates the presence of an α -helix within thymosin α_1 (Wüthrich, 1986). This conclusion is supported by fourteen short-range NH-NH ($i,i+1$) connectivities and five medium-range α CH-NH ($i,i+3$) and four NH-NH ($i,i+2$) connectivities observed between residues 16 to 26. The observed α CH-NH ($i,i+3$) connectivities were between the pairs of residues; Leu16/Lys19, Lys17/Lys20, Lys19/Val22, Glu21/Glu24 and Val22/Glu25. In the amide region of the spectrum, NH-NH ($i,i+2$) connectivities were observed between Leu16/Lys18, Glu18/Lys20, Lys20/Val22 and Val22/Glu24. A NH-NH ($i,i+3$) cross peak was also observed between Val23/Ala26. Two isolated NH-NH ($i,i+1$) cross peaks between Ala4/Val5 and Val5/Asp6 were also observed suggesting some type of stable secondary structure within this region of the peptide.

Distance geometry calculations using the observed NOE distance and volume restraints gave convergence for 11 out of 30 calculated structures for thymosin α_1 . The ratio of converged structure per structural calculation is quite low, which is a result of the small number of medium-range NOE measurements. The pattern of NOE connectivities and the results of the structural determination indicate that thymosin α_1 is composed of three structurally distinct conformations. Residues located at the amino terminal end (residues 1-4), within the central region (residues 9-15) and at the carboxyl terminal end (residues 27-28) appear to exist in an extended conformation. The most definitive secondary structural elements within the peptide is an α -helix between residues 16-26 and a turn between residues 5-8. The regions between residues 5 to 8 and 16 to 26 have a low coordinate RMSD. The helical region is well-defined in terms of N,N($i,i+3$) distances (Table VIII) and dihedral angles (Figure 35). An ideal helix would possess ϕ and ψ angles of -57° and -47° , respectively (Creighton, 1993) and

N,N(i,i+3) distances of 4.86 Å. The turn region is not as well-defined by its dihedral angles, but does possess N,N(i,i+3) distances much shorter than those expected for a random coil (Wagner, 1990). There is no evidence that either of the terminal regions fold back on the rest of the peptide, so the overall structure of the peptide is extended.

The determination of the N- and C-cap residues of the α -helix is based on the analysis of the dihedral angles and N,N(i,i+3) distances. Although the ϕ angle of Leu16 is not within the range of an α -helix, it does have a helix-like ψ angle and the N,N(i,i+3) distance between Leu16 and Lys19 is similar to that of an ideal α -helix. Therefore Leu16 is concluded to be the N-cap of the α -helix. Similarly, Ala26 has a ψ angle outside the range expected for an α -helix, but it does have a helix-like ϕ angle and the N,N(i,i+3) distance between Val23 and Ala26 is similar to that expected for an α -helix. Therefore Ala26 is concluded to be the C-cap of the α -helix.

As previously mentioned, only 11 out of 30 calculated structures gave acceptable convergence within the helical region of the peptide. The main reason for this low convergence rate is due to the low number of medium-range NOE connectivities. Within the low density of medium-range NOE measurements it is expected that more than one structure could satisfy the NOE distance restraints. Undoubtedly thymosin α_1 is very flexible in solution and the structure of this peptide cannot be represented accurately by an average structure or even by superimposing a group of molecules that give acceptable convergence. The structure of this peptide would best be represented as a movie in which each frame contained a structure that agreed with the experimental NOE distance restraints. The movie would show all of the conformations accessible to the peptide.

The amount of helicity predicted by the Chou-Fasman analysis (42.9%) agrees very well with the CD spectrum of thymosin α_1 in 30% (v/v) TFE (40.7%) and the NMR solution structure (39.3%) (Table X). In aqueous solution the CD analysis showed that only 17% of thymosin α_1 is in a helical conformation. Therefore the CD results do not agree with the Chou-Fasman analysis in aqueous solution. The Chou-Fasman analysis agrees with the CD and NMR results when the peptide is in its most stable conformation in a solution of 30% (v/v) TFE. The prediction derived using the Chou-Fasman analysis relies on the identity of a particular amino acid residue and the identity of the residues surrounding that residue. The Chou-Fasman analysis does not take into account different solvent conditions when determining the propensity of a residue sequence to form any type of secondary structure. It can be concluded that the results of the CD and NMR analysis of thymosin α_1 in 30% (v/v) TFE agree with the Chou-Fasman analysis.

A study was done in which 11 separate fragments of bovine growth hormone, a 191 residue protein, were synthetically prepared in order to study the effect of TFE on their α -helicity (Lehrman *et al.*, 1990). The peptides prepared corresponded to the following sequences in the parent protein: (1) residues 1-17; (2) residues 12-34; (3) residues 27-47; (4) residues 43-64; (5) residues 56-80; (6) residues 78-95; (7) residues 96-133; (8) residues 130-150; (9) residues 145-162; (10) residues 153-180; (11) residues 179-191 (Lehrman *et al.*, 1990). The helical content of each peptide in a 10 mol % TFE solution was measured by CD and compared to the predicted helical content for each peptide (Chou and Fasman, 1974) and the helical content of each segment in the corresponding x-ray crystallographic structure of the parent protein (Abdel-Meguid *et al.*, 1987). The results showed a better correlation between the TFE-enhanced α -helicity and the predicted α -helicity of the peptides, than

TABLE X

Comparison of the Helical Content of Thymosin α_1
Determined by Chou-Fasman, CD and NMR Analysis

<u>Method</u>	<u>% Helicity</u>	<u>No. of Residues</u>
Chou-Fasman	42.9	12.0
CD	40.7	11.4
NMR	39.3	11.0

the TFE-enhanced α -helicity and the helical content of the peptides in the corresponding protein structure (Lehrman *et al.*, 1990). The TFE-enhanced α -helicity agreed within 20% of the predicted α -helicity for 8 of the 11 peptides, while the TFE-enhanced α -helicity agreed within 20% of the α -helicity in the corresponding protein structure for only 3 of the 11 peptides (Lehrman *et al.*, 1990).

The results from the above experiments suggest that the Chou-Fasman predictive method is more accurate in determining the α -helical propensities of specific amino acid sequences than it is for their protein-linked conformations (Lehrman *et al.*, 1990). The Chou-Fasman analysis averages the conformational preferences of individual groups of amino acids and does not take into account any conformational preferences resulting from local environmental factors within the protein (Lehrman *et al.*, 1990). The results also show that the TFE-enhanced α -helicity of peptides derived from parent proteins is not always an accurate reflection of the amount of α -helicity contained in the corresponding sequence within the parent protein. The use of TFE in the stabilization of α -helical structures should be restricted to the study of small, linear native peptides. In addition, if the structure of a peptide derived from a parent protein is solved with the peptide dissolved in a TFE solution, it cannot be assumed that the sequence in the parent protein corresponding to the peptide possesses the same structure.

It is worth examining the sequence of residues that comprise the helical region of thymosin α_1 (Leu-Lys-Glu-Lys-Lys-Glu-Val-Val-Glu-Glu-Ala). Charged residues dominate within this sequence. Electrostatic, dipole and side-chain interactions have all been shown to contribute to helical stability (Shoemaker *et al.*, 1987). Electrostatic

interactions have been found to be particularly important in stabilizing helices in short synthetic peptides (Marqusee and Baldwin, 1987). In thymosin α_1 , Lys-17/Glu-21 and Lys-20/Glu-24 are most likely to form salt bridges. Such an arrangement of residues is similar in a group of peptides studied by Marqusee and Baldwin (Marqusee and Baldwin, 1987). They found that synthetic peptides with Glu and Lys residues with an (i,i+4) spacing stabilized the helical conformation relative to the (i,i+3) spacing. They also showed that the stabilization of the helical conformation was essentially equal when the Glu and Lys residues were reversed in the (i,i+4) spaced peptides. In the helical region of thymosin α_1 the spacing of the Lys and Glu residues is expected to contribute significantly to the stability of the helical conformation.

The CD titration profile using TFE clearly shows the presence of an isodichroic region between 202 and 207 nm (Figure 14), which suggests that two major structural elements prevail; α -helix and random coil. However, the structural transition that occurs during the titration with TFE involves more than two elements since an isodichroic region rather than an isodichroic point is observed (Khan *et al.*, 1990). There is a distinct possibility that the third structural element could be a β -turn comprising residues 6 to 9 as suggested by the analysis of the primary structure of the peptide. When the CD spectra of thymosin α_1 in 0% and 10% (v/v) TFE are compared (Figure 11), it is observed that as the concentration of TFE is increased, there is no change in the MRE_{222nm} , indicating that the α -helical content of the peptide has not significantly changed. However, there is a significant change in the MRE_{203nm} between the sample of thymosin α_1 in 0% TFE and 10% (v/v) TFE. In 0% (v/v) TFE the value of MRE_{203nm} is $-12\,499.24 \text{ deg}\cdot\text{cm}^2/\text{dmol}$ while in 10% (v/v) TFE MRE_{203nm} is equal to $-7788.67 \text{ deg}\cdot\text{cm}^2/\text{dmol}$. As the amount of TFE added to the peptide sample is

increased to 20% (v/v), the minimum absorption band shifts from 203 nm to about 207 nm, which is characteristic of α -helical secondary structure.

One interpretation of the observation that the formation of the β -turn within the peptide occurs before the formation of the α -helix. Such a result may have implications in the folding of the peptide. In order for the peptide to adopt a helical conformation the formation of the β -turn may be a prerequisite. The formation of the β -turn may lower the energy required for the formation of the α -helix, since it limits the space that the residues comprising the helix have to occupy. The lowering of the energy of formation may then permit the necessary hydrogen bonding between atoms required for the formation of the α -helix. Another explanation is that the turn region between residues 5 to 8 is a type 3 β -turn which has dihedral angles similar to that observed in an α -helix (O'Neil, personal communication). The formation of this turn may induce the transient formation of a series of turns between residues 9 to 15 which induces the formation of the helix between residues 16-26.

4.2) Stabilization of Thymosin α_1 by Trifluoroethanol

In the past it has been difficult to detect any stable secondary structure within small peptides in aqueous solution, mainly because small peptides are able to rapidly interconvert between more than one conformational state in aqueous solution (Dyson *et al.*, 1990). The addition of fluorinated alcohols, such as TFE, stabilize small helical-forming peptides which are predominantly random coils in aqueous solution, by increasing the equilibrium in favour of the helical conformation of the peptide (Dyson *et al.*, 1990). By this method the addition of the alcohol does not create any new structure

within the peptide, but merely stabilizes the helical structure the peptide already possesses (Dyson *et al.*, 1990). Thymosin α_1 contains a small measurable amount of helicity in aqueous solution (Figure 10) and the amount of helicity increases as more TFE (up to 30% (v/v)) is added to the peptide sample. Therefore the addition of TFE to thymosin α_1 pushes the equilibrium in favour of the helical over the random coil conformation.

The arrangement of residues in the helical region may provide some clues as to why thymosin α_1 shows little stable secondary structure in aqueous solution but is largely helical in 30% TFE. One suggestion is that in a lower dielectric constant environment, as such for TFE, charged pairs would interact more strongly than in aqueous solution (Khan *et al.*, 1990). In thymosin α_1 the addition of TFE would then be expected to increase the stabilization of the helical conformation mainly through ionic interactions between the side chain atoms of Lys17-Glu21 and Lys20-Glu24. In aqueous solution these residues would be expected to form strong ionic interactions with the solvent molecules.

Experiments performed by Zhou *et al.* (1993) offer a second explanation to the stabilization of helical structures by fluorinated alcohols. They prepared an amphipathic α -helical model peptide, Glu-Ala-Glu-Lys-Ala-Ala-Lys-Glu-Ala-Glu-Lys-Ala-Ala-Lys-Glu-Ala-Glu-Lys, and found that the amount of helicity within the peptide was pH dependent in aqueous solution but was pH independent in a solution containing 30% (v/v) TFE. The pH independency of the structure in TFE suggests that the effect of TFE in helix stabilization is not a result of its smaller dielectric constant, that should enhance ionic interactions between charged groups compared to water (Zhou

et al., 1993).

Other studies suggest that the stabilizing effect of TFE may be a result of its lower basicity than water (Llinas and Klein, 1975). The lower basicity of the solution would result in a decrease in hydrogen bonding between protons within the peptide to the solvent, and consequently strengthened hydrogen bonds between residues within the protein. Thus the pH independency in TFE of the model peptides used by Zhou *et al.*, (1993) would be a result of the strengthening of the hydrogen bonds between the side chains of the Lys and Glu residues.

Other results (Zhou *et al.*, 1993) have also shown that the more hydrophobic the nonpolar face of an amphipathic helix, the more stable the α -helix is in TFE solutions. The increased stability of a single-stranded α -helix is thus a result of enhancing the hydrophobic interactions between peptide and solvent molecules. This would result in the clustering of the hydrophobic side chains of the helical region. In the case of thymosin α_1 this would involve interactions between Leu16, Val22, Val23 and Ala26 with TFE molecules, which indeed all cluster along one face of the α -helix (Figure 36).

Since the helical region of thymosin α_1 is highly amphipathic, it is impossible to determine what causes the stabilizing effect of TFE on the peptide. If TFE stabilizes secondary structure within small peptides both electrostatically and hydrophobically, the arrangement of residues in the amphipathic helix of thymosin α_1 is optimal for stabilization by both effects. To more definitely determine by which method fluorinated alcohols stabilize structure within small peptides, synthetic non-amphipathic helical peptides (such as poly-L-lysine) should be studied. If fluorinated alcohols stabilize

helices by promoting intra-chain hydrogen bonds then adding one to an aqueous solution of poly-L-lysine should promote helix formation. If the effect is hydrophobically driven, then no helix should form.

Although the structure of thymosin α_1 in 30% (v/v) TFE-d₃ presented here cannot be absolutely ascertained to be physiologically correct, it is doubtful that the predominantly random coil conformation observed in aqueous solution is active. Considering the diverse activities attributed to this peptide it is most likely that it contains some type of stable secondary structure in its active form. The best method to determine the *in vivo* structure of thymosin α_1 is with the peptide bound to a receptor or any other polypeptide that it may interact with. Much is known about the activities possessed by thymosin α_1 , however little is known about its specific interactions with other polypeptides. Skeletal muscle MLCK is the only protein that thymosin α_1 has been shown to interact with directly (Galoyan *et al.*, 1992). To test the validity of the structure of thymosin α_1 in 30% (v/v) TFE-d₃, a structural study of thymosin α_1 in a solution containing the CaM-binding domain of skMLCK could be pursued. Circular dichroism could be used to determine if the helical content of thymosin α_1 is stabilized in the presence of the CaM-binding domain of skMLCK, to the extent it is stabilized in 30% (v/v) TFE. This experiment will not only test the validity of the structure of thymosin α_1 in 30% (v/v) TFE-d₃ but also confirm whether thymosin α_1 interacts with the same region of skMLCK that CaM does.

4.3) Modelling the Interaction of Thymosin α_1 with skMLCK

Thymosin α_1 , thymosin $\beta_4(1-39)$ and thymosin $\beta_4(16-38)$, have been shown to be high affinity activators of skMLCK, which is a well characterized Ca^{2+} /CaM-dependent enzyme. The solution structures of thymosin α_1 and thymosin β_4 are now known. The solution structure of the binding region of the CaM-binding domain of skMLCK complexed with CaM (Ikura *et al.*, 1992) as well as the crystal structure of the CaM-binding region of smMLCK complexed with CaM (Meador *et al.*, 1992) have been solved. All of these structures can be used in an attempt to show how the thymosin peptides interact with MLCK. The major difficulty in this is that CaM is a 145 residue protein, while the largest of the thymosin peptides is only 39 residues and the smallest contains only 23 residues. It would therefore be expected that the number of interactions between CaM and MLCK are much greater than those between the thymosin peptides and MLCK. Since CaM is so much larger than the other peptides, therefore all of the major forces expected in protein-protein interactions are observed. It is still worth attempting to find micro-regions within CaM that bind to MLCK and compare them to homologous regions in the thymosin peptides and also to try to find similarities in binding modes among the complexes.

In the solution structure of M13 (residues 577-602 of skMLCK) complexed with CaM, M13 was observed to adopt an α -helical conformation (Ikura *et al.*, 1992), which is popular for the binding regions of many proteins that interact with CaM (O'Neill and DeGrado, 1990). The sequence of M13 is Lys-Arg-Arg-Trp-Lys-Lys-Asn-Phe-Ile-Ala-Val-Ser-Ala-Ala-Asn-Arg-Phe-Lys-Lys-Ile-Ser-Ser-Ser-Gly-Ala-Leu (Ikura *et al.*, 1992) The interaction between M13 and CaM is stabilized mainly through

hydrophobic interactions. In addition to the hydrophobic interactions a large number of electrostatic interactions between M13 and CaM were deduced from the calculated simulated annealing (SA) structures (Ikura *et al.*, 1992). Ionic interactions were seen between the following pairs of negatively charged residues of CaM and basic residues of M13: Glu127/Arg3, Glu11/Lys5, Glu14/Lys6, Glu84/Asn15, Glu84/Arg16, Glu87/Lys18 and Glu83/Lys19 (Ikura *et al.*, 1992). All of the basic residues of M13 formed electrostatic interactions with Glu residues within the CaM molecule (Ikura *et al.*, 1992).

In the crystal structure of the CaM-binding region of smMLCK (chicken smMLCK residues 796 to 815) with CaM a large number of hydrophobic interactions were again observed, including all nine Met residues of CaM (Meador *et al.*, 1992). The sequence of the CaM-binding domain of smMLCK is Ala-Arg-Arg-Lys-Trp-Gln-Lys-Thr-Gly-His-Ala-Val-Arg-Ala-Ile-Gly-Arg-Leu-Ser-Ser (Meador *et al.*, 1992). Ionic interactions were seen between the following pairs of negatively charged residues of CaM and basic residues of CaM-binding domain of smMLCK: Glu114/Lys4, Glu120/Lys4, Glu7/Gln6, Glu11/Gln6, Glu14/Lys7, Glu114/Lys7, Glu84/Arg13 and Glu84/Arg17 (Meador *et al.*, 1992). All seven basic residues of the smMLCK peptide make salt bridges with negatively charged residues within the CaM molecule (Meador *et al.*, 1992).

In the structures of the CaM-binding domains of smMLCK and skMLCK bound to CaM, hydrophobic interactions dominate (Meador *et al.*, 1992; Ikura *et al.*, 1992). The primary structures of the thymosin α_1 , thymosin $\beta_4(1-39)$, and thymosin $\beta_4(16-38)$ are not dominated by hydrophobic residues (Figures 5 and 41). Regions within the peptides, thymosin $\beta_4(5-16)$ and $(30-39)$ and thymosin $\alpha_1(16-26)$, that contain

stable secondary structure are dominated by hydrophilic residues.

Since the thymosin peptides are not large proteins, there is a limit to the ways they can interact with MLCK. The MLCK stimulating ability of the polypeptides was found to be in the order: thymosin $\beta_4(1-39)$ > thymosin $\beta_4(16-38)$ > $\text{Ca}^{2+}/\text{CaM}$ > thymosin α_1 . If the thymosin peptides are all high affinity MLCK stimulators then there must be some region of structural homology within all three of them. The solution structures of thymosin α_1 and thymosin β_4 (Zarbock *et al.*, 1990) have been solved. Since thymosin $\beta_4(1-39)$ and thymosin $\beta_4(16-38)$ both possess a high-degree of activity it is apropos to assume that they contain the analogous structures that were found in the full peptide. This suggests that thymosin $\beta_4(1-39)$ and thymosin $\beta_4(16-38)$ possess a common α -helical segment between residues 30-38. Therefore this is the most likely MLCK binding region within the two thymosin β_4 peptides. The sequence between residues 30 and 38 contains only one hydrophobic residue (Ile34), thus it is reasonable to assume that its interaction with MLCK is polar in nature.

In thymosin α_1 there are only two structural elements: a β -turn between residues 5 to 8 and an α -helix between residue 16 to 26. Since it is also a high-affinity MLCK stimulator, its mode of binding must be similar to that of the thymosin β_4 peptides. Thus there must be some sequence homology between the helical segments in all three of the thymosin peptides. Examining the helical wheel diagrams for each peptide (Figures 36 and 42) shows that the highest homology occurs in the position of the two glutamic acid residues, Glu21 and Glu24 of thymosin α_1 and Glu32 and Glu35 of thymosin β_4 . This alignment also places Glu25 of thymosin α_1 in structurally homologous positions as Gln36 of both thymosin β_4 peptides.

The modelling studies using the solution structure of thymosin α_1 and the binding domain of skMLCK show that the electrostatic interaction between negatively charged groups on thymosin α_1 and positively charged groups of skMLCK results in a system with lower total energy than a system based on hydrophobic interactions between the two peptides. The modelling studies along with an examination of the amino acid content of the helical segments of the thymosin peptides, suggest that the peptides interact with MLCK predominantly through ionic interactions. The mode of interaction between thymosin α_1 and MLCK is in direct contrast to the interaction of MLCK with CaM which is predominantly hydrophobic, with a small amount of ionic interactions contributing to the stabilization of the CaM/MLCK complex (O'Neil and DeGrado, 1990).

4.4) How Does Thymosin α_1 Cure Hepatitis B?

The major clinical application being investigated for thymosin α_1 is its ability to act as a hepatitis B anti-viral agent (Mutchnick *et al.*, 1991). Now that we have determined the three-dimensional structure of thymosin α_1 , it is left to at least attempt to take the results and speculate on the mechanism by which thymosin α_1 acts as a hepatitis B virus therapy. Very recent results measuring the levels of thymosin α_1 and prothymosin α in normal HepG2 cells and also HepG2 cells transfected with the hepatitis B virus have provided some interesting results (Sasaki, personal communication). Prothymosin α is a highly acidic, 109 residues protein that has been implicated in cell division (Sburlati *et al.*, 1993). The first 28 residues of prothymosin α are identical to the 28 residues of thymosin α_1 (Sburlati *et al.*, 1993). An antibody raised against thymosin α_1 was used to detect the presence of thymosin α_1 and prothymosin α . It was observed that the level of prothymosin α in the nuclei of cells that were infected with

the hepatitis B virus was five-fold greater than in normal cells (Sasaki, personal communication). It was assumed that all of the antigen detected with the antibody was prothymosin α since thymosin α_1 does not contain a karyophilic sequence and would not be expected to occupy the nucleus. When the transfected cells were grown in the presence of thymosin α_1 the levels of prothymosin-like antigen were significantly reduced (Sasaki, personal communication). The decrease in the levels of prothymosin-like antigen suggests that thymosin α_1 interferes with prothymosin α production at one or more levels of protein synthesis in the cell.

An increase in the level of prothymosin α has previously been observed in malignant tissues when compared to healthy tissue (Tsitsiloni *et al.*, 1993). In particular the level of prothymosin α in cancerous breast tissue was found to be 17.9-fold greater than in healthy breast tissue (Tsitsiloni *et al.*, 1993). Higher levels of prothymosin α mRNA have been observed in leukemic leukocytes compared to healthy leukocytes (Gomez-Marquez *et al.*, 1989). The results of the above studies suggest that the increased levels of prothymosin α are tied to an increase in cell proliferation of the malignant tissues.

It has also been shown that the transcription of the prothymosin α gene increases in the presence of active c-Myc protein, a well established proto-oncogene (Eilers *et al.*, 1991). Northern blot (mRNA) analysis has shown that both the prothymosin α and c-Myc genes were overexpressed in human colorectal cancer cells as compared to adjacent healthy tissue (Mori *et al.*, 1993). The findings suggested that prothymosin α gene expression is associated with, or under the control of the c-Myc gene in human colorectal cancer (Mori *et al.*, 1993).

The activation of the c-Myc gene has been a consequence of both hepadna virus infection (Tiollais *et al.*, 1991) and HBV X protein (Koike *et al.*, 1987; Koike *et al.*, 1989). The c-Myc gene encodes a "basic-helix-loop-helix" (bHLH) protein which binds to DNA (Van Antwerp *et al.*, 1992). Within the sequence of the bHLH protein a cluster of basic residues have been shown to be important for DNA binding, while the helix-loop-helix region of the protein is important for dimerization of the c-Myc protein (Voronova and Baltimore, 1990). The binding to DNA is greatly enhanced when the bHLH protein is a dimer (Davis *et al.*, 1990; Murre *et al.*, 1989), although the DNA binding domain is not involved in dimer formation (Davis *et al.*, 1990). The DNA binding domain is 14 amino acids long and is characterized by two clusters of basic residues at each end of the sequence (Van Antwerp *et al.*, 1992).

The sequences of the DNA binding domains of nine other basic helix-loop-helix proteins have been determined and are compared in Figure 46 (Murre *et al.*, 1989). Within the sequences is a highly conserved basic region near the amino terminal and in particular an Arg residue at position two. There are also homologous residues at positions six (Asn6), nine (Glu9), ten (Arg10) and twelve (Arg12) (Murre *et al.*, 1989). In all of the sequences, except the three myc proteins, an Arg residue appears at position eight. In the three Myc proteins this position is occupied with a Leu residue (Murre *et al.*, 1989).

If HBV infection results in an increase in the transcription of the c-Myc gene then an increase in the levels of the bHLH protein encoded within this gene would also be expected. If this bHLH protein is also the one responsible for the activation of the prothymosin α gene mRNA, then an increase in the bHLH protein level would lead to an

c-Myc Lys-Arg-Arg-Thr-His-Asn-Val-Leu-Glu-Arg-Gln-Arg-Arg-Asn-Glu
L-Myc Lys-Arg-Lys-Asn-His-Asn-Phe-Leu-Glu-Arg-Lys-Arg-Arg-Asn-Asp
N-Myc Arg-Arg-Arg-Asn-His-Asn-Ile-Leu-Glu-Arg-Gln-Arg-Arg-Asn-Asp
MyoD Arg-Arg-Lys-Ala-Ala-Thr-Met-Arg-Glu-Arg-Arg-Arg-Leu-Ser-Lys
E12 Arg-Arg-Val-Ala-Asn-Asn-Ala-Arg-Glu-Arg-Leu-Arg-Val-Arg-Asp
E47 Arg-Arg-Met-Ala-Asn-Asn-Ala-Arg-Glu-Arg-Val-Arg-Val-Arg-Asp
da Arg-Arg-Gln-Ala-Asn-Asn-Ala-Arg-Glu-Arg-Val-Arg-Val-Arg-Asp
twist Gln-Arg-Val-Met-Ala-Asn-Val-Arg-Glu-Arg-Gln-Arg-Thr-Gln-Ser
As-C T4 Gln-Arg-Arg-----Asn-Ala-Arg-Glu-Arg-Asn-Arg-Val-Lys-Gln
As-C T5 Ile-Arg-Arg-----Asn-Ala-Arg-Glu-Arg-Asn-Arg-Val-Lys-Gln

Figure 46. Amino Acid Homologies Within the Basic Domains of Basic-Helix-Loop-Helix Proteins. The sequences are aligned to show the maximum degree of homology. Sequences are from: human c-Myc (residues 347-361) (Battey et al., 1983); human L-Myc (residues 289-303) and human N-Myc (residues 392-406) (DePinho et al., 1987); MyoD (residues 109-123) (Davis et al., 1987); E12 (residues 337-351), E47 (residues 337-351) and da (residues 555-569) (Caudy et al., 1988); twist (residues 358-372) (Thisse et al., 1988); As-C T4 (residues 102-115) and As-C T5 (residues 27-40) (Villares and Cabrera, 1987).

increase in the levels of prothymosin α mRNA. If the increased levels of prothymosin α mRNA were translated into prothymosin α protein then the increased levels of prothymosin α could possibly result in an increase in the rate of cell division and could lead to cancerous growth. Somewhere along this pathway is where thymosin α_1 must arrest the production of prothymosin α .

Some evidence (see above) suggests that thymosin α_1 interferes with the production of prothymosin α mRNA. If the c-Myc protein is a transcription factor for regulating the production of prothymosin α mRNA, this would require thymosin α_1 to bind to this protein and prevent it from binding to the prothymosin α gene. The inhibition of the production of prothymosin α mRNA could be accomplished in one of two ways. The first way would be a direct interaction between the negatively charged residues of thymosin α_1 with the cluster of basic residues within the DNA-binding domain of the c-Myc protein. The interaction would be analogous to the electrostatic interaction observed in the modelling studies of the interaction between thymosin α_1 and skMLCK. The thymosin α_1 /c-Myc complex would block the DNA-binding domain of c-Myc from binding to DNA and prevent the transcription of the prothymosin α gene. A second way that thymosin α_1 could prevent the transcription of the prothymosin α_1 gene is by way of a feedback inhibition. Since the 28 residues of thymosin α_1 are identical to the first 28 residues of prothymosin α it is possible that thymosin α_1 interacts with the group of basic residues on the DNA-binding domain of the c-Myc protein, in such a way that it is recognized as prothymosin α . The thymosin α_1 interaction would trick the c-Myc protein into believing that there is a high concentration of prothymosin α in the cell. The c-Myc protein would then cease to produce any more prothymosin α mRNA.

The main conclusion reached in this research project is that thymosin α_1 is comprised of a turn between residues 5 and 8 and an α -helix comprised of residues 16 to 26 in a 30% (v/v) TFE-d₃ solution. The helical region is highly amphipathic with a cluster of Glu residues making up one face of the helix. Modelling studies suggest that these Glu residues interact with a cluster of positively charged residues within the CaM-binding domain of skMLCK which results in the activation of skMLCK. The interaction between the negatively charged residues within the helical region of thymosin α_1 and positively charged residues within the DNA binding domain of the c-Myc protein may be a possible mechanism by which the peptide cures hepatitis B.

REFERENCES

Abdel-Meguid, S. S., Shieh, H.-S., Smith, W. W., Dayringer, H. E., Violand, B. N. and Bentle, L. A. (1987) Three-dimensional structure of a genetically engineered variant of porcine growth hormone. *Proc. Natl. Acad. Sci. U.S.A.* **84**, 6434-6437.

Adler, A. J., Greenfield, N. J. and Fasman, G. D. (1973) Circular dichroism and optical rotatory dispersion of proteins and polypeptides. *Methods Enzymol.* **27**, 675-735.

Aisenberg, A. C. and Wilkes, B. (1965) Partial immunological restoration of neonatally thymectomized rats with thymus-containing diffusion chambers. *Nature* **205**, 716-717.

Anfinsen, C. B. (1973) Principles that govern the folding of protein chains. *Science* **181**, 223-230.

Bach, J. F., Dardenne, M., Goldstein, A. L., Guha, A. and White, A. (1971) Appearance of T-cell markers in bone marrow rosette-forming cells after incubation with thymosin, a thymic hormone. *Proc. Natl. Acad. Sci. U.S.A.* **68**, 2734-2738.

Bagchi, I. C., Huang, Q. and Means, A. R. (1992) Identification of amino acids essential for calmodulin binding and activation of smooth muscle myosin light chain kinase. *J. Biol. Chem.* **267**, 3024-3029.

Barcia, M. G., Castro, J. M., Jullien, C. D., Gonzalez, C. G. and Freire, M. (1992) Prothymosin α is phosphorylated by casein kinase-2. *FEBS Let.* **312**, 152-156.

Basus, V. J. (1984) Observation of 2D nuclear overhauser effect crosspeaks involving amide protons in H₂O solutions of proteins. *J. Magn. Reson.* **60**, 138-142.

Batley, J., Moulding, C., Taub, R., Murphy, W., Stewart, T., Potter, H., Lenoir, G. and Leder, P. (1983) The human *c-myc* oncogene: structural consequences of translocation into the IgH locus in Burkitt lymphoma. *Cell* **34**, 779-787.

Bax, A. and Freeman, R. (1981) Investigation of complex networks of spin-spin coupling by two-dimensional NMR. *J. Magn. Reson.* **44**, 542-561.

Bidlingmeyer, B. A., Cohen, S. A. and Tarvin, T. L. (1984) Rapid analysis of amino acids using pre-column derivatization. *J. Chromatogr.* **336**, 93-104.

Blumenthal, D. K. and Stull, J. T. (1982) Effects of pH, ionic strength, and temperature on activation by calmodulin and catalytic activity of myosin light chain kinase. *Biochemistry* **21**, 2386-2391.

Blumenthal, D. K., Takio, K., Edelman, A. M., Charbonneau, H., Titani, L., Walsh, K. A. and Krebs, E. G. (1985) Identification of the calmodulin-binding domain of skeletal muscle myosin light chain kinase. *Proc. Natl. Acad. Sci. U.S.A.* **82**, 3187-3191.

Braunschweiler, L. and Ernst, R. R. (1983) Coherence transfer by isotropic mixing: application to proton correlation spectroscopy. *J. Magn. Reson.* **53**, 521-528.

Bustelo, X. R., Otero, A., Gomez-Marquez, J. and Freire, M. (1991) Expression of the rat prothymosin α gene during T-lymphocyte proliferation and liver regeneration. *J. Biol. Chem.* **266**, 1443-1447.

Caudy, M., Vassin, H., Brand, M., Tuma, R., Jan, L. Y. and Jan, Y. N. (1988) *daughterless*, a Drosophila gene essential for both neurogenesis and sex determination, has sequence similarities to *myc* and the *achaete-scute* complex. *Cell* **55**, 1061-1067.

Charbonneau, H., Kumar, S., Novack, J. P., Blumenthal, D. K., Griffin, P. R., Shabanowitz, J., Hunt, D. F., Beavo, J. A. and Walsh, K. A. (1991) Evidence for domain organization within the 61-kDa calmodulin-dependent cyclic nucleotide phosphodiesterase from bovine brain. *Biochemistry* **30**, 7931-7940.

Chou, P. Y. and Fasman, G. D. (1974a) Conformational parameters for amino acids in helical, β -sheet, and random coil regions calculated from proteins. *Biochemistry* **13**, 211-221.

Chou, P. Y. and Fasman, G. D. (1974b) Prediction of protein conformation. *Biochemistry* **13**, 222-245.

Conteas, C. N., Mutchnick, M. G., Palmer, K. C., Weller, F. E., Luk, G. D., Naylor, P. H., Erdos, M. R., Goldstein, A. L., Paneerselvam, C. and Horecker, B. L. (1990) Cellular levels of thymosin immunoreactive peptides are linked to proliferative events: evidence for a nuclear site of action. *Proc. Natl. Acad. Sci. U.S.A.* **87**, 3269-3273.

Cook D. A. (1967) The relation between amino acid sequence and protein conformation. *J. Mol. Biol.* **29**, 167.

Creighton, P. E. (1992) *In Proteins: Structures and molecular properties*. pp. 140-142. W. H. Freeman, New York.

Crippen, G. M. and Havel, T. F. (1978) Stable calculation of coordinates from distance information. *Acta. Cryst.*, **A34**, 282.

Dauphinee, M. J., Talal, N., Goldstein, A. L. and White, A. (1974) Thymosin corrects the abnormal DNA synthetic response of NZB mouse thymocytes. *Proc. Natl. Acad. Sci. U.S.A.* **71**, 2637-2641.

Davis R. L., Weintraub, H. and Lassar, A. B. (1987) Expression of a single-transfected cDNA converts fibroblasts to myoblasts. *Cell* **51**, 987-1000.

Davis R. L., Cheung, P.-F., Lassar, A. B. and Weintraub, H. (1990) The MyoD DNA binding domain contains a recognition code for muscle-specific gene activation. *Cell* **60**, 733-746.

DePinho, R. A., Hatton, K. S., Tesfaye, A., Yancopoulos, G. D. and Alt, F. W. (1987) The human *myc* gene family: structure and activity of L-*myc* and an L-*myc* pseudogene. *Genes Dev.* **1**, 1311-1326.

Dominiguez, F., Magdalena, C., Cancio, E., Roson, E., Paredes, J., Loidi, L., Zalvide, J., Fraga, M. and Forteza, J. (1993) Tissue concentrations of prothymosin α : A novel proliferation index of primary breast cancer. *Eur. J. Cancer* **29**, 893-897.

Dyson, H. J., Rance, M., Houghten, R. A., Lerner, R. A. and Wright, P. E. (1988a) Folding of immunogenic peptide fragments of proteins in water solution. I. Sequence requirements for the formation of a reverse turn. *J. Mol. Biol.* **201**, 161-200.

Dyson, H. J., Rance, M., Houghten, R. A., Wright, P. E. and Lerner, R. A. (1988b) Folding of immunogenic peptide fragments of proteins in water solution. II. The nascent helix. *J. Mol. Biol.* **201**, 201-217.

Easthope, P. and Havel, T. F. (1988) Computational experience with an algorithm for tetrahedron inequality bound smoothing. *Bull. Math. Biol.* **51**, 173-194.

Eilers, M., Schirm, S. and Bishop, J. M. (1991) The MYC protein activates transcription of the α -prothymosin gene. *EMBO J.* **10**, 133-141.

Ernst, R. R., Bodenhausen, G. and Wokaun, A. (1987) *Principles of nuclear magnetic resonance in one and two dimensions*. Oxford, Clarendon Press.

Eschenfeldt, W. H. and Berger, S. L. (1986) The human prothymosin α gene is polymorphic and induced upon growth stimulation: evidence using a cloned cDNA. *Proc. Natl. Acad. Sci. U.S.A.* **83**, 9403-9407.

Eschenfeldt, W. H., Marrow, R. E., Krug, M. S. and Berger, S. L. (1989) Isolation and partial sequencing of the human prothymosin α gene family. *J. Biol. Chem.* **264**, 7546-7555.

Fitzsimons, D. P., Herring, B. P., Stull, J. T. and Gallagher, P. J. (1992) Identification of basic residues involved in activation and calmodulin binding of rabbit smooth muscle light chain kinase. *J. Biol. Chem.* **267**, 23903-23909.

Franco, J. F., Diaz, C., Barcia, M. and Freire, M. (1992) Thymosin α_1 is a native peptide in several tissues. *Biochimica et Biophysica Acta.* **1120**, 43-48.

Freifelder, D. (1982) *Physical biochemistry. Applications to biochemistry and molecular biology.* W. H. Freeman and Company, New York.

Freire, M., Hannapel, E., Rey, M., Freire, J. M., Kido, H. and Horecker, B. L. (1981) Purification of thymus mRNA coding for a 16 000-dalton polypeptide containing the thymosin α_1 sequence. *Proc. Natl. Acad. Sci. U.S.A.* **78**, 192-195.

Gallagher, P. J., Herring, B. P., Trafny, A., Sowadski, J. and Stull, J. T. (1993) A molecular mechanism for autoinhibition of myosin light chain kinases. *J. Biol. Chem.* **268**, 26578-26582.

Galoyan, A. A., Gurvitis, B. Ya., Shuvalova, L. A., Davis, M. T., Shively, J. E. and Lee, T. D. (1992) A hypothalamic activator of calmodulin-dependent enzymes is thymosin $\beta_4(1-39)$. *Neurochem. Res.* **17**, 773-777.

Giedroc, D. P., Ling, N. and Puett, D. (1983) Identification of β -endorphin residues 14-25 as a region involved in the inhibition of calmodulin-stimulated phosphodiesterase activity. *Biochemistry* **22**, 5584-5591.

Glasoe, P. K. and Long, F. A. (1960) Use of glass electrodes to measure acidities in deuterium oxide. *J. Phys. Chem.* **64**, 188-190.

Goldstein, A. L. and White, A. (1970) *Biochemical Actions of Hormones* (G. Litwak, ed.), pp. 465-502, Academic Press, New York.

Goldstein, A. L., Guha, A., Zatz, M. M., Hardy, M. A. and White, A. (1972) Purification and biological activity of thymosin, a hormone of the thymus gland. *Proc. Natl. Acad. Sci. U.S.A.* **69**, 1800-1803.

Goldstein, G. (1974) Isolation of bovine thymosin: a polypeptide hormone of the thymus. *Nature* **247**, 11-14.

Goldstein, A. L., Cohen, G. H., Rossio, J. L., Thurman, G. B., Brown, C. N. and Ulrich, J. T. (1976) Use of thymosin in the treatment of primary immunodeficiency diseases and cancer. *Med. Clin. N. Am.* **60**, 591-606.

Gomez-Marquez, J., Segade, F., Dosil, M., Pichel, J. G., Bustelo, X. R. and Freire, M. (1989) The expression of prothymosin α gene in T lymphocytes and leukemic lymphoid cells is tied to lymphocyte proliferation. *J. Biol. Chem.* **264**, 8451-8454.

Goodall, G. J., Dominguez, F. and Horecker, B. L. (1986) Molecular cloning of cDNA for human prothymosin α . *Proc. Natl. Acad. Sci. U.S.A.* **83**, 8926-8928.

Gooley, P. R. and MacKenzie, N. E. (1988) Location of an α -helix in fragment 96-133 of bovine somatotropin by ^1H NMR spectroscopy. *Biochemistry* **27**, 4032-4040.

Greenfield, N. and Fasman, G. D. (1969) Computed circular dichroism spectra for the evaluation of protein conformation. *Biochemistry* **8**, 4108-4116.

Haritos, A. A., Goodall, G. and Horecker, B. L. (1984) Prothymosin α : isolation and properties of the major immunoreactive form of thymosin α_1 in rat thymus. *Proc. Natl. Acad. Sci. U.S.A.* **81**, 1008-1011.

Haritos, A. A., Blacher, R., Stein, S., Caldarella, J. and Horecker, B. L. (1985) Primary structure of rat thymus prothymosin α . *Proc. Natl. Acad. Sci. U.S.A.* **82**, 343-346.

Hartshorne, D. J. (1987) *Physiology of the Gastrointestinal Tract* (Johnson, L. R., Ed.) 2nd ed., Vol. I, pp 423-482, Raven Press, New York.

Havel, T. F. (1990) The sampling of properties of some distance geometry algorithms applied to unconstrained polypeptide chains: a study of 1830 independently computed conformations. *Biopolymers* **29**, 1565.

Havel, T. F. (1991) An evaluation of computational strategies for use in the determination of protein structure from distance constraints obtained by nuclear magnetic resonance. *Progr. Biophys. Mol. Biol.* **56**, 43-78.

Herring, B. P. (1991) Basic residues are important for Ca^{2+} /calmodulin binding and activation but not autoinhibition of rabbit skeletal muscle myosin light chain kinase. *J. Biol. Chem.* **266**, 11838-11841.

Hooper, J. A., McDaniel, M. C., Thurman, G. B., Cohen, G. H., Schulof, R. S. and Goldstein, A. L. (1975) Purification and properties of bovine thymosin. *Ann. N.Y. Acad. Sci.* **249**, 125-144.

Ikura, M., Clore, G. M., Gronenborn, A. M., Zhu, G., Klee, C. B. and Bax, A. (1992) Solution structure of a calmodulin-target peptide complex by multidimensional NMR. *Science* **256**, 632-638.

Ito, M., Guerriero, V., Jr., Chen, X. and Hartshorne, D. J. (1991) Definition of the inhibitory domain of smooth muscle myosin light chain kinase by site-directed mutagenesis. *Biochemistry* **30**, 3498-3503.

Jeener, J. (1971) Ampere International Summer School. Basko Polje, Yugoslavia.

Kemp B. E., Pearson, R. B., Guerriero, V., Jr., Bagchi, I. C. and Means, A. R. (1987) The calmodulin binding domain of chicken smooth muscle myosin light chain kinase contains a pseudosubstrate sequence. *J. Biol. Chem.* **262**, 2542-2548.

Khan, N., Graslund, A., Ehrenberg, A. and Shriver, J. (1990) Sequence-specific ^1H NMR assignments and secondary structure of porcine motilin. *Biochemistry* **29**, 5743-5751.

King, G. and Wright, P. E. (1983) Application of two-dimensional relayed coherence transfer experiments to ^1H NMR studies of macromolecules. *J. Magn. Reson.* **54**, 328-332.

Kyte, J. and Doolittle, R. F. (1982) A simple method for displaying the hydrophobic character of a protein. *J. Mol. Biol.* **157**, 110.

LaPorte, D. C., Wierman, B. W. and Storm, D. R. (1980) Calcium-induced exposure of a hydrophobic surface on calmodulin. *Biochemistry* **19**, 3814-3819.

Lehrman, S. R., Tuls, J. L. and Lund, M. (1990) Peptide α -helicity in aqueous trifluoroethanol: correlations with predicted α -helicity and the secondary structure of the corresponding regions of bovine growth hormone. *Biochemistry* **29**, 5590-5596.

Llinas, M. and Klein, M. P. (1975) Charge relay at the peptide bond. A proton magnetic resonance study of solvation effects on the amide electron density distribution. *J. Am. Chem. Soc.* **97**, 4731-4737.

Low, T. K. L., Thurman, G. B., McAdoo, M., McClure, J., Rossio, J. L., Naylor, P. H. and Goldstein, A. L. (1979) The chemistry and biology of thymosin. I. Isolation, characterization, and biological activities of thymosin α_1 and polypeptide β_4 from calf thymus. *J. Biol. Chem.* **254**, 981-986.

Low, T. K. L. and Goldstein, A. L. (1979) The chemistry and biology of thymosin. II. Amino acid sequence analysis of thymosin α_1 and polypeptide β_4 . *J. Biol. Chem.* **254**, 987-995.

Lukas, J. L., Burgess, W. H., Prendergast, F. G., Lau, W. and Watterson, D. M. (1986) Calmodulin binding domains: Characterization of a phosphorylation and calmodulin binding site from myosin light chain kinase. *Biochemistry* **25**, 1458-1464.

Markus, M. A., Nakayama, T., Matsudaira, P. and Wagner, G. (1994) Solution structure of villin 14T, a domain conserved among actin-severing proteins. *Protein Science* **3**, 70-81.

Marqusee, S. and Baldwin, R. L. (1987) Helix stabilization by $\text{glu}^- \cdots \text{lys}^+$ salt bridges in short peptides of *de novo* design. *Proc. Natl. Acad. Sci. U.S.A.* **84**, 8898-8902.

Meador, W. E., Means, A. R. and Quioco, F. A. (1992) Target enzyme recognition by calmodulin: 2.4 Å structure of a calmodulin-peptide complex. *Science* **257**, 1251-1255.

Miller, J. F. A. P. (1961) Immunological function of the thymus. *Lancet* **2**, 784-789.

Mori, M., Barnard, G. F., Staniunas, R. J., Jessup, J. M., Steele, G. D. and Chen, L. B. (1993) Prothymosin α mRNA expression correlates with that of *c-myc* in human colon cancer. *Oncogene* **8**, 2821-2826.

Müller, N., Ernst, R. R. and Wüthrich, K. (1986) Multiple-quantum-filtered two-dimensional correlated NMR spectroscopy of proteins. *J. Am. Chem. Soc.* **108**, 6482-6492.

Murre, C., McCaw, P. S. and Baltimore, D. (1989) A new DNA binding and dimerization motif in immunoglobulin enhancer binding, daughterless, MyoD, and c-myc proteins. *Cell* **56**, 777-783.

Murre, C., McCaw, P. S., Vaessin, H., Caudy, M., Jan, L. Y., Jan, Y. N., Cabrera, C. V., Buskin, J. N., Hauschka, S. D., Lassar, A. B., Weintraub, H. and Baltimore, D. (1989) Interactions between heterologous helix-loop-helix proteins generate complexes that bind specifically to a common DNA sequence. *Cell* **58**, 537-544.

Mutchnick, M. G., Appelman, H. D., Chung, H. T., Aragona, E., Gupta, T. P., Cummings, G. D., Waggoner, J. G., Hoofnagle, J. H. and Shafritz, D. A. (1991) Thymosin treatment of chronic hepatitis B: A placebo-controlled pilot trial. *Hepatology* **14**, 409-415.

Nagayama, K., Kumar, A., Wüthrich, K. and Ernst, R. R. (1980) Experimental techniques of two-dimensional correlated spectroscopy. *J. Magn. Reson.* **40**, 321-334.

Nagayama, K. and Wüthrich, K. (1981) Systematic application of two-dimensional ¹H nuclear-magnetic-resonance techniques for the studies of proteins. 1. Combined use of spin-echo-correlated spectroscopy and J-resolved spectroscopy for the identification of complete spin systems of non-labile protons in amino-acid residues. *Eur. J. Biochem.* **114**, 365-374.

Novak, J. P., Charbonneau, H., Bentley, J. K., Walsh, K. A. and Beavo, J. A. (1991) Sequence comparison of the 63-, 61-, and 59-kDa calmodulin-dependent cyclic nucleotide phosphodiesterases. *Biochemistry* **30**, 7940-7947.

O'Neil, J. D. J. (1994) personal communication.

O'Neil, K. T. and DeGrado, W. F. (1990) How calmodulin binds its targets: sequence independent recognition of amphiphilic α -helices. *Trends in Biochem. Sci.* **15**, 59-64.

Papamarcaki, T. and Tsolas, O. (1994) Prothymosin α binds to histone H1 in vitro. *FEBS Lett.* **345**, 71-75.

Perrillo, R. P., Schiff, E. R., Davis, G. L., Bodenheimer, H. C., Lindsay, K., Payne, J., Dienstag, J. L., O'Brien, C., Tamburro, C., Jacobson, I. M., Sampliner, R., Feit, D., Lefkowitz, J., Kuhns, M., Meschievitz, C., Sanghvi, B., Albrecht, J. and Gibas, A. (1990) A randomized, controlled trial of interferon alfa-2b alone and after prednisone withdrawal for the treatment of chronic hepatitis B. *N. Engl. J. Med.* **323**, 295-301.

Piantini, U., Sørensen, O. W. and Ernst, R. R. (1982) Multiple quantum filters for elucidating NMR coupling networks. *J. Am. Chem. Soc.* **104**, 6800-6801.

Ptitsyn O. B. (1969) Statistical analysis of the distribution of amino acid residues among helical and non-helical regions in globular proteins. *J. Mol. Biol.* **42**, 501-510.

Putkey, J. A., Slaughter, G. R. and Means, A. R. (1985) Bacterial expression and characterization of proteins derived from the chicken calmodulin cDNA and a calmodulin processed gene. *J. Biol. Chem.* **260**, 4704-4712.

Ramsay, G., Evan, G. I. and Bishop, J. M. (1984) The protein encoded by the human proto-oncogene *c-myc*. *Proc. Natl. Acad. Sci. U.S.A.* **81**, 7742-7746.

- Rance, M. and Wright, P. E. (1986) Analysis of ^1H NMR spectra of proteins using multiple-quantum coherence. *J. Magn. Reson.* **66**, 372-378.
- Reid, R. E., Garipey, J., Saund, A. K. and Hodges, R. S. (1981) Calcium-induced protein folding. *J. Biol. Chem.* **256**, 2742-2751.
- Ross, P. D. and Subramanian, S. (1981) Thermodynamics of protein association reactions: forces contributing to stability. *Biochemistry* **20**, 3096-3102.
- Roth, S. M., Schneider, D. M., Strobel, L. A., Van Berkum, M. F. A., Means, A. R. and Wand, A. J. (1992) Characterization of the secondary structure of a calmodulin in complex with a calmodulin-binding domain peptide. *Biochemistry* **31**, 1443-1451.
- Sasaki, D. M. (1994) personal communication.
- Sburlati, A. R., De La Rosa, A., Batey, D. W., Kurys, G. L., Manrow, R. E., Pannell, L. K., Martin, B. M., Sheeley, D. M. and Berger, S. L. (1993) Phosphorylation of human and bovine prothymosin α *in vivo*. *Biochemistry* **32**, 4587-4596.
- Schafer, L. A., Goldstein, A. L., Gutterman, J. U. and Hersh, E. M. (1976) *In vitro* and *in vivo* studies with thymosin in cancer patients. *Ann. N.Y. Acad. Sci.* **277**, 607-620.
- Scheinberg, M. A., Goldstein, A. L. and Cathcart, E. S. (1976) Thymosin restores T cell function and reduces the incidence of amyloid disease in casein-treated mice. *J. Immunol.* **116**, 156-158.

Scholtz, J. M., Marqusee, S., Baldwin, R. L., York, E. J., Stewart, J. M., Santord, M. and Bolen, D. W. (1991) Calorimetric determination of the enthalpy change for the α -helix to coil transition of an alanine peptide in water. *Proc. Natl. Acad. Sci. U.S.A.* **88**, 2854-2858.

Shirley, B. A., Stanssens, P., Hahn, U. and Pace, C. N. (1992) Contribution of hydrogen bonding to the conformational stability of ribonuclease T1. *Biochemistry* **31**, 725-732.

Smith, M. R., Al-Katib, A., Mohammad, R., Silverman, A., Szabo, P., Khilnani, S., Kohler, W., Nath, R. and Mutchnick, M. G. (1993) Prothymosin α gene expression correlates with proliferation, not differentiation, of HL-60 cells. *Blood* **82**, 1127-1132.

States, D. J., Haberkorn, R. A. and Ruben, D. J. (1982) A two-dimensional nuclear overhauser experiment with pure absorption phase in four quadrants. *J. Magn. Reson.* **48**, 286-292.

Tappin, M. J., Pastore, A., Norton, R. S., Freer, J. H. and Campbell, I. D. (1988) High-resolution ^1H NMR study of the solution structure of δ -hemolysin. *Biochemistry* **27**, 1643-1647.

Thisse, B., Stoezel, C., Gorostiza-Thisse, C. and Perrin-Schmitt, F. (1988) Sequence of the twist gene and nuclear localization of its protein in endomesodermal cells of early *Drosophila* embryos. *EMBO J.* **7**, 2175-2183.

Tiollais, P., Pourcel, C. and Dejean, A. (1985) The hepatitis B virus. *Nature* **317**, 489-495.

Toniolo, C. (1970) Circular dichroism of some aliphatic amino acid derivatives. Reexamination. *J. Phys. Chem.* **74**, 1390-1392.

Toniolo, C., Bonora, G. M., Salardi, S. and Mutter, M. (1979) A circular dichroism study of α -helix and β -structure formation in solution by homooligo-L-methionines. *Macromolecules* **12**, 620-625.

Trong, H. L., Beier, N., Sonnenburg, W. K., Stroop, S. D., Waish, K. A., Beavo, J. A. and Charbonneau, H. (1990) Amino acid sequence of the cyclic GMP stimulated cyclic nucleotide phosphodiesterase from bovine heart. *Biochemistry* **29**, 10280-10288.

Tsitsiloni, O. E., Stiakakis, J., Koutselinis, A., Gogas, J., Markopoulos, C., Yialouris, P., Bekris, S., Panoussopoulos, D., Kiortsis, V., Voelter, W. and Haritos, A. A. (1993) Expression of α -thymosins in human tissues in normal and abnormal growth. *Proc. Natl. Acad. Sci. U.S.A.* **90**, 9504-9507.

Van Antwerp, M. E., Chen, D. G., Chang, C. and Prochownik, E. V. (1992) A point mutation in the MyoD basic domain imparts c-Myc-like properties. *Proc. Natl. Acad. Sci. U.S.A.* **89**, 9010-9014.

Van Berkum, M. F. A. and Means, R. A. (1991) Three amino acid substitutions in domain I of calmodulin prevent the activation of chicken smooth muscle myosin light chain kinase. *J. Biol. Chem.* **266**, 21488-21495.

Villares, R. and Cabrera, C. V. (1987) The *achaete-scute* gene complex of *D. melanogaster*: conserved domains in a subset of genes required for neurogenesis and their homology to *myc*. *Cell* **50**, 415-424.

Voronova, A. and Baltimore, D. (1990) Mutations that disrupt DNA binding and dimer formation in the E47 helix-loop-helix protein map to distinct domains. *Proc. Natl. Acad. Sci. U.S.A.* **87**, 4722-4726.

Wagner, G., Kumar, A. and Wüthrich, K. (1981) Systematic application of two-dimensional ^1H nuclear-magnetic-resonance techniques for studies of proteins. 2. Combined use of correlated spectroscopy and nuclear overhauser spectroscopy for sequential assignments of backbone resonances and elucidation of polypeptide secondary structures. *Eur. J. Biochem.* **114**, 375-384.

Wagner, G. (1990) NMR investigations of protein structure. *Prog. NMR Spec.* **22**, 101-134.

Waldmann, R., Hanson, P. I. and Schulman, H. (1990) Multifunctional Ca^{2+} /calmodulin-dependent protein kinase make Ca^{2+} independent for functional studies. *Biochemistry* **29**, 1679-1684.

Walsh, M. P., Dabrowska, R., Hinkins, S. and Hartshorne, D. J. (1982) Calcium-independent myosin light chain kinase of smooth muscle. Preparation by limited chymotryptic digestion of the calcium ion dependent enzyme, purification, and characterization. *Biochemistry* **21**, 1919-1925.

Wara, D. W., Goldstein, A. L., Doyle, W. and Ammann, A. J. (1975) Thymosin activity in patients with cellular immunodeficiency. *N. Engl. J. Med.* **292**, 70-74.

Wara, D. W. and Ammann, A. J. (1976) Thymic cells and humoral factors as therapeutic agents. *Pediatrics* **57**, 643-646.

Williamson, M. P. and Waltho, J. P. (1992) Peptide structure from NMR. *Chem. Soc. Rev.* **21**, 227-236.

Wishart, D. S., Sykes, B. D. and Richards, F. M. (1991) Relationship between nuclear magnetic resonance chemical shift and protein secondary structure. *J. Mol. Biol.* **222**, 311-333.

Wüthrich, K., Billeter, M. and Braun, W. (1984) Polypeptide secondary structure determination by nuclear magnetic resonance observation of short proton-proton distances. *J. Mol. Biol.* **180**, 715-740.

Wüthrich, K. (1986) *NMR of proteins and nucleic acids*. J. Wiley and Sons, New York.

Zagorski, M. G., Norman, D. G., Barrow, C. J., Iwashita, T., Tachibana, K. and Patel, D. J. (1991) Solution structure of pardaxin P-2. *Biochemistry* **30**, 8009-8017.

Zarbock, J., Oschkinat, H., Hannappel, E., Kalbacher, H., Voelter, W. and Holak, T. A. (1990) Solution conformation of thymosin β_4 : A nuclear magnetic resonance and simulated annealing study. *Biochemistry* **29**, 7814-7821.

Zhang, M., Yuan, T. and Vogel, H. J. (1993) A peptide analog of the calmodulin-binding domain of myosin light chain kinase adopts an α -helical structure in aqueous trifluoroethanol. *Protein Science* **2**, 1931-1937.

Zhang, M., Li, M., Wang, J. H. and Vogel, H. J. (1994) The effect of met \rightarrow leu mutations on calmodulin's ability to activate cyclic nucleotide phosphodiesterase. *J. Biol. Chem.* **269**, 15546-15552.

Zhou, N. E., Kay, C. M., Sykes, B. D. and Hodges, R. S. (1993) A single-stranded amphipathic α -helix in aqueous solution: design, structural characterization, and its application for determining α -helical propensities of amino acids. *Biochemistry* **32**, 6190-6197.

Zisblatt, M., Goldstein, A. L., Lilly, F. and White, A. (1970) Acceleration by thymosin of the development of resistance to murine sarcoma virus-induced tumor in mice. *Proc. Natl. Acad. Sci. U.S.A.* **66**, 1170-1174.

PART B

**Two-dimensional Nuclear Magnetic Resonance
Studies of RNase A in the Presence
of Uridine Vanadate**

CHAPTER FIVE

INTRODUCTION

5.1) Ribonuclease A

5.1.a) Specificity and Enzymatic Mechanism

Ribonucleases (RNases) are a class of enzymes which are responsible for the digestion, processing and turnover of various classes of ribonucleic acids (RNA). Different RNases display particular specificities for a certain type of base within a RNA chain, hydrolyzing only after purines or pyrimidines, or differ in their catalytic mechanism (Eftink and Biltonen, 1987). Some particular RNases catalyze the degradation or processing of single stranded RNA much better than double stranded RNA (Eftink and Biltonen, 1987).

The most extensively studied member of this class of enzymes is bovine pancreatic RNase A. The primary reasons for its popularity is that it is readily available in large quantities, is highly stable, and is small in size (MW 13.7 kDa) (Eftink and Biltonen, 1987). The protein is comprised of a single chain of 124 amino acid residues (Figure 47). RNase A is secreted by the pancreas and is responsible for the digestion of single stranded RNA. The enzyme is specific for phosphodiester linkages with a uridine or cytidine base at the 3'-position, since a guanine or adenine ring is too large to fit into the active site without severely distorting it (Eftink and Biltonen, 1987). The uracil or cytosine ring binds within the active site through several hydrogen bonds with Thr45

1 Lys-Glu-Thr-Ala-Ala-Ala-Lys-Phe-Glu-Arg
11 Gln-His-Met-Asp-Ser-Ser-Thr-Ser-Ala-Ala
21 Ser-Ser-Ser-Asn-Tyr-Cys-Asn-Gln-Met-Met
31 Lys-Ser-Arg-Asn-Leu-Thr-Lys-Asp-Arg-Cys
41 Lys-Pro-Val-Asn-Thr-Phe-Val-His-Glu-Ser
51 Leu-Ala-Asp-Val-Gln-Ala-Val-Cys-Ser-Gln
61 Lys-Asn-Val-Ala-Cys-Lys-Asn-Gly-Gln-Thr
71 Asn-Cys-Tyr-Gln-Ser-Tyr-Ser-Thr-Met-Ser
81 Ile-Thr-Asp-Cys-Arg-Glu-Thr-Gly-Ser-Ser
91 Lys-Tyr-Pro-Asn-Cys-Ala-Tyr-Lys-Thr-Thr
101 Gln-Ala-Asn-Lys-His-Ile-Ile-Val-Ala-Cys
111 Glu-Gly-Asn-Pro-Tyr-Val-Pro-Val-His-Phe
121 Asp-Ala-Ser-Val

Figure 47. The Primary Structure of Bovine Pancreatic RNase A (Smyth *et al.*, 1963).

(Eftink and Biltonen, 1987). The nature of the rest of the interaction between RNase A and the RNA chain is primarily electrostatic. A series of nine positively charged Lys and Arg side chains form salt bridges with the negatively charged phosphate backbone of RNA (Eftink and Biltonen, 1987).

Even before the three-dimensional structure of RNase A was known, much information about the catalytic mechanism of the enzyme was already deduced (Eftink and Biltonen, 1987). The enzyme displays maximum activity at a pH value of 7.0, and the plot of reaction rate versus pH is bell-shaped. Since the optimum pH value for catalytic activity was 7.0, this result led investigators to propose that two His residues participated in catalysis, one in the basic form and the other in the acidic form (Findlay *et al.*, 1962). The imidazole ring of His plays a critical role in the function of a number of proteins (Markley, 1975a). The usefulness of His arises from its acid-base properties, since it is the only amino acid which can behave as either an acid or base at physiological pH (Markley, 1975a). It has been shown that by reacting RNase A with iodoacetate, the imidazole ring of either His12 or His119, but not both in the same protein molecule, is carboxymethylated (Blackburn and Moore, 1982). This chemical modification results in an inactive enzyme. Substrates or competitive inhibitors protecting His12 and His119 from modification prevent the inactivation of the enzyme by iodoacetate (Blackburn and Moore, 1982). These findings suggested that His12 and His119 are near each other in the active site and play a critical role in the catalytic mechanism. X-ray crystallographic studies eventually confirmed the presence of His12 and His119 in the active site of the enzyme (Kantha, 1967; Avey *et al.*, 1967).

The catalytic mechanism of RNase A is believed to consist of a two-step process

(Richards and Wyckoff, 1971). The first step is a transphosphorylation in which the 3'-5'-phosphodiester linkage is transesterified to a cyclic 2',3'-phosphate. The second step is a hydrolysis, in which the cyclic 2',3'-phosphate is converted to a 3'-phosphate. Three residues play a critical role in the mechanism: His12, His119, and Lys41. The transphosphorylation reaction begins with the acceptance of a proton from the 2'-OH group of the nucleotide by the un-ionized form of His12 (Figure 48). At the same time the protonated form of His119 donates its proton to the 5'-O and the 2'-O begins to form a bond with the phosphorous atom, which becomes transiently bonded to five oxygen atoms. This pentacovalent transition state is electrostatically stabilized by the nearby positively charged side chain of Lys41 (not shown). The bond between the phosphorous atom and the 5'-O breaks when a proton from the His119 side chain is completely transferred to this oxygen atom. At the same time a bond between the phosphorous atom and the 2'-O becomes fully formed, producing the 2',3'-cyclic intermediate. The subsequent hydrolysis reaction is essentially the reverse of the transphosphorylation reaction (Figure 49). Histidine 119 removes a proton from a water molecule positioned within the active site. The leftover OH⁻ ion then attacks the phosphorous atom, while at the same time His12 donates a proton back to the 2'-O causing the bond between this oxygen atom and the central phosphorous atom to rupture. The final product contains a hydroxyl group at the 2'-position and a free 3'-phosphate group in the nucleotide complex. The shortened RNA chain is then released from the active site of the enzyme.

5.1.b) Structure

Ribonuclease A is composed of 124 amino acid residues giving it a molecular weight of 13 700 Da. The enzyme contains four disulfide bonds between the following residues:

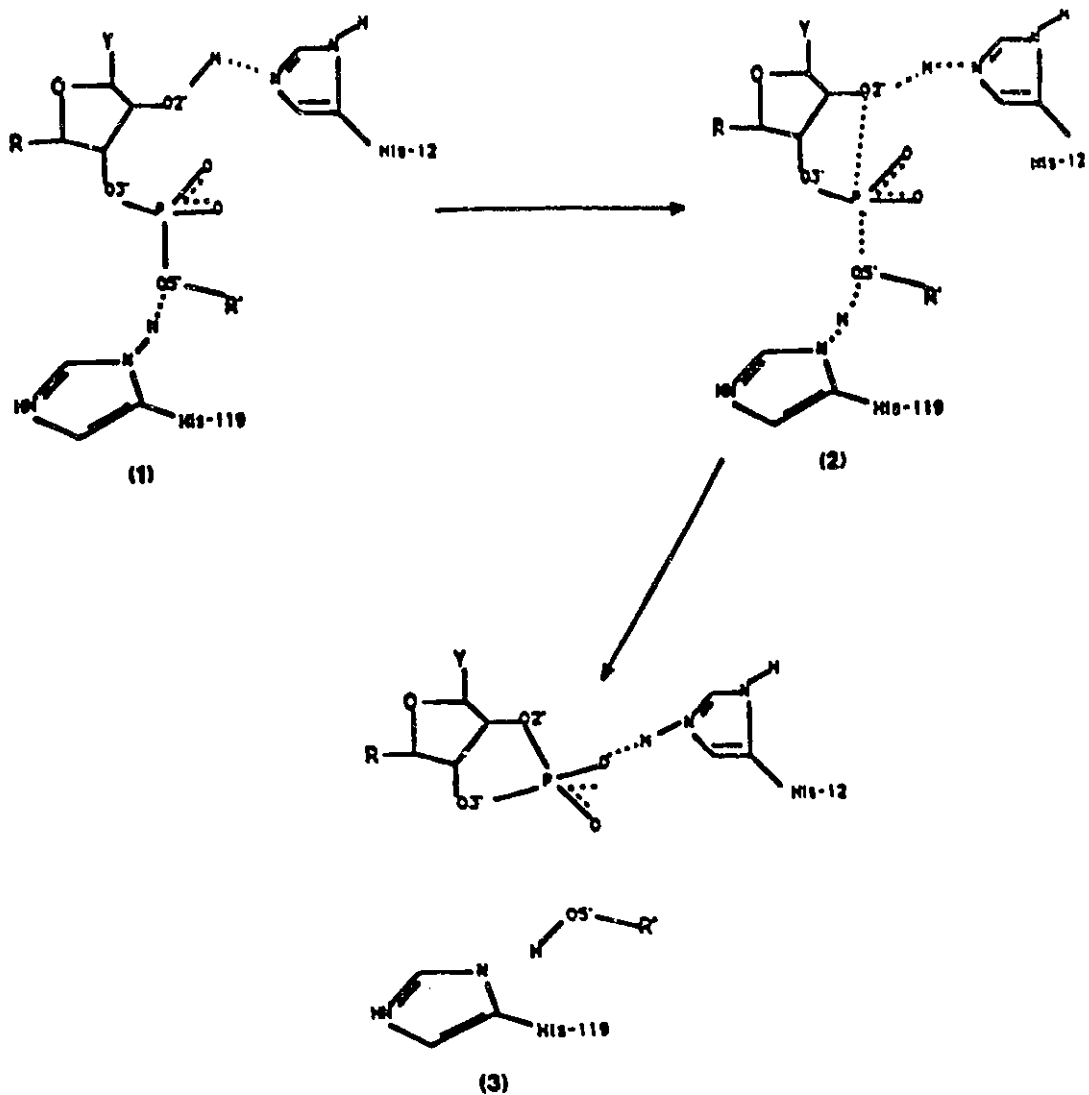


Figure 48. Transphosphorylation Mechanism of RNase A. Histidine 119 acts as an acid and His12 acts as a base in the formation of the cyclic intermediate (3) in the digestion of RNA by the enzyme (Richards and Wyckoff, 1971).

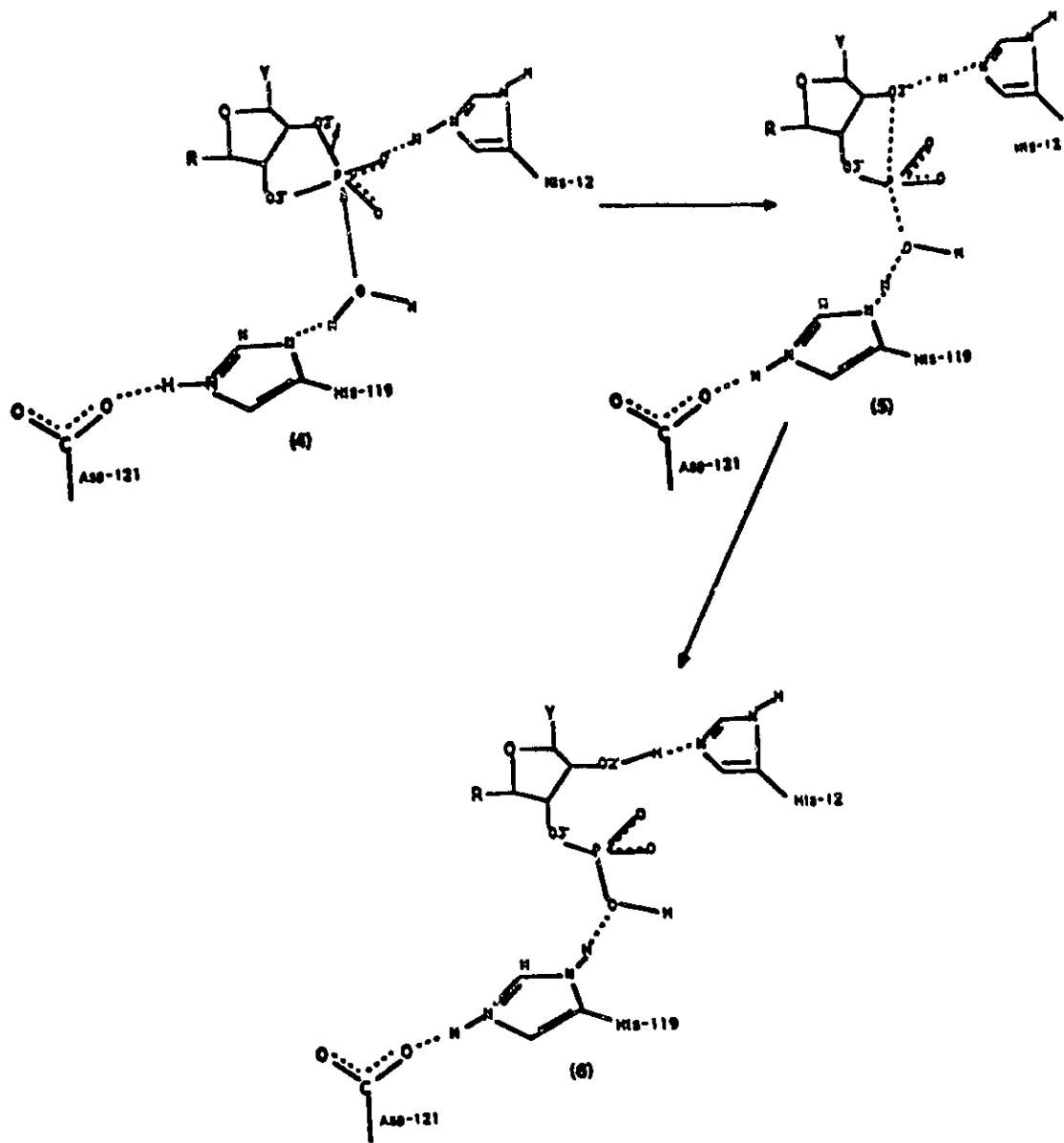


Figure 49. Hydrolytic Mechanism of RNase A. Histidine 119 acts as a base and His12 acts as an acid in the hydrolysis of the cyclic intermediate (4). Aspartic acid 121 is hydrogen bonded to His119 in the hydrolytic reaction, increasing the basicity of His119. The result is a shortened RNA chain with a free 3'-phosphate group (6) (Richards and Wyckoff, 1971).

Cys26/Cys84, Cys40/Cys95, Cys58/Cys110, and Cys65/Cys72. In the late 1960's, the crystal structure of RNase A was solved independently by two groups with essentially identical results (Avey *et al.*, 1967; Kartha, 1967). In the 1980's, a resurgence in the investigation of the crystal structure of the enzyme occurred. The data for the crystal structure of the enzyme was refined to a resolution of 2.5 Å (Wlodawer, 1980) and later to 1.45 Å (Borkakoti *et al.*, 1982). The results of these studies are also essentially identical (Eftink and Biltonen, 1987).

The three-dimensional structure RNase A is shown in Figure 50. RNase A is a U-shaped protein, with dimensions of 35 x 45 x 31 Å (Borkakoti *et al.*, 1982). It contains three sections of helix and an extensive region of β -pleated sheet made up of three antiparallel chains (Borkakoti *et al.*, 1982). One of the stretches of helix, running between residues 3 to 13 in the amino terminus region of the protein, forms one of the walls of a cleft which harbours the active site of RNase A. A second stretch of helix runs between Asn24 to Arg33 and includes a turn of 3_{10} -helix. The third region of helix lies between residues 50 to 60. The three chains of antiparallel β -sheet are formed by residues 42 to 48, 71 to 92 and 94 to 110. The peptide bonds of Pro93 and Pro114 are in a *cis* configuration and are involved in the reversal of the chain direction (Wlodawer, 1980).

The structure of RNase A was refined jointly with neutron and X-ray diffraction data extending to 2.0 Å (Wlodawer and Sjolín, 1983). Through the use of neutron diffraction data, the position of hydrogen and deuterium atoms could be determined. This work allowed the location of 128 water sites to be established in the protein crystal, as well as, unambiguously defined the position of several amino acid side chains whose positions

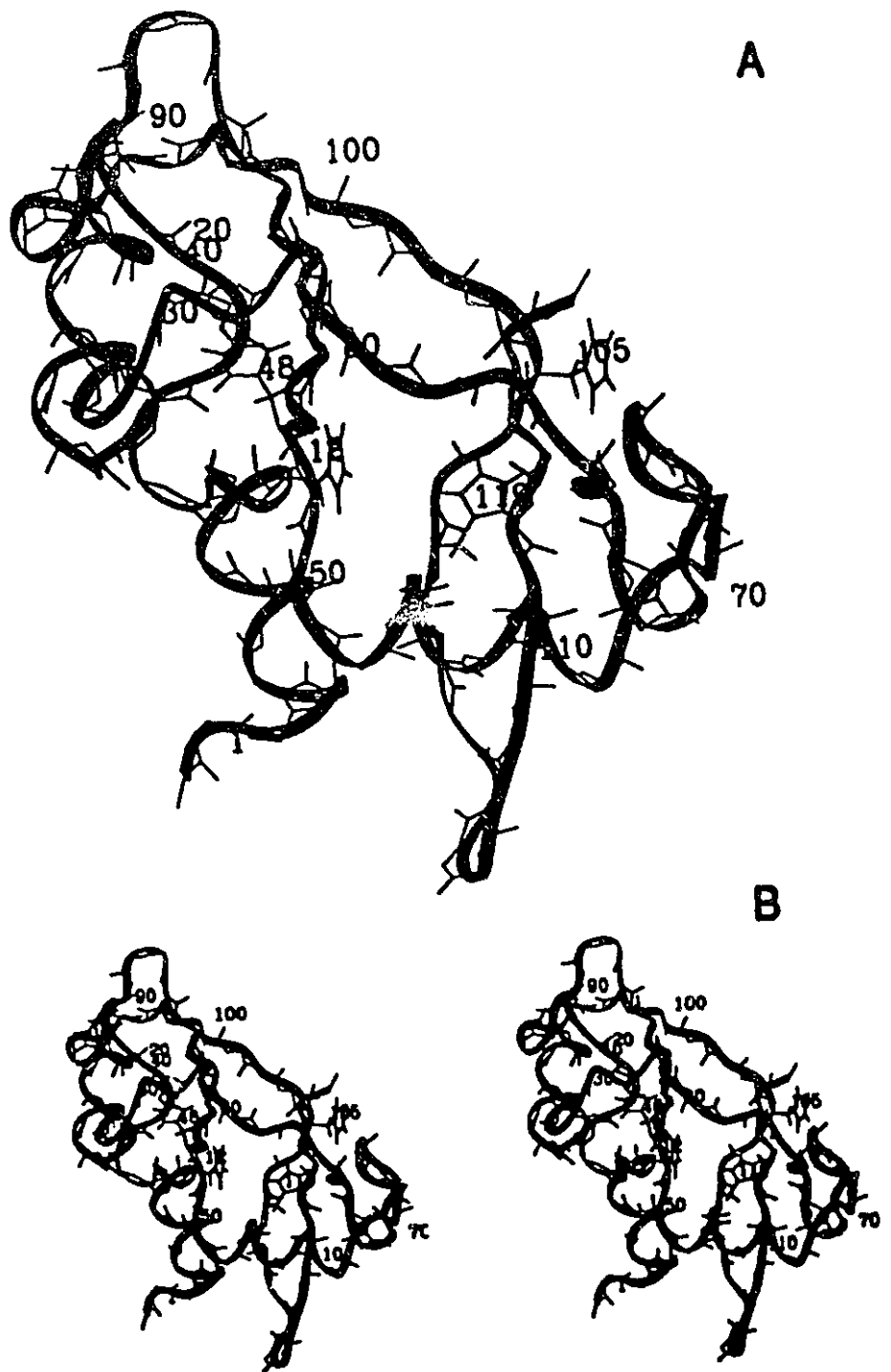


Figure 50. The Three-Dimensional Structure of RNase A. The positions of the four His residues are shown and labelled in (A). Only the backbone atoms of the remaining residues are shown. A stereoview of the three-dimensional structure of RNase A is shown in (B). (Bernstein *et al.*, 1977; Wlodawer *et al.*, 1982) (Protein Data Bank, reference 5RSA). 169

had been unclear up to that point. Some of the significant refinements included the repositioning of residues Asn44, Val124, Lys7, Lys37 and Lys41. The repositioning of the Lys41 side chain was a major refinement, since it is near the active site of the enzyme. A wide variation in the position of the Lys41 side chain had been observed in various X-ray diffraction studies of RNase A, with the distance from N ζ of Lys41 to the phosphorous atom of the active site-bound phosphate molecule ranging anywhere from 9.4 Å to about 4.0 Å. The refinement of the neutron diffraction data indicated that the side chain of Lys41 is located relatively close to the phosphorous atom of the bound ligand. This repositioning in the side chain of Lys41 was significant, since it had been proposed that the charged side chain of this residue moves towards the phosphate group of the substrate during catalysis, thus increasing the stability of the transition state of the substrate (Richards and Wyckoff, 1971; Holmes *et al.*, 1978).

5.2) Position of Histidine 119 and Histidine 12

As previously mentioned, the two most important catalytic residues within RNase A are His12 and His119. In the neutron diffraction structure of RNase A crystals grown in 43% t-butyl alcohol at pH 5.3 with no phosphate molecule bound in the active site, both His12 and His119 occupied unique positions (Wlodawer and Sjolín, 1981). In the X-ray crystallographic structure of RNase A crystals grown in 60% aqueous ethanol, at pH 5.2 to 5.7, with a molecule of sulfate bound to the active site, the His119 side chain was observed in two discrete locations (Borkakoti *et al.* 1982). The two observed positions of His119 are shown in Figure 51. The relative occupancies of the two positions were estimated at 0.80 for the major position, termed position A, or His119A, and 0.20 for the minor position, termed position B, or His119B. The side-chain torsion

angles corresponding to the two positions of His119 are: $\chi_1(\text{N-C}\alpha\text{-C}\beta\text{-C}\gamma) = 149^\circ$ and $\chi_2(\text{C}\alpha\text{-C}\beta\text{-C}\gamma\text{-C}\delta) = -101^\circ$ for His119A and $\chi_1 = -69^\circ$, $\chi_2 = -63^\circ$ for His119B. The relative positions of His119A and His119B are shown in Figure 51.

It was soon postulated that the ability of His119 to occupy two discrete positions may be catalytically important to the enzyme (Borkakoti, 1983). In studies of the active site dynamics of RNase A, His119 was observed to undergo dihedral angle transitions in some of the simulations, which confirmed the suggestion that this freedom of movement might be catalytically important (Brunger *et al.*, 1985). Harris *et al.*, (1987) using the coordinates of a refined crystal structure of the enzyme at 1.45 Å resolution (Borkakoti *et al.*, 1984), calculated the non-bonded potential energy contributions of all residues having at least one atom within 10 Å of His119. An energy map was constructed for values of χ_1 and χ_2 , each varying from 0 to 360° in steps of 20°. The nonbonded potential energy map revealed two discrete side chain positions for His119 located at points of minimum energy (Harris *et al.*, 1987). These positions, which correspond to the crystallographically observed A and B positions, were also linked by a low-energy pathway. These early results showing the flexibility of the His119 side chain, led many other groups to investigate the position of this residue in the presence of various inhibitors attempting to explain what role it might play in the mechanism of the enzyme. Table XI gives a list of some of the several structural studies of the position of His119 in the presence and absence of various ligands bound to the active site of RNase A.

One of the first major crystallographic studies of the active site structure of different inhibitor/enzyme complexes involved the three inhibitors 8-oxo-guanosine 2'-phosphate (O⁸-2'-GMP), cytidine-N(3)-oxide 2'-phosphate (O³-2'-CMP), and

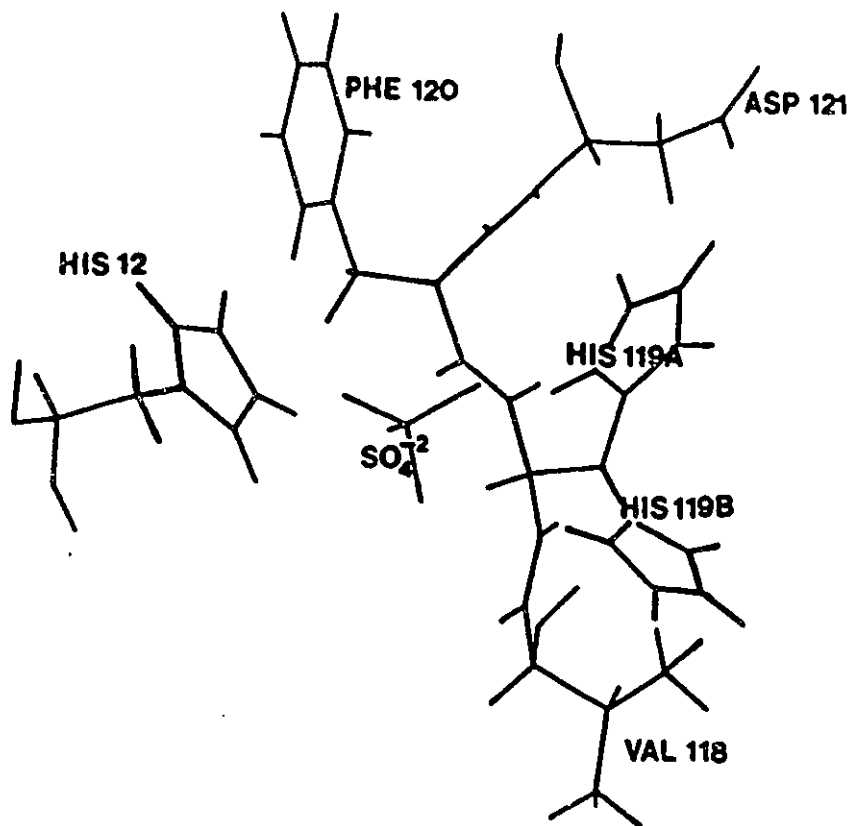


Figure 51. The Observed Positions of His119 of RNase A. Histidine 119 is able to occupy two discrete positions within the active site of the enzyme. The major position with the highest occupancy rate, in the crystal structure of the enzyme with a sulfate molecule bound to the active site, was termed His119A ($\chi_1=149^\circ$, $\chi_2=-101^\circ$) and the minor position was termed His119B ($\chi_1=-69^\circ$, $\chi_2=-63^\circ$) (Borkakoti *et al.*, 1982; Bernstein *et al.*, 1977; Włodawer *et al.*, 1982) (Protein Data Bank, reference 5RSA).

TABLE XI

Position of Histidine 119 in the Crystal Structures of RNase A
with Various Active Site Ligands

Active Site ^a	Conditions ^b	A ^c (%)	B ^d (%)	Reference
Ligand-free	55% t-butanol	100	0	Wlodawer et al., 1988.
SO ₄ ²⁻	30-40% ethanol, pH 5.2-5.7	100	0	Palmer et al., 1991.
SO ₄ ²⁻	60% ethanol	80	20	Borkakoti et al., 1982.
PO ₄ ³⁻	43% t-butanol, pH 5.3	100	0	Wlodawer et al., 1983.
0 ⁸ -2'GMP	40% ethanol, pH 5.2-5.7	100	0	Borkakoti et al., 1983.
2'GMP	40% ethanol, pH 5.2-5.7	80	20	Borkakoti et al., 1983.
0 ³ -2'GMP	40% ethanol, pH 5.2-5.7	0	100	Borkakoti et al., 1983.
U-V	43% t-butanol, pH 5.3	100	0	Borah et al., 1985.
U-H119 ^e	28% (NH ₄) ₂ SO ₄ , pH 5.1	-	x ^f	Nachman et al., 1990.
T-H129	28% (NH ₄) ₂ SO ₄ , pH 5.1	x	- ^f	Nachman et al., 1990.
SO ₄ ^{2-h}	1.3 M (NH ₄) ₂ SO ₄ , pH 5.2	0	100	detel et al., 1992.

^aligand found within the active site of enzyme crystal.

^bconditions under which the enzyme was crystallized.

^cpercentage of His119 residues found in the A position.

^dpercentage of His119 residues found in the B position.

^e[[[3'-deoxy-3'-uridiny]amino]carbonylmethyl] bound to N81 of His119.

^frelative occupancies of two positions not given.

^g[[[3'-deoxy-3'-thymidiny]amino]carbonylmethyl] bound to N22 of His12.

^hsemisynthetic RNase A

cytidine 2'-monophosphate (2'-CMP) (Table XI) (Borkakoti, 1983). The inhibitor/enzyme complexes were prepared by soaking native RNase A crystals, prepared in 40% ethanol at pH 5.2-5.7, in solutions of the individual nucleotide complexes. In the O⁸-2'-GMP/RNase A complex, His119 is observed to be in the A position, and a solvent molecule was seen in the B position. The binding of O³-2'-CMP in the active site had a stabilizing effect of His119 in the B position. The side chain rearrangement was essential as the A position was blocked by the 3'-O of the sugar ring. With 2'-CMP bound to the active site of the enzyme, no effect was seen on the equilibrium position of the side chain of His119 (Borkakoti, 1983).

Two groups investigated the position of His119 of RNase A with a phosphate molecule bound to the active site (Wlodawer *et al.*, 1983) and with the enzyme free of phosphate (Wlodawer and Sjolín, 1981). Both crystals were grown from 43% t-butyl alcohol under identical conditions and both showed His119 solely in the A position. The structure of phosphate-free RNase A with crystals grown in 55% t-butyl alcohol also showed His119 exclusively in the A position (Table XI) (Wlodawer *et al.*, 1983).

The molecular packing of six crystal forms of RNase A, grown in t-butanol, ethanol, ammonium sulfate, and polyethylene glycol 4000 have been compared (Crosio *et al.*, 1992). The number of intermolecular contacts and the amount of surface area covered between contacts, were different in the six packings. Active site His119 is observed to occur in position A or position B, in the six forms, and is highly solvent accessible (Lee and Richards, 1971). In each of the six different molecular packings of RNase A, His119 is not involved in any intermolecular contacts (Crosio *et al.*, 1992). Therefore, crystal packing effects are not responsible for the differences observed in the position of

His119.

5.3) Nuclear Magnetic Resonance Studies of RNase A

Proton NMR assignments have been made for 121 of the 124 residues of RNase A (Robertson *et al.*, 1989; Rico *et al.*, 1989). The NOESY spectrum of phosphate-bound RNase A at pH 4.0 and 35°C (Santoro *et al.*, 1993) showed a strong NOE between one of the methyl signals of Val118 and the H ϵ 1 proton of His119, placing His119 in the vicinity of Val118, which abuts the B position. Such a cross peak would not be predicted by the X-ray crystallographic structure of RNase A, since the distance between the methyl groups of Val118 and the H ϵ 1 proton of His119 in the A position ranges from 7.7 to 11.4 Å (Wlodawer *et al.*, 1982). This result suggests that there is a difference in the position of the His119 side chain between the solution and the crystal structures.

5.4) Interaction with Uridine Vanadate

Shortly after the observation of two discrete positions for His119 in the X-ray crystallographic structure of RNase A, the neutron diffraction structure of RNase A in the presence of uridine vanadate (U-V) was solved (Wlodawer *et al.*, 1983). The structure of U-V is shown in Figure 52. Uridine vanadate has been postulated to be a transition-state analog for RNase A (Lindquist *et al.*, 1973). A transition-state analog for an enzyme is a stable compound that resembles the structure of the substrate portion of the transition state of the enzymatic reaction (Lienhard, 1973). The hypothesis that U-V is a transition-state analog for RNase A is based on kinetic evidence (Lindquist *et al.*, 1973). The kinetic data were obtained by measuring the dissociation constants for

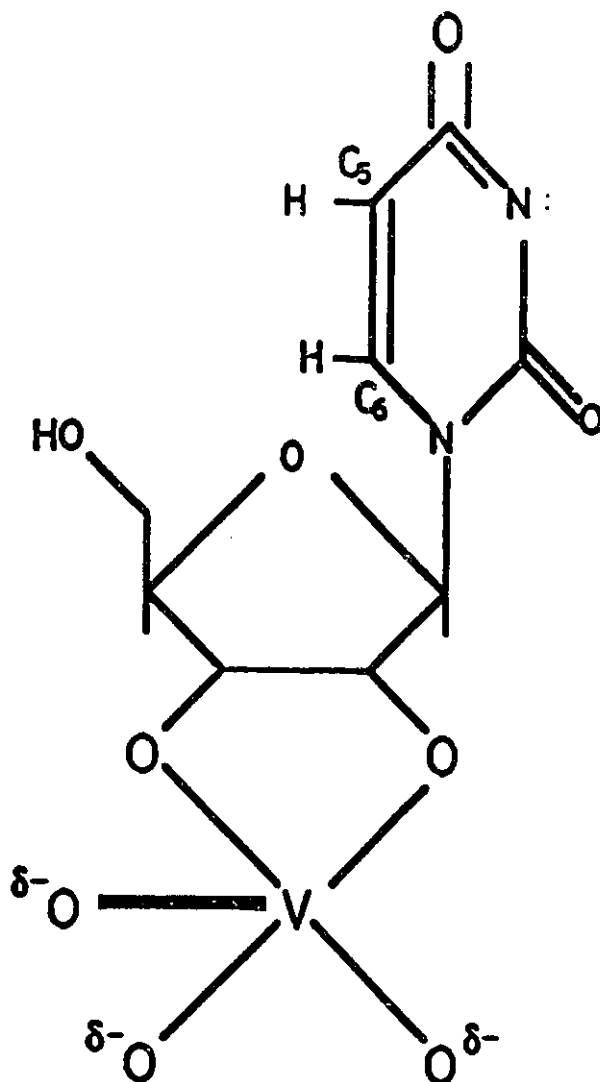


Figure 52. The Structure of Uridine Vanadate. The position of the C₅H and C₆H atoms on the uridine base are labelled.

the binding of U-V(IV) and U-V(V) complexes to RNase A and comparing them to the dissociation constants for uridine-2',3'-phosphate (U-2',3'-P) and uridine-3'-phosphate (U-3'-P), which are, respectively the substrate and product of the hydrolysis reaction catalyzed by RNase A (Lindquist *et al.*, 1973). The dissociation constant for the binding of the U-V(IV) complex to RNase A was 0.008 mM which is over 1000 times smaller than for the dissociation constant of the substrate, and over 40 times smaller than the dissociation constant for the product. Similarly, the dissociation constant for the binding of U-V(V) complex to RNase A was 0.011 mM which is almost 1000 times smaller than the dissociation constant for the substrate, and 40 times smaller than the dissociation constant for the product (Lindquist *et al.*, 1973).

Since there was no structural data by which to postulate what was the cause of the unusually strong binding of the vanadium complexes to the enzyme, the following possible explanations were postulated. First, one or more groups at the active site of the enzyme may coordinate to vanadium. V(IV) itself had been observed to be an effective inhibitor of the enzyme having a dissociation constant of 0.065 mM, which is 160 times smaller than the dissociation constant of U-2',3'-P (Lindquist *et al.*, 1973). The second possible explanation was that the inhibitor possesses a structure that is similar to the substrate portion of the transition state for the RNase A catalyzed reaction, suggesting the inhibitor is a transition-state analog for this enzyme (Lindquist *et al.*, 1973).

The neutron diffraction structure of the enzyme-transition state analog complex was solved using crystals of RNase A, grown in 43% t-butyl alcohol (pH 5.3), which had been soaked in a solution of U-V (Wlodawer *et al.*, 1983). The structure of the U-V/RNase A complex showed that the vanadium complex forms a trigonal bipyramidal

structure within the active site of the enzyme, in the same region where the phosphate group of the substrate is normally observed (Wlodawer *et al.*, 1983). The same position for His12 as found in all previous structural studies of RNase A was observed. As well, His119 was seen exclusively in the A position (Wlodawer *et al.*, 1983). It was also observed that the side chain of Lys41 was hydrogen bonded to the oxygen atom that His12 transfers a proton to in the hydrolysis of the cyclic phosphate intermediate (Borah *et al.*, 1985). This observation was a direct contradiction of the accepted mechanism of the enzymatic reaction in which both His12 and His119 are involved in proton transfer, while Lys41 is thought to provide a stabilization role for the transition-state complex (Richards and Wyckoff, 1971). The distance between the Nε2 proton of the His12 imidazole ring and the O2' atom of U-V was only 3.0 Å, so proton transfer was still entirely possible although no evidence of a hydrogen bond between these two atoms was observed (Borah *et al.*, 1985).

5.5) Objectives of This Research

Much has been deduced about the structure and catalytic mechanism of RNase A. One of the more puzzling aspects of the structure of RNase A lies in the flexibility of the active site residue His119. This residue has been shown to occupy two discrete positions and the relative occupancy of these positions depends on the conditions under which the structure of the enzyme is examined. Our purpose is to examine the positions of His119 and His12 in the presence of U-V, a transition-state analog for this enzyme (Lindquist *et al.*, 1973). The positions of these two residues are examined in solution using nuclear Overhauser enhancement spectroscopy. The positions of His12 and His119 are then compared to their positions in the combined neutron and 2 Å resolution x-ray

diffraction analyses of the structure of the U-V/RNase A complex (Bernstein *et al.*, 1977; Borah *et al.*, 1985; Wlodawer *et al.*, 1983) (Protein Data Bank, reference 6RSA). The results of this study may help to explain the role the flexibility of His119 plays in the catalytic mechanism of the enzyme and define which step in the catalytic mechanism of the enzyme, for which U-V acts as a transition-state analog.

CHAPTER SIX

MATERIALS AND METHODS

6.1) Materials

6.1.a) Proteins

RNase A (R-5125) was purchased from Sigma Chemical Company (St. Louis, MO 63178).

6.1.b) Chemicals

Cytidine 3'-monophosphate (3'-CMP) (C-1133), and uridine (U-3750) were purchased from Sigma Chemical Company. Ammonium metavanadate (NH_4VO_3) (B10027-34) was purchased from BDH Inc. (Toronto, Ontario M8Z 1K5).

6.2) Instrumentation

One-dimensional ^{51}V -NMR spectra were acquired at 52.58 MHz using a AC-200 NMR spectrometer manufactured by Bruker Spectrospin Ltd. (Milton, Ontario L9T 1Y6).

One- and two-dimensional ^1H -NMR spectra were acquired at 300 MHz using a AC-300 NMR spectrometer manufactured by Bruker Spectrospin Ltd.

6.3) Methodology

6.3.a) NMR Spectroscopy

^{51}V -NMR measurements were carried out on a Bruker AC-200 spectrometer operating at a frequency of 52.58 MHz. The one-dimensional ^{51}V -NMR spectra were recorded using the following parameters: 10 kHz spectral window; 8K data points; 0.393 acquisition time; 1 μs pulse width; 0 s relaxation delay. Since the ^{51}V nucleus has such a short T_1 relaxation time, it is possible to use a very short pulse width with a 0 s relaxation delay to increase the number of possible transients that can be acquired in a suitable time period. The spectrum of NH_4VO_3 was comprised of 100 transients, while the spectrum of uridine vanadate (U-V) was comprised of 149 000 scans. Both spectra were recorded at 295 K.

All one- and two-dimensional ^1H -NMR measurements were carried out at 300 MHz on a Bruker AC-300 spectrometer at 303 K. The spectra were recorded using a 5 mm ^1H selective probe in quadrature detection mode. The one-dimensional ^1H -NMR spectra were recorded using the following parameters: 16K data points, 60° pulse width, relaxation delay of 2 s and 500 to 800 scans. In all one-dimensional ^1H -NMR experiments involving the U-V/RNase A complex, a relaxation delay of 4 s was used. The two-dimensional NOESY spectrum of the U-V/RNase A complex was recorded using a phase sensitive mode with presaturation of solvent (Bodenhausen *et al.*, 1984) and a mixing time of 200 ms. In the NOESY experiment, 2048 data points were collected in the t_2 domain. Typically 512 time increments were acquired in the t_1 domain and the

FID's were zero-filled to 2048 data points prior to Fourier transformation. Spectral widths of 3.6 kHz in the F1 direction and 1.8 kHz in the F2 direction were used. Prior to Fourier transformation, the NOESY data were multiplied by a sinebell function of 0.32 in both directions. The spectrum was symmetrized after Fourier transformation.

6.3.b) pH* Titration of RNase A

A 2.79 mM sample of RNase A was prepared by dissolving 17.6 mg of the enzyme in 0.3 M NaCl and 0.5 mM DSS in D₂O. The total volume of the sample was 0.5 mL. The sample was then transferred to a 5 mm NMR tube. The pH* of the sample was adjusted to 3.0 and heated at 60°C for one hour to exchange the backbone amide protons with deuterons. pH* refers to the direct pH meter reading uncorrected for the deuterium isotope effect (Glasoe and Long, 1960). The ¹H-NMR spectrum of the sample was then acquired at 300 MHz. Subsequent ¹H-NMR spectra of the sample were acquired at various pH* values between 3.0 and 9.0, and 303 K. The pH* of the sample was adjusted by the addition of small aliquots of 1N DCl or 1N NaOD. The chemical shifts of the His12, His105, and His119 Hε1 resonances were recorded.

6.3.c) 3'-Cytidine Monophosphate Titration of RNase A

A sample of RNase A was prepared by dissolving 12.1 mg of the enzyme in a 0.5 mL solution of 0.3 mM NaCl and 0.5 mM DSS in D₂O. The concentration of the sample determined spectrophotometrically was 1.57 using an extinction coefficient at 280 nm of 7.3 (Worthington Enzymes). The sample was then transferred to a 5 mm NMR tube.

The pH* of the sample was adjusted to 3.0 and then heated at 60°C for one hour. The pH* of the sample was then adjusted to 5.48 for ¹H-NMR acquisition. A 5.0 mg sample of 3'-CMP was prepared in 2.0 mL of 0.3 M NaCl and 0.5 mM DSS in D₂O. The concentration of the sample was determined spectrophotometrically ($\epsilon_{279}=12\ 400$) to be 7.58 mM.

¹H-NMR spectra of RNase A were recorded at 303 K with various amounts of 3'-CMP added to the sample. The pH* of the sample was maintained near 5.50 by small additions of 1N DCl or NaOD. The pH* of the sample was measured before and after each spectrum was acquired. The chemical shifts of the His12, His105, and His119 H ϵ 1 resonances were recorded.

6.3.d) pH* Titration of 3'-CMP/RNase A Complex

A 4.38 mM sample of RNase A was prepared by dissolving 21.7 mg of the enzyme in 0.4 mL of a solution of 0.3 M NaCl and 0.5 mM DSS in D₂O. The sample was transferred to a 5 mm NMR tube and the pH* of the sample was adjusted to 2.94. The sample was heated at 60°C for one hour. To this sample, 0.4 mL of a 4.97 mM sample of 3'-CMP prepared in 0.3 M NaCl and 0.5 mM DSS, was added. The final NMR sample contained concentrations of 2.19 mM RNase A and 2.49 mM 3'-CMP resulting in a molar ratio of 3'-CMP:RNase A of 1.14. The pH* of the sample was adjusted to 3.75 and a series of ¹H-NMR spectra of the complex at various pH* values were recorded at 303 K. The chemical shifts of the H ϵ 1 resonances of His12, 105, and 119 were recorded.

6.3.e) ^{51}V -NMR of Uridine Vanadate

For ^{51}V -NMR experiments, a 79 mM sample of NH_4VO_3 was prepared by dissolving 7.4 mg of the compound in 0.8 mL of D_2O containing 0.2 M sodium acetate (CH_3COONa). The pH^* of the sample was 7.49. The ^{51}V -NMR spectrum of this sample was recorded at 295 K.

U-V was prepared using the method of Borah (Borah *et al.*, 1985). A sample of U-V was prepared by dissolving 4.9 mg of NH_4VO_3 in 1.5 mL of D_2O and 14.9 mg of uridine in a separate 1.5 mL aliquot of D_2O . 1.4 mL of the uridine sample ([uridine] = 42.2 mM by O.D.) was added to the NH_4VO_3 sample ([NH_4VO_3] = 27.9 mM by weight). The sample was heated at 65°C for 15 minutes. The final concentrations in the sample were 20.4 mM uridine and 14.4 mM NH_4VO_3 . A 0.5 mL aliquot of this sample was added to a 5 mm NMR tube for ^{51}V -NMR acquisition. The final pH^* was 6.20.

6.3.f) Uridine Vanadate Titration of RNase A

Uridine vanadate was prepared using the method of Borah *et al.* (1985). A 42.2 mM solution of uridine was prepared in 0.3 M NaCl and 0.5 mM DSS in D_2O . A 27.9 mM solution of NH_4VO_3 was prepared using the same solvent conditions. 1.5 mL of the NH_4VO_3 solution was added to 1.4 mL of the uridine solution to give a final concentration of uridine of 20.4 mM and a final concentration of NH_4VO_3 of 14.1 mM. This solution was then heated at 60°C for 15 minutes to form the U-V complex. The final concentration of U-V was taken to be 14.1 mM. The pH^* of the sample was adjusted to 5.6 with small additions of 1N DCl and 1N NaOD.

A 2.8 mM sample of RNase A was prepared by dissolving 23.0 mg of the protein in 0.6 mL of a 0.3 M NaCl and 0.5 mM DSS solution prepared in D₂O. The RNase A sample was adjusted to pH* 3.0 and heated at 60°C for one hour after which time it was adjusted to pH* 5.6 for ¹H-NMR acquisition. A series ¹H-NMR spectra of RNase A, with increasing amounts of U-V added, were acquired. Spectra corresponding to the following U-V to RNase A molar ratios were collected: 0.00, 0.43, 0.86, 1.29 and 2.14. All of the spectra were recorded at 303 K and pH 5.6, with the pH* of the sample being recorded before and after every spectrum acquired.

6.3.g) pH* Titration of U-V/RNase A Complex

The sample prepared in the U-V titration of RNase A, which contained final concentrations of 4.2 mM U-V and 1.98 mM RNase A ([U-V]:[RNase A] = 2.14) was used to perform a pH titration of the complex. A series of ¹H-NMR spectra of the U-V/RNase A complex were recorded at 303 K within the pH* range of 3.0 to 9.6. The chemical shifts of the Hε1 resonances of His12, His105 and His119 were recorded.

6.3.h) Preparation of the Sample for Two-dimensional ¹H-NMR Studies

A 60.8 mM sample of uridine was dissolved in 0.3 M NaCl and 0.5 mM DSS in D₂O. Ammonium metavanadate was added to a final concentration of 58.1 mM and the sample was heated at 60°C for 15 minutes to form the U-V complex. The final concentrations of uridine and vanadate in the sample were 60.8 mM and 58.1 mM, respectively. Since U-V forms at a maximum uridine to vanadate ratio of about 1.2:1 (Borah *et al.*, 1985) the concentration of U-V is taken to be about 50 mM. A ¹H-NMR spectrum of this sample

was acquired and showed only resonances characteristic of U-V.

A RNase A sample was prepared by dissolving 36.0 mg of the protein into 0.32 mL of 0.3 M NaCl and 0.5 mM DSS in D₂O. The concentration of the protein in this sample was determined spectrophotometrically to be 8.21 mM. The sample was heated at 60°C for 1 hour at pH* 3.0 to exchange the backbone amide protons. To this, 0.08 mL of the U-V sample prepared above was added. The final composition of the sample was 6.57 mM RNase A and 10 mM U-V. The RNase A to U-V ratio of 1:1.5 ensures that the enzyme is saturated with the inhibitor.

6.3.i) Modelling the Interaction of U-V with RNase A

Modelling the interaction of U-V with RNase A was performed on a Silicon Graphics Indigo R4000 computer. The combined neutron and 2 Å resolution x-ray diffraction structure of RNase A complexed with U-V (Bernstein *et al.*, 1977; Borah *et al.*, 1985; Wlodawer *et al.*, 1983) (Protein Data Bank, reference 6RSA) was used to generate molecular graphic images using the MidasPlus software system from the Computer Graphics Laboratory, University of California, San Francisco (Ferrin *et al.*, 1988) and Discover (Havel, 1991) which is part of the INSIGHT II software package (Biosym Technologies, San Diego, California). Distances between protons within the active site of the U-V/RNase A were measured by selecting the appropriate atoms and using the DISTANCE command within the INSIGHTII software package.

The total energy of RNase A and the U-V/RNase A complex was monitored at various χ_1 (N-C α -C β -C γ) and χ_2 (C α -C β -C γ -C δ) angles for the His119 side chain using the

ROTOR command in the Discover module of the INSIGHTII software package. The x-ray crystallographic structure of RNase A (Wlodawer *et al.*, 1982) (Protein Data Bank, reference 5RSA), without an active site ligand, was used as the initial structure for RNase A. The combined neutron and 2 Å x-ray diffraction structure of the U-V/RNase A complex (Bernstein *et al.*, 1977; Borah *et al.*, 1985; Wlodawer *et al.*, 1983) (Protein data bank, reference 6RSA) was used as the initial structure for the U-V/RNase A complex. The central vanadium atom of the U-V molecule was replaced with a phosphorous atom and a bond between this atom and the O2' atom of the ribose ring was created. The result is a central phosphorous atom bound to five oxygen atoms. The replacement of the vanadium atom with a phosphorous atom was necessary in order to remove any undefined valences within the U-V molecule. The computer program would not accept a structure with a central vanadium atom bound to five oxygen atoms, since this structure does not meet the required valences for all of the oxygen atoms. No other significant structural changes were made to this molecule. Both RNase A and the U-V/RNase A complex were energy minimized before initiating the rotation of the His119 side chain. The χ_1 and χ_2 angles of His119 were rotated from -180° to $+180^\circ$ in steps of 18° and the total energy of the system was monitored at each angle. A contour plot of the total energy versus the change in χ_1 and χ_2 angles was prepared showing areas of minimum total energy.

CHAPTER SEVEN

RESULTS

7.1) pH* Titration of RNase A

The pH* titration of the He1 protons of His12, His105, and His119 of RNase A that have been previously characterized and assigned (Bradbury and Scheraga, 1966; Meadows *et al.*, 1968; Bradbury and Teh, 1975; Markley, 1975b; Patel *et al.*, 1975; Shindo *et al.*, 1976; Lenstra *et al.*, 1979) is shown in the ¹H-NMR spectra in Figure 53. The positions of the He1 resonances of His12 (○), His105 (●), and His119 (◻) are labelled. Figure 54 shows a plot of the chemical shifts of the He1 resonances of the His residues versus the pH* of the sample. The residues His12, His105, and His119 exhibit continuous titration curves, while the titration curve of His48 is discontinuous. The He1 resonance of His48 broadens out at low pH* and disappears near pH 5.0. A curve was fitted to the data using a non-linear least squares fitting routine based on the following equation (Markley, 1975a).

$$\delta_{\text{obs}} = \delta_{\text{A}} + (\delta_{\text{B}} - \delta_{\text{A}}) \cdot (K^n) / (K^n + [\text{H}]^n) \quad (\text{A})$$

where δ_{obs} is the observed chemical shift in ppm, δ_{A} is the chemical shift of the protonated species, δ_{B} is the chemical shift of the deprotonated species, K is the dissociation constant and n is the Hill coefficient. A complete summary of the chemical shift positions of the He1 resonances of the His residues versus the pH* of the sample is given in Table XII. The pKa values of His12, His105 and His119 were calculated to be

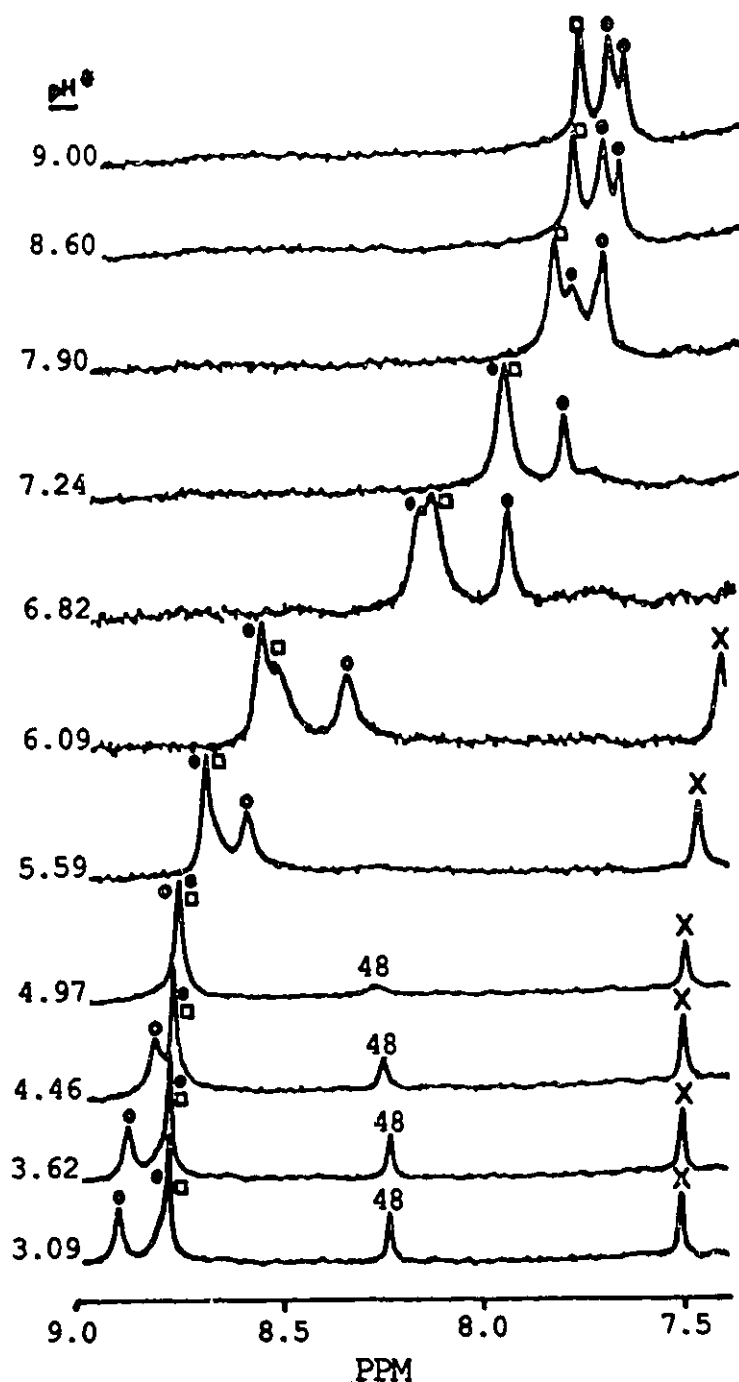


Figure 53. pH* Titration of RNase A. 300 MHz ^1H -NMR spectra of the low-field region (9.0 to 7.4 ppm) of 1.57 mM RNase A in 0.3 M NaCl and 0.5 mM DSS at 300 K at various pH* values. The H ϵ 1 resonances of the histidyl residues are indicated as follows: His12 (o), His105 (●), and His119 (□). The H δ 2 resonance of His105 is indicated by (x).

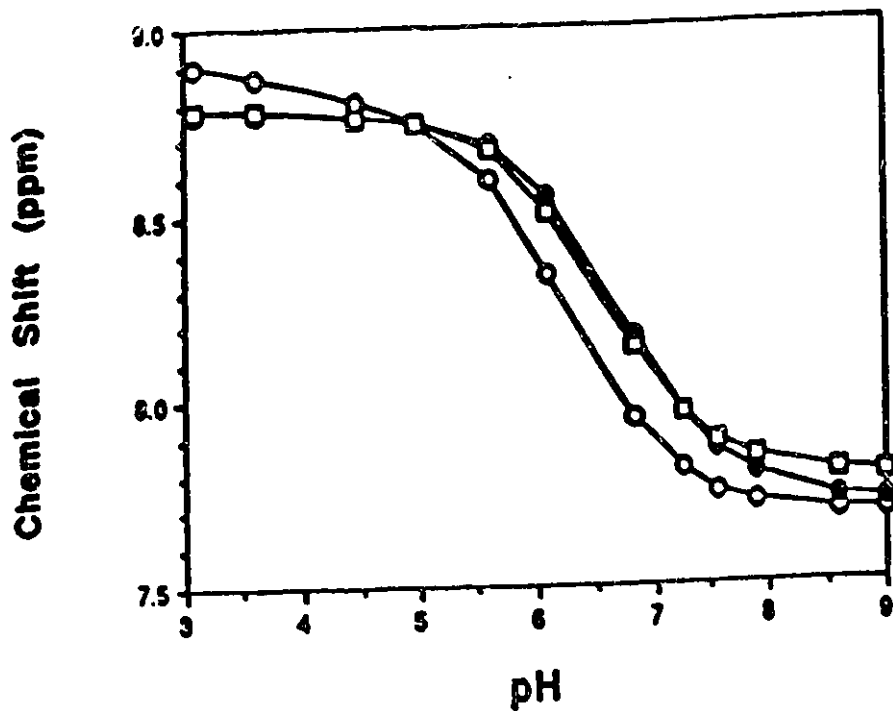


Figure 54. pH* Titration Curves of the Histidyl Resonances of RNase A. Plot of the chemical shifts of the His H ϵ 1 resonances of RNase A versus pH*. The resonances are indicated as follows: His12 (o), His105 (\bullet), and His119 (\square).

TABLE XII

pH* Titration Chemical Shift Data
of the Histidyl Residues of RNase A

<u>pH*</u>	<u>His12</u>		<u>His119</u>		<u>His105</u>	
	<u>δ_{exp}^a</u>	<u>δ_{cal}^a</u>	<u>δ_{exp}</u>	<u>δ_{cal}</u>	<u>δ_{exp}</u>	<u>δ_{cal}</u>
3.09	8.896	8.872	8.785	8.780	8.775	8.774
3.62	8.868	8.867	8.779	8.779	8.772	8.773
4.46	8.805	8.833	8.762	8.771	8.760	8.766
4.97	8.747	8.770	8.747	8.751	8.747	8.749
5.59	8.595	8.587	8.677	8.673	8.690	8.684
6.09	8.337	8.332	8.508	8.515	8.551	8.547
6.82	7.956	7.949	8.147	8.139	8.172	8.170
7.24	7.809	7.814	7.963	7.965	7.963	7.961
7.55	7.749	7.755	7.884	7.885	7.863	7.856
7.90	7.714	7.717	7.838	7.835	7.793	7.784
8.60	7.688	7.685	7.796	7.797	7.723	7.728
9.00	7.686	7.679	7.790	7.791	7.720	7.718

δ_{exp} : experimentally observed chemical shift

δ_{cal} : calculated chemical shift

^aall chemical shift values are reported in parts per million

6.19, 6.69, and 6.55 respectively. The complete pH* titration data is listed in Table XIII.

7.2) 3'-CMP Titration of RNase A

A series of $^1\text{H-NMR}$ spectra of the aromatic region of RNase A (7.5 to 9.0 ppm) with increasing amounts of 3'-CMP added to the protein at pH* 5.5 are shown in Figure 55. The $^1\text{H-NMR}$ spectrum of free RNase A contains peaks in the aromatic region that were assigned to the H ϵ 1 resonances of His12 (8.643 ppm), His105 (8.711 ppm), His119 (8.696 ppm) and the C δ H resonance of His105 (7.485 ppm). As increasing amounts of 3'-CMP are added to the RNase A sample the position of the His12 H ϵ 1 resonance gradually shifts downfield. The position of the His105 and His119 H ϵ 1 resonances remain essentially unchanged. Histidine 12 continues to move downfield until a [3'-CMP]:[RNase A] ratio of about 1.5 is achieved. No change in the position of the H ϵ 1 resonance of His12 is observed at higher [3'-CMP]:[RNase A] ratios. Figure 56 shows a plot of the chemical shift values of the H ϵ 1 resonances of the His residues versus the [3'-CMP]/[RNase A]. The effect on the position of the H ϵ 1 resonance of His12 is much greater than the effect on the H ϵ 1 resonances of His105 and His119. The shift in the position of the His12 resonance suggests that the H ϵ 1 proton of this residue is within close proximity of the phosphate group of 3'-CMP, when the inhibitor is bound to the active site of RNase A. There are no discontinuities in the titration curves for any of the histidyl residues of RNase A. A summary of the chemical shifts of the H ϵ 1 resonances of the His residues versus the [3'-CMP]/[RNase A] is given in Table XIV. Very little change is observed in the shape of any of the His resonances as increasing amounts of 3'-CMP are added to the sample.

TABLE XIII

RNase A pH Titration Parameters^a

	<u>His12</u>	<u>His119</u>	<u>His105</u>
pKa	6.19 (0.02) ^d	6.55 (0.01)	6.69 (0.01)
Hill Coefficient	0.84 (0.03)	0.95 (0.02)	0.94 (0.01)
δ_{AH} (ppm) ^b	8.88 (0.01)	8.78 (0.01)	8.78 (0.01)
δ_A (ppm) ^c	7.67 (0.01)	7.79 (0.01)	7.71 (0.01)

^aTitration parameters are derived from a least squares fit of the data to equation (A).

^bChemical shift of the protonated species.

^cChemical shift of the unprotonated species.

^dStandard deviation

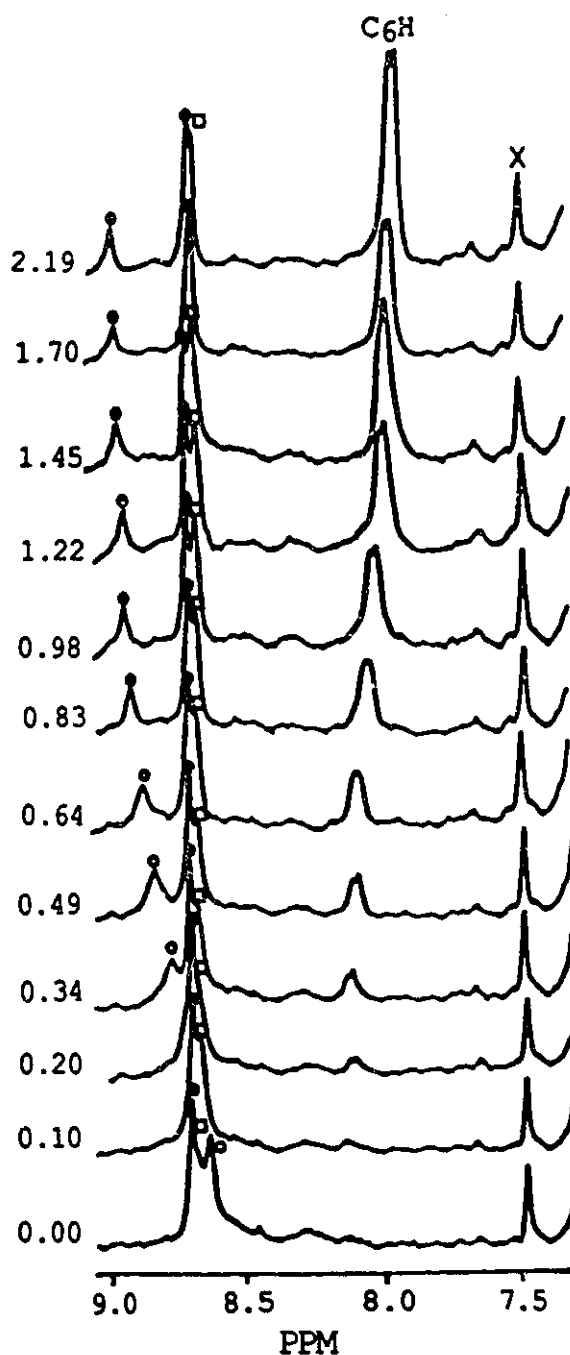


Figure 55. 3'-CMP Titration of RNase A. 300 MHz ^1H -NMR spectra of the low-field region (9.1 to 7.3 ppm) of 1.57 mM RNase A in 0.3 M NaCl and 0.5 mM DSS, pH 5.5 at increasing molar ratios of 3'-CMP:RNase A. The H ϵ 1 resonances of the histidyl residues are indicated as follows: His12 (O), His105 (●), and His119 (◻). The H δ 2 resonance of His105 is indicated by (x) and the C $_6$ H proton of 3'-CMP by (C $_6$ H).

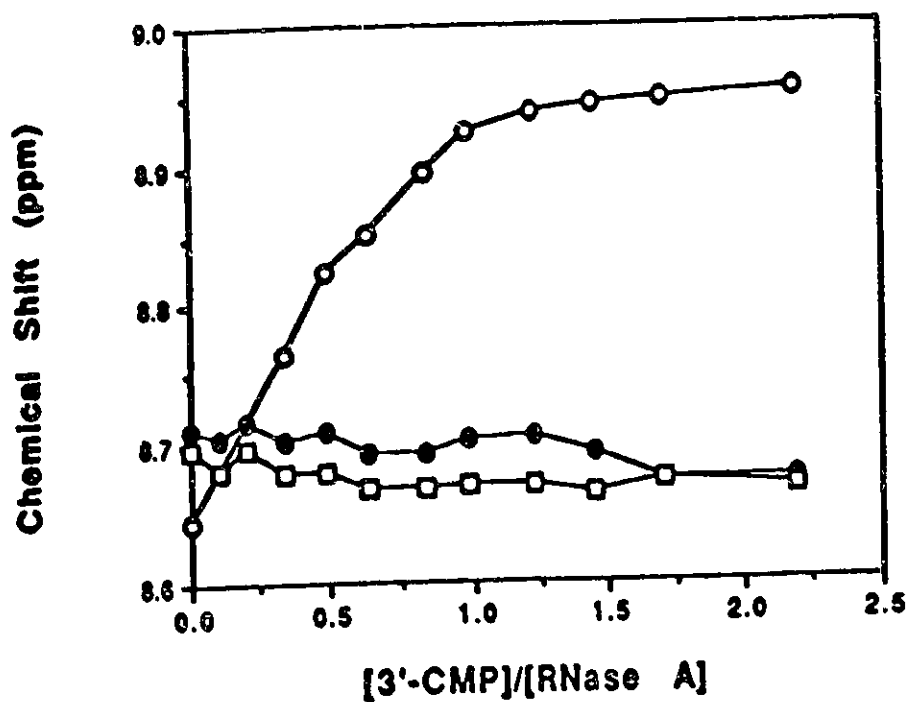


Figure 56. Chemical Shift Dependence of the Histidine Resonances of RNase A in the Presence of 3'-CMP. The effect of increasing molar ratios of 3'-CMP:RNase A on the H α 1 resonances of His12 (o), His105 (●), and His119 (□) of RNase A. The experimental conditions are as given in Figure 55.

TABLE XIV

Chemical Shift Data of the Histidyl Residues
in the 3'OMP Titration of RNase A

<u>3'OMP/RNase A</u>	<u>Chemical Shift (ppm)</u>		
	<u>His-12</u>	<u>His-119</u>	<u>His-105</u>
0.00	8.643	8.696	8.711
0.10	8.682	8.682	8.705
0.20	8.717	8.696	8.717
0.34	8.764	8.679	8.702
0.49	8.825	8.679	8.708
0.64	8.851	8.667	8.693
0.83	8.895	8.667	8.693
0.98	8.924	8.670	8.702
1.22	8.939	8.670	8.705
1.45	8.945	8.664	8.693
1.70	8.948	8.673	8.673
2.19	8.954	8.673	8.667

7.3) pH* Titration of the 3'CMP/RNase A Complex

A series of ^1H -NMR spectra of the aromatic region (7.5 to 9.2 ppm) of the 3'CMP/RNase A complex acquired at several pH* values between 3.75 and 9.82 is shown in Figure 57. Figure 58 shows a plot of the chemical shift values of the H ϵ 1 resonances of His12, 105, and 119 versus the pH* of the sample. As the pH* is raised from 3.75 to 5.15, there is a downfield shift in the position of the H ϵ 1 resonance of His12 and an upfield shift in the same resonance of His119. As the pH* is raised, the H ϵ 1 resonances of the His residues titrate normally throughout the pH* range. A complete summary of the chemical shift positions of the H ϵ 1 resonances of the His residues versus the pH* of the sample is given in Table XV. The pKa values of His12, His105, and His119 were calculated to be 6.95, 6.69 and 7.17, respectively. The pH* titration curves of the H ϵ 1 resonances of His12, 105, and 119 are continuous in the 3'-CMP/RNase A complex. The complete pH* titration data of the 3'CMP/RNase A complex are listed in Table XVI.

7.4) ^{51}V -NMR of Uridine Vanadate

The ^{51}V -NMR spectrum of NH_4VO_3 showed the presence of two components (Figure 59). The larger peak (B), representing 84.2% of the total area, was assigned an arbitrary position of 0 ppm. This intense peak has been previously assigned to the ^{51}V resonance of H_2VO_4^- (Borah *et al.*, 1985). The unidentified minor peak (A) located at -8.5 ppm, represented 15.8% of the total area.

The ^{51}V -NMR spectrum of the sample of uridine and NH_4VO_3 (Figure 60) ([uridine]:[NH_4VO_3] = 1.42) showed a large decrease in the resonance assigned to

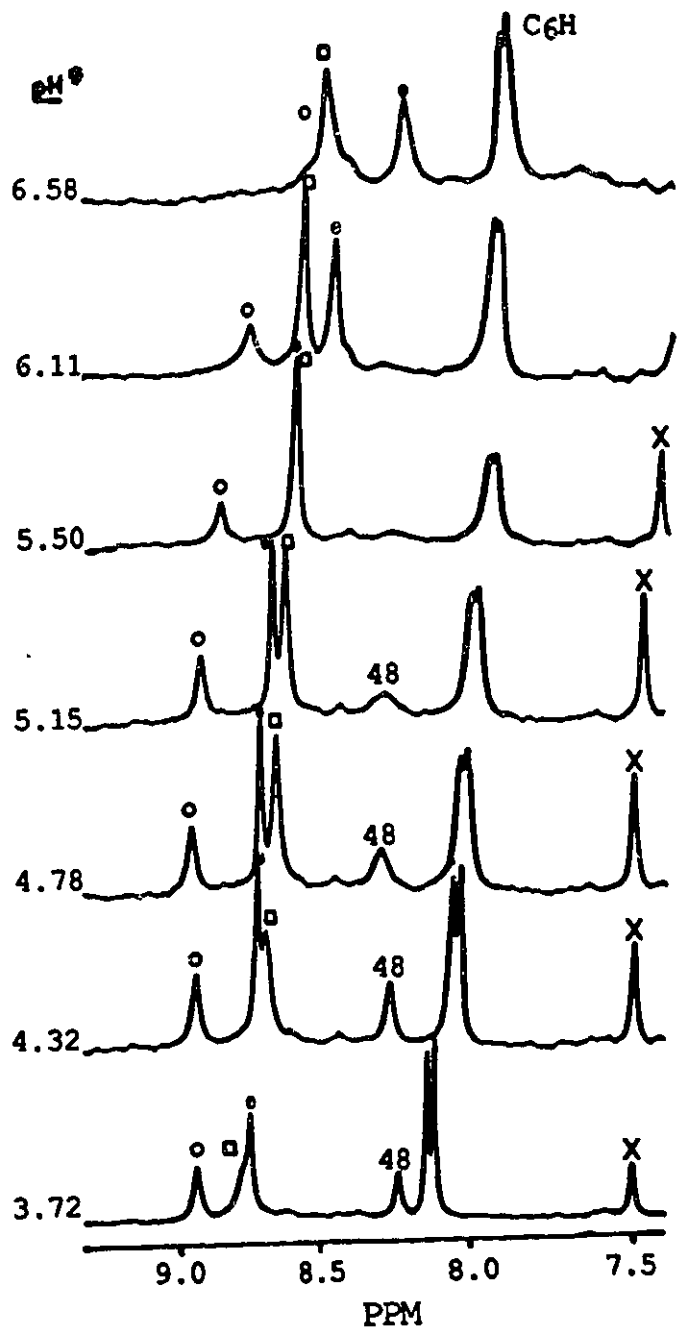


Figure 57. pH Titration of the 3'-CMP/RNase A Complex. 300 MHz ^1H -NMR spectra of the low-field region (9.3 to 7.4 ppm) of 3'-CMP/RNase A (molar ratio 1.14) in 0.3 M NaCl and 0.5 mM DSS at various pH values. The H ϵ 1 resonances of the His residues are indicated as follows: His12 (o), His105 (●), His119 (◻) and His48 (48). The H δ 2 resonance of His105 is indicated by (x) and the C $_6$ H proton of 3'-CMP by (C $_6$ H).

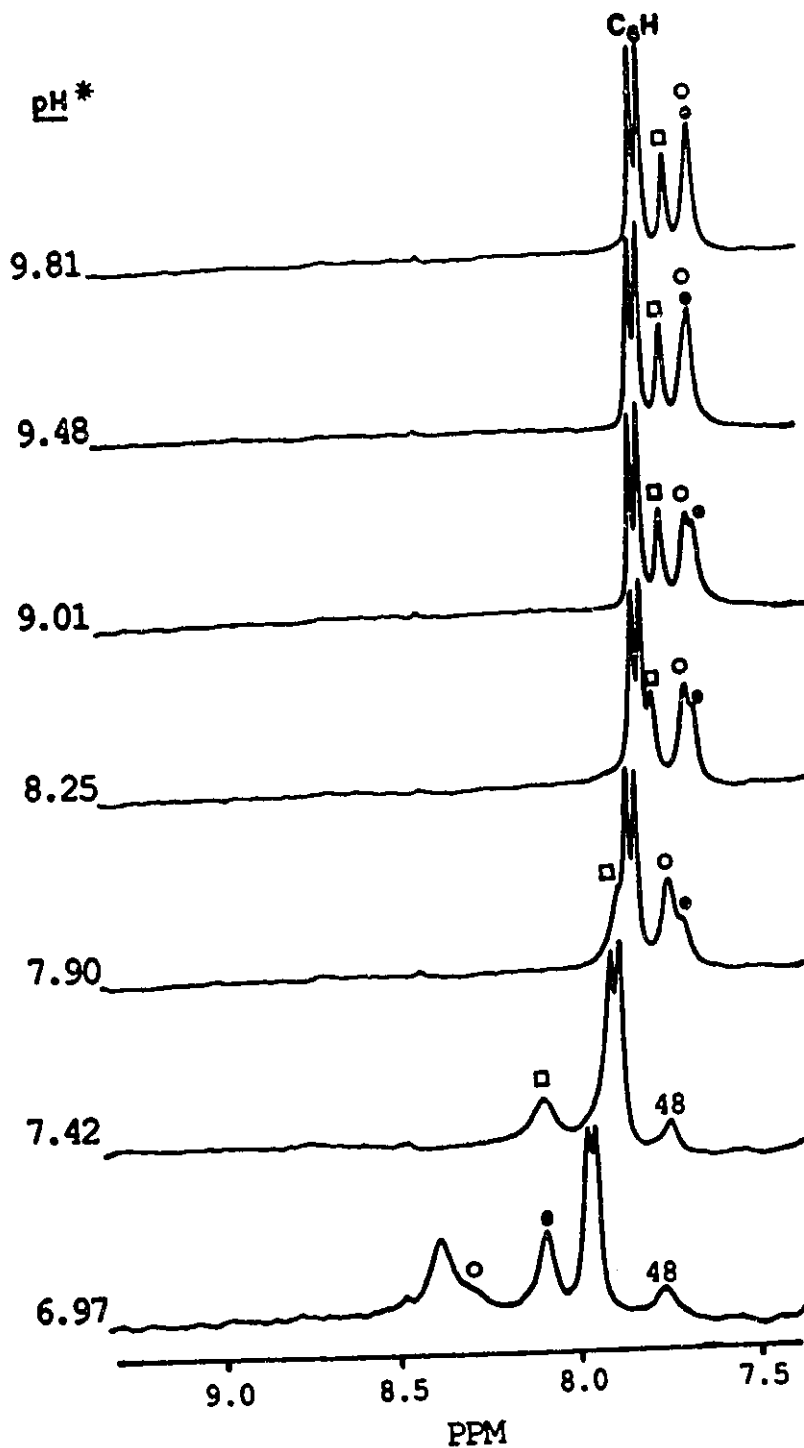


Figure 57 (continued). pH* Titration of the 3'-CMP/RNase A Complex. The H ϵ 1 resonances of the His residues are indicated as follows: His12 (O), His105 (●), His119 (◻) and His48 (48). The H δ 2 resonance of His105 is indicated by (x) and the C₆H proton of 3'-CMP by (C₆H).

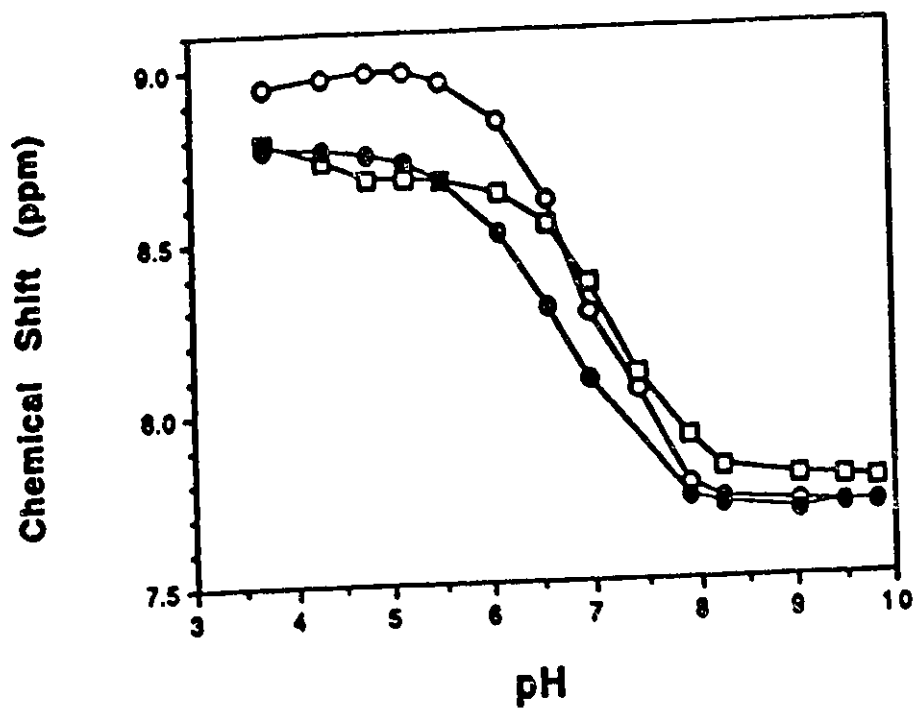


Figure 58. pH^{*} Titration Curves of the Histidine Resonances in the 3'-CMP/RNase A Complex. Plot of the observed chemical shifts of the His Hε1 resonances of the 3'-CMP/RNase A complex versus pH^{*}. The resonances are indicated as follows: His12 (○), His105 (●) and His119 (□).

TABLE XV

pH* Titration Chemical Shift Data of the Histidyl Residues
of RNase A in the 3'-CMP/RNase A Complex

	<u>His12</u>		<u>His119</u>		<u>His105</u>	
<u>pH*</u>	<u>δ_{exp}^a</u>	<u>δ_{cal}^a</u>	<u>δ_{exp}</u>	<u>δ_{cal}</u>	<u>δ_{exp}</u>	<u>δ_{cal}</u>
3.72	8.948	8.981	8.781	8.712	8.769	8.759
4.32	8.971	8.979	8.728	8.712	8.760	8.755
4.78	8.982	8.974	8.684	8.710	8.745	8.744
5.15	8.985	8.963	8.672	8.705	8.719	8.724
5.50	8.950	8.940	8.666	8.696	8.666	8.686
6.11	8.836	8.825	8.628	8.645	8.514	8.527
6.58	8.602	8.603	8.538	8.531	8.298	8.295
6.97	8.283	8.327	8.368	8.356	8.084	8.075
7.42	8.099	8.020	8.099	8.110	-	-
7.90	7.780	7.823	7.917	7.916	7.742	7.766
8.25	7.733	7.755	7.827	7.843	7.713	7.728
9.01	7.718	7.706	7.792	7.788	7.695	7.699
9.48	7.707	7.699	7.786	7.781	7.707	7.694
9.81	7.710	7.697	7.780	7.779	7.710	7.693

δ_{exp} : experimentally observed chemical shift

δ_{cal} : calculated chemical shift

^aall chemical shift values are reported in parts per million

TABLE XVI

3'-CMP/RNase A Complex pH Titration Parameters^a

	<u>His12</u>	<u>His119</u>	<u>His105</u>
pKa	6.95 (0.04) ^d	7.17 (0.04)	6.70 (0.02)
Hill Coefficient	1.01 (0.09)	1.04 (0.09)	0.94 (0.05)
δ_{AH} (ppm) ^b	8.98 (0.02)	8.71 (0.01)	8.76 (0.01)
δ_{A} (ppm) ^c	7.70 (0.02)	7.78 (0.02)	7.69 (0.01)

^aTitration parameters are derived from a least squares fit of the data to equation (A).

^bChemical shift of the protonated species.

^cChemical shift of the unprotonated species.

^dStandard deviation

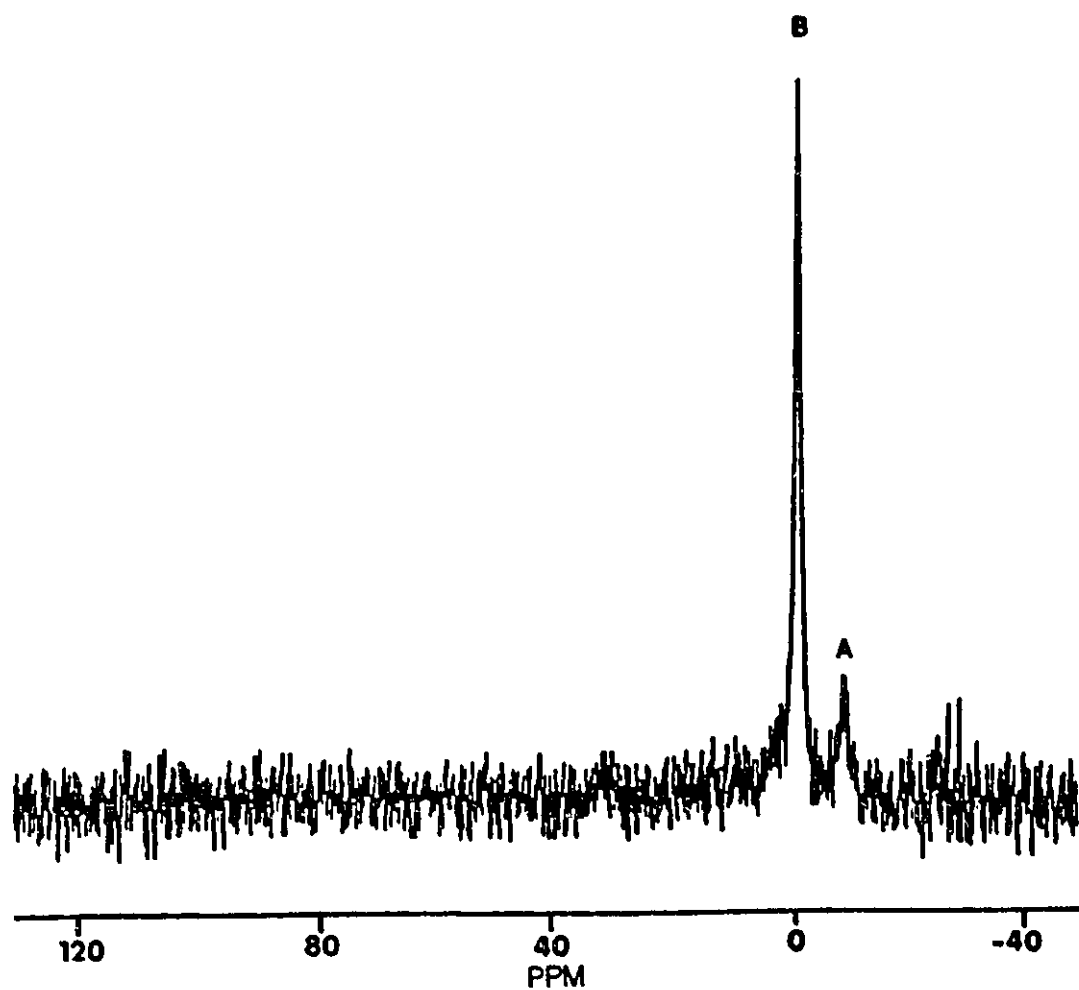


Figure 59. ^{51}V -NMR of Ammonium Metavanadate. The 52.58 MHz ^{51}V -NMR spectrum of a 79 mM sample of NH_4VO_3 at pH* 7.49, in 0.2 M CH_3COONa in D_2O showed two peaks. The large peak (B) has been assigned to the ^{51}V resonance of H_2VO_4^- (Borah *et al.*, 1985). Peak (A) has not been assigned.

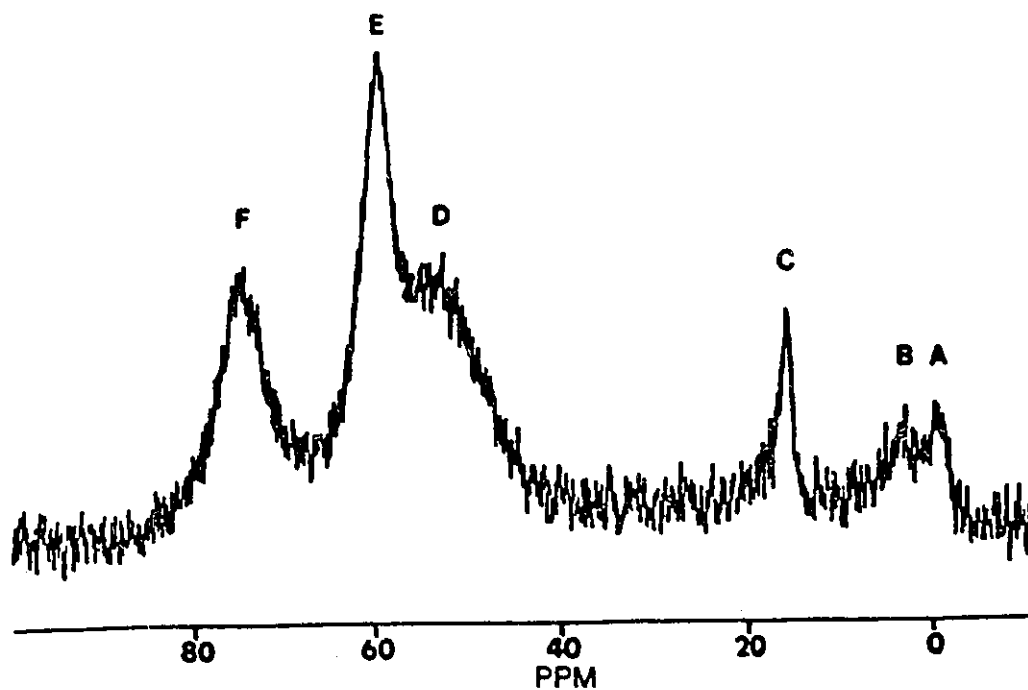


Figure 60. ^{51}V -NMR of Uridine Vanadate. The ^{51}V -NMR spectrum of a 14.4 mM sample of U-V at pH* 6.20 in D_2O showed six major peaks. The largest peak (D) has been assigned to the ^{51}V resonance of U-V (Borah *et al.*, 1985).

[H₂VO₄]⁻ at 0 ppm. Four new peaks were observed at 3.0 (B), 16.0 (C), 53.1 (D), 60.1 (E) and 75.5 (F) ppm. The largest peak, representing 38% of the total area, at 53.1 ppm, has been assigned to the ⁵¹V resonance of U-V (Borah *et al.*, 1985). Two other large peaks at 60.1 and 75.5 ppm, representing 31% and 23% of the total area respectively, are unassigned and were not observed previously in the ⁵¹V-NMR spectrum of U-V (Borah *et al.*, 1985). The remaining peaks at 0.0, 3.0 and 16.0 ppm represented roughly 8% of the total area.

7.5) Uridine Vanadate Titration of RNase A

A series of ¹H-NMR spectra of RNase A with increasing amounts of U-V added were acquired at pH* 5.5 and 303 K (Figure 61). The ¹H-NMR spectrum of free RNase A at pH* 5.5 showed peaks in the aromatic region which corresponded to the Hε1 resonance of His12 (8.54 ppm), His119 (8.63 ppm), and His105 (8.68 ppm). After U-V was added to a [U-V]:[RNase A] ratio of 0.43, the resonance position for His105 was unchanged, but the resonances corresponding to His12 and His119 had decreased in intensity, while four new peaks appeared at 8.85, 8.54, 7.86 and 7.45 ppm. The resonances at 8.84 and 7.86 ppm have been assigned as protonated (His119P) and unprotonated (His119U) forms of His119 respectively, in a slow exchange process, and the resonances at 8.54 and 7.45 have been similarly assigned to protonated (His12P) and unprotonated (His12U) forms of His12, respectively (Borah *et al.*, 1985). Slow exchange means that the lifetime of the protonated and unprotonated species of the two histidyl residues is long compared to the NMR time scale. A lower limit can be put on each state by determining the chemical shift difference of the resonances, and substituting that value into the following equation (Markley *et al.*, 1970):

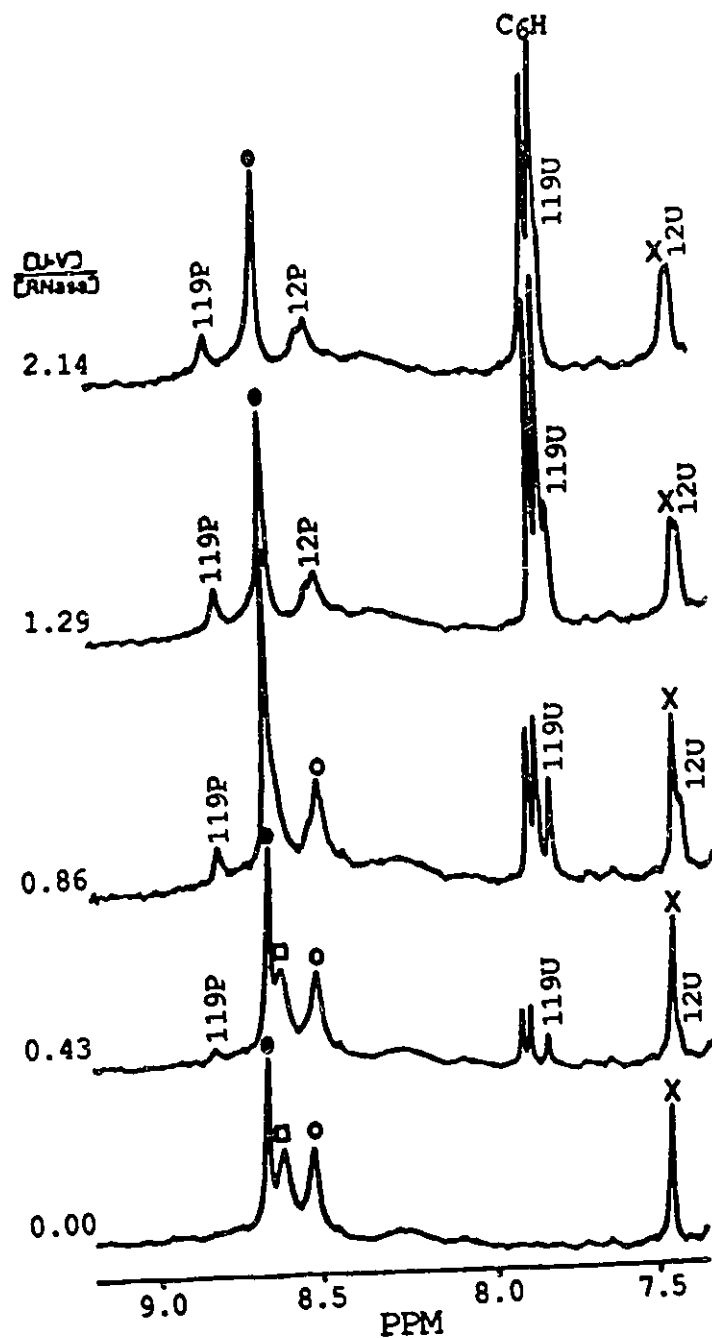


Figure 61. Uridine Vanadate Titration of RNase A. 300 MHz ^1H -NMR spectra of the low-field region (7.3 to 9.2 ppm) of RNase A in 0.3 M NaCl and 0.5 mM DSS, pH 5.5, at increasing molar ratios of U-V:RNase A. The resonances are labelled as follows: His12 (o); His105 H ϵ 1 (●); His119 (◐); His12P, His12 protonated; His12U, His12 unprotonated; His119P, His119 protonated; His119U, His119 unprotonated; His105 H δ 2 (x); C₆H proton of U-V, (C₆H).

$$\tau > \frac{1}{(2\pi)\delta(\nu)}$$

There is a chemical shift difference of 0.98 ppm or 294 Hz for the His119U and His119P resonances which indicates that each state must exist for at least 0.5 ms. The lifetime for the protonated and unprotonated forms of His12 must be at least 0.49 ms.

The doublet assigned to the C₆H resonance of the uridine base of U-V was observed at 7.87 and 7.90 ppm, increased in intensity as the concentration of U-V was increased. The H ϵ 1 resonances of His12 and His119 continued to decrease in intensity as the concentration of U-V increased, while the intensity of the four new resonances continued to increase. At a [U-V]:[RNase A] of 1.29 the H ϵ 1 resonances of His12 and His119 had disappeared. As the concentration of U-V increased further, no change in the intensity of the four new resonances was observed, which suggests that the enzyme is saturated with U-V. No effect on the H ϵ 1 resonance of His105 was observed throughout the U-V titration of RNase A. A summary of the chemical shifts of the H ϵ 1 resonances of His12 and His119 versus the [U-V]/[RNase A] is given in Table XVII.

7.6) pH* Titration of U-V/RNase A Complex

A series of ¹H-NMR spectra of the U-V/RNase A complex was acquired at various pH* values from 3.0 to 9.6 at 30^oC (Figure 62). The ratio of [U-V]/[RNase A] was 2.14, ensuring that the enzyme is saturated with U-V. The H ϵ 1 resonances of His12, His119 and His105 all titrated normally over the pH range 3.01 to 4.90. The next pH* value used in the titration was 5.37. At this pH* value the H ϵ 1 resonances of His12 and

TABLE XVII

Chemical Shift Data of Histidyl Residues 12 and 119
in the U-V Titration of RNase A

<u>[U-V/RNase A]</u>	<u>Chemical Shift (ppm)</u>		
	<u>His12</u>	<u>His12U*</u>	<u>His12Pt</u>
0.00	8.5367	-	-
0.43	8.5323	7.4468	-
0.86	8.5382	7.4432	-
1.29	-	7.4468	8.5411
2.14	-	7.4497	8.5323

<u>[U-V/RNase A]</u>	<u>Chemical Shift (ppm)</u>		
	<u>His119</u>	<u>His119U*</u>	<u>His119Pt</u>
0.00	8.6303	-	-
0.43	8.6421	8.8454	7.8564
0.86	-	8.8454	7.8564
1.29	-	8.8425	7.8579
2.14	-	8.8396	7.8769

*Unprotonated histidyl residue.

†Protonated histidyl residue.

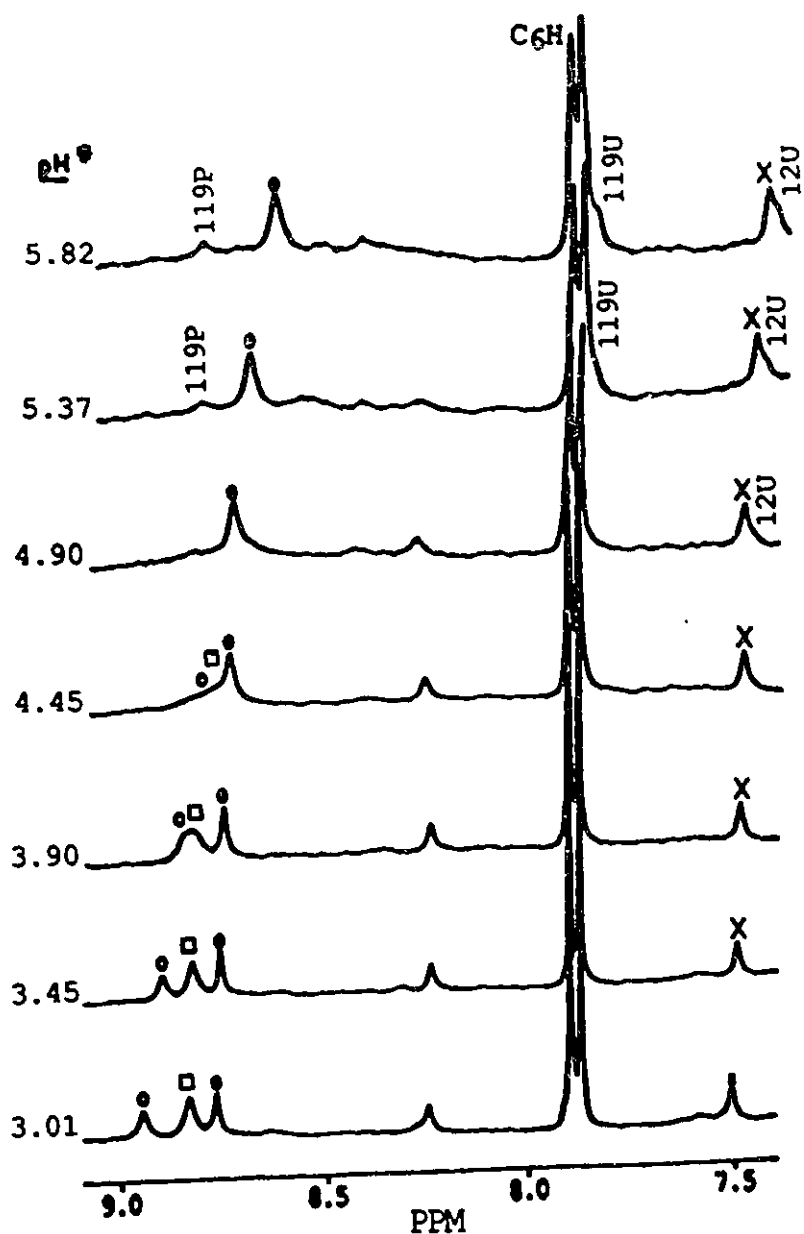


Figure 62. pH Titration of the U-V/RNase A Complex. 300 MHz ^1H -NMR spectra of the low-field region (7.4 to 9.1 ppm) of U-V/RNase A (molar ratio 2.14) in 0.3 M NaCl and 0.5 mM DSS at 303 K at various pH* values. The resonances are labelled as follows: His12 (o); His105 He1 (●); His119 (□); His12P, His12 protonated; His12U, His12 unprotonated; His119P, His119 protonated; His119U, His119 unprotonated; His105 H δ 2 (x); C $_6$ H proton of U-V, (C $_6$ H).

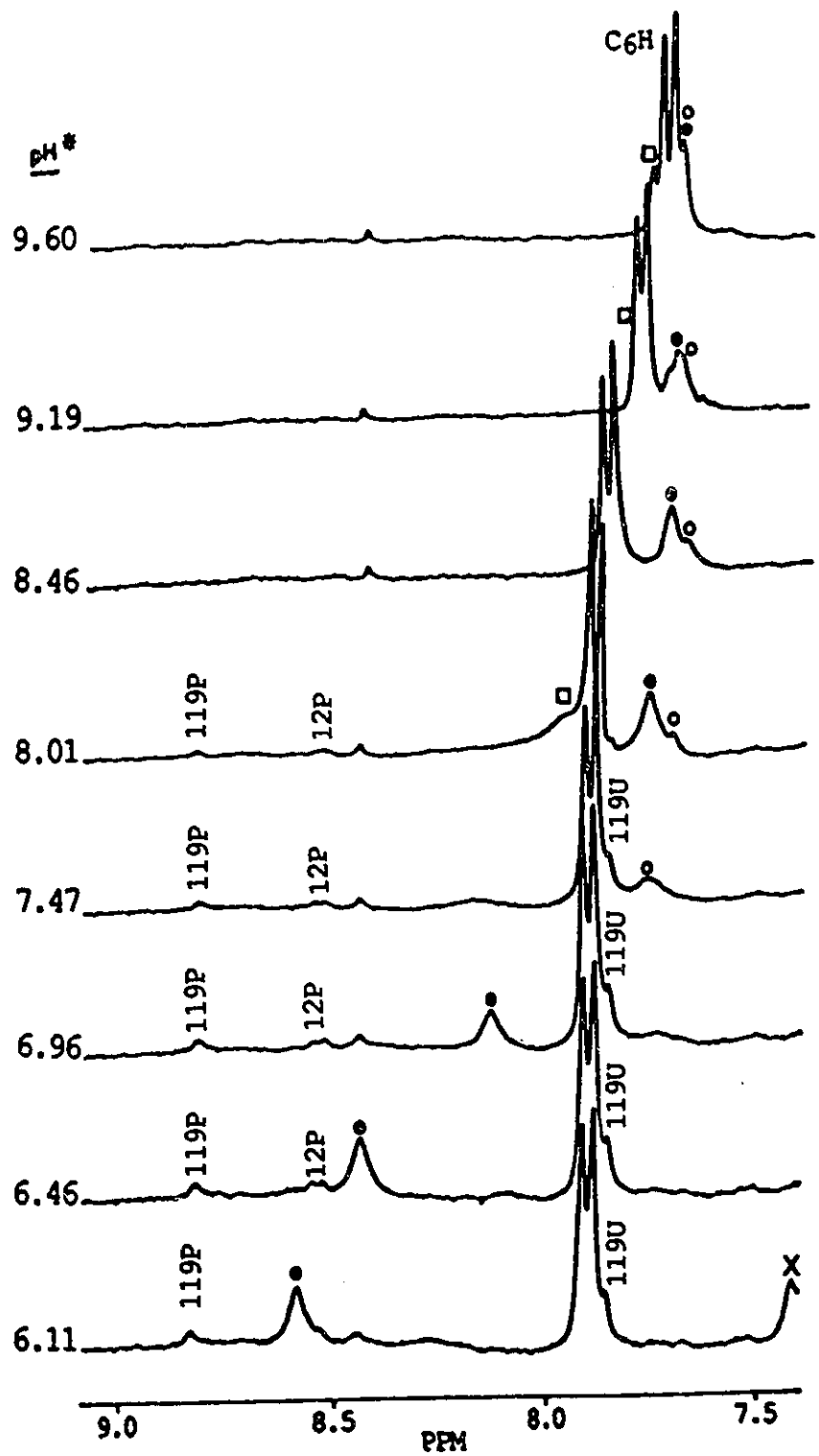


Figure 62 (continued). pH Titration of the U-V/RNase A Complex. The resonances are labelled as follows: His12 (o); His105 Hε1 (●); His119 (□); His12P, His12 protonated; His12U, His12 unprotonated; His119P, His119 protonated; His119U, His119 unprotonated; His105 Hδ2 (x); C₆H proton of U-V. (C₆H).

His119 disappeared and four new resonances, corresponding to the protonated and unprotonated forms of His12 (His12P and His12U) and His119 (His119P and His119U) appeared. The H ϵ 1 resonance of His105 continued to titrate normally as in free RNase A. The H ϵ 1 resonances of His12P, His12U, His119P and His119U observed did not change in position up to pH* 8.01. At the next pH* value, 8.54, these resonances disappeared and the H ϵ 1 resonances of His12 and His119 reappeared and titrated normally to pH* 9.60, which was the last value used in the titration. Plots showing the chemical shifts of the H ϵ 1 resonances of His12, His119 and His105 in the presence of U-V at various pH* values are shown in Figures 63, 64 and 65, respectively. The complete list of the chemical shifts of the H ϵ 1 resonances of His12 and His119 versus the pH* values for the U-V/RNase A complex are listed in Table XVIII. The pKa value for His105 was calculated to be 6.83 which is comparable to the pKa of His105 in free RNase A (6.69). The pKa values of His12 and His119 could not be calculated, since their titration curves were discontinuous in the presence of U-V.

7.7) Two-Dimensional NMR of U-V/RNase A Complex

The contour plot of the aromatic region (5.5 to 9.0 ppm) of the homonuclear NOESY spectrum of the U-V/RNase A complex is shown in Figure 66. The aromatic region shows cross peaks between the C₆H and C₅H resonances of the uridine base of U-V, which are 2.42 Å apart based on the coordinates of the combined neutron diffraction and x-ray crystallographic structure of the U-V/RNase A complex (Bernstein *et al.*, 1977; Borah *et al.*, 1985; Wlodawer *et al.*, 1983) (Protein Data Bank, reference 6RSA). A cross peak was observed between the C₆H resonance and one of the aromatic protons of Phe120. The distances between these protons varies from 4.57 to 8.91 Å in the

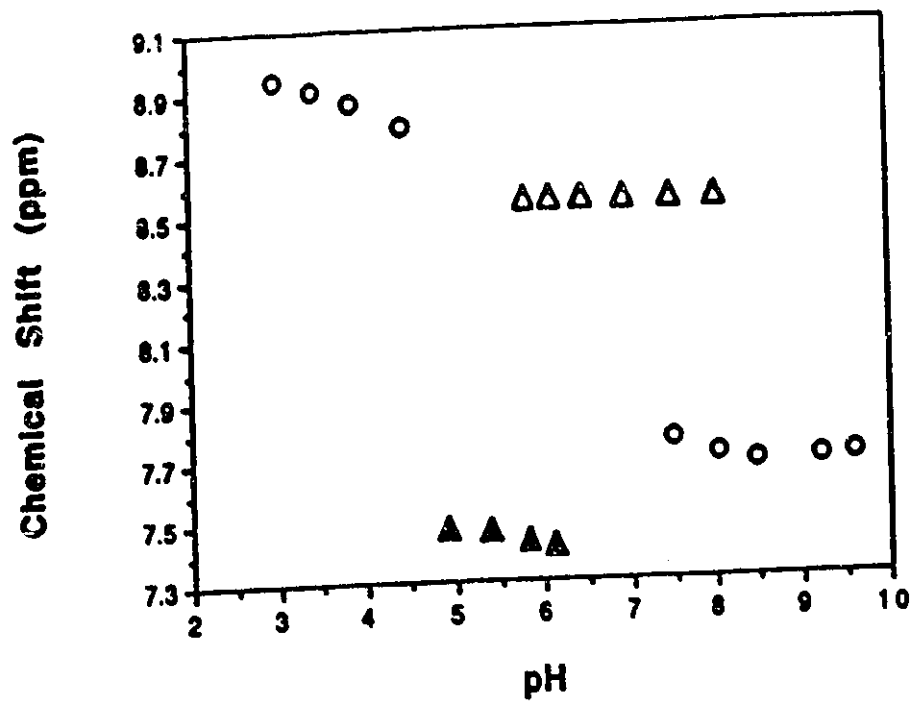


Figure 63. pH Titration Curve of His12 in the U-V/RNase A Complex. Plot of the observed chemical shifts of the His12 resonances versus pH* for the U-V/RNase A complex. The His12 resonances are indicated as follows: His12 (o); His12P (▲); His12U (△).

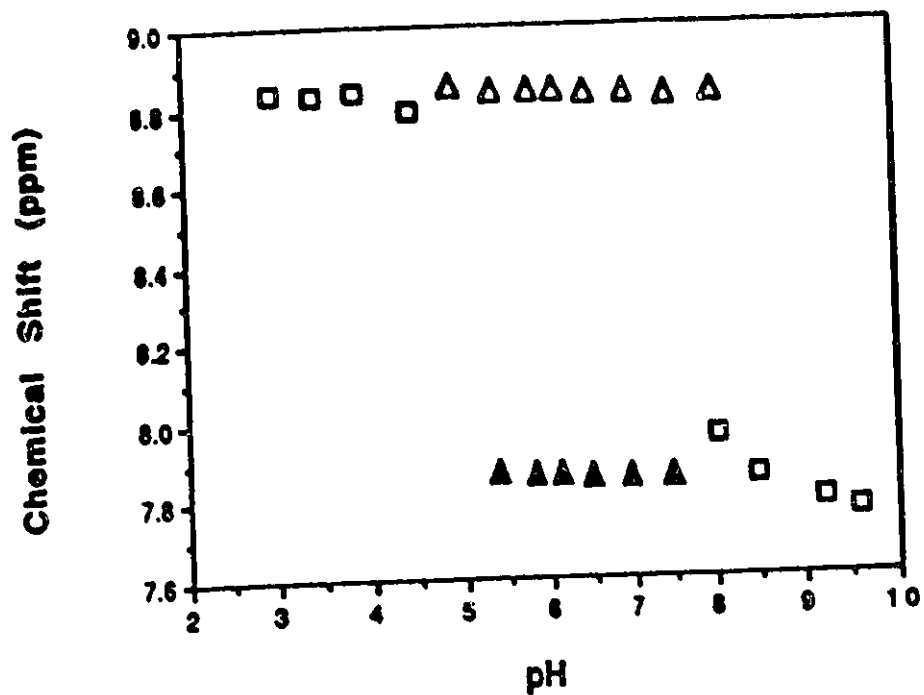


Figure 64. pH Titration Curve of His119 in the U-V/RNase A Complex. Plot of the observed chemical shifts of the His119 resonances versus pH* of the U-V/RNase A complex. The His119 resonances are indicated as follows: His119 (□); His119P (△); His119U (▲).

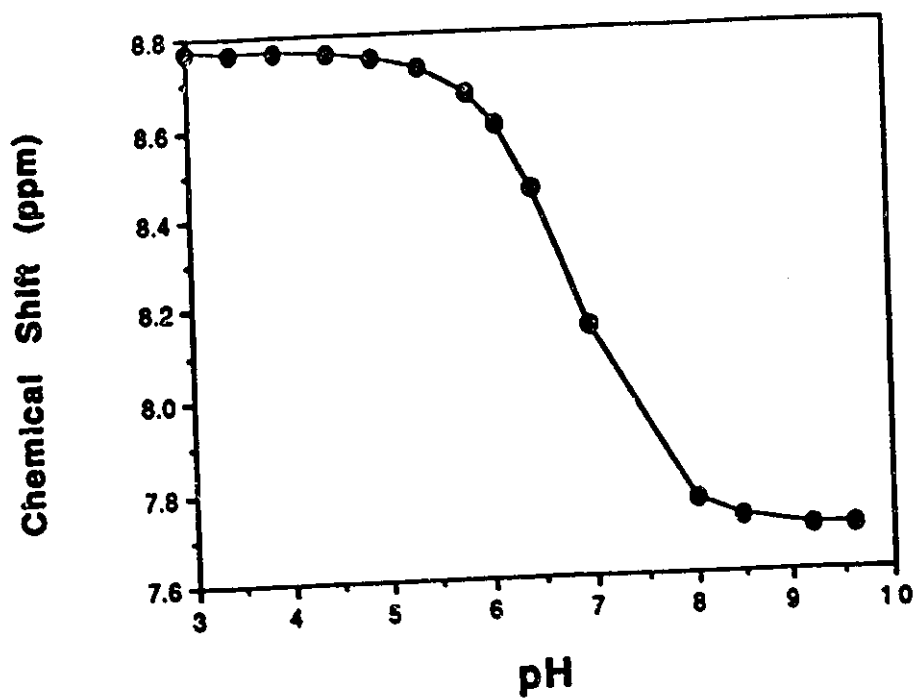


Figure 65. pH Titration Curve of His105 in the U-V/RNase A Complex. Plot of the observed chemical shifts of the H ϵ 1 resonance of His105 (●) versus pH* for the U-V/RNase A complex.

TABLE XVIII

Chemical Shift Data for Histidyl Residues 12 and 119
in the pH* Titration of the U-V/RNase A Complex

pH*	Chemical Shift (ppm)					
	His119	His119 ^a	His119 ^b	His12	His12 ^a	His12 ^b
3.01	8.837	-	-	8.945	-	-
3.45	8.832	-	-	8.905	-	-
3.90	8.841	-	-	8.863	-	-
4.45	8.790	-	-	8.790	-	-
4.90	-	8.848	-	-	-	7.475
5.37	-	8.841	7.870	-	-	7.463
5.82	-	8.840	7.861	-	8.545	7.432
6.11	-	8.835	7.861	-	8.547	7.416
6.46	-	8.828	7.856	-	8.543	-
6.96	-	8.829	7.856	-	8.540	-
7.47	-	8.826	7.856	-	8.540	-
8.01	7.962	8.834	-	7.707	8.540	-
8.46	7.858	-	-	7.685	-	-
9.19	7.799	-	-	7.690	-	-
9.60	7.772	-	-	7.700	-	-

^aUnprotonated histidyl residue

^bProtonated histidyl residue

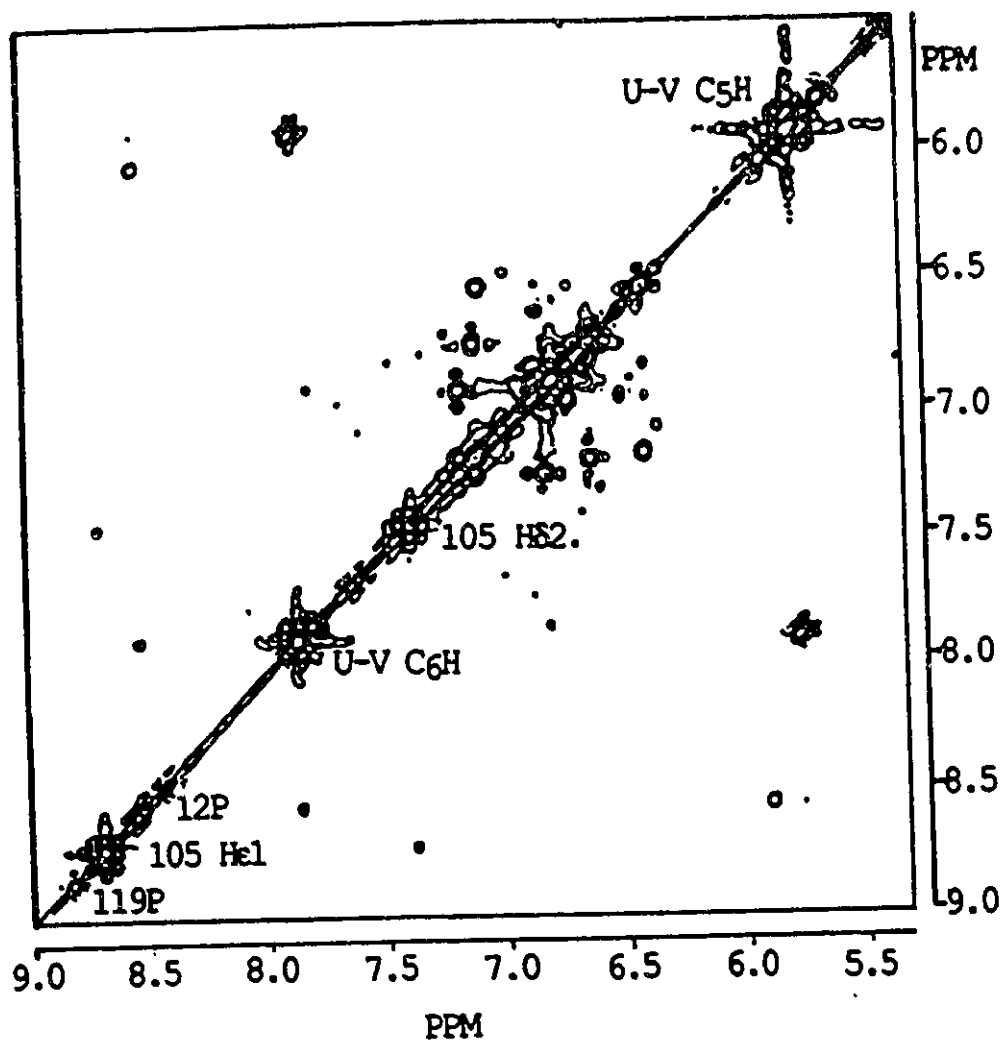


Figure 66. NOESY spectrum of the Aromatic Region of the U-V/RNase A Complex. Contour plot of the phase-sensitive NOESY spectrum of U-V bound to RNase A at pH* 5.5 and 303 K. RNase A and U-V concentrations are 6.57 and 10 mM respectively , in 0.3 M NaCl and 0.5 mM DSS in D₂O.

combined neutron diffraction and x-ray crystallographic structure of the U-V/RNase A complex (Bernstein *et al.*, 1977; Borah *et al.*, 1985; Wlodawer *et al.*, 1983) (Protein Data Bank, reference 6RSA). A third cross peak is observed for the He1 and Hδ2 protons of His105, which are 4.25 Å apart. The resonance assigned to the He1 proton of the protonated form of His12 displays a cross peak with both the C₅H and C₆H protons of U-V suggesting that U-V is within approximately 5 Å of His12. The reason for the absence of cross peaks corresponding to the interaction between the unprotonated form of His12 and U-V is not clear. No cross peaks were observed between the C₆H and C₅H resonances of U-V and any of the resonances associated with His119. The lack of cross peaks between His119 and U-V, indicates that the uridine base of U-V is not in the vicinity of His119. Outside of the aromatic region of the spectrum, a crosspeak was observed between one of the methyl proton resonances of Val118 and the He1 proton of the protonated form of His119 (Figure 67).

7.8) Modelling the Interaction Between RNase A and Uridine Vanadate

The joint neutron and 2 Å x-ray diffraction structure of the U-V/RNase A complex (Bernstein *et al.*, 1977; Borah *et al.*, 1985; Wlodawer *et al.*, 1983) (Protein Data Bank, reference 6RSA) was used to generate molecular graphic images of the complex. The neutron diffraction structure shows His119 to occupy the A position in the complex. The distances between the He1 proton of His12 and the C₅H and C₆H protons of U-V are 5.54 Å and 6.74 Å, respectively. In the A position, the same distances between the He1 proton of His-119 and the C₅H and C₆H protons of U-V are 4.89 Å and 6.61 Å, respectively, which places the He1 proton of His119 nearer to the C₅H and C₆H protons of U-V, than the He1 proton of His-12. Figure 68 shows the active site residues His12

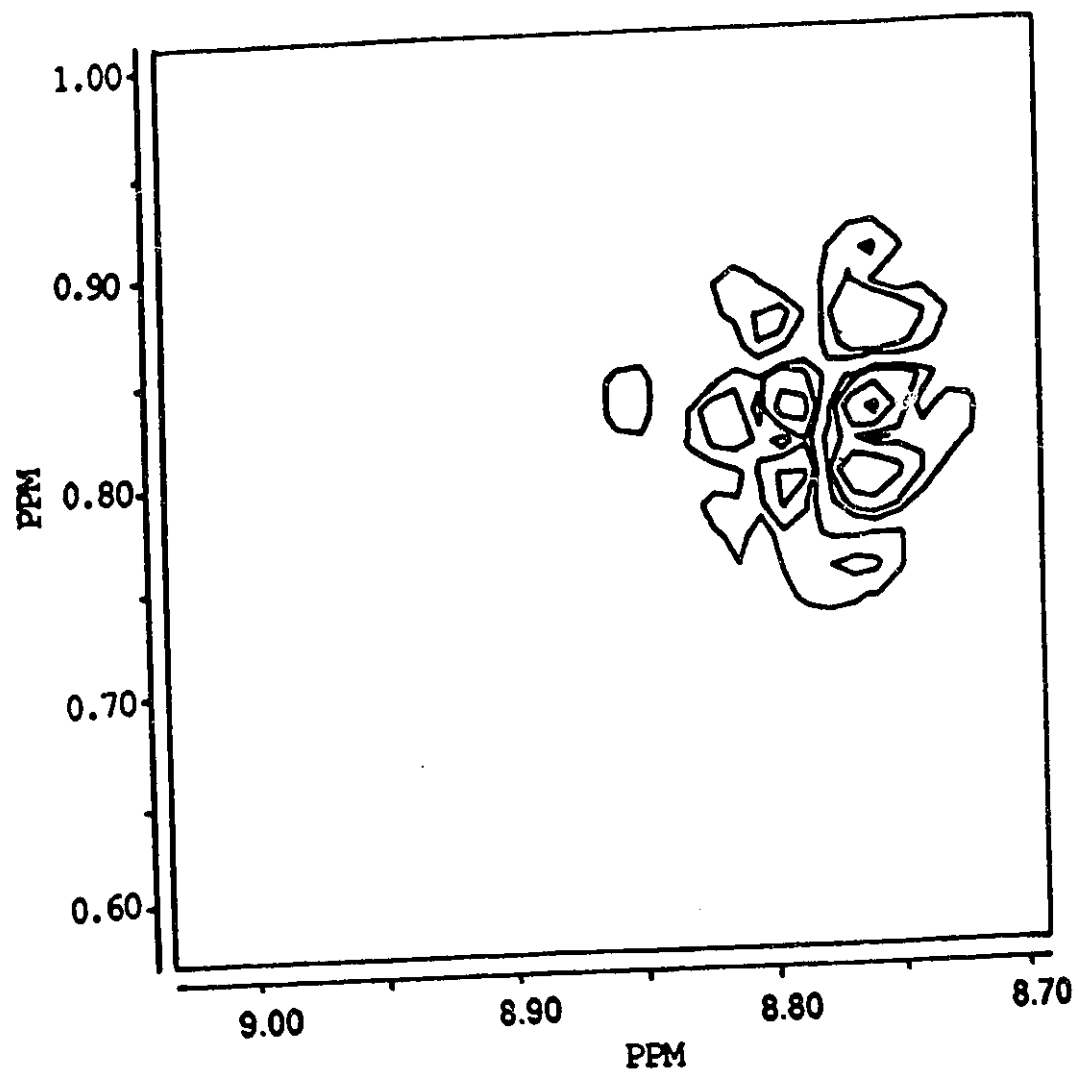


Figure 67. NOE Cross Peak Between His119P and Val118 in the U-V/RNase A Complex. Contour plot of the phase-sensitive NOESY spectrum of the U-V/RNase A complex showing the cross peak between His119P and one of the methyl protons of Val118 based on the assignments of Robertson *et al.*, (1989). The experimental conditions are the same as those listed in Figure 66.

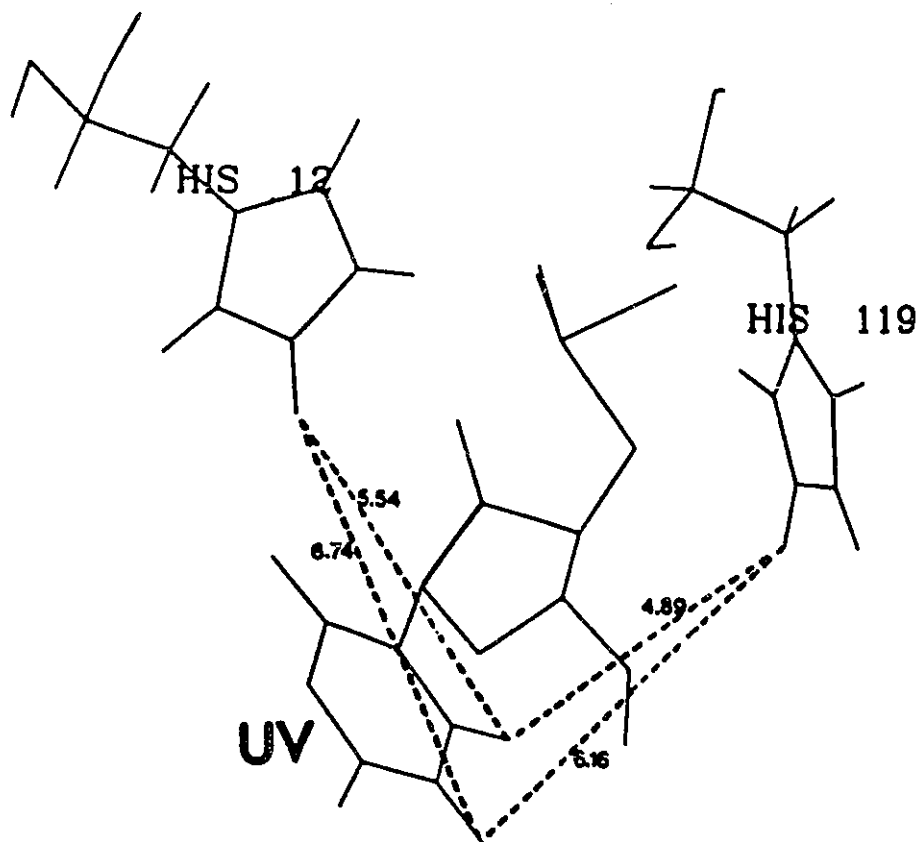


Figure 68. Distances Within the Active Site of the X-ray Crystallographic Structure of the U-V/RNase A Complex. The above diagram shows some of the distances between the H ϵ 1 protons of His12 and 119 and the C₅H and C₆H protons of U-V, based upon the coordinates of the combined neutron and 2 Å x-ray crystallographic structure of the U-V/RNase A complex (Bernstein et al., 1977; Borah et al., 1985; Wlodawer et al., 1983) (Protein Data Bank, reference 6RSA).

and His119A in the presence of U-V, with the above mentioned distances indicated.

The His-119 side chain was then swung into the B position by applying a rotation to the dihedral angles χ_1 (N-C α -C β -C γ) and χ_2 (C α -C β -C γ -C δ). The new dihedral angles were $\chi_1 = -69^\circ$ and $\chi_2 = -63^\circ$ (Borkakoti *et al.*, 1982). In this position, the distances between the H ϵ 1 proton of His119 and the C $_5$ H and C $_6$ H protons of U-V are 11.25 Å and 12.85 Å, respectively, which is well outside of the observable NOE range (Wüthrich, 1986). The distance between the H ϵ 1 proton of His119B and the closest proton of Val118 is 3.81 Å. Figure 69 shows the active site residues His12, His119B, and Val118 in the presence of U-V with the above mentioned distances indicated.

7.9) Energy Changes in the U-V/RNase A Complex as a Consequence of Varying the Position of the His119 Side Chain

The energy of RNase A was measured with the position of His119 side chain in various locations. The energy calculations were performed using the x-ray crystallographic coordinates of RNase A (Bernstein *et al.*, 1977; Wlodawer *et al.*, 1982) (Protein Data Bank, reference 5RSA) with no ligand bound to the active site. The two dihedral angles χ_1 and χ_2 of His119 were varied between -180° and $+180^\circ$ in steps of 18° and the energy of the system was measured at each angle variation. Figure 70 shows a contour plot of the areas of lowest energy versus the dihedral angles χ_1 and χ_2 of His119. The lowest contour level is at 889 kcal/mol and the outer contours increase by 2 kcal/mol. The A and B positions of His119 were both located in areas of minimum energy and these positions were connected by a low energy pathway. Two other areas of minimum energy were located at approximately $\chi_1 = 160^\circ$, $\chi_2 = 80^\circ$ and $\chi_1 = -120^\circ$, $\chi_2 = 80^\circ$.

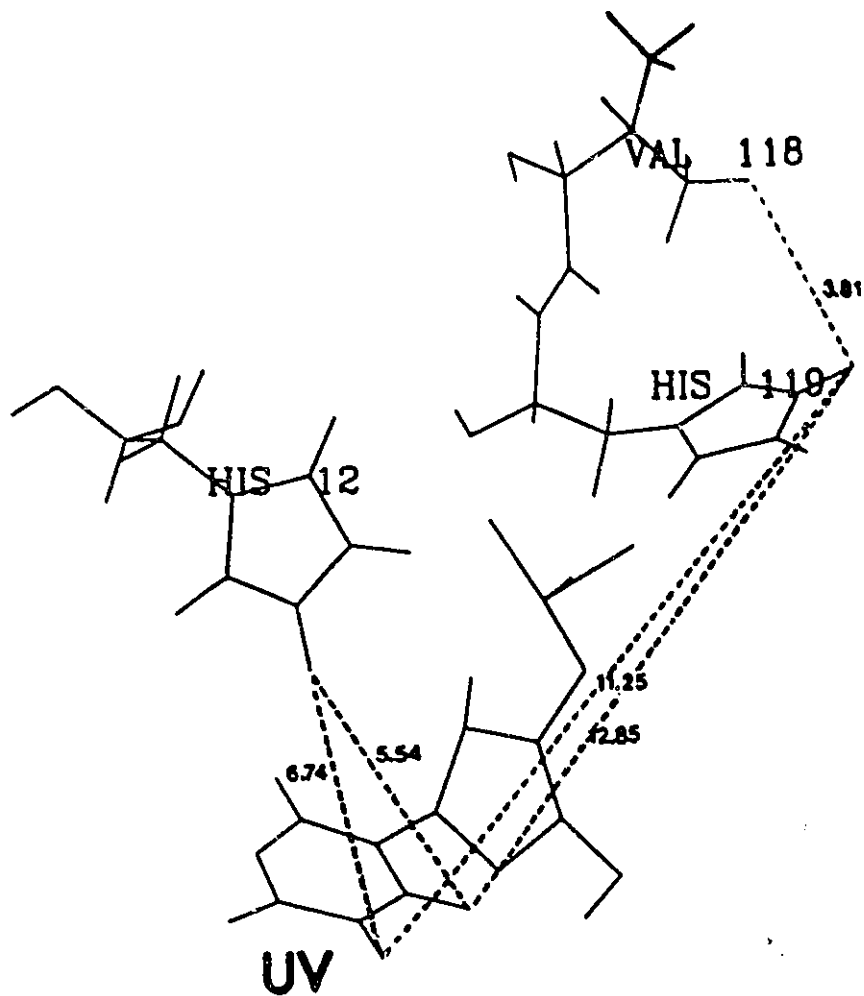


Figure 69. Distances Within the Active Site of the U-V/RNase A Complex with His119 in the B Position. The above diagram shows some of the distances between the He1 protons of His12 and 119 and the C₅H and C₆H protons of U-V and between the He1 proton of His119 and the closest methyl proton of Val118, with His119 in the B position based upon the coordinates of the combined neutron and 2 Å x-ray crystallographic structure of the U-V/RNase A complex (Bernstein et al., 1977; Borah *et al.*, 1985; Wlodawer et al., 1983) (Protein Data Bank, reference 6RSA).

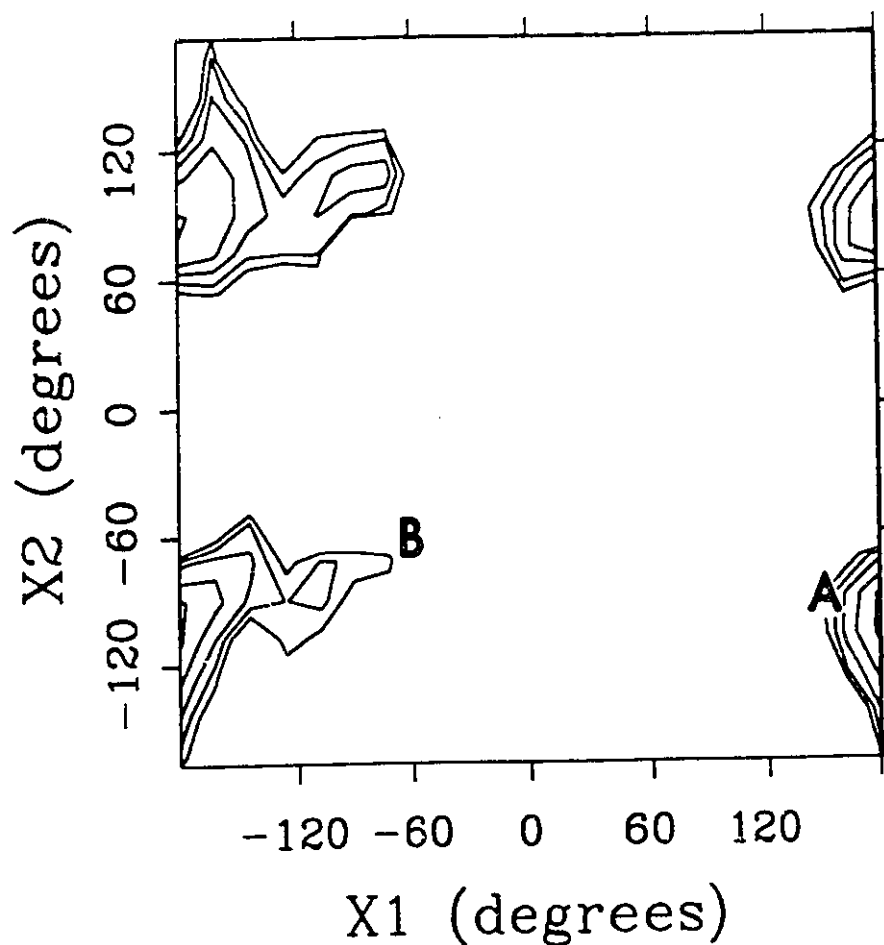


Figure 70. Contour Plot of the Energy of RNase A Versus the χ_1 and χ_2 Angles of His119. The χ_1 (N-C α -C β -C γ) and χ_2 (C α -C β -C γ -C δ) angles of His119 were each rotated through 360° and the energy of RNase A was measured at each new angle. The lowest energy level is 889 kcal/mol and each outer contour increases by 2 kcal/mol. The dihedral angles representing the A and B positions of His119 are labelled on the plot. The coordinates used were from Wlodawer *et al.*, 1982 (Protein Data Bank, reference 5RSA).

The same calculation was repeated using the neutron diffraction coordinates of the U-V/RNase A complex (Protein data bank, reference 6RSA). Since the U-V portion of the complex had several undefined valences, the substrate portion was altered so that a phosphorous atom replaced the vanadium atom. Therefore, a penta-coordinate phosphorous atom now occupies the active site. No other significant atomic changes were made to the U-V molecule. The two dihedral angles χ_1 and χ_2 of His119 were varied between -180° and $+180^\circ$ in steps of 18° and the energy of the system was measured at each angle variation. Figure 71 shows a contour plot of the areas of lowest energy versus the dihedral angles χ_1 and χ_2 of His119. The lowest contour level is at 950 kcal/mol and the outer contours increase by 10 kcal/mol.

Two areas with total energy less than 1000 kcal/mol were located on the plot. The position representing His119 in the A position ($\chi_1=149^\circ$, $\chi_2=-101^\circ$) is labelled on the plot and is within one of the areas with low energy. The second area with low energy possesses a similar χ_1 angle but there is a large change in the χ_2 angle. The contour with the lowest energy in this second area has χ_1 and χ_2 angles of 160° and 80° , respectively. The position of His119B is also labelled on the graph, but is not within an area of minimum energy.

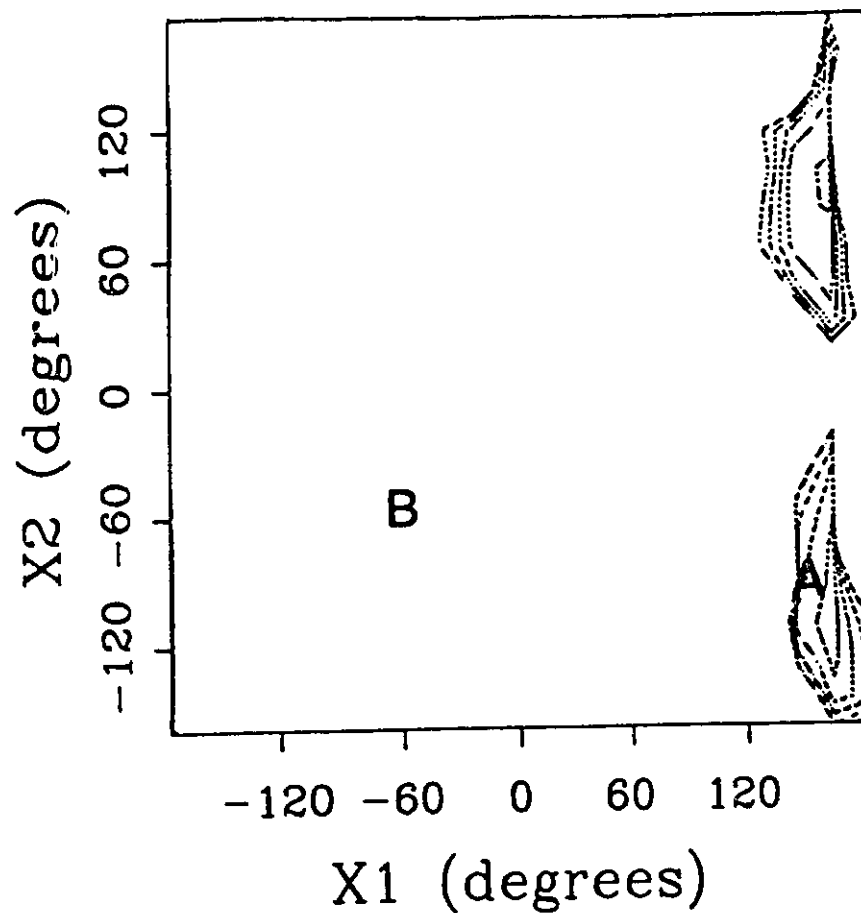


Figure 71. Contour Plot of the Energy of the U-V/RNase A Complex Versus the χ_1 and χ_2 Angles of His119. The χ_1 (N-C α -C β -C γ) and χ_2 (C α -C β -C γ -C δ) angles of His119 were each rotated through 360° and the energy of the U-V/RNase A complex was measured at each new angle. The lowest energy level is 950 kcal/mol and each outer contour increases by 10 kcal/mol. The dihedral angles representing the A and B positions of His119 are labelled on the plot.

CHAPTER EIGHT

DISCUSSION

8.1) pH* Titration of RNase A

The pH* titration curves of the H ϵ 1 resonances of His12, His105 and His119 are continuous in the pH range of 3.0 to 9.0 (Figure 54). The titration curve of the H ϵ 1 proton of His48 is discontinuous, as this resonance is not observed in the pH* range 5.0 to 8.0. The resonance of the H ϵ 1 proton of His48 is only observed in the presence of acetate and propionate; in the presence of other salts, it is not observed due to slow exchange broadening (Figure 53) near its pKa (Markley, 1975b). The calculated pKa values for H ϵ 1 protons of the observable His residues are as follows: His12, 6.19; His105, 6.69; His119, 6.55 (Table XIII). The pKa values are similar to the pKa values determined under identical salt concentration and temperature conditions, where the pKa values of His12, His105 and His119 were found to be 6.01, 6.40 and 6.72, respectively (Markley and Finkenstadt, 1975; Markley, 1975b).

8.2) Titration of RNase A with 3'-CMP

The titration of RNase A with 3'-CMP was done at pH* 5.5 and was monitored by ¹H-NMR at 30°C (Figure 55). 3'-CMP is an inhibitor of RNase A. The structure of 3'-CMP, with its free 3'-phosphate group, is identical to the structure of the nucleotide bound directly to the active site of the enzyme after RNA catalysis. The binding constant of 3'-CMP to RNase A at pH 7.0 is equal to 1770 M⁻¹ (Pollard and Nagyvary, 1973) and

at pH 5.0 the binding constant increases to 7530 M^{-1} (Anderson *et al.*, 1968). The effect of adding increasing amounts of 3'-CMP to the RNase A sample is manifested by a downfield shift in the position of the H ϵ 1 resonances of His12 with no observable change in the line-shape of this resonance or the other His resonances. The total downfield shift for the H ϵ 1 resonances of His12 was about 0.3 ppm. There is no significant effect on the H ϵ 1 resonances of His119 therefore this proton does not directly interact with the phosphate group of the inhibitor. The observation that His12 and His119 are differentially affected by the binding of 3'-CMP to the active site of RNase A, agrees with previous reports on the binding of this inhibitor as well as 2'-CMP and 5'-CMP to the enzyme (Meadows *et al.*, 1969). The ^1H -NMR resonances of the H ϵ 1 and H δ 2 protons of His105 are not affected by the introduction of 3'-CMP suggesting there is no interaction between this residue and the inhibitor. The effect on the position of the His12 resonance occurs gradually (Figure 56) and is continuous as 3'-CMP is added to the enzyme solution until the enzyme becomes saturated with inhibitor at a [3'CMP]/[RNase A] molar ratio of about 1.5.

8.3) pH* Titration of the 3'-CMP/RNase A Complex

In the pH* titration of RNase A with 3'-CMP bound to the active site, the H ϵ 1 resonances of His12, His105, His119, and His48 could be observed clearly within the aromatic region (7.4 to 9.2 ppm) of the ^1H -NMR spectrum (Figure 57) at low pH*. The H ϵ 1 resonances of His12, His105 and His119 exhibited continuous titration curves throughout the pH* range (3.72 to 9.81) (Figure 58). The titration curve of the H ϵ 1 proton of His48 is discontinuous as was observed in the pH* titration of the free enzyme (Figure 53). The calculated pKa values for His12, 105 and 119 were 6.95, 6.69 and

7.17, respectively (Table XVI). Compared to the pH* titration of the free enzyme (Table XIII) the pKa values of His12 and His119 in the 3'-CMP/RNase A complex increased 0.76 and 0.62 pKa units, respectively. No significant change was observed in the pKa of His105. The large increase in the pKa values of His12 and His119 is expected, since the binding of 3'-CMP within the active site places a negatively charged phosphate group within the vicinity of these two residues. No change was expected in the pKa value of His105, since this residue is not near the active site of the enzyme (Borkakoti *et al.*, 1982). The effect on the pH* titration curves of the active site His residues induced by 3'-CMP is typical of that observed in several titration studies of these residues in the presence of various RNase A inhibitors (Gorenstein *et al.*, 1976; Haar *et al.*, 1974; Markley, 1975b; Meadows *et al.*, 1969). In general, the binding of a negatively charged ligand to the active site of RNase A results in an increase in the pKa of His12 and His119.

8.4) Titration of RNase A with U-V

The titration of RNase A with U-V was performed at pH* 5.6. ¹H-NMR spectra were recorded at five different [U-V]:[RNase A] ratios: 0.00, 0.43, 0.86, 1.29 and 2.14 (Figure 61). With no U-V added the His resonances of the free enzyme were observed in the aromatic region (7.4 to 9.2 ppm) of the spectrum. As the concentration of U-V is increased the Hε1 resonances of His12 and His119 decrease in intensity and the resonances of His12P, His12U, His119P and His119U appear and increase in intensity. As U-V binds to the active site, the normal Hε1 resonances of His-12 and 119 begin to lose intensity with no change in their position evident other than the appearance of the four resonances assigned to protonated and unprotonated forms of these residues in slow

exchange (Borah *et al.*, 1985). The change in the positions of the H ϵ 1 resonances of His12 and His119 is not continuous and occurs suddenly as U-V binds within the active site of RNase A. The ^1H -NMR resonances of the H ϵ 1 and H δ 2 protons of His105 are not affected by the introduction of U-V suggesting no interaction with this residue. The resonances of free His-12 and His-119 were no longer observable at a [U-V]:[RNase A] molar ratio of 1.29 and no change in the spectrum was observed at a ratio of 2.14. Therefore the enzyme is essentially saturated with U-V at a maximum ratio of 1.29. These results confirm the tight binding of U-V to RNase A and may substantiate its proposed transition-state analog role (Lindquist *et al.*, 1973). This result is significant, since it is important to verify that the enzyme is saturated with U-V before performing any pH titration studies or two-dimensional NOESY experiments. The U-V titration profile of RNase A observed by ^1H -NMR is similar to that observed by Borah *et al.* (1985).

Although the ^{51}V -NMR spectrum of the U-V molecule acquired at pH* 6.20 was not identical to the spectrum of U-V acquired at pH* 6.80 observed by Borah *et al.* (1985), the largest resonance in the spectrum is assignable to the ^{51}V resonance of U-V based on the assignments of Borah *et al.* (1985). Two other resonances were observed in the spectrum presented here that were not observed in the spectrum of U-V acquired by Borah *et al.* (1985). The reasons for this are not clear. The extra peaks could be a result of the different pH values that the two spectra were acquired at. During the course of this study a crystal developed in the NMR sample used to acquire the ^{51}V -NMR spectrum of U-V. The structure of this crystal was subsequently solved by x-ray diffraction, and found to be $\text{V}_{10}\text{O}_{28}$. Therefore, one of the extra peaks could be this molecule. The most convincing evidence that it is indeed U-V that is binding to the active

site of RNase A, is the observed effect on His12 and His119. The results of the $^1\text{H-NMR}$ experiments showing the binding of the U-V sample to RNase A presented here, are similar to that observed by Borah *et al.* (1985). No previous research has shown the binding of $\text{V}_{10}\text{O}_{28}$, or any molecule similar to this structure, to RNase A. If $\text{V}_{10}\text{O}_{28}$ is an impurity within the U-V sample it would not interfere with the study of the effect of U-V on the active site histidyl residues.

8.5) pH* Titration of the U-V/RNase A Complex

The pH* titration of the U-V/RNase A complex is quite unusual (Figure 62). Unlike the binding of 3'-CMP and other inhibitors to RNase A where the effects on the active site His residues are gradual as the pH is raised or lowered, U-V saturates the enzyme as soon as the pH* hits 5.0. Also since the titration curves of His12 and His119 are now discontinuous, the pKa values of these residues cannot be calculated. In the pH* titration of the 3'-CMP/RNase A complex, both His12 and His119 have continuous titration curves and the effect of the binding of the inhibitor on these residues is manifested by an increase in their calculated pKa values. There were no significant effects on the resonances of His105 or His48, as expected since neither of these residues is within the active site of the enzyme and do not interact directly with U-V.

8.6) Binding of U-V to RNase A

As shown above, U-V exhibits very peculiar binding characteristics to the active site of RNase A. U-V binds to the enzyme only within the pH* range of 5.0 to 8.0 and absolutely no evidence of binding to the enzyme is observable outside of this pH range.

The reason for this particular binding phenomenon is not known. It could be a result of a change in the protonation state of one of the active site histidine residues. Either His12 or His119 must become unprotonated, allowing the U-V to bind tightly and rapidly into the active site of RNase A. The displacement of U-V from the active site at pH* 8.0 would thus be preceded by the complete deprotonation of the second histidine residue. Histidine 12 is most likely the residue deprotonated at pH* 5.0 since its pKa in the free enzyme is 6.19. The pKa of His119 in the free enzyme is 6.55, therefore it would be the deprotonated residue at pH* 8.0. The problem with this explanation is that at pH 5.0 a very small percentage of the His12 (pKa 6.19) residues would be unprotonated and almost 100% of the His119 (pKa 6.55) residues would be completely unprotonated at about pH 7.6. Indeed if the deprotonation of an active site His residue were required for the release of U-V at pH* 8.0, a gradual decrease in the intensity of one of the resonances attributed to the protonated forms of His12 or His119 would be expected. Both His12P and His119P are observed throughout the pH* range from 5.0 to 8.0 (Figures 63 and 64) (Borah *et al.*, 1985) with no observable change in their intensities (Borah *et al.*, 1985). If U-V traps the active site His residues in a slow protonation/deprotonation exchange the protonation state of the active site residues would not be expected to change within the pH* range 5.0 to 8.0. Therefore, no alteration of the protonation state of these residues could occur which would be required for the release of U-V.

A second explanation for the strange binding behaviour of U-V to RNase A is that it may be a result of an overall structural change in the enzyme occurring at pH* values 5.0 and 8.0. This theory would require a subtle change in the conformation of the active site at pH* 5.0. This conformational change would accommodate the binding of U-V.

Another conformational change at pH* 8.0, unfavourable for the binding of U-V, would cause the release of the transition-state analog from the active site of the enzyme. Such a structural change was postulated by Markley (1975b) when he was investigating the titration profile of His48 of RNase A. The titration profile of this residue was known to be discontinuous, and in titrations from low to high pH, began to broaden out and disappear near pH* 5.0 and then reappear again at pH* 8.0. It was postulated that the discontinuous titration curve of His48 was a result of structural changes in the region near His48. The distances between the C α atoms of His48 and His119, and His48 and His12 are 16.07 Å and 8.88 Å, respectively, as measured in the combined neutron and x-ray diffraction structure of the U-V/RNase A complex (Bernstein *et al.*, 1977; Borah *et al.*, 1985; Wlodawer *et al.*, 1983) (Protein Data Bank, reference 6RSA). If a structural transition is occurring within RNase A which affects His48 between pH* 5.0 and 8.0, it is also possible that the same conformational transition could result in changes in the active site of RNase A in the vicinity of His12 and possibly His119.

8.7) Position of His119 in the U-V/RNase A Complex

The NOESY spectrum of the U-V/RNase A complex showed no cross peaks between any of the resonances attributed to His119 and the C₅H and C₆H resonances of U-V (Figure 66). Cross peaks between the H ϵ 1 resonance of His12P and the C₅H and C₆H resonances of U-V were observed (Figure 66). Although the associated distances of 5.54 Å and 6.74 Å, respectively, (Figure 68) approach the upper limit of inter-proton distances normally observed by through-space correlation, the observation of cross peaks suggests that on a time average in solution, these protons are close to each other. The distances were determined from the coordinates of the combined neutron and 2 Å

resolution x-ray diffraction structure of the U-V/RNase A complex (Bernstein *et al.*, 1977; Borah *et al.*, 1985; Wlodawer *et al.*, 1983) (Protein Data Bank, reference 6RSA). The distances between the H ϵ 1 proton of His119 and the C₅H and C₆H protons of U-V are shorter than the distances between the H ϵ 1 proton of His12 and the C₅H and C₆H protons of U-V based on the coordinates of the neutron diffraction structure of the U-V/RNase A complex (Borah *et al.*, 1985) which places His119 in the A position (Figure 68). This result along with the cross peak observed between the H ϵ 1 resonance of His119P and one of the methyl resonances of Val118 (Figure 67), suggests that His119 occupies a position more closely related to the B position (Borkakoti *et al.*, 1982) in the U-V/RNase A complex in solution. A cross peak between the H ϵ 1 proton of His119 and one of the methyl protons of Val118 would be predicted if His119 were in the B position (Figure 69). With His119 in the B position, no cross peak would be expected between the H ϵ 1 proton of His119 and the C₅H and C₆H protons of U-V (Figure 69). Therefore the position of His119 in the U-V/RNase A complex in solution is different from that observed in the neutron diffraction structure of the complex (Borah *et al.*, 1985).

The energy of RNase A was measured with the position of the His119 side chain in various positions by altering the dihedral angles χ_1 and χ_2 of this residue (Figure 70). An area of minimum energy was located at $\chi_1=160^\circ$, $\chi_2=-80^\circ$ for His119 which is similar to the A position for this residue ($\chi_1=149^\circ$, $\chi_2=-101^\circ$) (Borkakoti *et al.*, 1982). An area of minimum energy was also observed for the system with His119 near the B position ($\chi_1=-69^\circ$, $\chi_2=-63^\circ$) (Borkakoti *et al.*, 1982).

The energy of the U-V/RNase A complex was measured with the position of the His119 side chain in various positions by altering the dihedral angles χ_1 and χ_2 of this

residue (Figure 71). Two areas of minimum energy were located at $\chi_1=160^\circ$, $\chi_2=80^\circ$ and $\chi_1=160^\circ$, $\chi_2=-80^\circ$ which is similar to the A position for His119 ($\chi_1=149^\circ$, $\chi_2=-101^\circ$) (Borkakoti *et al.*, 1982). No area of minimum energy was observed for the system with His119 in the B position ($\chi_1=-69^\circ$, $\chi_2=-63^\circ$) (Borkakoti *et al.*, 1982). This result does not preclude His119 from being able to occupy the B position, as there is no evidence from the NMR data that U-V binds within the active site of the enzyme in the exact position as in the crystallographic structure. Indeed in the combined neutron and x-ray diffraction structure, the position and orientation of the ribose sugar ring of U-V was ambiguous and the final structure of this moiety is distorted (Borah *et al.*, 1985).

The observed differences in the position A and B of His119 of RNase A may be a function of differences in crystals and solution structure. The possibility does exist that the differences in the position of His119 may be a result of differences in experimental conditions. Histidine 119 is seen primarily in the A position in RNase A crystallized from alcohol, such as 40-60% ethanol at pH 5.2-5.7 and 43% t-butanol at pH 5.3. (Borkakoti *et al.*, 1982; Wlodawer and Sjolín, 1983; Wlodawer *et al.*, 1983). Histidine 119 is observed in the B position in RNase A crystallized from salt solutions such as ammonium sulfate at pH 5.2 (Martin *et al.*, 1987; deMel *et al.*, 1992). In the NOE spectra of the phosphate/RNase A complex in aqueous solution in 0.2 M NaCl at pH 4.0, a cross peak was observed between His119 and one of the methyl protons of Val118 (Santoro *et al.*, 1993), which places the side chains of these two residues within close proximity of one another. An arrangement in which the side chains of His119 and Val118 are close to one another abuts the B position (Santoro *et al.*, 1993).

It has been postulated that U-V is a better transition-state analog for the hydrolysis step than for transphosphorylation in the catalytic mechanism of RNase A (Lindquist *et al.*, 1973). This implies that His119 in the U-V complex should be closer to position A. In the A position, His119 makes a hydrogen bond with Asp121, thereby making it a better base for abstracting a proton off the water molecule that attacks the tetrahedral phosphonate in the cyclic nucleotide (Figure 49) (Brooks *et al.*, 1986). The ionic strength of our NMR sample (0.3 M NaCl) may weaken this interaction between His119 and Asp121. This would allow His119 to move away from the A position, possibly closer to an axial oxygen atom of U-V, which has a larger electrostatic potential than the equatorial ones (Krauss and Basch, 1992).

8.8) Modelling the Catalytic Mechanism of RNase A

U-V is proposed to be a transition-state analogue for RNase A (Lindquist *et al.*, 1973). It has been shown in the x-ray crystallographic structure of the U-V/RNase A complex that U-V forms a pentacoordinate trigonal bipyramidal structure with the central vanadium atom bound to five oxygen atoms (Wlodawer *et al.*, 1983). This structure mimics the pentacoordinate trigonal bipyramidal phosphorous transition state that is encountered in both the transphosphorylation (Figure 48) and hydrolysis (Figure 49) catalytic mechanisms of RNase A.

In the neutron diffraction structure of the U-V/RNase A complex (Borah *et al.*, 1985), His119 formed a hydrogen bond with the apical oxygen O2V of U-V, although the distance to the O3 equatorial atom was 0.31 Å shorter. Histidine 12 made a hydrogen bond with an equatorial oxygen and Lys41 was hydrogen bonded to an apical oxygen. This

observed location of His12 is in contradiction to the accepted mechanism of the enzyme. Histidine 12 is responsible for the proton transfer to the apical oxygen and Lys41 provides stabilization of the transition-state complex (Alber *et al.*, 1983). One explanation for this apparent discrepancy is that the flexibility of the Lys-41 side chain allows this residue to search for and bind to the more electronegative apical oxygen (Krauss *et al.*, 1992). It was concluded that U-V is not a suitable transition-state analog for the study of His12 and Lys41, but is a useful analogue for the study of His119 (Krauss *et al.*, 1992).

Modelling studies placing U-V in the active site of semisynthetic RNase A show that the distance between the O2 atom of U-V and ND1 of His-119A is 2.96 Å and the same distance with His119 in the B position is 3.13 Å (deMel *et al.*, 1992). The O2 atom of U-V has been proposed to mimic the oxygen of the water molecule involved in the hydrolytic reaction performed by RNase A (Lindquist *et al.*, 1973). Thus His119 in the A position is closer to the atom that is attacked in the hydrolytic step.

A second modelling study involved placing the substrate uridylyl-3',5'-adenosine (UpA), with a methylene group in place of the 5'-oxygen, into the active site of semisynthetic RNase A (deMel *et al.*, 1992). When UpA is placed into the active site, the distance between the C4P1 atom in this molecule, which has replaced the O5' atom in the actual substrate, UpA, and the ND1 atom of His119, when in position A, is 3.26 Å. When His119 is placed in the B position the corresponding distance is 2.68 Å. The overall results of the above modelling studies are that His119 in site A is closer to the substrate atom that is attacked in the hydrolytic step, while His119 in position B is closer to the atom that is attacked in the transphosphorylation step. The results of this modelling

study suggest that His119 in the A position is catalytically important for the hydrolysis reaction, and His119 in the B position is important for the transphosphorylation reaction. However, His119 in the more distant site is still within a suitable distance to react effectively with the appropriate substrate atom. Therefore in our NMR studies, U-V is mimicing the transphosphorylation step instead of the hydrolytic reaction, since His119 is in a location more closely related to the B position, when U-V is bound within the active site.

In the neutron diffraction structure of the U-V/RNase A complex, the vanadate existed in the dianion form, and both His12 and His119 are doubly protonated (Borah *et al.*, 1985). In solution, the vanadate species exists as a monoanion and the extent of protonation of the two active site histidine residues are about 58% for His12 and 26% for His119 (Borah *et al.*, 1985). It has been suggested that the vanadate dianion models a step in the hydrolysis mechanism and that the monoanion form of the vanadate mimics a step earlier in the catalytic mechanism, presumably transphosphorylation (Krauss *et al.*, 1992). Thus the difference seen in the positions of His119 in the crystal and solution structure may be a result of the difference in the ionization state of the vanadate.

As mentioned above, the degree of protonation of His12 and His119 was observed to be about 58% and 26% respectively (Borah *et al.*, 1985). Although the spectra presented here are less resolved, on the surface they appear to support this result (Figure 61). What is peculiar is that at pH* 5.0, where the binding of U-V to RNase A is initiated, His119 would be expected to be fully protonated, since its pKa in free RNase A was calculated to be 6.55 (Table XIII). Even at pH* 5.5 at which the U-V titration of RNase

A experiments were performed, the extent of protonation of His119 would be expected to be much greater than 26%. The extent of protonation of His119 should be substantially greater than that for His12 at pH* 5.0 and 5.5, since His12 has a pKa value about 0.3 pH units less than that of His119. Although the experiments are examining a dynamic event and the extent of protonation of either residue would be expected to change upon the binding of U-V, the extent of protonation of the two His residues appears to correlate with the formation of the cyclic intermediate. In the formation of the cyclic intermediate, His119 gives up its proton while His12 accepts a proton from the substrate. During the hydrolysis step of the mechanism, His119 abstracts a proton from the substrate, while His12 donates a proton. Thus the extent of protonation observed for these two residues is more indicative of transphosphorylation in which His119 relinquishes a proton.

The major difficulty in attempting to determine which step in the catalytic mechanism of RNase A that U-V acts as a transition-state analog for, is that a mechanism is a dynamic event. The mechanism of RNase A can be crudely divided up into a few steps such that a penta-coordinate phosphorous atom exists twice; once during the middle of the transphosphorylation step and once during the hydrolytic step. In reality, there are several environments around the penta-coordinate phosphorous transition-state throughout the course of the digestion of RNA by the enzyme. These environments are dependent on the degree of protonation of the two active site histidyl residues. Therefore, several different penta-coordinate phosphorous transition-states exist for the enzyme and it is difficult to definitively determine which point of the mechanism that U-V is acting as a transition-state analog for.

With all of the structural studies done attempting to determine the importance of the flexibility of the His119 side chain in the catalytic mechanism of RNase A, little progress appears to be made. It may be possible that the flexibility is not catalytically important and is only a result of the conditions in which the structural studies were carried out. The enzyme semisynthetic RNase A, prepared through a non-covalent association of RNase A (1-118) and a synthesized tetradecapeptide comprising the carboxyl terminus of the enzyme, retains 98% of the activity of native RNase A. In the 1.8 Å resolution x-ray structure of crystals of semisynthetic RNase A, grown from concentrated salt solutions at pH 5.2, His119 is seen exclusively in the B position (Martin *et al.*, 1987). The results from the crystal structure of semisynthetic RNase A suggest that His119 in the B position is still totally functional in the digestion of RNA.

Overall the results from the two-dimensional homonuclear NOESY spectrum suggest that the position of His119 of RNase A in the presence of U-V differs from that observed crystallographically (Borah *et al.*, 1985). The lack of NOE cross peaks between His119 and U-V and the presence of a cross peak between His119 and one of the methyl protons of Val118 suggests that His119 occupies a position closely related to the B position observed for this residue in solution (Borkakoti *et al.*, 1982).

REFERENCES

- Aguilar, C. F., Thomas, P. J., Moss, D. S., Mills, A. and Palmer, R. A. (1991) Novel non-productively bound ribonuclease inhibitor complexes -high resolution X-ray refinement studies on the binding of RNase-A to cytidylyl-2',5'-guanosine (2',5' CpG) and deoxycytidylyl-3',5'-guanosine (3',5' dCpdP) *Biochimica et Biophysica Acta*. **1118**, 6-20.
- Alber, T., Gilbert, W. A., Ponzi, D. R. and Petsko, G. A. (1973) The role of mobility in the substrate binding and catalytic machinery of enzymes. *Ciba Found. Symp.* **93**, 4-24.
- Anderson, D. G., Hammes, G. G. and Walz, F. G. Jr. (1968) Relaxation spectra of ribonuclease. VI. Interaction of ribonuclease with uridine 3'-monophosphate. *Biochemistry* **7**, 1637-1645.
- Avey, H. P., Boles, M. O., Carlisle, C. H., Evans, S. A., Morris, S. J., Palmer, R. A., Woolhouse, B. A. and Shall, S. (1967) Structure of ribonuclease. *Nature* **213**, 557-562.
- Bernstein, F. C., Koetzle, T. F., Williams, G. J. B., Meyer, E. F., Brice, M. D., Rodgers, J. R., Kennard, O., Shimanouchi, T. and Tasumi, M. (1977) The protein data bank: a computer-based archival file for macromolecular structures. *J. Mol. Biol.* **112**, 535-542.

Blackburn, P. and Moore, S. (1982) Pancreatic Ribonuclease. in *The Enzymes*. Vol. XV. Academic Press, New York. 317-433.

Bodenhausen, G., Kogler, H. and Ernst, R. R. (1984) Selection of coherence-transfer pathways in NMR pulse experiments. *J. Magn. Res.* **58**, 370-388.

Borah, B., Chen, C., Egan, W., Miler, M., Wlodawer, A. and Cohen, J. S. (1985) Nuclear magnetic resonance and neutron diffraction studies of the complex of ribonuclease A with uridine vanadate, a transition-state analogue. *Biochemistry* **24**, 2058-2067.

Borkakoti, N., Moss, D. S. and Palmer, R. A. (1982) Ribonuclease A: Least-squares refinement of the structure at 1.45 Å resolution. *Acta. Crystallogr. Sect. B Struct. Sci.* **38**, 2210-2217.

Borkakoti, N. (1983) The active site of ribonuclease A from the crystallographic studies of ribonuclease-A-inhibitor complexes. *Eur. J. Biochem.* **132**, 89-94.

Borkakoti, N., Moss, D. S., Stanford, M. J. and Palmer, R. A. (1984) The refined structure of ribonuclease at 1.45 Å resolution. *J. Cryst. Spectr. Res.* **14**, 467-494.

Bradbury, J. H. and Scheraga, H. A. (1966) Structural studies of ribonuclease. XXIV. The application of nuclear magnetic resonance spectroscopy to distinguish between the histidine residues of ribonuclease. *J. Am. Chem. Soc.* **88**, 4240-4246.

Bradbury, J. H. and Teh, J. S. (1975) Reassignment of the histidine ^1H nuclear magnetic resonances of ribonuclease-A. *Chem. Commun.* **52**, 936-937.

Brooks III, C., Brünger, A., Francl, M., Haydock, K., Allen, L. C. and Karplus, M. (1986) Role of active site residues and solvation in RNase A. *Ann. N.Y. Acad. Sci.* **471**, 295-298.

Brünger, A. T., Brooks, C. L. and Karplus, M. (1985) Active site dynamics of ribonuclease. *Proc. Natl. Acad. Sci. U.S.A.* **82**, 8458-8462.

Crosio, M. P., Janin, J. and Jullien, M. (1992) Crystal packing in six crystal forms of pancreatic ribonuclease. *J. Mol. Biol.* **228**, 243-251.

deMei, V. S. J., Martin, P. D., Doscher, M. S. and Edwards, B. F. P. (1992) Structural changes that accompany the reduced catalytic efficiency of two semisynthetic ribonuclease analogs. *J. Biol. Chem.* **267**, 247-256.

Eftink, M. R. and Biltonen, R. L. (1987) Pancreatic ribonuclease: the most studied endoribonuclease. *In Hydrolytic Enzymes*. A. Neuberger, and K. Brocklehurst, editors. Elsevier, Amsterdam. 333-376.

Ferrin, T. E., Huang, C. C., Jarvis, L. E. and Langridge, R. (1988) The MIDAS display system. *J. Mol. Graphics* **6**, 13-27.

Findlay, D., Herries, D. G., Mathias, A. P., Rabin, B. R. and Ross, C. A. (1962) The active site and mechanism of action of bovine pancreatic ribonuclease. *Biochem. J.* **35**, 152-153.

Glasoe, P. K. and Long, F. A. (1960) Use of glass electrodes to measure acidities in deuterium oxide. *J. Phys. Chem.* **64**, 188-190.

Gorenstein, D. G., Wyrwicz, A. and Bode, J. (1976) Proton and phosphorous NMR study on the binding of cytidine monophosphate inhibitors to ribonuclease A. *J. Am. Chem. Soc.* **98**, 2308-2314.

Gutte, B., Lin, M. C., Caldi, D. G. and Merrifield, R. B. (1972) Reactivation of des(119-, 120-, or 121-124) ribonuclease A by mixture with synthetic COOH-terminal peptides of varying length. *J. Biol. Chem.* **247**, 4763-4767.

Haar, W., Maurer, W. and Rüterjans, H. (1974) Proton-magnetic-resonance studies of complexes of pancreatic ribonuclease A with pyrimidine and purine nucleotides. *Eur. J. Biochem.* **44**, 201-211.

Harris, G. W., Borkakoti, N., Moss, D. S., Palmer, R. A. and Howlin, B. (1987) Ribonuclease A. Analysis of the hydrogen bonding geometry, and spatial accessibility at the active site. *Biochim. Biophys. Acta.* **912**, 348-356.

Havel, T. F. (1991) An evaluation of computational strategies for use in the determination of protein structure from distance constraints obtained by nuclear magnetic resonance. *Prog. Biophys. Mol. Biol.* **56**, 43-78.

Holmes, R. R., Deiters, J. A. and Galluci, J. C. (1978) Computer simulation of ribonuclease action of uridylyl-(3'-5')-adenosine. *J. Am. Chem. Soc.* **100**, 7393-7402.

Kartha, G. (1967) Tertiary structure of ribonuclease. *Nature* **214**, 234-240.

Kim, E. E., Varadarajan, R., Wyckoff, H. W. and Richards, F. M. (1992) Refinement of the crystal structure of ribonuclease S. Comparison with and between the various ribonuclease A structures. *Biochemistry* **31**, 12304-12314.

Krauss, M. and Basch, H. (1992) Is the vanadate anion an analogue of the transition state of RNase A? *J. Am. Chem. Soc.* **114**, 3630-3634.

Lee, B. and Richards, F. M. (1971) The interpretation of protein structures: estimation of static accessibility. *J. Mol. Biol.* **55**, 379-400.

Lenstra, J. A., Bolscher, B. G. J. M., Stob, S., Beintema, J. J. and Kaptein, R. (1979) The aromatic residues of bovine pancreatic ribonuclease studied by ¹H nuclear magnetic resonance. *Eur. J. Biochem.* **98**, 385-397.

Lienhard, G. E. (1973) Enzyme catalysis and transition-state theory. *Science* **180**, 149-154.

Lindquist, R. N., Lynn, J. L. and Lienhard, G. E. (1973) Possible transition-state analogs for ribonuclease. The complexes of uridine with oxovanadium (IV) ion and vanadium (V) ion. *J. Am. Chem. Soc.* **95**, 8762-8769.

Markley, J. L., Williams, M. N., and Jardetzky, O. (1970) Nuclear magnetic resonance studies of the structure and binding sites in enzymes, XII. A conformational equilibrium in *Staphylococcal* nuclease involving a histidine residue. *Proc. Natl. Acad. Sci. U.S.A.* **65**, 645-651.

Markley, J. L. (1975a) Observation of histidine residues in proteins by means of nuclear magnetic resonance spectroscopy. *Accts. Chem. Res.* **8**, 70-80.

Markley, J. L. (1975b) Correlation proton magnetic resonance studies at 250 MHz of bovine pancreatic ribonuclease. I. Reinvestigation of the histidine peak assignments. *Biochemistry* **14**, 3546-3554.

Markley, J. L. (1975c) Correlation proton magnetic resonance studies at 250 MHz of bovine pancreatic ribonuclease. II. pH and inhibitor-induced conformational transitions affecting histidine-48 and one tyrosine residue of ribonuclease A. *Biochemistry* **14**, 3554-3561.

Markley, J. L. and Finkenstadt, W. R. (1975) Correlation proton magnetic resonance studies at 250 MHz of bovine pancreatic ribonuclease. III. Mutual electrostatic interaction between histidine residues 12 and 119. *Biochemistry* **14**, 3562.

Martin, P. D., Doscher, M. S. and Edwards, B. F. P. (1987) The refined crystal structure of a fully active semisynthetic ribonuclease at 1.8-Å resolution. *J. Biol. Chem.* **262**, 15930-15938.

Maurer, W., Haar, W. and Ruterjans, H. (1971) Proc. 1st Eur. Biophys. Congr., vol. 4, pp. 375-379, Verlag der Wiener Medizinischen Akademie, Vienna, Austria.

Meadows, D. H., Jardetzky, O., Epand, R. M., Rüterjans, H. H. and Scheraga, H. A. (1968) Assignment of the histidine peaks in the nuclear magnetic resonance spectrum of ribonuclease. *Proc. Natl. Acad. Sci. U.S.A.* **60**, 766-772.

Meadows, D. H., Roberts, G. C. K. and Jardetzky, O. (1969) Nuclear magnetic resonance studies of the structure and binding sites of enzymes. VIII. Inhibitor binding to ribonuclease. *J. Mol. Biol.* **45**, 491-511.

Nachman, J., Miller, M., Gilliland, G. L., Carty, R., Pincus, M., and Wlodawer, A. (1990) Crystal structure of two covalent nucleoside derivatives of ribonuclease A. *Biochemistry* **29**, 928-937.

Patel, D. J., Canuel, L. L. and Bovey, F. A. (1975) Reassignment of the active site histidines in ribonuclease A by selective deuteration studies. *Biopolymers* **14**, 987-997.

Pollard, D. R. and Nagyvary, J. (1973) Inhibition of pancreatic ribonuclease A by arabinonucleotides. *Biochemistry* **12**, 1063-1066.

Richards, F. M. and Wyckoff, H. W. (1971) Bovine pancreatic ribonuclease. In *The Enzymes*. P. D. Boyer, ed. vol. IV, 3rd ed., Academic Press, New York. 647-806.

Rico, M., Bruix, M., Santoro, J., Gonzalez, C., Neira, J. L., Nieto, J. L. and Herranz, J. (1989) Sequential ^1H -NMR assignment and solution structure of bovine pancreatic ribonuclease A. *Eur. J. Biochem.* **183**, 623-638.

Rico, M., Santoro, J., Gonzalez, C., Bruix, M., Neira, J. L., Nieto, J. L. and Herranz, J. (1991) 3D structure of bovine pancreatic ribonuclease A in aqueous solution: an approach to tertiary structure determination from a small basis of ^1H NMR NOE correlations. *J. Bio. NMR* **1**, 283-298.

Robertson, A. D., Purisima, E. O., Eastman, M. A. and Scheraga, H. A. (1989) Proton NMR assignments and regular backbone structure of bovine pancreatic ribonuclease A in aqueous solution. *Biochemistry* **28**, 5930-5938.

Santoro, J., Gonzalez, C., Bruix, M., Neira, J. L., Neito, J. L. and Herranz, J. (1993) High-resolution three-dimensional structure of ribonuclease A in solution by nuclear magnetic resonance spectroscopy. *J. Mol. Biol.* **229**, 722-734.

Shindo, H., Hayes, M. B. and Cohen, J. S. (1976) Nuclear magnetic resonance titration curves of histidine ring protons. *J. Biol. Chem.* **251**, 2644-2647.

Smyth, D. G., Stein, W. H. and Moore, S. (1963) The sequence of amino acid residues in bovine pancreatic ribonuclease: revisions and confirmations. *J. Biol. Chem.* **238**, 227-234.

Wlodawer, A. (1980) Studies of ribonuclease-A by X-ray and neutron diffraction. *Acta Crystallogr. Sect. B. Struct. Sci.* **36**, 1826-1831.

Wlodawer, A. and Sjolín, L. (1981) Orientation of histidine residues in RNase A: a neutron diffraction study. *Proc. Natl. Acad. Sci. U.S.A.* **78**, 2853-2855.

Wlodawer, A., Bott, R. and Sjolín, L. (1982) The refined crystal structure of ribonuclease A at 2.0 Å resolution. *J. Biol. Chem.* **257**, 1325-1332.

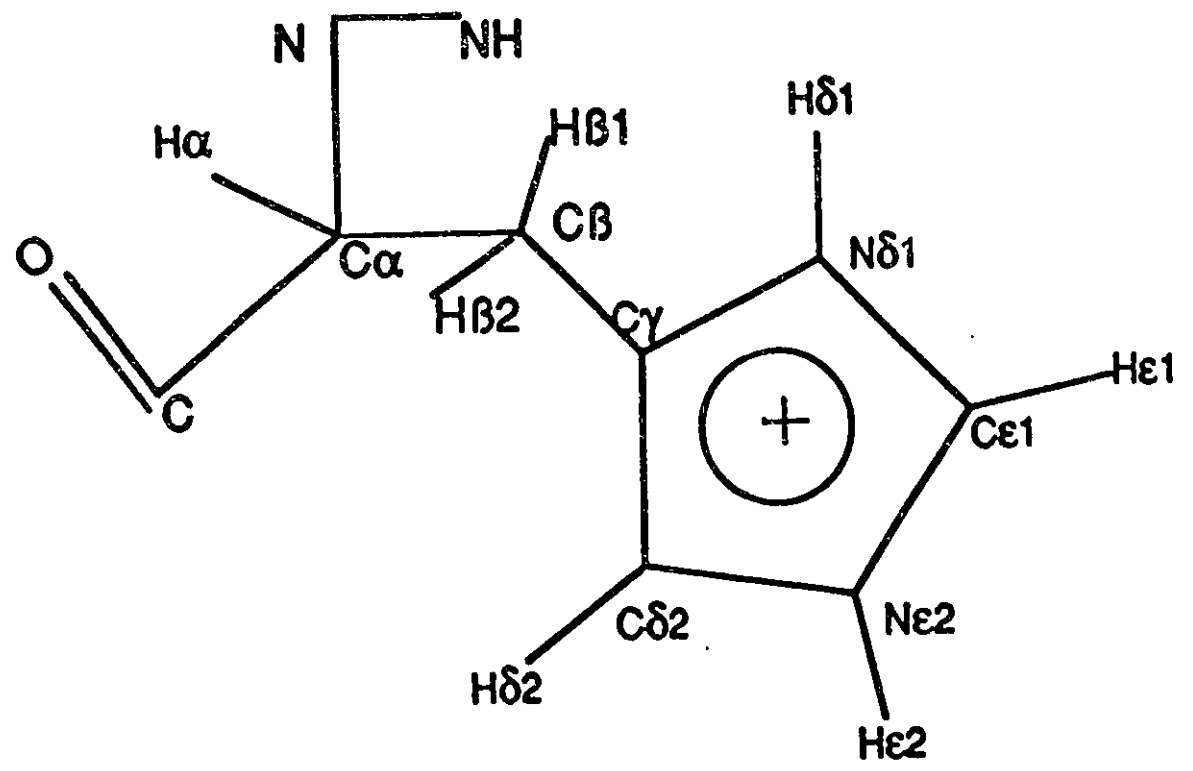
Wlodawer, A. and Sjolín, L. (1983) Structure of ribonuclease A: results of joint neutron and X-ray refinement at 2.0-Å resolution. *Biochemistry* **22**, 2720-2728.

Wlodawer, A., Miller, M. and Sjolín, L. (1983) Active site of RNase: neutron diffraction study of a complex with uridine vanadate, a transition-state analog. *Proc. Natl. Acad. Sci. U.S.A.* **80**, 3628-3631.

Wlodawer, A., Svensson, L. A., Sjolín, L., and Gilliland, G. L. (1988) Structure of phosphate-free ribonuclease A refined at 1.26 Å. *Biochemistry* **27**, 2705-2717.

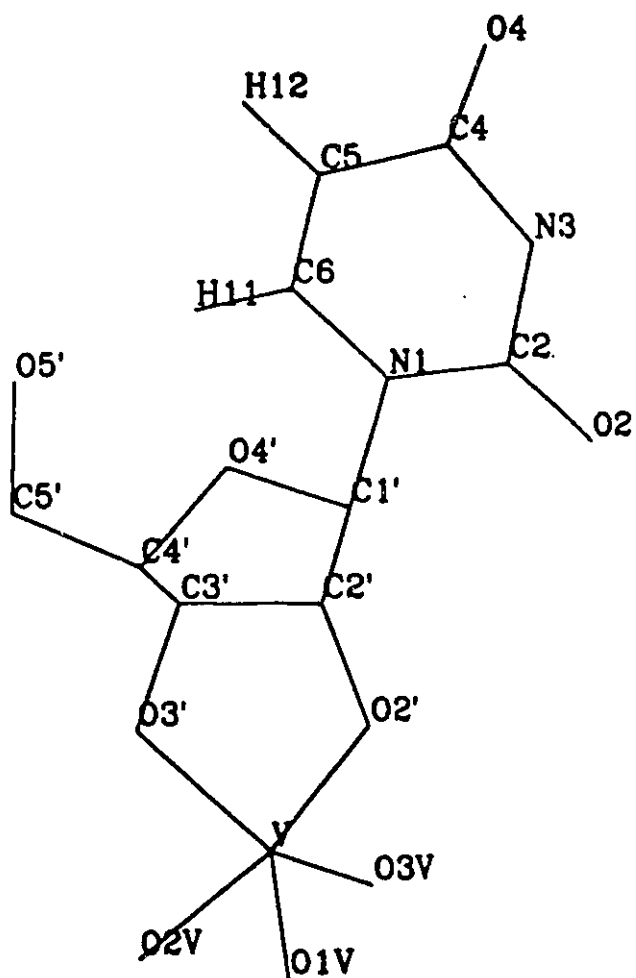
Wüthrich, K. (1986) *NMR of proteins and nucleic acids*. J. Wiley and Sons, New York.

Nomenclature of Atoms in Histidine



Appendix 2

Nomenclature of Atoms in Uridine Vanadate



Appendix 3

NOE Restraint File Used in the Generation of the Three-Dimensional Structure of Thymosin α_1

The following file is a list of hydrogen bond restraints, chirality restraints
NOE distance restraints and NOE volume restraints used in the generation of the
three-dimensional structure of Thymosin α_1

The column definitions are as follows:

- a the smallest separation between the pair of atoms in Å
- b the greatest separation between the pair of atoms in Å
- c force constant applied when atoms are closer than the lower bound ($\text{kcal mol}^{-1} \text{Å}^{-2}$)
- d force constant applied when atoms are farther apart than the upper bound ($\text{kcal mol}^{-1} \text{Å}^{-2}$)
- e limit on the magnitude of force ($\text{kcal mol}^{-1} \text{Å}^{-1}$)
- f the asymmetric atom center
- g the desired chirality at the center
- h mixing times
- i maximum upper bound of the separation of the pair of atoms in Å
- j lower bound on the NOE volume for mixing time 1
- k upper bound on the NOE volume for mixing time 1
- l lower bound on the NOE volume for mixing time 2
- m upper bound on the NOE volume for mixing time 2
- n lower bound on the NOE volume for mixing time 3
- o upper bound on the NOE volume for mixing time 3

IBIOSYM restraint 1

distance		a	b	c	d	e
1:LEU_16:O	1:LYS+_20:HN	1.800	2.300	10.00	10.00	1000.00
1:LYS+_17:O	1:GLU-_21:HN	1.800	2.300	10.00	10.00	1000.00
1:GLU-_18:O	1:VAL_22:HN	1.800	2.300	10.00	10.00	1000.00
1:LYS+_19:O	1:VAL_23:HN	1.800	2.300	10.00	10.00	1000.00
1:LYS+_20:O	1:GLU-_24:HN	1.800	2.300	10.00	10.00	1000.00
1:GLU-_21:O	1:GLU-_25:HN	1.800	2.300	10.00	10.00	1000.00
1:VAL_22:O	1:ALA_26:HN	1.800	2.300	10.00	10.00	1000.00
1:LEU_16:O	1:LYS+_20:N	2.500	3.300	10.00	10.00	1000.00
1:LYS+_17:O	1:GLU-_21:N	2.500	3.300	10.00	10.00	1000.00
1:GLU-_18:O	1:VAL_22:N	2.500	3.300	10.00	10.00	1000.00
1:LYS+_19:O	1:VAL_23:N	2.500	3.300	10.00	10.00	1000.00
1:LYS+_20:O	1:GLU-_24:N	2.500	3.300	10.00	10.00	1000.00
1:GLU-_21:O	1:GLU-_25:N	2.500	3.300	10.00	10.00	1000.00
1:VAL_22:O	1:ALA_26:N	2.500	3.300	10.00	10.00	1000.00

chiral	f	g
1:SERN_1:CA	S	S
1:ASP-_2:CA	S	S
1:ALA_3:CA	S	S
1:ALA_4:CA	S	S
1:VAL_5:CA	S	S
1:ASP-_6:CA	S	S
1:THR_7:CA	S	S
1:SER_8:CA	S	S
1:SER_9:CA	S	S
1:GLU-_10:CA	S	S
1:ILE_11:CA	S	S
1:THR_12:CA	S	S
1:THR_13:CA	S	S
1:LYS+_14:CA	S	S
1:ASP-_15:CA	S	S
1:LEU_16:CA	S	S
1:LYS+_17:CA	S	S
1:GLU-_18:CA	S	S
1:LYS+_19:CA	S	S
1:LYS+_20:CA	S	S
1:GLU-_21:CA	S	S
1:VAL_22:CA	S	S
1:VAL_23:CA	S	S
1:GLU-_24:CA	S	S
1:GLU-_25:CA	S	S
1:ALA_26:CA	S	S
1:GLU-_27:CA	S	S
1:ASNC_28:CA	S	S
1:THR_7:CB	S	S
1:ILE_11:CB	S	S
1:THR_12:CB	S	S
1:THR_13:CB	S	S

#NOE_distance									
IATOM 01		ATOM 02							
I		J		a	b	l	c	d	e
1: ILE_11:HN	1: THR_12:HN	1.800	4.000	5.000	10.00	10.00	1000.00		
1: LYS_14:HN	1: ASP_15:HN	1.800	3.000	5.000	10.00	10.00	1000.00		
1: ASP_15:HN	1: LEU_16:HN	1.800	3.000	5.000	10.00	10.00	1000.00		
1: LEU_16:HN	1: LYS_17:HN	1.800	3.000	5.000	10.00	10.00	1000.00		
1: GLU_18:HN	1: LYS_19:HN	1.800	5.000	5.000	10.00	10.00	1000.00		
1: LYS_19:HN	1: LYS_20:HN	1.800	4.000	5.000	10.00	10.00	1000.00		
1: GLU_21:HN	1: VAL_22:HN	1.800	3.000	5.000	10.00	10.00	1000.00		
1: VAL_22:HN	1: VAL_23:HN	1.800	3.000	5.000	10.00	10.00	1000.00		
1: VAL_23:HN	1: GLU_24:HN	1.800	3.000	5.000	10.00	10.00	1000.00		
1: GLU_24:HN	1: GLU_25:HN	1.800	3.000	5.000	10.00	10.00	1000.00		
1: GLU_25:HN	1: ALA_26:HN	1.800	4.000	5.000	10.00	10.00	1000.00		
1: VAL_5:HN	1: ASP_6:HN	1.800	5.000	5.000	10.00	10.00	1000.00		
1: LEU_16:HN	1: GLU_18:HN	1.800	4.000	5.000	10.00	10.00	1000.00		
1: GLU_10:HN	1: ILE_11:HN	1.800	4.000	5.000	10.00	10.00	1000.00		
1: LYS_20:HN	1: VAL_22:HN	1.800	4.000	5.000	10.00	10.00	1000.00		
1: VAL_22:HN	1: GLU_24:HN	1.800	4.000	5.000	10.00	10.00	1000.00		
1: VAL_23:HN	1: ALA_26:HN	1.800	5.000	5.000	10.00	10.00	1000.00		
1: GLU_21:HN	1: GLU_24:HN	1.800	5.000	5.000	10.00	10.00	1000.00		
1: ALA_4:HN	1: VAL_5:HN	1.800	5.000	5.000	10.00	10.00	1000.00		
1: VAL_22:HA	1: VAL_23:HN	1.800	3.000	5.000	10.00	10.00	1000.00		
1: GLU_21:HG*	1: GLU_21:HA	1.800	4.000	5.000	10.00	10.00	1000.00		
1: GLU_24:HG*	1: GLU_24:HN	1.800	5.000	5.000	10.00	10.00	1000.00		
1: GLU_21:HG*	1: GLU_21:HN	1.800	5.000	5.000	10.00	10.00	1000.00		
1: VAL_23:HA	1: GLU_24:HN	1.800	3.000	5.000	10.00	10.00	1000.00		
1: VAL_5:HA	1: ASP_6:HN	1.800	3.000	5.000	10.00	10.00	1000.00		
1: ALA_4:HA	1: VAL_5:HN	1.800	4.000	5.000	10.00	10.00	1000.00		
1: GLU_18:HB*	1: VAL_22:HN	1.800	5.000	5.000	10.00	10.00	1000.00		
1: LEU_16:HA	1: LYS_19:HN	1.800	4.000	5.000	10.00	10.00	1000.00		
1: LEU_16:HB*	1: LYS_19:HN	1.800	5.000	5.000	10.00	10.00	1000.00		
1: ALA_26:HA	1: GLU_27:HN	1.800	5.000	5.000	10.00	10.00	1000.00		
1: GLU_21:HA	1: VAL_22:HN	1.800	3.000	5.000	10.00	10.00	1000.00		
1: LYS_19:HA	1: VAL_22:HN	1.800	4.000	5.000	10.00	10.00	1000.00		
1: ALA_3:HA	1: ALA_4:HN	1.800	5.000	5.000	10.00	10.00	1000.00		
1: GLU_24:HA	1: GLU_25:HN	1.800	4.000	5.000	10.00	10.00	1000.00		
1: ILE_11:HA	1: THR_12:HN	1.800	4.000	5.000	10.00	10.00	1000.00		
1: THR_12:HA	1: THR_13:HN	1.800	4.000	5.000	10.00	10.00	1000.00		
1: LYS_14:HA	1: ASP_15:HN	1.800	4.000	5.000	10.00	10.00	1000.00		
1: ASP_15:HA	1: LEU_16:HN	1.800	4.000	5.000	10.00	10.00	1000.00		
1: LEU_16:HA	1: LYS_17:HN	1.800	4.000	5.000	10.00	10.00	1000.00		
1: LYS_17:HA	1: GLU_18:HN	1.800	4.000	5.000	10.00	10.00	1000.00		
1: GLU_18:HA	1: LYS_19:HN	1.800	4.000	5.000	10.00	10.00	1000.00		
1: LYS_19:HA	1: LYS_20:HN	1.800	4.000	5.000	10.00	10.00	1000.00		
1: LYS_20:HA	1: GLU_21:HN	1.800	4.000	5.000	10.00	10.00	1000.00		
1: LYS_20:HA	1: VAL_23:HN	1.800	5.000	5.000	10.00	10.00	1000.00		
1: SER_8:HA	1: SER_9:HN	1.800	5.000	5.000	10.00	10.00	1000.00		
1: LYS_17:HA	1: LYS_20:HN	1.800	5.000	5.000	10.00	10.00	1000.00		
1: VAL_22:HA	1: GLU_25:HN	1.800	5.000	5.000	10.00	10.00	1000.00		
1: GLU_18:HA	1: GLU_21:HN	1.800	5.000	5.000	10.00	10.00	1000.00		
1: LYS_20:HA	1: VAL_22:HN	1.800	5.000	5.000	10.00	10.00	1000.00		
1: ALA_3:HB*	1: ALA_4:HN	1.800	4.000	5.000	10.00	10.00	1000.00		
1: VAL_5:HG*	1: ASP_6:HN	1.800	5.000	5.000	10.00	10.00	1000.00		
1: GLU_24:HB*	1: GLU_25:HN	1.800	3.000	5.000	10.00	10.00	1000.00		
1: GLU_24:HG*	1: GLU_25:HN	1.800	5.000	5.000	10.00	10.00	1000.00		
1: ILE_11:HG*	1: THR_12:HN	1.800	4.000	5.000	10.00	10.00	1000.00		
1: THR_12:HG*	1: THR_13:HN	1.800	4.000	5.000	10.00	10.00	1000.00		

		a	b	i	c	d	e
1:THR_13:HO*	1:LYS+_14:HN	1.000	5.000	5.000	10.00	10.00	1000.00
1:LYS+_14:HB*	1:ASP-_15:HN	1.000	5.000	5.000	10.00	10.00	1000.00
1:ALA_26:NB*	1:GLU-_27:HN	1.000	5.000	5.000	10.00	10.00	1000.00
1:LEU_16:NB*	1:LYS+_17:HN	1.000	5.000	5.000	10.00	10.00	1000.00
1:GLU-_18:NB*	1:LYS+_19:HN	1.000	5.000	5.000	10.00	10.00	1000.00
1:LYS+_19:NB*	1:VAL_22:HN	1.000	5.000	5.000	10.00	10.00	1000.00
1:LYS+_19:HG*	1:VAL_22:HN	1.000	5.000	5.000	10.00	10.00	1000.00
1:GLU-_21:NB*	1:GLU-_24:HN	1.000	3.000	5.000	10.00	10.00	1000.00
1:LEU_16:NB*	1:LYS+_20:HN	1.000	5.000	5.000	10.00	10.00	1000.00
1:GLU-_21:HA	1:GLU-_24:HN	1.000	5.000	5.000	10.00	10.00	1000.90
1:GLU-_21:HG*	1:VAL_22:HN	1.000	5.000	5.000	10.00	10.00	1000.00
1:LYS+_17:NB*	1:GLU-_18:HA	1.000	5.000	5.000	10.00	10.00	1000.00
1:ASP-_15:NB*	1:LEU_16:NB*	1.000	5.000	5.000	10.00	10.00	1000.00
1:VAL_22:NB	1:VAL_23:HG*	1.000	3.500	5.000	10.00	10.00	1000.00
1:VAL_5:HG*	1:VAL_5:HA	1.000	4.500	5.000	10.00	10.00	1000.00
1:VAL_5:NB*	1:SER_8:HA	1.000	5.500	5.500	10.00	10.00	1000.00
1:VAL_5:HG*	1:SER_9:HA	1.000	5.500	5.500	10.00	10.00	1000.00
1:ILE_11:HA	1:THR_12:HG*	1.000	5.000	5.000	10.00	10.00	1000.00
1:VAL_23:HG*	1:GLU-_24:HA	1.000	5.500	5.500	10.00	10.00	1000.00
1:LEU_16:NB*	1:LYS+_17:HA	1.000	4.000	5.000	10.00	10.00	1000.00
1:VAL_23:HG*	1:GLU-_24:HA	1.000	5.500	5.500	10.00	10.00	1000.00
1:THR_7:HG*	1:SER_9:HA	1.000	4.000	5.000	10.00	10.00	1000.00
1:VAL_5:HG*	1:VAL_5:HN	1.000	5.500	5.500	10.00	10.00	1000.00
1:GLU-_27:NB*	1:GLU-_27:HN	1.000	5.000	5.000	10.00	10.00	1000.00
1:VAL_23:HN	1:VAL_23:HG*	1.000	3.500	5.000	10.00	10.00	1000.00
1:VAL_22:HN	1:VAL_22:HG*	1.000	3.500	5.000	10.00	10.00	1000.00
1:VAL_22:EG*	1:VAL_23:HN	1.000	3.500	5.000	10.00	10.00	1000.00
1:VAL_23:HG*	1:GLU-_24:HN	1.000	4.500	5.000	10.00	10.00	1000.00
1:VAL_22:HG*	1:GLU-_25:HN	1.000	5.500	5.500	10.00	10.00	1000.00
1:VAL_23:HG*	1:ALA_26:HN	1.000	5.500	5.500	10.00	10.00	1000.00
1:LEU_16:NB*	1:LYS+_17:HN	1.000	5.000	5.000	10.00	10.00	1000.00
1:ILE_11:NB	1:THR_12:HN	1.000	3.000	5.000	10.00	10.00	1000.00
1:ILF_11:NB	1:ILE_11:HN	1.000	3.000	5.000	10.00	10.00	1000.00
1:LYS+_14:HG*	1:LYS+_14:HN	1.000	5.000	5.000	10.00	10.00	1000.00
1:LYS+_14:NB*	1:LYS+_14:HN	1.000	3.000	5.000	10.00	10.00	1000.00
1:ILE_16:HG	1:LYS+_17:HN	1.000	5.000	5.000	10.00	10.00	1000.00
1:LYS+_17:NB*	1:LYS+_17:HN	1.000	4.000	5.000	10.00	10.00	1000.00
1:LYS+_17:HG*	1:LYS+_17:HA	1.000	5.000	5.000	10.00	10.00	1000.00
1:GLU-_18:NB*	1:GLU-_18:HN	1.000	3.000	5.000	10.00	10.00	1000.00
1:LYS+_17:NB*	1:GLU-_18:HN	1.000	4.000	5.000	10.00	10.00	1000.00
1:GLU-_18:HG*	1:GLU-_21:HG*	1.000	4.000	5.000	10.00	10.00	200.00
1:GLU-_18:NB*	1:GLU-_21:HG*	1.000	4.000	5.000	10.00	10.00	200.00
1:LYS+_19:NB*	1:LYS+_19:HN	1.000	3.000	5.000	10.00	10.00	1000.00
1:LYS+_19:NB*	1:LYS+_20:HN	1.000	3.000	5.000	10.00	10.00	1000.00
1:LYS+_19:NB*	1:LYS+_20:HA	1.000	4.000	5.000	10.00	10.00	750.00
1:LYS+_19:HG*	1:VAL_22:HA	1.000	5.000	5.000	10.00	10.00	500.00
1:LYS+_20:HG*	1:VAL_23:HA	1.000	5.000	5.000	10.00	10.00	500.00
1:LYS+_20:NB*	1:LYS+_20:HN	1.000	3.000	5.000	10.00	10.00	1000.00
1:VAL_22:HG*	1:VAL_22:HA	1.000	3.500	5.000	10.00	10.00	1000.00
1:VAL_22:HG*	1:VAL_23:HA	1.000	4.500	5.000	10.00	10.00	500.00
1:VAL_22:HA	1:VAL_23:HG*	1.000	4.500	5.000	10.00	10.00	500.00
1:VAL_23:HG*	1:GLU-_24:HG*	1.000	5.500	5.000	10.00	10.00	500.00
1:VAL_23:HG*	1:GLU-_25:NB*	1.000	5.500	5.000	10.00	10.00	500.00
1:GLU-_24:NB*	1:GLU-_24:HN	1.000	2.000	5.000	10.00	10.00	1000.00
1:GLU-_24:NB*	1:GLU-_25:HA	1.000	4.000	5.000	10.00	10.00	1000.00
1:GLU-_24:HG*	1:GLU-_25:HB*	1.000	4.000	5.000	10.00	10.00	500.00
1:ALA_4:NB*	1:VAL_5:HN	1.000	5.000	5.000	10.00	10.00	1000.00
1:ALA_4:NB*	1:ALA_4:HN	1.000	3.000	5.000	10.00	10.00	1000.00
1:ALA_4:NB*	1:VAL_5:HA	1.000	5.000	5.000	10.00	10.00	1000.00
1:VAL_5:NB	1:VAL_5:HN	1.000	4.000	5.000	10.00	10.00	1000.00
1:THR_7:HG*	1:SER_8:HA	1.000	5.000	5.000	10.00	10.00	1000.00
1:VAL_22:NB	1:ALA_26:HA	1.000	5.000	5.000	10.00	10.00	500.00

		a	b	l	c	d	e
1:GLU-_10:HG1	1:ILE_11:NA	1.800	5.000	5.000	10.00	10.00	1000.00
1:GLU-_18:HB*	1:VAL_22:NA	1.800	4.000	5.000	10.00	10.00	1000.00
1:GLU-_21:HB*	1:GLU-_24:NA	1.800	5.000	5.000	10.00	10.00	1000.00
1:GLU-_25:HB*	1:ALA_26:HN	1.800	4.000	5.000	10.00	10.00	1000.00
1:GLU-_24:HG*	1:GLU-_25:NA	1.800	5.000	5.000	10.00	10.00	1000.00
1:GLU-_18:HB*	1:LYS+_19:NA	1.800	5.000	5.000	10.00	10.00	1000.00
1:LYS+_17:NA	1:GLU-_18:HB*	1.800	5.000	5.000	10.00	10.00	1000.00
1:ALA_3:HB*	1:ALA_4:NA	1.800	5.000	5.000	10.00	10.00	1000.00
1:THR_13:HG*	1:LYS+_14:HB*	1.800	5.000	5.000	10.00	10.00	1000.00
1:LYS+_17:HD*	1:LYS+_20:HB*	1.800	5.000	5.000	10.00	10.00	1000.00
1:VAL_5:HN	1:SER_8:NA	1.800	5.000	5.000	10.00	10.00	1000.00
1:LEU_16:HB*	1:LEU_16:HN	1.800	4.000	5.000	10.00	10.00	1000.00
1:LEU_16:HG	1:LEU_16:HN	1.800	4.000	5.000	10.00	10.00	1000.00
1:ASP-_2:HB1	1:ASP-_2:HN	1.800	5.000	5.000	10.00	10.00	1000.00
1:ASP-_2:HB2	1:ASP-_2:HN	1.800	5.000	5.000	10.00	10.00	1000.00
1:ASP-_6:HB2	1:ASP-_6:HN	1.800	3.500	5.000	10.00	10.00	1000.00
1:ASP-_6:HB1	1:ASP-_6:HN	1.800	3.500	5.000	10.00	10.00	1000.00

!

!

!

!

!

!

!

!mixing_times h

0.075 0.150 0.300

!

!NOE_volume

!

		j	k	l	m	n	o	c	d
1:ALA_4:HN	1:VAL_5:HN	0.000	0.025	0.000	0.050	0.000	0.100	1000.0	1000.0
1:VAL_5:HN	1:ASP-_6:HN	0.000	0.025	0.000	0.050	0.000	0.100	1000.0	1000.0
1:GLU-_10:HN	1:ILE_11:HN	0.050	0.100	0.150	0.250	0.150	0.250	1000.0	1000.0
1:ILE_11:HN	1:THR_12:HN	0.000	0.050	0.025	0.100	0.075	0.150	1000.0	1000.0
1:LYS+_14:HN	1:ASP-_15:HN	0.000	0.050	0.025	0.100	0.000	0.100	1000.0	1000.0
1:ASP-_15:HN	1:LEU_16:HN	0.000	0.050	0.050	0.125	0.075	0.150	1000.0	1000.0
1:LEU_16:HN	1:LYS+_17:HN	0.000	0.075	0.050	0.150	0.100	0.200	1000.0	1000.0
1:GLU-_18:HN	1:LYS+_19:HN	0.000	0.050	0.000	0.100	0.050	0.150	1000.0	1000.0
1:LYS+_19:HN	1:LYS+_20:HN	0.050	0.125	0.075	0.150	0.125	0.175	1000.0	1000.0
1:GLU-_21:HN	1:VAL_22:HN	0.000	0.050	0.025	0.100	0.075	0.150	1000.0	1000.0
1:VAL_22:HN	1:VAL_23:HN	0.000	0.050	0.000	0.100	0.050	0.125	1000.0	1000.0
1:VAL_23:HN	1:GLU-_24:HN	0.000	0.050	0.075	0.125	0.150	0.250	1000.0	1000.0
1:GLU-_24:HN	1:GLU-_25:HN	0.000	0.050	0.025	0.075	0.050	0.125	1000.0	1000.0
1:GLU-_25:HN	1:ALA_26:HN	0.000	0.050	0.025	0.075	0.050	0.100	1000.0	1000.0
1:LEU_16:HN	1:GLU-_18:HN	0.000	0.050	0.050	0.100	0.075	0.125	1000.0	1000.0
1:LYS+_20:HN	1:VAL_22:HN	0.000	0.050	0.025	0.075	0.075	0.150	1000.0	1000.0
1:VAL_22:HN	1:GLU-_24:HN	0.000	0.050	0.000	0.050	0.025	0.075	1000.0	1000.0
1:VAL_23:HN	1:ALA_26:HN	0.000	0.050	0.050	0.100	0.125	0.175	1000.0	1000.0
1:ASNC_28:HB1	1:ASNC_28:HN	0.000	0.100	0.050	0.150	0.100	0.200	1000.0	1000.0
1:VAL_22:HA	1:VAL_23:HN	0.200	0.250	0.350	0.450	0.475	0.575	1000.0	1000.0
1:ASNC_28:HB2	1:ASNC_28:HN	0.050	0.100	0.100	0.125	0.125	0.175	1000.0	1000.0
1:GLU-_24:HG*	1:GLU-_24:HN	0.075	0.125	0.100	0.150	0.125	0.200	1000.0	1000.0
1:GLU-_21:HG*	1:GLU-_21:HN	0.075	0.125	0.125	0.200	0.175	0.225	1000.0	1000.0
1:VAL_23:NA	1:GLU-_24:HN	0.250	0.325	0.425	0.475	0.600	0.700	1000.0	1000.0
1:VAL_5:NA	1:ASP-_6:HN	0.200	0.300	0.350	0.450	0.500	0.600	1000.0	1000.0
1:ALA_4:NA	1:VAL_5:HN	0.050	0.125	0.250	0.300	0.300	0.375	1000.0	1000.0
1:LYS+_19:HN	1:VAL_22:HN	0.000	0.050	0.025	0.075	0.050	0.125	1000.0	1000.0
1:LYS+_20:NA	1:VAL_23:HN	0.050	0.100	0.100	0.150	0.150	0.200	1000.0	1000.0
1:GLU-_21:HN	1:GLU-_24:HN	0.000	0.025	0.050	0.125	0.100	0.150	1000.0	1000.0

		j	k	l	m	n	o	c	d
1:GLU_-21:HA	1:VAL_22:HN	0.075	0.125	0.130	0.190	0.250	0.350	1000.0	1000.0
1:LYS+_19:HA	1:VAL_22:HN	0.125	0.175	0.200	0.250	0.250	0.300	1000.0	1000.0
1:ALA_3:HA	1:ALA_4:HN	0.025	0.075	0.100	0.150	0.200	0.275	1000.0	1000.0
1:GLU_-24:HA	1:GLU_-25:HN	0.150	0.200	0.200	0.300	0.300	0.400	1000.0	1000.0
1:ILE_11:HA	1:THR_12:HN	0.100	0.200	0.200	0.300	0.300	0.400	1000.0	1000.0
1:THR_13:HA	1:LYS+_14:HN	0.050	0.100	0.100	0.150	0.150	0.250	1000.0	1000.0
1:LYS+_14:HA	1:ASP_-15:HN	0.050	0.150	0.150	0.200	0.225	0.275	1000.0	1000.0
1:ASP_-15:HA	1:LEU_16:HN	0.050	0.100	0.100	0.150	0.175	0.225	1000.0	1000.0
1:LEU_16:HA	1:LYS+_17:HN	0.200	0.300	0.350	0.450	0.400	0.500	1000.0	1000.0
1:LYS+_17:HA	1:GLU_-18:HN	0.200	0.300	0.300	0.350	0.350	0.450	1000.0	1000.0
1:GLU_-18:HA	1:LYS+_19:HN	0.150	0.250	0.250	0.325	0.350	0.450	1000.0	1000.0
1:LYS+_19:HA	1:LYS+_20:HN	0.200	0.300	0.300	0.400	0.450	0.550	1000.0	1000.0
1:LYS+_20:HA	1:GLU_-21:HN	0.200	0.300	0.350	0.425	0.400	0.500	1000.0	1000.0
1:GLU_-21:HA	1:GLU_-24:HN	0.100	0.200	0.225	0.300	0.350	0.400	1000.0	1000.0
1:SER_8:HA	1:SER_9:HN	0.050	0.100	0.100	0.200	0.150	0.250	1000.0	1000.0
1:LEU_16:HA	1:LYS+_19:HN	0.150	0.225	0.200	0.250	0.325	0.375	1000.0	1000.0
1:LYS+_17:HA	1:LYS+_20:HN	0.050	0.100	0.100	0.150	0.170	0.225	1000.0	1000.0
1:VAL_22:HA	1:GLU_-25:HN	0.000	0.025	0.000	0.050	0.050	0.125	1000.0	1000.0
1:GLU_-18:HA	1:GLU_-21:HN	0.000	0.050	0.050	0.125	0.100	0.175	1000.0	1000.0
1:LYS+_20:HA	1:VAL_22:HN	0.000	0.050	0.025	0.075	0.025	0.100	1000.0	1000.0
1:ALA_3:HB*	1:ALA_4:HN	0.025	0.075	0.125	0.175	0.275	0.325	1000.0	1000.0
1:VAL_5:HG*	1:ASP_-6:HN	0.025	0.075	0.175	0.225	0.275	0.325	1000.0	1000.0
1:GLU_-24:HB*	1:GLU_-25:HN	0.200	0.300	0.500	0.600	0.700	0.800	1000.0	1000.0
1:GLU_-24:HG*	1:GLU_-25:HN	0.075	0.125	0.075	0.150	0.150	0.200	1000.0	1000.0
1:LEU_16:HB*	1:LYS+_20:HN	0.000	0.025	0.000	0.025	0.025	0.075	1000.0	1000.0
1:GLU_-21:HG*	1:GLU_-21:HA	0.025	0.075	0.025	0.100	0.075	0.150	1000.0	1000.0
1:LYS+_17:HB*	1:GLU_-18:HA	0.000	0.050	0.025	0.100	0.100	0.150	1000.0	1000.0
1:ASP_-15:HB*	1:LEU_16:HB*	0.000	0.025	0.025	0.075	0.075	0.150	1000.0	1000.0
1:VAL_22:HB	1:VAL_23:HG*	0.450	0.550	0.750	0.850	1.100	1.200	1000.0	1000.0
1:VAL_5:HG*	1:VAL_5:HA	0.125	0.200	0.175	0.250	0.300	0.350	1000.0	1000.0
1:VAL_5:HG*	1:SER_8:HA	0.000	0.025	0.025	0.075	0.125	0.200	1000.0	1000.0
1:VAL_5:HG*	1:SER_9:HA	0.000	0.025	0.025	0.100	0.125	0.200	1000.0	1000.0
1:ILE_11:HA	1:THR_12:HG*	0.050	0.100	0.050	0.125	0.125	0.200	1000.0	1000.0
1:VAL_23:HG*	1:GLU_-24:HA	0.000	0.050	0.025	0.075	0.075	0.125	1000.0	1000.0
1:VAL_22:HG*	1:GLU_-24:HA	0.000	0.075	0.025	0.100	0.100	0.150	1000.0	1000.0
1:THR_7:HG*	1:SER_9:HA	0.025	0.075	0.150	0.225	0.225	0.275	1000.0	1000.0
1:THR_12:HG*	1:THR_13:HN	0.025	0.075	0.200	0.300	0.250	0.350	1000.0	1000.0
1:THR_13:HG*	1:LYS+_14:HN	0.000	0.050	0.025	0.075	0.125	0.200	1000.0	1000.0
1:LYS+_14:HB*	1:ASP_-15:HN	0.100	0.150	0.200	0.300	0.250	0.350	1000.0	1000.0
1:LEU_16:HB*	1:LYS+_17:HN	0.000	0.050	0.075	0.125	0.100	0.150	1000.0	1000.0
1:GLU_-18:HB*	1:LYS+_19:HN	0.075	0.125	0.125	0.200	0.125	0.200	1000.0	1000.0
1:LYS+_19:HB*	1:VAL_22:HN	0.000	0.025	0.050	0.100	0.125	0.175	1000.0	1000.0
1:LEU_16:HD*	1:LYS+_17:HA	0.150	0.250	0.150	0.250	0.250	0.350	1000.0	1000.0
1:VAL_5:HG*	1:VAL_5:HN	0.125	0.175	0.225	0.275	0.225	0.300	1000.0	1000.0
1:VAL_23:HN	1:VAL_23:HG*	0.175	0.250	0.450	0.550	0.650	0.750	1000.0	1000.0
1:VAL_22:HN	1:VAL_22:HG*	0.200	0.250	0.350	0.450	0.500	0.600	1000.0	1000.0
1:GLU_-25:HB*	1:ALA_26:HN	0.150	0.200	0.225	0.275	0.275	0.325	1000.0	1000.0
1:GLU_-24:HG*	1:GLU_-25:HA	0.000	0.050	0.000	0.050	0.025	0.100	1000.0	1000.0
1:GLU_-18:HB*	1:LYS+_19:HA	0.100	0.200	0.300	0.400	0.700	0.800	1000.0	1000.0
1:LYS+_17:HA	1:GLU_-18:HB*	0.000	0.050	0.025	0.075	0.075	0.125	1000.0	1000.0
1:ALA_3:HB*	1:ALA_4:HA	0.000	0.050	0.025	0.100	0.125	0.175	1000.0	1000.0
1:THR_13:HG*	1:LYS+_14:HB*	0.000	0.025	0.000	0.025	0.050	0.150	1000.0	1000.0
1:LYS+_17:HD*	1:LYS+_20:HB*	0.025	0.075	0.050	0.100	0.150	0.250	1000.0	1000.0
1:VAL_5:HN	1:SER_8:HA	0.000	0.050	0.025	0.075	0.100	0.200	1000.0	1000.0
1:LEU_16:HB*	1:LEU_16:HN	0.200	0.250	0.275	0.325	0.375	0.450	1000.0	1000.0

		j	k	i	m	n	o	c	d
1:VAL_22:HG*	1:VAL_23:HN	0.150	0.200	0.225	0.275	0.350	0.425	1000.0	1000.0
1:VAL_23:HG*	1:GLU-_24:HN	0.025	0.100	0.100	0.150	0.175	0.225	1000.0	1000.0
1:VAL_22:HG*	1:GLU-_25:HN	0.025	0.100	0.050	0.100	0.075	0.125	1000.0	1000.0
1:VAL_23:HG*	1:ALA_26:HN	0.000	0.025	0.000	0.025	0.000	0.050	1000.0	1000.0
1:LEU_16:HD*	1:LYS+_17:HN	0.000	0.050	0.025	0.075	0.050	0.100	1000.0	1000.0
1:ILE_11:HB	1:THR_12:HN	0.350	0.450	0.650	0.750	1.250	1.350	1000.0	1000.0
1:ILE_11:HB	1:ILE_11:HN	0.250	0.300	0.325	0.375	0.500	0.600	1000.0	1000.0
1:LYS+_14:HG*	1:LYS+_14:HN	0.000	0.050	0.025	0.075	0.075	0.125	1000.0	1000.0
1:LYS+_14:HB*	1:LYS+_14:HN	0.400	0.500	0.600	0.700	0.650	0.750	1000.0	1000.0
1:LEU_16:HG	1:LYS+_17:HN	0.000	0.050	0.025	0.075	0.050	0.125	1000.0	1000.0
1:LYS+_17:HB*	1:LYS+_17:HN	0.025	0.075	0.100	0.200	0.300	0.400	1000.0	1000.0
1:LYS+_17:HB*	1:GLU-_18:HN	0.000	0.100	0.100	0.200	0.250	0.350	1000.0	1000.0
1:LYS+_17:HG*	1:LYS+_17:HA	0.025	0.075	0.050	0.125	0.075	0.150	1000.0	1000.0
1:GLU-_18:HG*	1:GLU-_21:HG*	0.075	0.125	0.150	0.200	0.175	0.250	1000.0	1000.0
1:GLU-_18:HB*	1:GLU-_21:HG*	0.000	0.050	0.050	0.100	0.100	0.200	1000.0	1000.0
1:LYS+_19:HB*	1:LYS+_19:HN	0.500	0.600	0.700	0.800	0.800	0.900	1000.0	1000.0
1:LYS+_19:HB*	1:LYS+_20:HN	0.550	0.650	0.750	0.850	0.950	1.050	1000.0	1000.0
1:LYS+_19:HB*	1:LYS+_20:HA	0.200	0.300	0.250	0.350	0.350	0.425	1000.0	1000.0
1:LYS+_19:HG*	1:VAL_22:HA	0.000	0.000	0.000	0.025	0.000	0.025	1000.0	1000.0
1:LYS+_20:HG*	1:VAL_23:HA	0.025	0.075	0.075	0.125	0.100	0.200	1000.0	1000.0
1:LYS+_20:HB*	1:LYS+_20:HN	0.700	0.800	1.300	1.200	1.800	1.900	1000.0	1000.0
1:GLU-_21:HB*	1:GLU-_24:HN	0.100	0.150	0.175	0.225	0.300	0.350	1000.0	1000.0
1:VAL_22:HG*	1:VAL_22:HA	0.100	0.200	0.250	0.350	0.475	0.575	1000.0	1000.0
1:VAL_22:HG*	1:VAL_23:HA	0.075	0.125	0.175	0.250	0.200	0.300	1000.0	1000.0
1:VAL_22:HA	1:VAL_23:HG*	0.175	0.225	0.225	0.275	0.375	0.425	1000.0	1000.0
1:VAL_23:HG*	1:GLU-_24:HG*	0.000	0.025	0.000	0.025	0.025	0.075	1000.0	1000.0
1:VAL_23:HG*	1:GLU-_25:HB*	0.000	0.025	0.000	0.050	0.025	0.075	1000.0	1000.0
1:GLU-_24:HB*	1:GLU-_24:HN	0.300	0.400	0.500	0.600	0.750	0.850	1000.0	1000.0
1:GLU-_24:HB*	1:GLU-_25:HA	0.075	0.125	0.125	0.175	0.275	0.325	1000.0	1000.0
1:GLU-_24:HB*	1:GLU-_25:HB*	0.600	0.700	0.800	0.900	1.200	1.300	1000.0	1000.0
1:GLU-_24:HG*	1:GLU-_25:HB*	0.000	0.050	0.075	0.125	0.125	0.175	1000.0	1000.0
1:ALA_4:HB*	1:VAL_5:HN	0.000	0.050	0.025	0.075	0.100	0.200	1000.0	1000.0
1:ALA_4:HB*	1:ALA_4:HN	0.100	0.175	0.275	0.350	0.500	0.600	1000.0	1000.0
1:ALA_4:HB*	1:VAL_5:HA	0.000	0.025	0.000	0.050	0.025	0.075	1000.0	1000.0
1:VAL_5:HB	1:VAL_5:HN	0.100	0.150	0.200	0.300	0.325	0.425	1000.0	1000.0
1:THR_7:HG*	1:SER_8:HA	0.050	0.100	0.150	0.225	0.200	0.250	1000.0	1000.0
1:VAL_22:HB	1:ALA_26:HA	0.000	0.025	0.000	0.025	0.000	0.050	1000.0	1000.0
1:GLU-_10:HG1	1:ILE_11:HA	0.000	0.025	0.000	0.050	0.000	0.075	1000.0	1000.0
1:LEU_16:HG	1:LEU_16:HN	0.075	0.125	0.175	0.225	0.250	0.300	1000.0	1000.0
1:ASP-_2:HB1	1:ASP-_2:HN	0.000	0.025	0.025	0.075	0.050	0.125	1000.0	1000.0
1:ASP-_2:HB2	1:ASP-_2:HN	0.000	0.025	0.025	0.075	0.075	0.125	1000.0	1000.0
1:ALA_3:HB*	1:ALA_3:HN	0.150	0.250	0.400	0.450	0.400	0.500	1000.0	1000.0
1:ASP-_6:HB2	1:ASP-_6:HN	0.050	0.100	0.100	0.150	0.150	0.250	1000.0	1000.0
1:ASP-_6:HB1	1:ASP-_6:HN	0.050	0.100	0.100	0.150	0.100	0.150	1000.0	1000.0

APPENDIX 4

COMPARISON OF RMSD VALUES OF THE ELEVEN CALCULATED STRUCTURES OF THYMOSIN α_1

Structure	1	2	3	4	5	6	7	8	9	10	11
1	0.00	5.59	6.21	3.89	5.51	4.55	6.42	4.60	2.88	5.69	3.29
2	5.59	0.00	4.52	6.17	5.09	4.88	5.93	7.34	6.73	6.54	5.94
3	6.21	4.52	0.00	6.87	5.87	6.68	4.89	5.85	6.49	6.07	7.44
4	3.89	6.17	6.87	0.00	6.41	5.47	7.70	4.37	4.02	7.42	4.64
5	5.51	5.09	5.87	6.41	0.00	5.51	7.94	5.47	6.30	5.71	5.01
6	4.55	4.88	6.68	5.47	5.51	0.00	6.42	6.31	5.94	6.63	4.41
7	6.42	5.93	4.89	7.70	7.94	6.42	0.00	6.23	6.69	7.34	8.03
8	4.60	7.34	5.85	4.37	5.47	6.31	6.23	0.00	3.81	6.59	5.25
9	2.88	6.73	6.49	4.02	6.30	5.94	6.69	3.81	0.00	6.18	4.47
10	5.69	6.54	6.07	7.42	5.71	6.63	7.34	6.59	6.18	0.00	5.53
11	3.29	5.94	7.44	4.64	5.01	4.41	8.03	5.25	4.47	5.53	0.00

APPENDIX 5

COMPARISON OF RMSD VALUES OF RESIDUES 16 TO 26 OF THE ELEVEN CALCULATED STRUCTURES OF THYMOSIN α_1

Structure	1	2	3	4	5	6	7	8	9	10	11
1	0.00	0.41	0.50	0.97	0.41	0.85	0.41	0.89	0.50	1.20	0.89
2	0.41	0.00	0.39	0.94	0.55	0.81	0.30	0.82	0.63	1.18	0.80
3	0.50	0.39	0.00	1.03	0.60	0.95	0.42	0.97	0.69	1.17	0.88
4	0.97	0.94	1.03	0.00	0.92	0.81	1.00	0.81	0.82	1.35	1.03
5	0.41	0.55	0.60	0.92	0.00	0.99	0.48	0.96	0.37	1.09	0.91
6	0.85	0.81	0.95	0.81	0.99	0.00	0.89	1.03	0.85	1.45	1.19
7	0.41	0.30	0.42	1.00	0.48	0.89	0.00	0.91	0.53	1.20	0.88
8	0.89	0.82	0.97	0.81	0.96	1.03	0.91	0.00	1.00	1.51	1.02
9	0.50	0.63	0.69	0.82	0.37	0.85	0.53	1.00	0.00	1.15	0.97
10	1.20	1.18	1.17	1.35	1.09	1.45	1.20	1.51	1.15	0.00	0.84
11	0.89	0.80	0.88	1.03	0.91	1.19	0.88	1.02	0.97	0.84	0.00

APPENDIX 6

COMPARISON OF RMSD VALUES OF RESIDUES 5 TO 8 OF
THE ELEVEN CALCULATED STRUCTURES OF THYMOSIN α_1

Structure	1	2	3	4	5	6	7	8	9	10	11
1	0.00	1.10	1.34	1.57	0.88	1.56	1.75	0.61	0.84	1.75	0.71
2	1.10	0.00	0.87	1.60	1.08	1.77	1.26	1.04	1.38	1.89	1.10
3	1.34	0.87	0.00	1.43	1.43	1.48	1.00	1.27	1.45	1.82	1.06
4	1.57	1.60	1.43	0.00	1.64	1.48	1.65	1.64	1.25	2.10	1.38
5	0.88	1.08	1.48	1.64	0.00	1.72	1.80	0.66	1.15	1.76	1.09
6	1.56	1.77	1.00	1.48	1.72	0.00	1.50	1.54	1.47	1.62	1.34
7	1.75	1.26	1.00	1.65	1.80	1.50	0.00	1.71	1.80	1.90	1.60
8	0.61	1.04	1.27	1.64	0.66	1.54	1.71	0.00	1.02	1.81	0.84
9	0.84	1.38	1.45	1.25	1.15	1.47	1.80	1.02	0.00	0.96	0.73
10	1.75	1.89	1.82	2.10	1.76	1.62	1.90	1.81	1.15	0.00	1.74
11	0.71	1.10	1.06	1.38	1.09	1.34	1.60	0.84	0.96	1.74	0.00

APPENDIX 7

PHI ANGLES OF THE RESIDUES OF THE ELEVEN
STRUCTURES OF THYMOSIN C1

RESIDUE	1	2	3	4	5	6	7	8	9	10	11
Ser1	0.0	0.0	0.0	0.0	0.0	0.0	0.0	0.0	0.0	0.0	0.0
Asp2	-48.4	173.7	-52.7	110.7	141.2	65.5	-78.0	85.6	-90.0	-172.8	157.4
Ala3	138.8	125.6	147.7	132.5	-151.5	127.3	147.8	128.3	-112.3	140.7	124.6
Ala4	-176.0	-110.3	128.3	127.6	128.0	125.6	136.4	103.8	117.9	129.8	-147.3
Val5	92.0	117.5	76.6	170.4	100.9	155.2	146.6	-101.2	82.6	134.7	8.5
Asp6	134.7	122.3	151.7	131.9	148.7	118.3	158.1	137.5	80.1	-81.1	130.4
Thr7	-164.5	-172.9	88.5	-142.3	171.1	157.2	122.7	167.0	-45.3	-38.1	77.6
Ser8	96.2	112.4	-31.3	-12.8	146.4	108.4	158.1	167.8	125.5	-177.1	90.4
Ser9	23.7	-166.1	-24.7	80.6	54.8	114.1	-95.1	97.3	87.9	107.2	6.8
Glu10	105.4	-85.8	171.6	-0.6	109.9	89.8	31.8	102.1	123.9	24.0	-46.5
Ile11	138.9	166.1	125.1	-156.1	169.8	118.9	-103.4	111.2	126.3	167.3	118.5
Thr12	49.8	100.1	74.4	135.6	-69.6	41.5	49.7	-31.1	47.9	-69.7	71.7
Thr13	84.5	84.9	69.9	73.1	131.4	115.4	88.2	69.8	63.0	8.1	-23.5
Lys14	-65.8	-174.9	101.6	103.0	85.9	83.6	148.2	102.8	88.9	-70.9	173.0
Asp15	-17.8	154.2	-179.1	105.7	25.1	123.9	-170.5	108.6	-69.6	59.3	110.3
Leu16	-85.7	-83.0	92.6	-32.9	-4.3	71.1	102.9	101.8	54.0	133.7	61.8
Lys17	-36.5	-26.9	-0.8	12.5	14.0	-14.6	-27.7	-83.5	10.1	-38.2	-60.1
Glu18	-8.2	-47.6	-42.0	-36.4	-28.1	-80.2	-45.9	-70.5	-29.2	-110.0	-6.9
Lys19	-172.4	-165.9	168.3	-160.7	173.2	-149.8	-166.7	-159.2	-161.2	-4.0	-0.3
Lys20	-95.6	-93.9	-94.3	-112.7	-93.0	-108.6	-92.5	-89.0	-111.9	-86.4	-115.0
Glu21	-42.2	-49.9	-43.0	-52.7	-36.9	-42.4	-48.7	-53.2	-53.6	-79.4	-86.7
Val22	-56.8	-47.7	-50.0	-22.5	-54.8	-17.8	-48.1	-56.4	-44.1	-45.5	-47.6
Val23	-26.0	-22.8	-47.0	-23.7	-23.6	-13.8	-25.7	-24.3	11.5	-31.1	-30.7
Glu24	-48.1	-49.9	-62.2	-55.9	-48.5	-50.7	-49.0	-58.8	-18.1	-58.1	-59.9
Glu25	-93.0	-93.8	-70.5	-31.8	-92.5	-21.7	-93.7	-97.0	-72.6	-97.6	-74.9
Ala26	-39.1	-62.9	-53.7	168.9	-87.9	-53.9	-74.6	131.7	-58.9	-51.2	-38.1
Glu27	178.1	179.7	55.3	76.2	95.9	96.2	-40.8	22.7	-60.8	113.9	-48.9
Asn28	-179.3	92.8	143.3	46.1	99.1	143.2	152.2	27.4	158.6	-162.9	-45.6

APPENDIX 8

PSI ANGLES OF THE RESIDUES OF THE ELEVEN
STRUCTURES OF THYMOSIN α1

RESIDUE	STRUCTURE										
	1	2	3	4	5	6	7	8	9	10	11
Ser1	-122.5	30.9	12.5	127.4	-97.8	104.2	-118.8	-101.7	-91.4	-100.9	-111.5
Asp2	-37.7	-157.7	168.8	40.0	163.7	33.9	39.7	-28.6	6.0	109.8	-4.2
Ala3	-90.2	-124.0	88.9	124.8	83.0	80.8	117.4	57.7	149.8	-142.8	-77.4
Ala4	-113.9	21.9	31.3	-135.0	89.0	146.2	-137.9	-126.3	113.0	-95.8	64.2
Val5	3.1	124.9	95.3	107.6	137.3	13.5	102.3	7.6	6.44	-47.5	0.9
Asp6	-68.1	-72.5	-67.9	86.1	-74.6	14.2	-88.7	-81.6	53.8	9.8	-0.1
Thr7	-127.6	-140.1	-90.5	-110.6	-112.1	146.9	107.1	-71.7	-179.1	20.7	-131.7
Ser8	-22.9	104.7	-44.5	-39.5	-121.8	129.9	7.6	-89.6	-63.6	65.3	-19.5
Ser9	157.3	-105.7	-153.9	98.6	68.4	-130.5	175.9	-160.0	-113.5	159.9	89.3
Glu10	-82.3	-17.4	-122.0	36.8	-31.1	-138.1	-34.4	-135.9	-59.1	34.9	26.7
Ile11	159.3	170.8	155.4	110.8	-111.1	159.2	-152.3	151.6	158.0	-150.0	163.5
Thr12	130.6	-81.5	-148.7	145.8	165.9	153.5	110.7	62.0	110.1	138.8	64.2
Thr13	10.4	-106.7	-117.7	-135.5	-120.6	-151.9	-108.7	-114.8	-23.5	8.2	-101.6
Lys14	-43.6	-68.9	-40.6	9.2	-127.1	-130.4	-33.7	11.8	-11.3	26.3	-58.4
Asp15	-107.6	-141.8	-110.6	-139.7	-8.4	-155.8	-87.3	-155.6	-16.2	-133.9	-148.2
Leu16	-138.8	-111.5	-122.9	-48.9	-60.3	-92.2	-112.0	-94.9	-55.7	-159.1	-98.1
Lys17	-57.8	-52.8	-56.4	-53.1	-51.9	-73.7	-53.0	18.2	-51.9	-14.8	-58.1
Glu18	-42.8	-40.1	-41.8	-38.7	-46.1	-48.7	-39.8	-48.6	-43.9	-38.8	-63.7
Lys19	-101.7	-99.7	-108.5	-96.0	-110.2	-97.2	-99.6	-100.1	-95.5	-55.9	-50.7
Lys20	-32.1	-35.3	-34.9	-0.8	-39.8	-5.6	-36.9	-28.8	-8.1	-29.9	-56.0
Glu21	-2.9	-14.1	-12.3	-30.3	-14.3	-34.4	-12.8	-21.8	-8.4	-9.7	-8.5
Val22	-32.7	-55.9	-36.6	-56.7	-54.4	-71.0	-54.6	-55.2	-71.3	-54.9	-52.4
Val23	-26.2	-29.0	-11.2	-56.8	-28.6	-70.3	-25.4	-23.4	-48.4	-26.2	-24.9
Glu24	-101.6	-101.2	-97.8	-55.8	-102.6	-52.5	-105.6	-84.1	-95.2	-85.9	-85.7
Glu25	-107.3	-102.7	-106.0	-113.4	-104.7	-106.5	-109.2	-107.3	-95.9	-103.0	-90.4
Ala26	77.2	-144.5	-54.3	65.0	140.4	-38.9	-118.5	30.1	71.5	-42.6	-70.2
Glu27	-123.3	74.1	90.1	-176.0	120.2	71.8	-19.3	-129.5	79.4	61.6	40.5
Asn28	40.8	-155.2	-91.7	-124.8	82.7	-120.1	-80.7	-98.1	40.5	51.2	-102.3

Vita Auctoris

TIMOTHY DANIEL VEENSTRA

BIRTHDATE	May 21, 1966	
EDUCATION	1986-1990	Honours B.Sc. Chemistry Trent University, Peterborough, Ontario
	1990-present	Ph.D Candidate University of Windsor, Windsor, Ontario

SCHOLARSHIPS AND AWARDS

1993-1994	University of Windsor Tuition Scholarship
1993	Dr. William A. Redmond Honorary Bursary
1992	Merck Frosst Honorarium
1992	University of Windsor Graduate Studies Travel Grant

PUBLICATIONS AND PRESENTATIONS

Refereed Journals

1. Veenstra, T. D. and Lee, L. (1994) NMR study of the positions of His-12 and His-119 in the ribonuclease A-uridine vanadate complex. *Biophysical Journal* 67, 331-335.
2. Veenstra, T. D. and Lee, L. (1994) Sequence specific ^1H NMR assignments and secondary structure of thymosin α_1 . (submitted for publication).

Manuscripts in Preparation

3. Veenstra, T. D. and Lee, L. (1994) Solution structure of thymosin α_1 . (in preparation).
4. Baldwin, J. S., Veenstra, T. D. and Lee, L. (1994) A functional and structural investigation of the V2 fragment of bovine platelet factor 4. (in preparation).

Abstracts and Presentations

5. Veenstra, T. D. and Lee, L. (1994) Sequence specific ^1H NMR assignments and secondary structure of thymosin α_1 . Poster to be presented at the 1994 Canadian Federation of Biological Societies meeting in Montreal, Quebec.
6. Baldwin, J. S., Veenstra, T. D. and Lee, L. (1994) A functional and structural investigation of the V2 fragment of bovine platelet factor 4. Poster to be presented at the 1994 Canadian Federation of Biological Societies meeting in Montreal, Quebec.
7. Veenstra, T. D. and Lee, L. (1993) Secondary structure determination of thymosin α_1 by circular dichroism and nuclear magnetic resonance. Symposium lecture presented at the 1993 Canadian Federation of Biological Societies meeting in Windsor, Ontario.

8. Veenstra, T. D. and Lee, L. (1992) Nuclear magnetic resonance studies of the interaction of 3'-cytidine monophosphate with semisynthetic ribonuclease A. Symposium lecture presented at the 1992 Canadian Federation of Biological Societies meeting in Victoria, British Columbia.